Use of Carbon Nanofilaments in Producing Cementitious Composites with Improved Mechanical and Durability Performance

Salam Razaq Jasim Al-Rekabi

A thesis submitted in partial fulfilment of the requirements of the University of Brighton for the degree of Doctor of Philosophy

School of Environment and Technology
University of Brighton

September 2017

ABSTRACT

Reinforcement of cementitious materials is a common technique for improving mechanical performance and preventing crack propagation, and is typically applied at the macro-scale, meso-scale (millimetre scale) and/or at the micro-scale using macrofibres and microfibres, respectively. Cementitious material failure is a multi-scale process, however, and also occurs at the nano-scale (10^{-9} m). The use of nano-additives may therefore be valuable in reinforcing cement hydration products at the nano-scale, bridging nano and micro cracks to prevent initial crack propagation, and refining the pore structure to densify the cement matrix.

This research focuses on the use of carbon based nano-additives as nano-reinforcement agents in cementitious composites, with the aim of producing novel high performance nanocomposite materials for practical structural application (e.g. as repair materials). Four types of nano-additives were investigated: multiwall carbon nanotubes (MWCNTs), functionalised MWCNTs, carbon nanofibres (CNFs), and "few layer graphene oxides" (FLGO). The unique geometrical characteristics of these additives in particular, as well as their mechanical properties such as high strength, ductility and stiffness, were the motivation for this study.

In this work, extensive experimental studies have been conducted to develop practical and effective dispersion techniques for carbon nano-additives for cementitious application, and to produce novel cementitious composites with nano-additives (i.e. Nanofilaments Reinforced Cementitious Composites (NRCC)) and with hybrid nano-and-micro fibres (i.e Multiscale Hybrid Reinforced Cementitious Composites (MHRCC). The work has also focused on evaluating the efficiency of nanofilaments as nano reinforcement agents, controlling cracking and its impact on the durability of the produced composites. More specifically, test methods have been used to assess the shrinkage and cracking response of thin composite layers exposed to restrained shrinkage, and their sulfuric acid resistance. Furthermore, the potential application of the developed hybrid composites (MHRCC) as a layer repair/strengthening material was examined.

Carbon nano-additives (MWCNTs, functionalised MWCNTs, CNFs, and GO) have a high tendency to agglomerate due to their strong Van der Waals self-attraction and hydrophobic surfaces. To date, ensuring a uniform dispersion in water and in the cementitious composite

is the main challenge that hinders their effective use as a nano reinforcing agent. The present study focuses on a novel dispersion technique for dispersing the carbon nano-additives in water and in the cementitious composite. The effect of various intensities of sonication and treatment times, and the effect of surfactants and mineral admixtures on the dispersion behaviour were investigated. Nano-additive suspensions were semi-quantitatively and qualitatively analysed analysed using Ultraviolet–visible spectroscopy (Uv-vis) and Transmission Electron Microscopy (TEM). The mechanical properties and microstructure of the resulting composite material were characterised through compressive, direct tensile strength, and Scanning Election microscopy (SEM) tests. It was found that periodic and short-duration, high-intensity sonication achieved superior dispersion of the agglomerated carbon nano-additives at different concentrations, and led to cementitious composites with improved mechanical performance. The new composite material overcomes a number of issues associated with conventional cementitious composites, in particular their tendency to crack at the nanoscale under loading, and during shrinkage.

The obtained results on dispersion show that it is possible to produce composites reinforced (i) at the nano scale by incorporating a very low percentage of nanofilaments at 0.025% (by cement weight) and (ii) at nano-and-micro scale by incorporating a low percentage of nanofilaments at 0.025% (by cement weight) together with micro steel fibres (volume fraction of 2%). Addition of nanofilaments resulted in cementitious composites with improved tensile strength, drying and restrained shrinkage performance. Hybrid fibre composites exploit the synergistic effect between nano-and micro additives and can potentially lead to significant improvements in toughness and other mechanical properties. Encouraging results are reported suggesting that incorporating effectively dispersed nanotubes/fibres has the potential to produce composites with simultaneously improved mechanical performance and long-term durability. Repairing of reinforced concrete beams by using a thin layer (35 mm) of Multiscale Hybrid Reinforced Cementitious Composites(MHRCC) was found to have many advantages, such as increasing the ultimate load, stiffness, extending the service life, and potentially delaying crack formation and propagation.

TABLE OF CONTENTS

Chapter Four: Dispersion of MWCNTs for cementitious application: Effect of Sonication Intensity, Surfactants, and Mineral Admixtures

Chapter Nine: Conclusions and Further Work

LIST OF TABLES

LIST OF FIGURES

LIST OF ABBREVIATIONS

ASTM	American Society for Testing and Materials
CNTs	Carbon nanotubes (i.e. refer to the as received Multiwall carbon nanotubes)
CNFs	Carbon nanofibres (as received)
CNT/Fs	Carbon Nanotubes/fibres
CVD	Chemical Vapor Deposition
COOH	Carboxyl groups
CT-1	Dosage of CNTs (0.01) % by cement weight
CT-2	Dosage of CNTs (0.025) % by cement weight
CT-3	Dosage of CNTs (0.05) % by cement weight
ECC	Engineered Cementitious Composites
FRC	Fibre Reinforced Concrete
F-MWCNTs	Functionalised Multiwall Carbon Nanotubes (as received)
FLGO	Few Layer Graphene Oxide
GO	Graphene Oxide
G	Graphene
HSC	High Strength Concrete
HFC	Hybrid Reinforced Concrete
JSCE	Japan Society of Civil Engineering
LVDT	Linear Voltage Differential Transformation
MTS	Hydraulic Mechanical Testing System
MC	Methylcellulose
MWCNTs	Multiwall Carbon Nanotubes
MHRCC	Multiscale Hybrid Reinforced Cementitious Composites

MHRCC-CNT	Multiscale Hybrid Reinforced Cementitious Composites-based on CNT
MHRCC-CNF	Multiscale Hybrid Reinforced Cementitious Composites-based on CNF
NC	Normal Concrete
NSF	Naphthalene Sulfonates Formaldehyde
NRCC	Nanofilaments Reinforced Cementitious Composites
NRCC-CNT	Nanofilaments Reinforced Cementitious Composites- based on CNT
NRCC-CNF	Nanofilaments Reinforced Cementitious Composites- based on CNF
OPC	Ordinary Portland Cement
OH	Hydroxyl Groups
PCE	Polycarboxylate Ether
PC	Control mix of Portland Cement mortar
P	Porosity
RC	Reinforced Concrete
RILEM	The International Union of Laboratories and Experts in Construction Materials, Systems and Structures (RILEM, from the name in French)
SWCNTs	Single Wall Carbon Nanotubes
SEM	Scanning Electron Microscope
SD	Standard Deviation
TEM	Transmission Electron Microscopy
USF	Undensified Silica Fume
UV-Visible	Ultraviolet–visible Spectroscopy
UHPFRC	Ultrahigh Performance Fibre Reinforced Concrete

LIST OF NOMENCLATURES

$f_{c(frc)}$	Compressive Strength of FRC, MPa
f_{fs}	Flexural Strength of HPSFRC, MPa
$f_{c(hfc)}$	Compressive Strength of hybrid fibre composite, MPa
f_{dts}	Direct Tensile Strength of HPSFRC, MPa
f_{sts}	Splitting Tensile Strength of HPSFRC, MPa
f_{cp}	Compressive strength of PC, MPa
RI	Fibre reinforcing index
V_f	Volumetric ratio
FT_{δ}	Flexural Toughness Factor

Declaration

I declare that the research contained in this thesis, unless otherwise formally indicated within the text, is the original work of the author. The thesis has not been previously submitted to this or any other university for a degree, and does not incorporate any material already submitted for a degree.

Candidate: **Salam Razaq Jasim Al-Rekabi**

Signature :____  ____

Date: 20/ 09/ 2017

ACKNOWLEDGEMENTS

A mighty long way to have come and to realise that it is done, for this reason, it is just right to give unhindered thanks and praise to God Almighty for life, health and strength through it all. acknowledgement. I wish to express my gratitude to the Ministry of Higher Education and Scientific Research/Iraqi Cultural attaché in London for help and their financial support for this study.

I would like to take this opportunity to express my heartily gratitude to my supervisors, Prof. Andy Cundy, for his untiring support, encouragement and guidance from day one to completion of my thesis which enabled me to reach this stage.

I would also like to thank my other supervisors, Dr. Andreas Lampropoulos, Prof. Raymond Whitby, Dr Irina Savina, and Dr Hamid Eslimy-Isfahany, their input, support, and interest in the work has been invaluable.

I would like to thank staff members of the Doctoral College/University of Brighton especially the Director of the Doctoral College Prof. Neil Ravenscroft, and the Research Student Administrator Mrs Sarah Longstaff staff for their continual guidance. Thanks, are also extended to all staff members and technical staff of the School of Environment and Technology Engineering and School of Pharmacy and Biomolecular Sciences. Special gratitude is expressed to Dr Jonathan Salvage and Dr Andrew Flint for their assistance in the Scanning Electron Microscopy (SEM).

I also like to thank my great friend who made my life here colourful and pleasant, Mohammed Al-Majidi, I am so lucky to have your accompany in the last four years. To my friends Oday Almaamory and friend and roommates; Laura D'Amico, Richard Kulczak, and Hamed Mahjorian thank you for listening, offering me advice, and supporting me through this entire process.

Finally, I would like to thank my wife Baidaa Ibraheem for her love and support since we get married. Without her patient and understand in my tough time and taking care of my life during the PhD course, my thesis would hardly be completed “easily”. To my beloved

daughters Mariam and Mawj, I would like to express my thanks for being such a good girls always cheering me up.

Finally, I am very much grateful to my parents, my brothers and sisters and for all their supports and encourage though out my studies. I thank my mum for her unconditional love and her support and understanding throughout my PhD course.

Chapter One:

Introduction

1.1 General

The nanotechnology revolution has heavily impacted a variety of products, services, and industries, including the construction sector. The incorporation of nanomaterials in construction is expected to improve vital qualities of building materials (e.g., strength, durability, and lightness), offers new collateral functions (e.g., energy-saving, self-heating, and crack-free materials), and provides the main components for maintenance instruments such as structural health sensors(Mittal et al. 2015, Gdoutos et al. 2016). Moreover, nanotechnology has a promising role in developing smart, efficient, and sustainable construction materials and reducing carbon emissions, thus making concrete production, and the construction industry generally, more environmentally friendly. Nanotechnology in construction was selected as one of 10 targeted nanotechnology applications considered able to resolve the developing world's biggest problems (Zdenek et al. 2009, Rashid et al. 2012).

Cement-based composite (e.g. cement paste, cement grout, concrete) is a brittle material that has low tensile strength, strain capacity, and shows early development and propagation of micro cracks under relatively low tensile loads. Hence, extensive research efforts have been directed towards addressing some of the concerns related to concrete brittleness and its poor resistance to crack growth. The incorporation of short randomly distributed fibres, as reinforcement, can be effective in arresting cracks at both the micro- and macro-levels. At the micro-level, fibres inhibit the growth of cracks, and after the micro-cracks coalesce into macro-cracks, fibres provide mechanisms that abate their unstable propagation, provide effective bridging, and impart sources of strength gain, toughness and ductility (Banthia and Sappakittipakorn 2007).

New generation nanomaterials have the potential to act as reinforcement agents at the nano scale, preventing the formation of cracks as well as arresting their propagation. Carbon nanofilaments, such as carbon nanotubes and carbon nanofibres, have

therefore been the subject of many investigations as reinforcements for cementitious composite. These materials possess remarkable mechanical properties: such as a high Young's modulus (which for CNTs is around 1TPa), high tensile strength (ca. 50–200 GPa), and fracture strain as high as 280% (Siddique and Mehta 2014, Stynoski et al. 2015). The incorporation of carbon nanofilaments can inhibit crack formation and delay the failure process: cracks mechanism in cement-based materials is multi-scale process which is developed initially at the nanoscale, where microfibres fail to stop crack initiation(Lu et al. 2016). Moreover, additional benefits of using carbon nanotubes/fibres include: production of relatively lightweight and flexible composites, producing novel geometrical construction shapes which are easy to mould and install, and potential to generate materials which act as an isolating shield around reinforcement bars, and which prevent aggressive ions from penetrating and corroding the steel bars in the concrete structure, (Saptarshi et al. 2013). Use of nano engineered concrete can lead to considerable reduction in the dimensions of structural members which could result in much less consumption of cement and thereby reduction of CO2 release, and make the concrete materials to be very promising green and sustainable construction and building materials and have strong potential to be used in engineering practice.(Tian et al. 2015).

1.2 Current Problems in the use of Cement Based Composites

1.2.1 Durability

Cracking is the major cause of durability issues in structural members. Problems occur due to the tendency of cementitious materials to crack, which is the result of their brittle nature and low tensile strength. The formation of microcracks, which may later merge and develop into macrocracks, often allows the ingress of moisture and harmful chemicals (salts, acids) which lead to degradation of structural elements. The caused damage in the concrete materials and/or reinforcement steel (due to corrosion) can lead to reduced capacity, service lifetime and potentially complete structural failure(Tobias 2015).

To date, various preventative measures are undertaken, based on limiting crack propagation rather than crack prevention, such as: reducing the induced stresses, using of short and randomly distributed strengthening fibres, and increasing the effective reinforcing. Despite these design criteria, crack formation in cement based composites is effectively unavoidable, and thus durability issues resulting from cracking are still common (Richardson and Heather 2013).

1.2.2 Sustainability

Sustainability issues (economic and environmental) are essentially correlated with the durability issues (described above). For example, degradation of concrete structures requires periodic maintenance, and the ongoing maintenance cost often represents a significant portion of the total initial build cost. Reduction in crack formation/width can be translated directly into long term gains in durability because the structure remains less permeable to harmful chemical ions. An improvement in the durability therefore will reduce maintenance, repair, and if required replacement of a structure, thus impacting positively on the sustainability of the material (Zdenek et al. 2009, Tian et al. 2015).

Moreover, the cement industry is one of the most energy consuming industries, with a very high rate of carbon dioxide (CO_2) emissions(Rovnaník et al. 2016), of which 50% are from chemical manufacturing processes and 40% are from burning fuel. Overall emissions are responsible for approximately 7-10 % of total global CO_2 emissions, placing the construction sector third behind the energy and transportation sectors in terms of total CO_2 emissions (Tobias 2015). Significant efforts have been directed toward reducing the carbon footprint of the cement industry by; i) improving the efficiency of the cement manufacturing process, ii) reducing cement production which is either by using supplementary cementitious materials such as fly ash, ground granulated blast furnace slag, natural pozzolans, and silica fume (replacement with cement or by improving cement based composite properties to extend service life and reduce quantity required for maintenance(Passant 2015).

1.3 Motivation for Research

The motivation behind this research is to examine the use of nanotechnology in improving the performance, and enhancing the durability, of structural construction materials–specifically this thesis examines the use of carbon nano-additives in the development of new cementitious composites with improved mechanical performance and durability for structural application. Carbon based nanofilament reinforced cementitious materials are a potential solution to many durability and sustainability issues currently affecting the construction industry sector. Improving mechanical durability performance of structural materials will minimise maintenance requirements and reduce the demand for cement and concrete, and therefore improve overall economic and environmental sustainability.

Global production of carbon nano-additives has increased significantly, it has surpassed the kiloton level and is expected to more than double in the next few years as existing manufacturers increase production and new manufacturers emerge(Kerdnawee et al. 2017). With continuing advancements in cost reduction and production scale, the number and diversity of nano-additives and production technologies will continue to rise, and these materials have the potential to become major additives, alongside microfibres, for composite fabrication.

1.4 Research Objectives

The goal of the present study is to produce novel cementitious composites with improved mechanical and durability performance by incorporating various types of carbon based nano-additives, such as carbon nanotubes, carbon nanofibres, and graphene sheets, into the cement mixture. To fulfil this aim, it is important to overcome the relevant challenges associated with these additives to allow their effective and repeatable application. Within this broad aim, the research focused on the following key objectives:

1. With the use of ultrasonication techniques, optimise a facile and scalable technique for dispersion of nano-additives in cementitious composites (Chapter Four).

2. Use low amounts of nano-additives (0.025% wt.%), prepared following the proposed dispersion technique, to produce: (a) nano-additives cementitious composites (Chapter Five), and (b) multiscale hybrid reinforced cementitious composites (Chapter Six), with improved mechanical properties.
3. To investigate the durability performance of the produced composites, through tests including free drying shrinkage, cracking tendency (through based restrained, and end restrained tests), and resistance to sulfuric acid ingression (Chapter Seven).
4. To examine the potential application of using the proposed composites, i.e. multiscale hybrid reinforced cementitious composites based on carbon nanotubes and based on carbon nanofibres, as new repair/strengthening technique. This final objective focused on experiment determining if these composites could be effectively used to repair and strengthen reinforced concrete (RC) beams for improving their flexural behaviour (Chapter Eight).

Chapter Two:

Use of Nano-Additives in Producing Nano Cementitious Composites: Literature Review

2.1 Overview

During the past decade, the application of concrete technology has been undergoing rapid and widespread development and growth, not only for buildings but also for highways, bridges, underground mass transit facilities, wastewater treatment systems, and marine structures. The most recent efforts to modify the inherent brittle behaviour of cement-based materials have included the concept of nanotechnology. Nanoscience and nanotechnology have a central role to play in producing innovative concrete materials for the 21st century. Nanotechnology enables scientists to work at the molecular level, atom by atom, to develop new materials fundamentally with new physical and chemical properties(Sanchez and Sobolev 2010). Currently, combining new nano-sized materials such as carbon nanotubes, nanofibres and graphene with cement and concrete to produce improved performance composites is a dynamic and growing research area. Nano materials are defined as materials with at least one size dimension less than 100nm (1nm=10^{-9}m) (Passant 2015). Nano-ingredients have been incorporated in wide range of areas, such as in physics, chemistry, medicine etc., resulting in new research areas such as nano-physics, nano-medicine, and nano composites. (Anurag 2014). This work focuses on the latter area.

Use of nano-additives such as multiwall carbon nanotubes (MWCNTs), carbon nanofibres (CNFs), and graphene (G), in cementitious materials is at a relatively novel stage. These materials have emerged as a key potential technology to reinforce cementitious composites and prevent crack formation at the nano scale, prevent the growth and propagation of the cracks to a larger scale, and produce denser composites with improved mechanical performance. Reinforcing a cementitious composite at the nano scale has become a promising approach for creating a new generation of crack-free materials that offer significant potential to reduce durability problems associated with existing cementitious composites. Crack propagation in a cement matrix system

starts at (and develops from) the nano scale, leading to the accelerated penetration of water, oxygen, chlorides, acids and alkalis into the cement matrix, causing reinforcement corrosion and concrete deterioration.

The following sections first review the development of cementitious composites, relevant nano-additives properties, and the challenges influencing their use which are essential to the understanding of the subsequent composite behaviour. An extensive review of the experimental studies carried out in the last two decades is presented, then reviews about the possible application of nano-additives composites.

2.2 Development of Cement Based Composites

An overview on the development of cementitious composites and fibre reinforced cementitious composites is given below.

2.2.1 Cementitious Composites: Background and Historical Development

Cementitious materials (i.e. concrete, mortar, cement paste, etc.) are the main structural elements used in the construction field. Every year, global use of concrete in the construction field increases due to its ready availability, low cost and relatively low energy requirements (Stark 2011, Keitetsu et al. 2013). However, cementitious materials are known as being brittle materials with a low strain capacity, and poor resistance to crack growth. The cracks allow sulphates and other aggressive ions to permeate and damage reinforcing steel structures, causing lack of long-term durability. Therefore, cementitious composite to remain untracked is crucial to improve their durability, due to the ingression of aggressive ions is greatly reduced with compacted, dancer and untracked composite.(Chaipanich et al. 2010).

Since ancient times, significant efforts have been made to improve the inherent brittleness of concrete, by the introduction of third phases throughout its volume. The concept of fibre reinforcement came into being to improve the tensile properties of brittle materials. In ancient times, straw fibres were used to enhance the tensile strength of sun-baked bricks. Scientific research on fibre reinforced cementitious composites has widely increased since the 1960s. In principle, fibre-based composites

consist of cementitious materials and a reinforcement material, for example, cement based mixture reinforced with randomly distributed micro or macro fibres is termed a fibre reinforced composite. The most common reason why fibres are added to a material is to improve its tensile performance i.e. its tensile ductility or its tensile strength. (Anette 2011, Marks 2013). The influence of the fibres on cracking of cement-based composites is explained in Figure2.1, large single cracks are replaced with a dense systems of microcracks0, which is desirable from both safety and durability viewpoints(Brandt 2008).

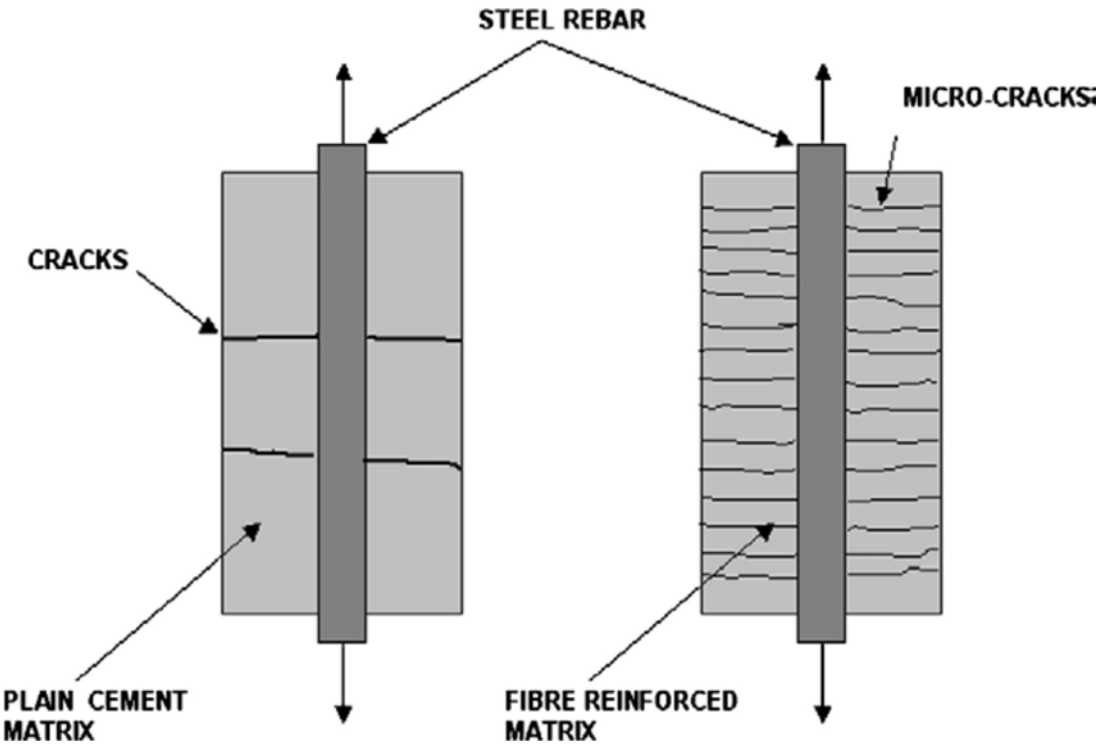

Figure 2.1 Crack patterns in reinforced concrete (RC) and fibre reinforced concrete (FRC) elements subjected to tension(Brandt 2008).

From the 1960s onwards research on fibre-based composites has advanced quickly, and today fibres of various kinds are used to reinforce concrete in structural applications. Composite systems improved by adding different types of fibres (manmade or natural) have been observed to enhance the post peak ductility performance, pre-crack tensile strength, fatigue strength, impact strength of cementitious materials, and eliminate temperature and shrinkage cracks (ACI544.1R-96 2002, Ezeokonkwo 2011).

Over the past decades, as a result of improvements in both fibre manufacturing and cementitious materials and admixtures, cementitious composite have been developed to produce High Performance Fibre Reinforced Cementitious Composites (HPFRCCs), and Ultra High Performance Fibre Reinforced Cementitious Composites (UHPFRCCs). UHPFRC is the latest innovation in the fibre composite sector developed by Bouygues SA, France, in 1995(SpaSojević 2008) and it can provide an effective alternative to typical fibre reinforced composites because of its high strain capacity under both bending and tensile loads, higher ductility, durability, and energy dissipation capacity (Martin Tr¨ubertini 2011).

HPFRCC materials undergo multiple cracking after first cracking, exhibiting a hardening behaviour, i.e., strength increases after first cracking. This material, therefore, is characterized by a pseudo-ductile tensile strain hardening behaviour with multiple cracking prior to failure. Figure 2.2 illustrates schematically the differences between the tensile response of Normal Concrete (NC), FRC, and HPFRCC, such as obtained from a uniaxial tension test. This figure emphasizes the transition from brittle concrete to quasi-brittle FRC (tension-softening) to ductile HPFRCC (strain-hardening). Specifically, during tension-softening, deformation is localized onto a single fracture plane, most appropriately described in terms of crack opening(Martin Tr¨ubertini 2011). During strain-hardening, deformation is composed of the opening of multiple subparallel fine cracks, and elastic stretching of the material between these cracks. Over a length scale that includes many such cracks, the deformation maybe considered as tensile “strain” smeared over a representative volume of material. As will be seen in the following sections, these distinctions between FRC and HPFRCC have significant ramifications in terms of load capacity and structural durability(Martin Tr¨ubertini 2011, Mechtcherine 2013).

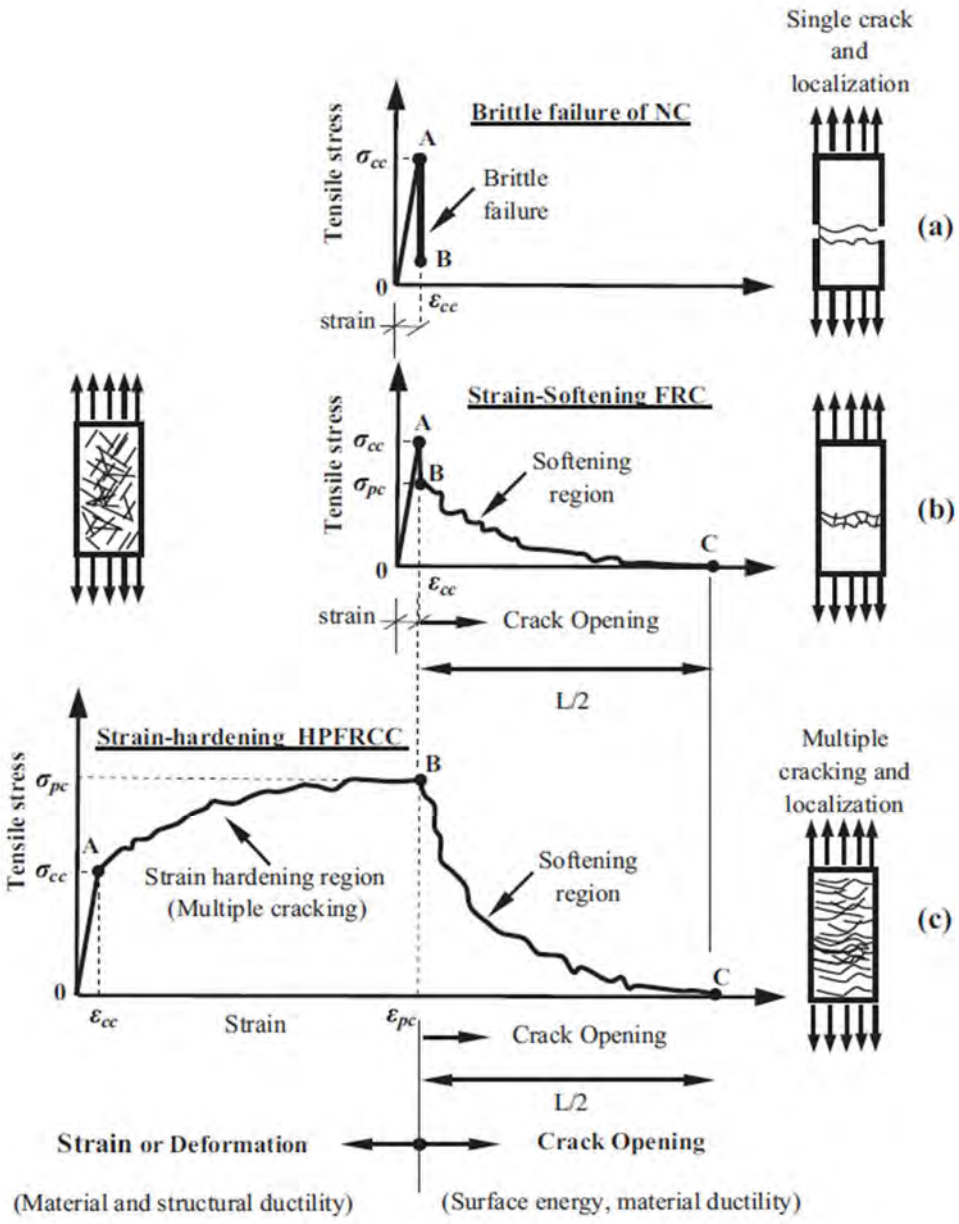

Figure 2.2 Typical tensile stress–strain or deformation relation up to failure of: (a) normal concrete (NC); (b) Fibre Reinforced Concrete (FRC); and (c) High Performance Fibre Reinforced Cementitious Composites (HPFRCC), adopted from(Fakharifar et al. 2014).

Due to its high stiffness, steel fibre is probably the most commonly used fibre material in civil engineering applications. Steel fibres have a range of shapes, they can be smooth, indented, crimped, coiled, with hooked ends, paddles, and buttons or other

anchorages. The most recent concept is to use twisted fibres; a design which results in excellent performance as is presented in (Antoine 2003).However, synthetic fibres are now gaining ground, and new materials are under continuous development (Khalifa 2015).

Since last two decades, the concept of fibre cementitious composites has extended to include many new classes. Examples of modern fibre reinforced cementitious composites are: Slurry Infiltrated Fibre Concrete, Engineered Cementitious Composites (ECC), Compact Reinforced Composite, Reactive Powder Concrete, Multiscale Fibre-Reinforced Cementitious Composites, and Hybrid Fibre Concrete(Ivan 2006, Victor Chabot 2013).

Engineered Cementitious Composites (ECC) was adopted by the original developers(Li 1992), and defined as the latest class of high performance fibre reinforced cementitious composite (HPFRCC). In 2006, the RILEM technical committee (RILEM 2006) emphasized the unique tensile strain-hardening response of this material as a constitutive law for structural engineering design, and gave the more descriptive name Strain Hardening Cementitious Composites (SHCC) to this class of materials. Japan Society of Civil Engineering (JSCE), however, emphasized these composites as "Multiple Fine Cracking Fibre Reinforced Cementitious Composites"(Keitetsu et al. 2013). While mechanical strength of typical ECC is moderate compared to HPFRCC (typical moderate tensile strength of 4-6MPa), higher strain-hardening (ductility of 3-5%) accompanied by multiple cracking (i.e. ultimate strength higher than their first cracking strength and the formation of multiple cracking during the inelastic deformation process) is the main feature of ECC(Said and Razak 2015, Tian et al. 2015). The spacing between multiple cracks in a typical ECC is between hundreds microns (even at large imposed deformation, the crack widths of ECC remain small (less than 60μm) and up to 6mm (Şahmaran et al. 2009). With this magnitude of crack width, the durability of material can be improved compared to conventional concrete material with similar deformation capacity. Figure 2.3 shows the strain capacity of ECC and crack width development.

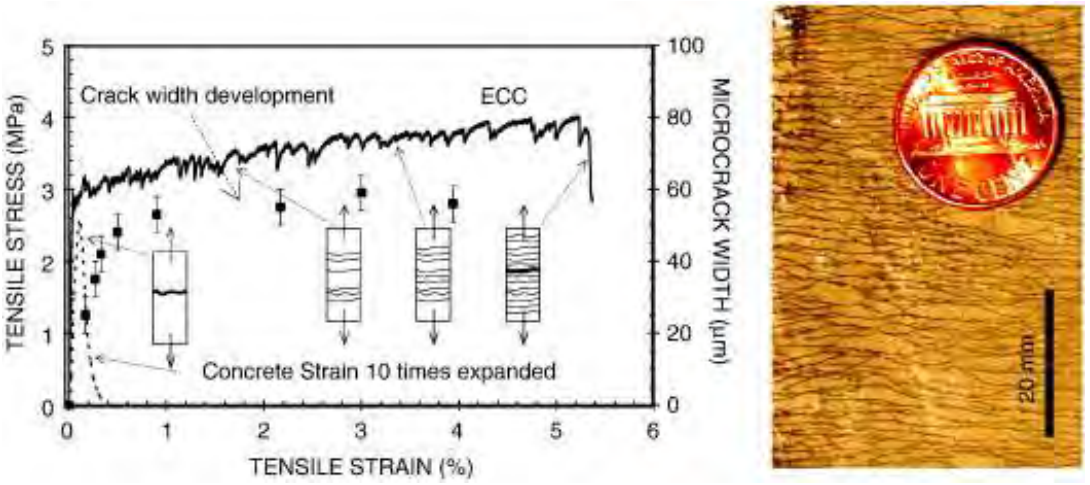

Figure 2.3 a) Typical tensile stress-strain curve and crack width development of ECC(Şahmaran et al. 2009).

Currently, a new class of Fibre Reinforced Composite (FRC) such as Cementitious Nanocomposite and Hybrid Fibre Concrete (HFC) is under development and their mechanical properties are still a subject of ongoing research. Use of two or more types of fibres in a suitable combination may potentially not only improve the overall properties of concrete, but may also result in performance synergy. The combining of fibres is often called hybridization. Hybrid Fibre Concretes (HFC) are characterised by high tensile and flexural strengths and high ductility, as well as with a high compressive strength and a very good workability(Martin Tr¨ubertini 2011). Figure 2.4 shows a typical tensile stress-strain behaviour of a hybrid cementitious composite.

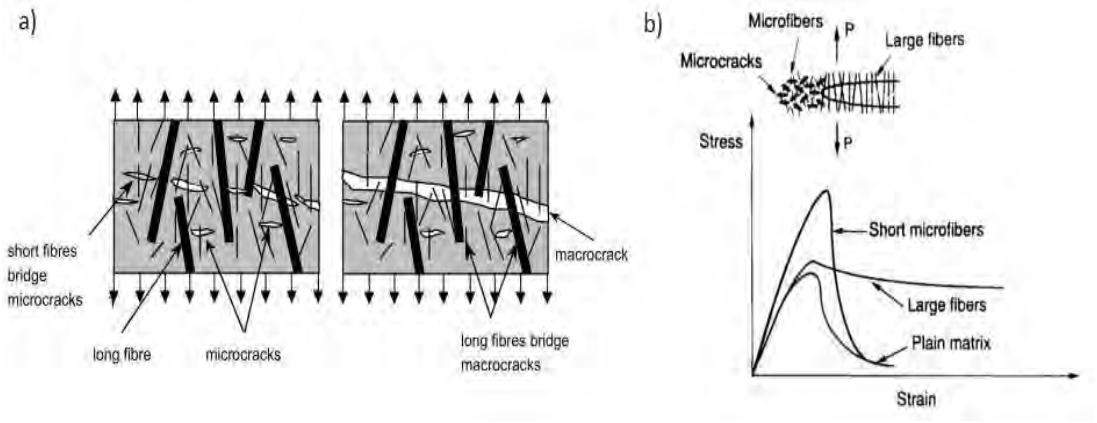

Figure 2.4 Hybrid Fibre Composite, a) scale at which different fibre types are active, b) influence of different fibres on the tensile behaviour (Ivan 2006, Pakravan et al. 2017).

2.2.2 Multiscale Hybrid Composites

The development of Hybrid Fibre Concretes (HFC) dates to the early 1980s, and many efforts have been made to improve the ductility and toughness of cementitious composites by incorporation of various types of short fibres(Martin-Gullon et al. 2006, Stähli and van Mier 2007). The motivation toward this type of fibre composite was the single fibre type in conventional fibre reinforced concrete can be effective only over a limited range of strain and crack opening. Moreover, failure of cement based materials is a multi-scale process, and each fibre type has a different scale function in the control of crack growth. Fibres bridge cracks and transfer the load, delaying the coalescence of cracks, however their influence in reinforcing the composite mainly depends on their scale. Microfibres and macrofibres are typically defined as fibres with diameters less than 50μm, and greater than 500μm, respectively(Mindess 2007). Macrofibres bridge the macrocracks and improve the post-peak behaviour, whereas microfibres, typically, bridge microcracks which could delay the propagation of microcracks in coalescing to form macrocracks (created microcracks are, in principle, discontinuous in a distributed manner, and coalesce to form lager cracks defined as macrocracks). However, cracks formation in cement based composite is a gradual multi-scale process initiated from the nanoscale, where microfibres are not effective(Stähli and van Mier 2007).

Hybrid reinforced concrete, also called multi-modal fibre reinforced concrete' (MMFRC), was first proposed by Rossi(Rossi 1987). It is defined as a combination of fibres made of the same type of material but with different geometry (shape and/or size), or another possibility is to use fibres made of different types of materials (Li 1992, Khalifa 2015, Xu et al. 2015). The most frequently used reinforcing fibres are organic fibres (such as polypropylene and nylon, polyvinyl alcohol fibres), natural cellulose (such as hardwood and softwood pulps), and inorganic fibres (such as steel, glass and carbon) (Musso et al. 2009, Yu et al. 2014). Steel fibres, polypropylene (pp) and recently polyvinyl alcohol fibres PVA have attracted most attention due to their outstanding toughness and mechanical performance (Şahin and Köksal 2011, Centonze et al. 2012, Syed Mazharul et al. 2012, Pan et al. 2015).

Recent developments in fibre reinforced composites have highlighted the positive effect of hybrid-fibre composites of micro and macro fibres or different type of micro fibres(Mohammed Alias et al. 2013, Nemkumar and Vivek 2013). The addition of fibres leads to an improvement of the properties of the composites at both micro- and macro-levels, where at micro-level, the fibres inhibit the initiation and growth of cracks(Banthia and Sappakittipakorn 2007). Therefore, one type/size of fibres can delay the propagation of microcracks, but they do not however stop their formation (Zoi et al. 2010, Han et al. 2011, Ahmed Sbia et al. 2014).

Recently, attempts have been made to incorporate of reinforcing agents at the nano scale (i.e. carbon nanotubes/fibres) to bridge nano-cracks during loading and transferring the load(Ahmed Ibrahim 2011, Hanus and Harris 2013, Siddique and Mehta 2014). They can delay the initiation of cracks at the nanoscale, and thus higher loads are required to form the crack, which improves the weak tensile strength of the cementitious matrix (Han et al. 2011). Carbon nanotube/fibres can inhibit crack formation where microfibres fail to stop crack initiation at nanoscale (Díez-Pascual et al. 2015). To date, there is only one published study on the synergistic effect of micro steel fibres and CNFs to achieve superior tensile strength and fracture toughness. Ahmed et al.(Ahmed Sbia et al. 2014) have optimised the effect of hybrid reinforcement system (i.e. a combination of steel fibres and CNFs) on the engineering properties of ultrahigh performance concrete (UHPC). The results of combination of

1.1 %(by mix volume) steel fibres and 0.04% of CNFs produced 50%, 240%, 2700%, 236%, 1200%, and 5% improvements in the flexural strength, maximum deflection, energy absorption capacity, impact resistance, abrasion resistance, and compressive strength of (plain) UHPC, respectively. The combination of nano and micro-scale reinforcement was found to enhance the reinforcing efficiency at different scales, where the nanofibres can bridge the cement hydration production in nanoscale while the micro fibres are more efficient in preventing the development of macro-cracks (Maria et al. 2010, Kawashima et al. 2013). The above study is very limited however and investigates only a single type of carbon nanofilament (i.e. CNFs).

2.3 Carbon Nano-Additives: Types and Fundamentals

2.3.1 General

Since the concept of nanotechnology was put forward by Nobel laureate Richard P. Feynman at the California Institute of Technology in 1959, many revolutionary developments in different sectors have been initiated, especially since the 1990's (after the development of scanning tunnelling microscopy and atomic force microscopy) (Sanchez and Sobolev 2010). In the past few decades, nanotechnology in general and carbon nano-additives in particular have been the subject of many studies in an array of fields including; Energy, Medicine, Environment, Electronics, Polymer Composites, and Civil Engineering. Research has demonstrated that the application of nanotechnology shows remarkable potential to achieve many goals by engineering a material at the nano level. Recent studies in civil engineering have tended to research the application of nanotechnology as a solution to key longstanding construction problems.

Types of commonly used nanofilaments (carbon nanotubes, and carbon nanofibres) and graphene sheets are discussed below:

2.3.2 Carbon Nanotubes (CNTs)

In the history of CNTs, many researchers have reported that the first discovery of carbon nanotubes (CNTs) was in 1952 by the Russian Scientists Radushkevich and Lukyanovich(Ahmed Ibrahim 2011, Frank et al. 2012). However, interest and worldwide attention in CNTs began in 1991 when Sumio Iijima, published the first article on CNTs in the journal Nature (Iijima 2002). Over the last two decades, the research interested to investigate the incorporation of CNTs within construction materials has seen dramatically increase (Jose 2014).

Carbon nanotubes available commercially can be categorized into two major forms, (Siddique and Mehta 2014). Figure 2.5 shows schematic drawings for SWCNTs, and MWCNTs.

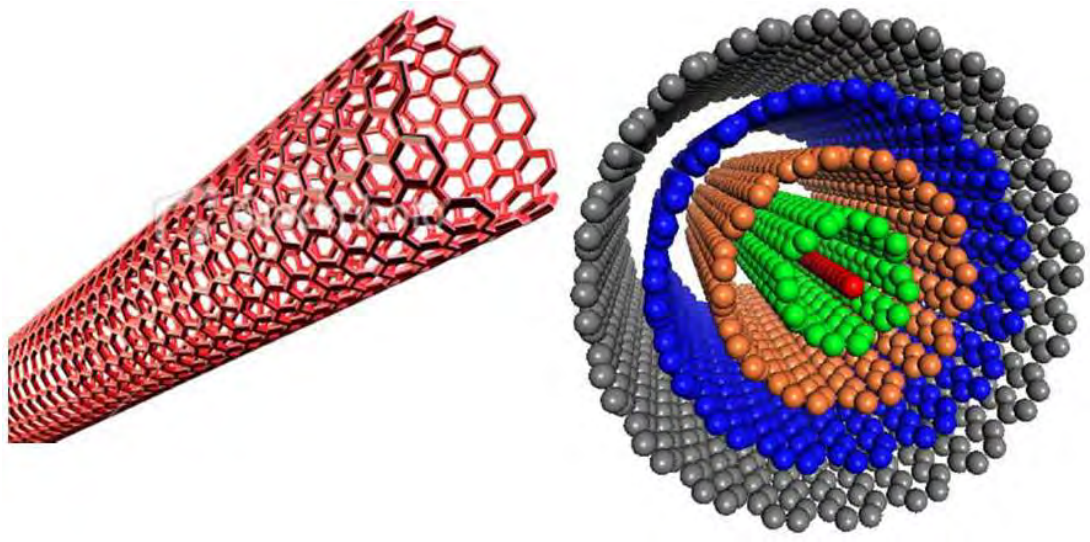

Figure 2.5 a) Schematic of a SWCNT, and b) MWCNT which are comprised of many concentric layers of carbon tubes(Ahmed Ibrahim 2011).

Various methods have been developed to produce large quantities of carbon nanotubes, including arc evaporation, laser ablation, chemical vapor deposition, electrolysis, flame synthesis etc(Ruoff et al. 2003, Zdenek et al. 2009). The arc

evaporation method, laser ablation and chemical vapor deposition are the techniques which are most commonly used for synthesis of CNTs, and chemical vapor deposition (CVD) in particular has been shown to be capable of synthesizing CNTs in sizeable quantities, at a promising price to unit ratio and with relatively high purity. This technique is based on using a metal catalyst to crack the molecules of carbon sources to form CNTs. Catalysts are heated for a specific time in a furnace to 600-1000 ^{o}C in the presence of high pressure hydrocarbon gas, then the produced carbon nanotubes are allowed to cool down in an inert gas rich environment to avoid reaction with oxygen (Zdenek et al. 2009, Liu et al. 2013). At lower temperatures (300–800^{o}C) multi wall carbon nanotubes (MWCNTs) are mainly formed, while single wall carbon nanotubes (SWCNTs) require higher temperatures (600–1000^{o}C). The drawbacks of this technique are that the relatively low operating temperatures associated with this method (300-800^{o}C) can lead to a number of lattice defects on the wall of CNTs, and mixtures of SWCNTs and MWCNTs are produced together (Hui et al. 2004).

CNTs possess highly unique mechanical, electrical and thermal properties, which play an important role in their application in composite materials. Properties of carbon nanotubes are highly dependent on morphology, size and diameter of the tubes. Various techniques have been applied to evaluate the individual properties of MWCNTs, with the first direct measurement done using atomic force microscopy. From this, an average Young's modulus of 1.28TPa and a bending strength of 14GPa was derived (Eric W. et al. 1997, Coleman et al. 2006). Other studies on mechanical and thermal properties indicate stiffness values up to 1 TPa, an elastic modulus of CNTs as high as 1 TPa, strength in the order of 100 GPa (about 100 times stronger than steel) with an ultimate strain capacity of more than 12% (about 60 times higher ductility than steel), and thermal conductivity of up to 6000 W. Moreover, the density of CNTs is about 1/6 of the density of mild steel; i.e. 1.3-1.4 g/cm^3 (Yu M 2000, Ruoff et al. 2003). Table 2.1 shows a comparison between the mechanical properties of common construction materials and CNTs (Coleman et al. 2006). The properties of carbon nanotubes have been found to be directly influenced by the number and types of defects on their walls, however the nature of these defects is closely related to the synthesis process, and significantly affects the mechanical strength and electric and

thermal transport (Mann 2006). At nano-scale the Van der Waals interaction forces between CNTs are relatively high, due to their high aspect ratio (diameters are much smaller than the lengths which ranged from hundreds of nm to several cm), and large surface area to volume ratios. This attraction causes the CNTs to be prone to agglomeration(Xu et al. 2015), and causes them to rapidly settle out of suspension if not properly treated with surfactants and mixed with an ultrasonic mixer (an ultrasonic mixer is a device that uses a high frequency driver to transmit acoustical energy throughout a liquid medium). In the ultrasonication technique, the energy in the shock waves is extremely high, which through the physical actions act to accelerates the chemical reactions, and breaks up the clumps and agglomerations of particles.

Table 2.1 Mechanical properties of most used construction materials and CNTs (Nanoshel 2014).

Material	Young's Modulus (GPa)	Tensile Strength (GPa)	Density ($g.cm^3$)
Concrete	30	0.007	2.3
Steel	208	1.0	7.8
Timber	16	0.008	0.6
CNTs	1054	150	1.4

Most applications of CNTs are mainly based on their excellent mechanical, electrical and thermal properties. A wide range of studies have been carried out to develop products which use these properties for industrial applications such as energy storage devices, electronics, sporting goods, automobiles, filters, sensors, etc (Zhu 2004).

However, few of these techniques can be applied to cementitious materials because of the chemical retardation (i.e., delay in the hydration process of the cement paste) caused by the surfactants used in dispersing the CNTs (Cwirzen et al. 2008). Carbon nanotubes do however seem to have a promising role in developing concrete composite materials with high strength, and which are ductile, crack free, durable etc. These nanotubes are useful for any application where robustness and flexibility are

necessary. Further, nanotubes are also stable under extreme chemical, and high temperatures environments. Use of nano engineered concretes could lead to a considerable reduction in the dimensions of the structural members, which could result in much less consumption of cement and thereby reduction of CO_2 release (Tian et al. 2015).

2.3.3 Functionalization of Carbon Nanotubes

Carbon nanotubes are commercially available either in their pure manufactured state (i.e. "as received" no surface fictionalization is applied), or with functionalised outer walls. As previously mentioned, the hydrophobic nature of the "as received" CNTs and strong Van der Waals forces are known to be the main reasons for the rapid agglomeration of CNTs, and mean that it is difficult to disperse them effectively into a matrix (Sham and Kim 2006, Rance et al. 2010). To achieve the advantages of CNTs and to enhance the dispersion and interaction properties of CNTs with a composite, various approaches can be used, including functionalization treatment (i.e. covalent and non-covalent functionalization of CNTs)(Peyvandi et al. 2013, Antonello Di et al. 2014). Nanotubes can be chemically treated to produce so-called functionalised carbon nanotubes, to facilitate dispersion and change their hydrophobic nature. Functional groups on the walls of the CNTs enhance their dispersion in the receiving solution and improve the bonding strength between CNTs and the host matrix (because of chemical reactions driven by the presence of carboxylic acid groups). This therefore enhances their reinforcement ability(Geng Ying et al. 2005).

Covalent functionalization is based on covalent linkages between carbon nanotubes and other functional groups. Functional groups such as carboxyl (COOH), hydroxyl (OH), hydrogenated (CH) or amine (NH_2) groups, are generated using strong acids and other oxidizing agents such as $H_2SO_4 + HNO_3$, $H_2SO_4 + KMnO_4$, HNO_3, and H_2O_2 (Sham and Kim 2006, Peng-Cheng et al. 2010). Covalent functionalisation leads to roughening of the tube surface and breaks in carbon-carbon bonds creating defect sites; this allows attachment of functional groups on the surface of carbon nanofilaments and enhances their long term dispersion stability. Despite the advantages of covalent fictionalization in enhancing the long-term dispersion and

interfacial interaction bonding with the surrounding matrix, drawbacks include use of toxic, difficulty to handle concentrated acids and strong oxidants, and alterations in the structural properties of carbon nanotubes leading to weaker monofilaments, smaller length and a lower aspect ratios (Abu Al-Rub RK 2012, Siddique and Mehta 2014).

The non-covalent functionalization approach has been used to avoid affecting the structure of carbon nanotubes and to enhance their dispersion in aqueous solution. Through this approach a surfactant, or a polymer molecule, is connected onto the nanotube without forming chemical bonds, by wrapping molecules around the CNTs. Polymers such as polystyrene (PS), epoxy, poly(m-phenylenevinylene-co-2,5-dioctyloxy-p-phenylenevinylene) (PmPV), and poly(phenylacetylene) (PPA) and surfactants such as sodium dodecyle benzene sulfonate (SDBS), sodium dodecyle sulfonate (SDS), and dodecyl trimethylammonium bromide are widely used in non-covalent functionalization to prevent the agglomeration of CNTs(Song et al. 2013, Antonello Di et al. 2014).

Proper functionalisation techniques that improve the nanotube dispersion play a crucial role in maintaining the nanotubes structures and the overall performance of nanocomposites. For example, shortening the length of nanotubes in reinforced nanocomposites means that they can less effectively transfer their stiffness or strength properties to the matrix. This results in premature failure of the composites. At the same time, besides good dispersion, interfacial bond development through the functional groups is necessary to provide effective reinforcement of the matrix.

2.3.4 Carbon Nanofibres (CNFs)

Carbon nanofibres (CNFs) belong to the new class of superior engineered nanomaterials because of their exceptional mechanical and electrical properties. Presently carbon fibre products are becoming commercially very important in a wide

range of sectors due to their low weight, easy production, good chemical resistance and cheap price (Khanna et al. 2008).

Carbon nanofibres (CNFs) are defined as a nanofilaments with an aspect ratio (length/diameter) greater than 100, derived from conventional carbon fibres. Their usage came to prominence in early 1950s after their structure had been analysed by electron microscopy (Santillan-Jimenez et al. 2015). CNFs have been synthesised (similar to CNTs) by various methods, such as vaporisation, arc discharge catalytic chemical vapour deposition and plasma-enhanced chemical vapour deposition (Iijima 2002), The Catalytic Chemical Vapour Deposition (CCVD) method is the most developed method for synthesising CNFs. The advantages of this method include the possibility to control the product morphology with improved alignments of nanofilaments, and obtaining large amounts of fibres at low cost compared with other methods (Liliana Olenic 2010). The shape of CNFs tends to stack in a truncated conical form, compared to a hollow cylinder for CNTs. Their geometry is microscopic in length (50-200μm) and nanoscopic in diameter (20-200nm), Figure 2.6 shows comparison of the diameter and shape of different types of carbon fibres.

CNFs are being used in many applications, including concrete, due to their unique mechanical, thermal, and electrical properties. They exhibit lower strength and smaller Young's modulus than that of CNTs, but they stay stronger and stiffer compared to steel. They typically exhibit a Young's modulus of 600 GPa, and tensile strength of 12 GPa, which is approximately 10-20 times stronger than steel. In recent decades, CNFs (and indeed CNTs) have had limited practical application due to their high production cost and availability, but recently they have become a feasible option as a reinforcing agent in many applications due to better techniques to synthesise these nanofilaments being developed (Khanna et al. 2008, George Turner 2014).

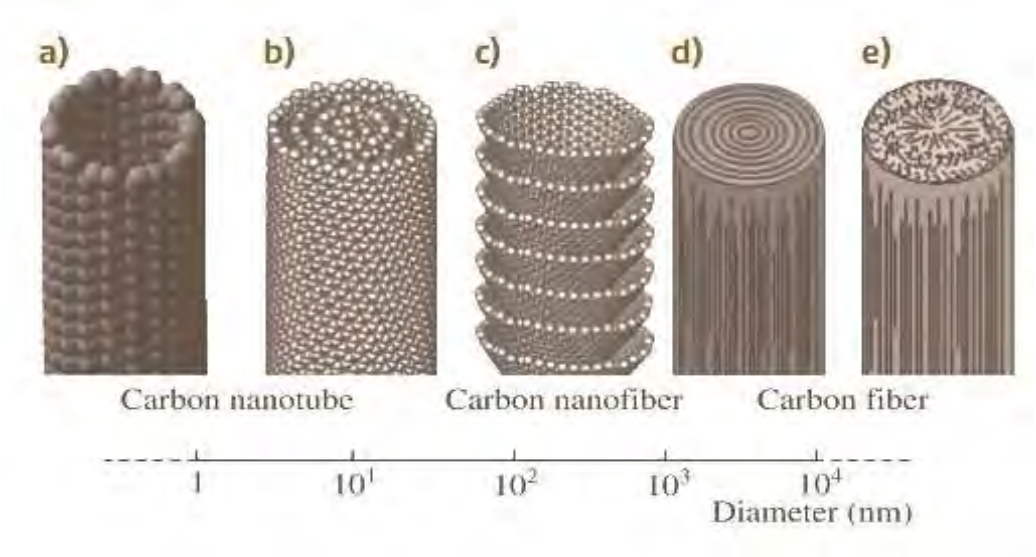

Figure 2.6 Schematic comparisons of the diameter dimensions on a log scale for various types of fibrous carbons (a) single walled CNTs. (b) b multi-walled CNTs. (c) carbon nanofibres. (d& e) carbon microfibre (Bhushan 2010).

2.3.5 Graphene

Graphene has been an emerging centre of research in various fields. Since the discovery of graphene, several industries have been benefitted including the composite industry (Mittal et al. 2015). Graphene was initially isolated by Geim and Novoselov at the University of Manchester(Chadwick 2008). They defined graphene as the thinnest material measured to date, where two dimensional crystallised allotropes of carbon atoms are bonded together in a hexagonal honeycomb lattice to form a one-dimensional layer, which they termed graphene. Graphene is the lightest material discovered (0.77milligrams per square metre), the strongest material known (three hundred times stronger than steel), and it has excellent tensile stiffness (about 10 TPa) and high tensile strength (130GPa). In addition, graphene has high electrical and thermal conductivity and a unique level of light absorption(Graphenea 2010).

Several approaches have now been devised and optimized for the synthesis of large quantities of graphene on a commercial scale. The exfoliation (peeling) technique was the first technique used to produce graphene sheets, and it was carried out by Novoselov (Novoselov 2004), whereby graphene is mechanically exfoliated from

small fraction of monocrystalline graphitic. Dispersion of graphite is a kind of exfoliation method described as the easiest technique to prepare graphene in the liquid phase, and it produces very high quality flakes compared with micromechanical exfoliation but the size of the obtained graphene is very small(Liu et al. 2013).

Chemical vapour deposition (CVD) and Epitaxial Growth (EG) are two methods used to prepare graphene directly on surfaces. The advantage of using CVD in producing graphene are, the layers diminutions of produced graphene are relatively very large, and easy to obtain in large quantity which are necessary for laboratory research and large applications, it also has low complexity and gives prefect control on the results (Victor Chabot 2013). In a synthesis context, versatile chemical oxidation of graphite followed by exfoliation offers a promising method to produce large quantities of graphene oxide (GO), but the drawback is that there are typically large defects on the structure, and therefore the mechanical and electrical properties are disrupted(Liu et al. 2013)

Graphene oxide is a compound derived from graphite oxide, which is achieved by chemical oxidation of graphite with a strongly oxidising mixture such as a combination of potassium chlorate ($KClO_3$) with nitric acid (HNO_3) or potassium permanganate ($KMnO_4$) and sulphuric acid (H_2SO_4) (Hantel 2013). However, further processes are required to reduce (chemically) graphite oxide on the surface from micron to nanometres, and then to exfoliate it into flakes of monolayer and few layer graphene oxide. Figure 2.7 shows a schematic diagram of the graphene exfoliation process

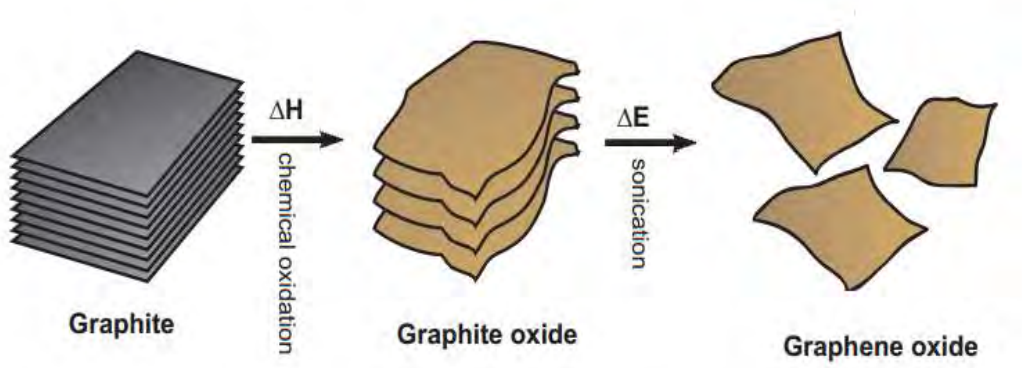

Figure 2.7 Schematic diagram for preparation of graphene nano sheets (Hantel 2013).

2.4 Challenges Influencing the Use of Carbon Nano-additives.

To date, the feasibility of effectively utilizing carbon nano-additives in cementitious materials is still under investigation as many challenges still need to be solved for repeatable and scalable application, including: Proper dispersion of the nano-additives in water and within the cementitious composite, the compatibility of the surfactant used in the dispersion process with cement hydration, and the effectiveness of the bond with the surrounding cement matrix (Rashid et al. 2012, Liu et al. 2013).

2.4.1 Dispersion of Carbon Nano-additives

2.4.1.1 General

The attractive Van der Waals interaction forces between nanotubes/fibres promote their existence in aggregated bundles and ropes. Dispersing nanofilaments in cement as in other matrices is still a challenge due to: the large Van der Waals' forces between the surfaces of the tubes/fibres(Zhu 2004, Bo et al. 2015), their poor wettability (Junrong et al. 2007), and large aspect ratio (Length-to-diameter ratio) (Rashid et al.

2012). Nanotubes/fibres tend to agglomerate and form bundles, which in turn hinder their dispersion in a liquid or in composites (Rashid et al. 2012, Mendoza et al. 2014).

Several studies on cementitious nanocomposites noted that poor dispersion of CNTs in the suspension and through the hardened cement composite prevents CNTs from effectively reinforcing the matrix (Chen et al. 2014, Stynoski et al. 2015). It can cause clusters and voids through the microstructure which could lead to drastic degradation and weakening of the composite or potential areas for concentrated stresses that can weaken the performance of the composite (Rashid et al. 2012, Sobolkina et al. 2012, Yan and Eugene 2012, Hanus and Harris 2013). A proper dispersion can guarantee a good distribution of CNTs within the matrix, enhance interfacial bonding with the surrounding matrix, evenly distribute the applied load and uniformly transfer load from matrix to CNTs (Xiao-Lin et al. 2005). Recently, utilization of mineral admixtures such as silica fume in CNT/cement composites was proposed as means of improving the dispersion of CNTs and to enhance the interfacial interaction between CNTs and the cement hydration products. The extremely fine particle size of silica fume could be intermixed with agglomerated CNTs and mechanically separate CNTs into dispersed tubes during the mixing process (Kim et al. 2014).

Chemical Approaches: This technique is based on chemical treatment (functionalization) of nanotube surfaces, in which therefore the interaction between the tube and the surroundings is affected. By choosing a specific type of functional group, it is possible to influence the interaction in different ways. This treatment enhances nanotube dispersion in different solvent and polymer systems. The main functionalization methods are based on acidic treatments. Functionalisation, in principle, cuts the nanotubes at sites with high structural damage or defect density, which leads to the production of shorter and decreased diameters nanotubes(Liu 2012, Antonello Di et al. 2014)

Physical approaches: These techniques are generally less destructive than chemical approaches on the carbon nanofilaments, and enable preparation of large scale nano-additives suspensions. The advantage of these techniques is that they do not destroy the conjugated system of the nanotubes sidewalls, and therefore do not affect the final

structural properties of the material. Among the different physical dispersion methods, the ultrasonication technique has proved to be an essential method for adequate dispersion of nano-additives into a base fluid with the presence of a dispersion agent (non-covalent functionalization) (Jose et al. 2014). Ultrasonication can be performed in both highly viscous polymers and low viscosity liquids (e.g. water, acetone and ethanol). Stirring or extrusion introduced by mechanical shear-mixing can also deliver a shear stress which leads to dispersion of aggregates or bundles of nanotubes and nanofibres. However, Yan and Eugene (Yan Yan and Eugene M. 2012) states that the delivered shear force is less effective and not enough to break up the binding Van der Waals force and is only suitable for highly viscous CNTs- polymers. Shear mixing is controlled by the rotational speed of the blade, container shape, and mixer geometry. Moreover, Huang explained that low shear stress is more effective to disperse CNTs in low aspect ratios without causing damage to the tubes, while, for high aspect ratio (ratio of length to diameter more than 1000) a sonicator delivers a sufficient energy which is higher than the binding force.

Below, a review on the effect of ultrasonication, surfactant, and mineral admixtures on dispersion of nano-additives is presented.

2.4.1.2 Effect of Ultrasonication Techniques

The ultrasonic dispersion mechanism is that ultrasonic waves in the solution induce rapidly collapsing cavitation bubbles which act to provide a highly localised shear force exceeding the tensile strength of the nanotubes, and thus can act to detach individual CNTs/Fs from bundles (Figure 2.8).

Ultrasonication is the most commonly adopted technique used for dispersion of nanotubes for civil engineering application. Ultrasonication treatment has been reported to significantly enhance the beneficial impact of incorporated nanotubes on the mechanical strength of composite materials (Gojny et al. 2003, Kim et al. 2012, Karabanova et al. 2013, Irshidat et al. 2015). However, limited attempts have been made to examine the effect of sonicator settings (i.e. intensities and treatment durations). These parameters are the main aspects affecting the dispersion process by

directly controlling the cavities distributions and then the shear stress produced (Vaisman et al. 2006, Frank et al. 2012).

Several past studies have used different sonication conditions to optimise the dispersion of carbon based nanofilaments in cementitious composites.

Of the studies which have addressed the effect of sonication duration, Makar (Makar 2005)used an ethanol/sonication treatment method for four hours to obtain a uniform dispersion of CNTs in cement-based materials, with results showing that this method was effective for dispersion and for acceleration of the cement hydration process at early curing ages. Li et al. (Li et al. 2005, Li et al. 2007) reported that use of chemically functionalized CNTs, dispersed for three hours in an ultrasonic bath at a concentration of 0.5% by weight of cement, led to improvements in compressive and flexural strength of 19% and 25% respectively. Tyson et al.(Tyson et al. 2011) and Rashid et al. (Rashid et al. 2012) found that the addition of nanofilaments (CNTs and CNFs) at concentrations of 0.1% and 0.2% (by cement weight) dispersed via an ultrasonic mixer with a probe for 20–30 min led to an improvement in ductility, modulus of elasticity, and modulus of toughness in the resulting composites. Extended sonication treatment however can modify suspension temperature and viscosity, and it has been reported to influence the nanotubes structure and reduce the tube aspect ratio, thereby reducing their reinforcing effectiveness (Adam J. et al. 2011, Farman et al. 2014).

To date, only two studies, those of Chen et al. and Bo et al. (Chen et al. 2014, Bo et al. 2015), have addressed the effect of different ultrasonication energies on dispersion of functionalized multi-walled CNTs in water, and their impact on the engineering properties of cementitious composites. Chen et al (Chen et al. 2014) optimized (theoretically) the effect of ultrasonication on the length and concentration of dispersed functionalised nanotubes, at different energies (from very low (25)J/ml to high (400)J/ml). These authors predicted that the concentration of dispersed nanotubes in water increases with ultrasonication energy and reaches a plateau after about 250J/ml. Lower energies (89J/m) were predicted to be optimal in generating higher bridging stress with a superior reinforcing effect. Bo et al (Bo et al. 2015) experimentally investigated the effects of ultrasonication energies on the engineering

properties of CNT–OPC pastes containing functionalized CNTs at 0.094%-1.88% by cement weight. Their results indicated that the amount of dispersed nanotubes in water increases with ultrasonication energy until a dispersion plateau is achieved after about 250J/ml. The optimal ultrasonication energy for improving composite mechanical properties was found to be between 50-and-150 J/ml, depending on the dosage of nanotubes. For example, the flexural strength of cement paste containing nanotubes at 0.038%, and 0.075% wt. was increased from 12% to 25%, and from 13% to 48%, respectively, with an increase in ultrasonication energy from 50 J/ml to 75J/ml. However, these studies are limited to one type of nanofilament (functionalised nanotubes) and did not investigate the effect of combined treatment duration/sonication intensity on dispersion and subsequent composite performance. The difficulty in uniformly dispersing the highly entangled bundles of nanotubes in water in a repeatable and cost-effective way limits the commercial applicability of these materials (Pacheco-Torgal and Jalali 2011, Hanus and Harris 2013). While the cost-effectiveness of dispersion techniques is not explicitly discussed in many previous studies, the need for repeatable, readily scalable and cost-effective techniques to generate effective dispersions of CNTs in fluid and matrices poses a tremendous hurdle that must be overcome prior to realizing wider applications of CNTs as, for example, reinforcement components in composites.

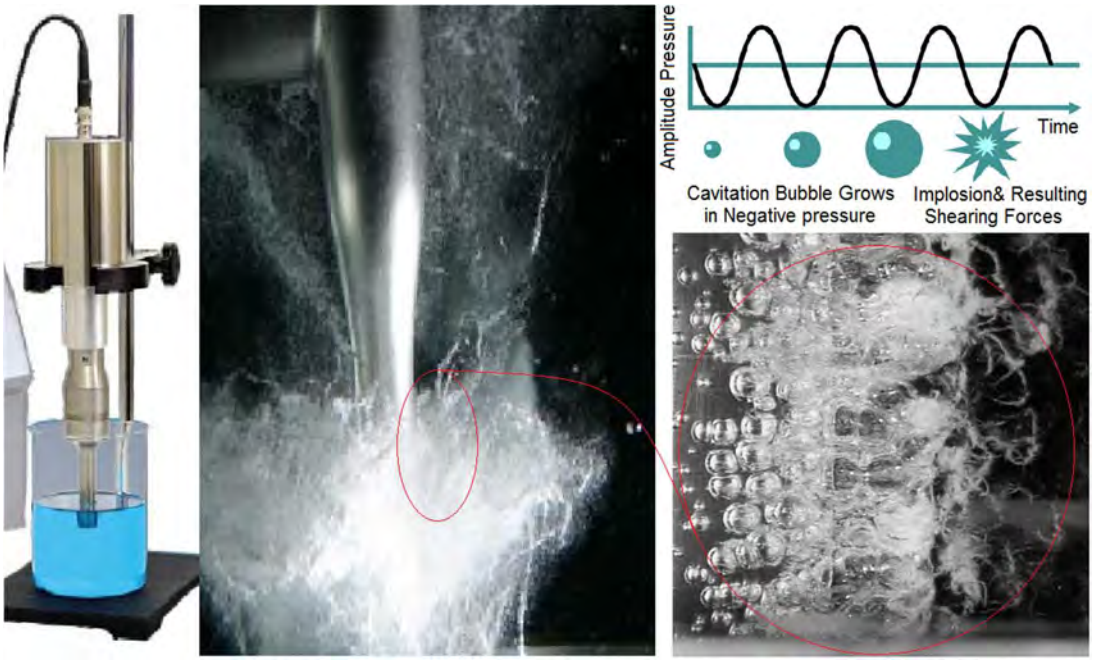

Figure 2.8 Mechanism of creating and collapsing cavitation bubbles created during ultrasonication(Alhelfi and Sundén 2016).

2.4.1.3 Effect of Surfactants:

- Surfactant Dispersion Mechanism

Surfactants are widely used to improve the dispersibility of CNTs in aqueous phases in combination with ultrasonic action. Several papers have investigated the effects of various types of polymers and surfactants on dispersibility of CNTs and their dispersive mechanisms(Krister et al. 2003, Datsyuk et al. 2009). These studies indicated that surfactants produce an effective coating on carbon nanomaterials and induce electrostatic or steric repulsions that can counterbalance Van der Waals attractions. The balance between repulsive and attractive forces creates a thermodynamic equilibrium, which regulates the dispersion and aggregation of CNTs. The balance between repulsive and attractive forces creates a thermodynamic equilibrium, which regulates the dispersion and aggregation of CNTs(Haghi and Sabu 2015).

The surfactant molecular structure consists of two parts: a head (which is hydrophilic), and a tail (hydrophobic).The latter are usually hydrocarbon chains. These chains

interact with the nanotubes/fibres surface while the hydrophilic heads orient towards water for dissolution(Datsyuk et al. 2009). A longer tail chain length gives a higher spatial volume, which in turn gives greater repulsive charge between individual nanofilaments. The hydrophobic nature of carbon nanotubes/fibres can be changed to hydrophilic during exfoliation using a sonicator in combination with a surfactant. (Bin Donga et al. 2011, Hoheneder 2012)

The addition of surfactants to nanofilament suspensions in combination with sonication produces charges on the nanofilament surfaces which can reduce the attractive force density between tubes, allowing suspension for a longer time period. The shear forces generated by the sonicator lead to the creation of gaps or spaces between the nano tubes or fibres, and the available functional groups will be adsorbed on the surfaces creating repulsive forces between the nanofilaments, generating separation (Junrong et al. 2007, Yan and Eugene 2012). The dispersion stability influenced significantly by the weak or strong of the created electrostatic repulsive force, which is often depends of the surfactant chain length and surface density. (Cwirzen et al. 2008, Mudimela et al. 2009).

- Surfactants used in past studies: Effect and Compatibility

As noted previously, to develop successful nano-additives cementitious composites, one of the major requirements is to attain uniform dispersion of CNTs in mixing water and in the final composite. The tendency of the nano-additives to agglomerate means that it is difficult to homogenously disperse them in water without use of a surfactant. Many past studies have been carried out on the effect of different types of surfactant on dispersion in water, and their impact on the final cementitious composite. The investigations have shown varying results in dispersing both CNTs and CNFs within aqueous solutions, and a wide range of surfactants have been shown to be effective in the dispersion of nanotubes/fibres in water. Some surfactants however can retard the hydration process of cement. Adresi et al. (Adresi et al. 2016) used different surfactants such as sodium dodecylbenzene sulfonate (NaDDBS), Triton X-100, and sodium dodecyl sulfate (SDS) to disperse high mass fractions of carbon nanotubes.

These surfactants were found to effectively disperse the nanotubes for wide range of polymers (Islam 2003, Ghorabi 2012, Sun 2016).

While the focus of this study is on nano-additives cement composites, the more recent studies on the effect of surfactant on dispersion of nano-additives for cementitious application reported here (Bastos et al. 2016). Chen et al., and Yazdanbakhsh et al (Chen et al. 2011, Yazdanbakhsh et al. 2012) reported that use of sodium dodecylbenzene sulfonate (NaDDBS) as a surfactant with nanotubes suspensions for cement composites introduces much more air into the cement paste (five times more than the normal range), which hinders initial setting of the cement paste for 24 hours. Also, these authors found that using an ultrasonic mixer with a commercial superplasticiser, ADVA Cast 575 (polycarboxylate-based water reducing admixture) was the most successful dispersion method compatible with cement, without affecting the hydration process.

Maria et al. (Maria et al. 2010) investigated the impact of ultrasonic energy combined with commercial surfactant on the properties of cement paste. Their results showed that for proper dispersion, the application of ultrasonic energy is required. Evidence from nanostructure analysis of the cement composite indicated that at a CNT to surfactant weight ratio within the range of 4.0 to 6.25, the nanotubes were well dispersed in the matrix.

Madhavi et al. (Madhavi et al. 2013) studied the strength durability properties of concrete containing CNTs at 0.015%, 0.03% and 0.045% of cement (by weight). The suspension was dispersed with the aid of super plasticizers–polycarboxylate at 0.25% by weight of cement. Results showed an increase in compressive and splitting-tensile strengths of the samples with increasing MWCNT content. 0.045% of MWCNT improved the 28 days' compressive strength by 27 % while the splitting tensile strength increased by 45%.

Wang et al.(Wang et al. 2013) in their study, examined the mechanical properties of cement/CNFs composites with low concentrations of CNFs at 0.05%, 0.075%, 0.1% and 0.2% by weight of cement. Ultrasonic processing and a commercially available surfactant, Methylcellulose (MC), was employed as CNFs dispersion method. The

maximum improvement in the flexural strength obtained was about 21% at 28 days. This enhancement showed the presence of strong interfacial bonds between CNFs and the matrix. Compressive strength of each mix sample was a little lower than that of the reference sample at multiple days, which the authors believed was because of the influence of the added surfactant on the composite.

Adresi et al(Adresi et al. 2016) found that a compatible surfactant with concrete compositions provides the best dispersion of MWCNTs. The authors studied the influence of various surfactants on the dispersion of 0.05 wt. % of MWCNTs in water and on the concrete compressive strength. Combinations of various surfactants and superplasticisers were introduced as an effective dispersion agents, omitting tributy1 phosphate as deformer was used at 0.02 wt. % with the mixture to eliminate air bubbles

. All prepared solutions (surfactant and MWCNTs in water) were stirred for 10 min with a magnetic stirrer (model, WIFESTEER MSH-20B) and then sonicated for 130min. The combination of Sodium Dodecyl Sulfate (SDS) and superplasticiser was introduced as a new surfactant composition that effectively disperses MWCNTs in aqueous solutions and maintains the mechanical properties of the composite as similar to that of plain concrete.

Despite of various surfactants that can be used with the dispersion process, there are very limited studies investigated the effect of surfactant/polymers options that can practically be used with cementitious materials. The nature and chemistry of the cement and its hydration process require certain surfactants that are compatible with cement, since many surfactants will delay or stop the hydration process of the cement paste. Hence, optimising effective type and concentration of surfactant that can practically be used to improve the dispersion of nano-additives and at the same time improve the cementitious materials properties is remain a subject of research that need to be extensively covered.

2.4.1.4 Effect of Mineral Admixtures

Many past studies have reported that although nanotubes were highly dispersed in the aqueous mixing solution, high numbers of clusters of nanotubes in the composites could be observed. This phenomenon was attributed to the large particle size of cement grains which did not contribute to the dispersion or prevent the re-agglomeration of nanotubes in the free water of the fresh matrix (Morsy et al. 2011, Nadiv et al. 2016, Torabian Isfahani et al. 2016). Therefore, several studies have examined the effects of the addition of ultrafine mineral.

In current practice, microsilica, and fly ash, are commonly added to cement-based composites (especially after the development of effective superplasticisers) to improve their mechanical and durability performance. In principle, due to their reactive nature and ultrafine size (much smaller than cement particle size), these materials fill in the composite pores, and accelerate the hydration process by providing nucleation sites for hydration products and contributing to faster dissolution of cement grains. Minerals containing calcium were found to influence the early stage of hydration as well (Carsten 2010).

Recently, some studies have attempted to use these minerals admixtures in combination with nano-additives in cement based composites. In particular, utilization of Silica Fume (SF), a by-product of the production of silicon metal or ferrosilicon alloys, in nanotubes/cement composites was recently proposed as means of surmounting the obstacles associated with the use of nanotubes, to produce improved material properties and increase the dispersion of microfibres in cement(Kim et al. 2014). SF particles are extremely fine with a particle size ranging from ca. 100–500 nm, which is about 100 times smaller than anhydrous cement particles and on the same scale as CNF diameters. Additionally, because of its very high amorphous silicon dioxide content (more than 80–85% SiO2), SF is a very reactive pozzolanic material that consumes calcium hydroxide during the hydration reactions of Portland cement to form additional C–S–H, giving improved hardened properties to the material(Sanchez and Ince 2009). Silica fume has been introduced within cementitious nanocomposites to improve the dispersion of nanoparticles as the extremely fine

particle size of silica fume could help to mechanically separate the agglomerate nanotubes/fibres into dispersed fibres during the mixing process. Figure 2.9 explains the effect of different silica fume contents on the dispersion of nanotubes. Moreover, due to their high pozzolanic activity, silica fume could effectively anchor CNTs, enhancing the interfacial interaction between CNTs and the hydration products(Kim et al. 2014).

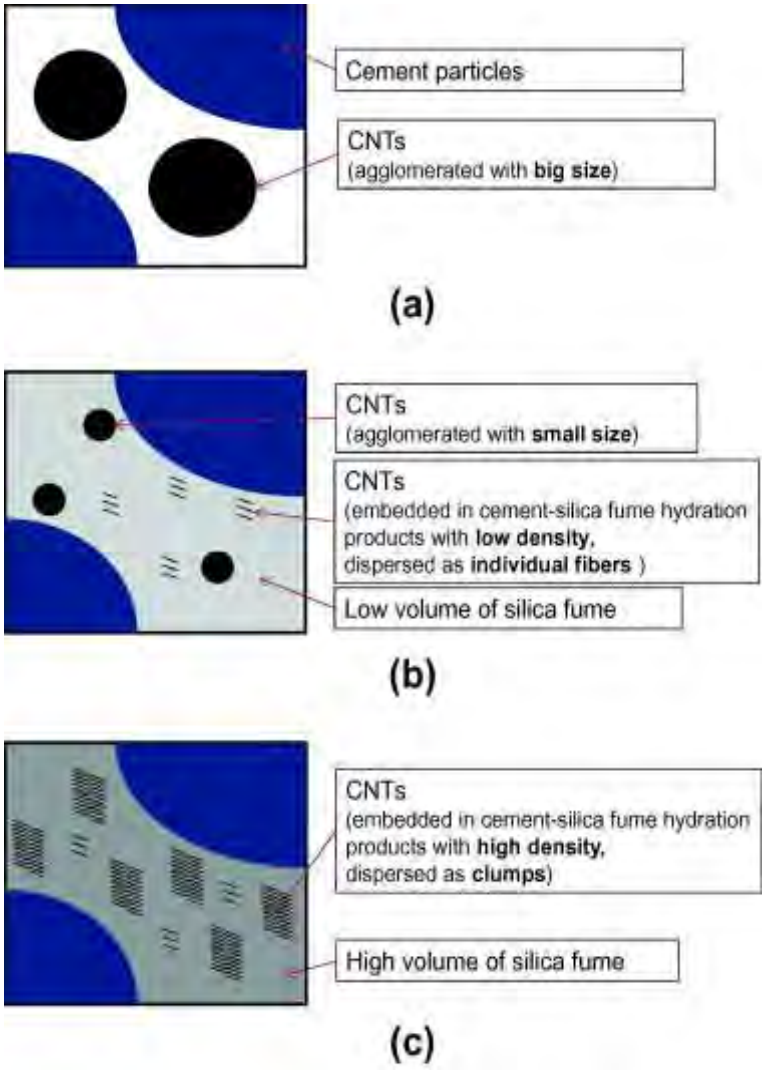

Figure 2.9 a) Schematics of dispersion of CNTs in cement matrix without silica fume, b) with low volume of silica fume, and c) with high volume of silica fume (Kim et al. 2014).

Sanchez and Ince (Sanchez and Ince 2009) investigated the performance of hybrid carbon nanofibres and silica fume (SF) in cement composites in terms of microstructural, physical, and mechanical (compressive and splitting tensile strengths) properties. The role of SF in facilitating CNFs dispersion and improving the interfacial interaction between the CNFs and the cement phases was reported. Carbon nanofibres were used in range of 0.005% to 2% per weight of cement, and SF replaced cement at a percentage of 10%. The results showed that the fine particle size of SF acted to improve nanofibres dispersion and improve the interfacial interaction bond between the CNFs and the cement phases. The CNFs were found as individual fibres well anchored in the hydration products throughout the paste, at pore/pocket edges and in clumps inside pockets created in the paste. Moreover, addition of CNFs to SF cement pastes did not show any net change in the compressive and splitting tensile strengths of the composites for all CNF loadings.

Kim et al 2014 (Kim et al. 2014) focused on enhancing the effect of CNTs on mechanical and electrical properties of cement composites by incorporation of silica fume. CNTs were used in three different concentrations (0%, 0.15%, and 0.3% by weight of cement) and silica fume in amounts of 0%, 10%, 20%, and 30% by weight of cement. Analysis through SEM images was carried out to observe the surface morphology and microstructure of the samples. The effects of silica fume addition on porosity, and the compressive strength of CNTs/cement composites were investigated. SEM images showed that in the case of CNTs/cement composites (without silica fume), large clusters of nanotubes were observed in the cement matrix. It was reported that for effectively dispersed CNTs which then enhance the mechanical and electrical properties of CNTs/cement composites, an appropriate amount of silica fume and CNTs are required. Small amounts of silica fume increased the compressive strength, but resulted in some smaller sizes of agglomerated CNTs. Higher amounts of silica fume increased the fraction of individual nanotubes, but at the same time, higher concentration increase the possibility of CNTs clumps formation which could adverse

effect the compressive strength of CNTs/cement composites(Kim and Reda Taha 2014).

Although, the utilisation of ultrasonication in combination with surfactants, and use of mineral admixtures with the composite are studies in previous investigations. Use of ultrafine reactive admixtures (such as unidentified silica fume) can be promising to enhance the dispersion degree of nano-additives, prevent the possibility of re-agglomeration, enhance the bond with the surrounding matrix, and therefore improve significantly their reinforcing efficiency through a cementitious composite.

2.4.2 Bond of Nano-additives with Cementitious Surrounding Matrix

The bond of the nano-additives with the surrounding matrix is another major aspect responsible for the load transfer capacity, and is one of the challenges limiting effective structural reinforcing efficiency within cementitious composites (Yazdanbakhsh et al. 2012, Torabian Isfahani et al. 2016). Properties such as; smooth surface, hydrophobic nature, and nonreactive surface and structural stability influence the reaction of the nanofilaments with the surrounding matrix, reducing the effectiveness of the CNT/Fs cement matrix bond. Hence, several methods have been developed to mitigate issues around weak bonding. Improving the wettability of nano-additives, through roughening their surfaces by treatment via covalent functionalization, and /or non-covalent wrapping with surfactants in combination with ultrasonic mixing, are the main methods followed to date (as shown in Figure 2.10)(Sham and Kim 2006, Wang et al. 2013). Rougher surfaces results in the outer walls possessing large surface areas, giving a higher contact area with the matrix and more mechanical interlocking sites(Zhang et al. 2004).

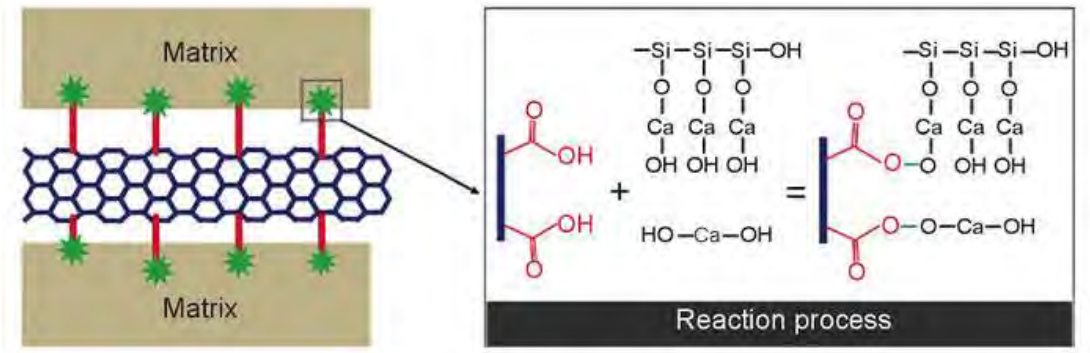

Figure 2.10 Schematic presentation of strength bonding between functionalised CNTs/CNFs and the matrix, and typical reaction process between functional groups (-COOH) and the hydration products(Wille and Loh 2010).

Past studies have reported that many parameters directly control the surface wettability nature of the nano-additives, such as treatment type and duration, concentration and the intensity of functionalizing agents (Pouria et al. 2011, Yazdanbakhsh et al. 2011). Poor wetting creates a weak interfacial interaction with the surrounding matrix which minimises the stress transfer from the matrix to the fibres and reduces the reinforcing efficiency. Whereas, the enhanced wettability of nano-additives on the one side, and the availability of reactive ultrafine materials in the mixture on the other, could improve the bond strength with the surrounding matrix and enhance the nanostructure and mechanical performance of composite (Mann 2006).

2.4.3 Cost and Availability of Carbon Nano-additives

One of the primary obstacles preventing the widespread use of nano-additives in large scale application is their availability and cost: a high synthesis cost (especially for carbon nanotubes and graphene) is widely considered one of the major issues blocking the application of nano-additives on a larger scale(Bastos et al. 2016). In construction applications, the cost of these carbon nano-additives is a key determining factor in

whether they will be used, regardless of how well they could be used. Siddique et al.(Siddique and Mehta 2014) reported that despite the tremendous potential benefits of nano materials, their availability and cost are the major challenges that are being faced in their usage. For bulk applications, such as fillers and reinforcing in composites, the quantities of nanotubes that can be manufactured still falls far short of what industry would need. The industry would need multiple tonnage quantities of nanotubes for such applications. However, if the cost and production challenges can be overcome, then carbon nanotubes/fibres can prove to be the most innovative and advantageous material in relation to concrete structures (Siddique and Mehta 2014).

As production is scaled up, the prices of large quantity nano-additives are reduced significantly compared to that of small quantity. For example the price (up to date) of multiwall carbon nanotubes (used in this research) is about $15 per gram, but with large quantity (more than 1kg) the priced reduced to $0.9 per gram(CheapTubes 2017). Therefore, research on the study and manipulation of matter at the nanoscale has been expanding exponentially, (see Figure 2.11 reveals that the scientific literature has significantly increased in the last decade). More than 100 companies around the world today are manufacturing carbon nanotubes using different techniques and this number is expected to increase to more than 200 within the next five years with an annual growth rate of 32.5% (Figure 2.12)(Nanowerk 2011). The chemical vapor deposition (CVD) method is reported as being the most promising technique in producing large volumes of nanotubes, for example, the manufacture of CNTs with a production rate of 595 kg/h was reported via decomposition of hydrocarbons by a catalytic chemical vapor deposition (CVD) method (Agboola et al. 2007). The possibility of mass production of CNTs has catalysed the vision to commercialize and apply CNT technology in large scale applications(Yit Thai et al. 2010).

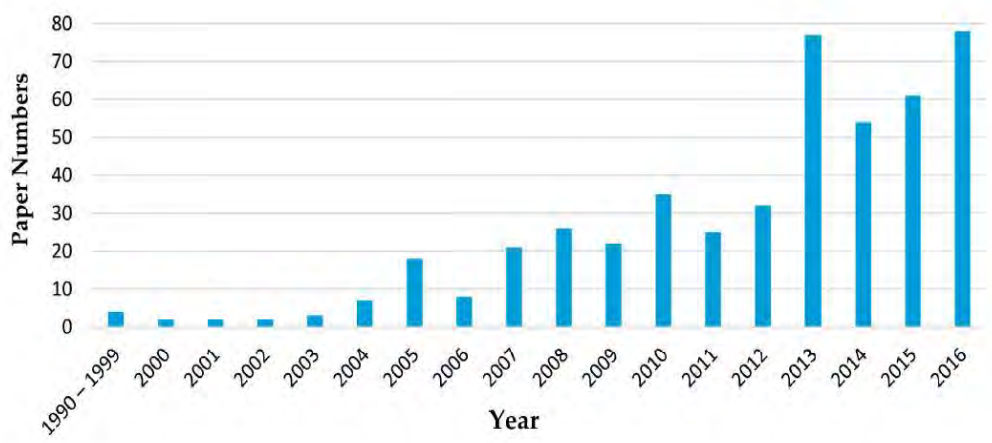

Figure 2.11 Number of published papers that, according to Scopus, include the terms cement and nanotechnology or nanomaterials in the title, abstract or keywords, limited to the fields of engineering and materials science(Bastos et al. 2016).

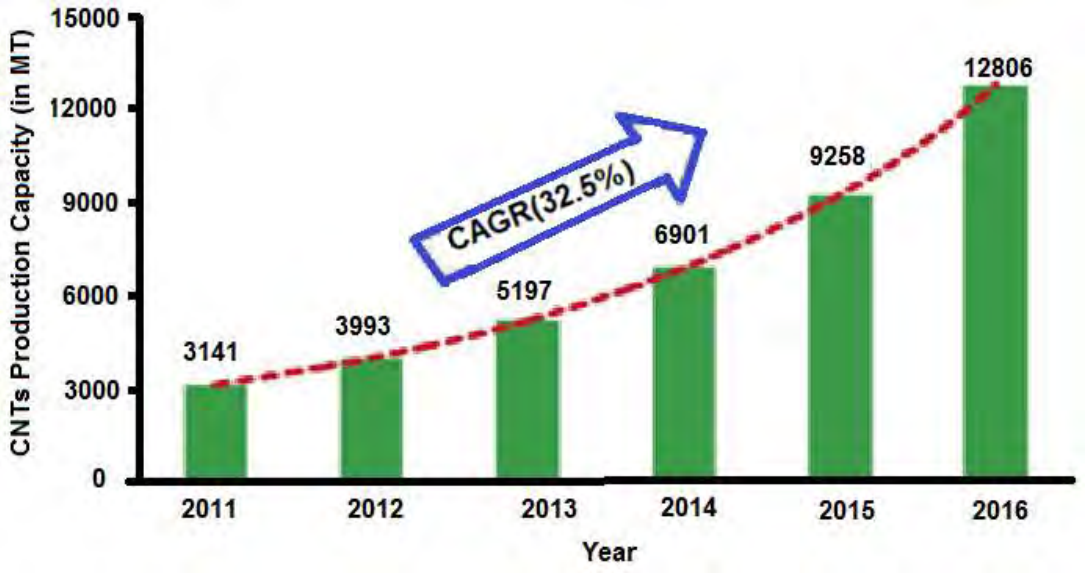

Figure 2.12 Next five years forecast (2011-2016) for global CNTs market, showing CNTs production capacity in MT (Global carbon nanotubes market)(Nanowerk 2011).

2.5 Review on the Use of Nano-additives in Cementitious Composites

2.5.1 Carbon Nanofilaments (nanotubes/fibres(CNTs/Fs))

The outstanding mechanical properties of Carbon nanotubes/fibres(CNTs/Fs) have motivated researchers to investigate the potential of using them to improve existing cementitious composites properties, or create new construction composites. Although CNTs/Fs are not specifically produced to be incorporated within cementitious composites, CNTs/Fs have a promising future when successfully incorporated with ordinary Portland cement due to their superlative mechanical and physical properties(Sanchez and Sobolev 2010, Jorge et al. 2013)

In recent decades, several studies have examined the potential to overcome the brittleness, low tensile strength and strain capacity of cement based materials by the incorporation of CNTs/Fs. CNT/Fs have been incorporated within cementitious composites by many different approaches, most of which show a positive effect of CNT/Fs on the strength performance of cementitious nanocomposites(Sanchez and Sobolev 2010, Tyson et al. 2011).

Since 2004 a range of studies have been carried out investigating CNT/Fs reinforced cementitious composites and its effect the composite mechanical strength and durability properties. Below, the findings of previous published studies on the effect of Nanofilaments on compressive strength, tensile strength, flexural strength and impact resistance, porosity, and abrasion resistance of concrete is summarised.

Li et al(Li et al. 2004) investigated the effect of adding MWCNTs, at concentration of 0.5% by cement weight, on compressive strength, tensile strength and porosity of nano cementitious composites. MWCNTs were treated with a strong oxidizing acid mixture and sonicated under ambient temperatures for three hours, which led to well dispersed functionalized suspensions. The results indicated a 19% increase in compressive strength, a 25% increase in flexural strength, and a 64% reduction in porosity. Inspection by SEM images revealed a good dispersion of the filaments within the fractured composite, and FT-IR spectra indicated that the covalent bond between functionalized CNTs and cement hydration products had been improved. In 2007 Li

et al.(Li et al. 2007) also investigated the impact of treated CNTs (using a mixed solution of H_2SO_4 and HNO_3) on compressive strength and flexural strength of cement paste compared to pastes containing untreated CNTs. The reported results show that incorporation of treated or untreated CNTs led to distinct improvements in compressive and flexural strength. Generally, treated CNTs produced higher mechanical strength (compressive strength about 2.7MPa, and tensile strength about 0.4MPa, higher than those of cement paste containing untreated CNTs).

Terttin (Trettin 2005) studied the effect of 0.5% MWCNTs (by cement weight) on compressive strength, and found a marginal increase in performance after 28 curing days, although the strength was shown to decrease as nanotubes dose increased to 2.5 % or more.

Geng et al.(Geng Ying et al. 2005) measured the porosity of a CNT-cementitious composite at same dose (0.5 weight % CNT by cement) by using mercury intrusion porosimetry (MIP). Results showed a dramatic decrease in porosity, near to 64%, compared to the standard mortar, and the total porosity was 10.8% by volume. Moreover, CNTs filled the larger pores within cement hydration products producing more compacted mortar, which enhanced the strength and potentially decreased the damage caused by permeation of aggressive ions from the surrounding environment.

Maria et al.(Maria et al. 2010) also investigated the effect of incorporation of low amounts of MWCNTs (only 0.048 weight % by cement). Dispersion was carried out using a commercial surfactant and ultrasonication. These authors observed a 45% increase in the Young's modulus and a 25% increase in the flexural strength. The authors believed that addition of CNTs into the cementitious matrix increased the stiffness of cement hydration products and decreased the porosity. Previous studies (Li et at (Li et al. 2004)) had incorporated ten times this amount of MWCNTs to produce the same relative increase in flexural strength, and this indicated that a very low quantity of well-dispersed CNTs might enough to achieve a significant enhancement of the mechanical properties of the composites. Cwirzen et al. (Cwirzen et al. 2008) have also used treated MWCNTs (using a polyacrylic acid agent and sonication) to investigate the impacts of incorporation of small quantities of CNTs

(0.045-0.15 wt.% by cement) on workability and compressive strength. These authors found a significant improvement in compressive strength of nearly 50% and 10 % in flexural strength, in addition to production of a homogeneous paste with good workability. The strong covalent bond formed between CNTs and the matrix was again argued to be the main reason for the improvements in performance.

Musso et al (Musso et al. 2009) evaluated the compressive and flexural strength of pristine, annealed and functionalised MWCNTs–cementitious composites (0.5% by mass of cement). They claimed that functionalized CNTs caused significant reduction in both compressive strength and flexural strength of approximately two and half times in comparison to plain cement. Pristine and annealed MWCNTs produced improvements in compressive strength of 10-20% and of approximately 9-34% in flexural strength.

Chaipanich et al. (Chaipanich et al. 2010) investigated the impact of adding two different concentrations of CNTs by weight of fly ash cement matrix (0.5% and 1%), and showed that CNTs act as a filler agent filling up the voids in between the cement hydration products, resulting in a very dense microstructure and a significant improvement in compressive strength which became close to 100 % after 28 curing days compared to the reference fly ash mix.

Musso et al. (Musso et al. 2009) explained the impact of adding carbon nanotubes on mechanical and electrical properties of cement paste. Their analysis on COOH-MWCNTs cement composites confirmed that high amounts of lattice defects and carboxylic groups can justify a strong hydrophilic behaviour (Figure 2.13) that is probably responsible for the incomplete hydration of cement paste added with nanotubes which initially retained the water during concrete preparation and then released it progressively during air curing.

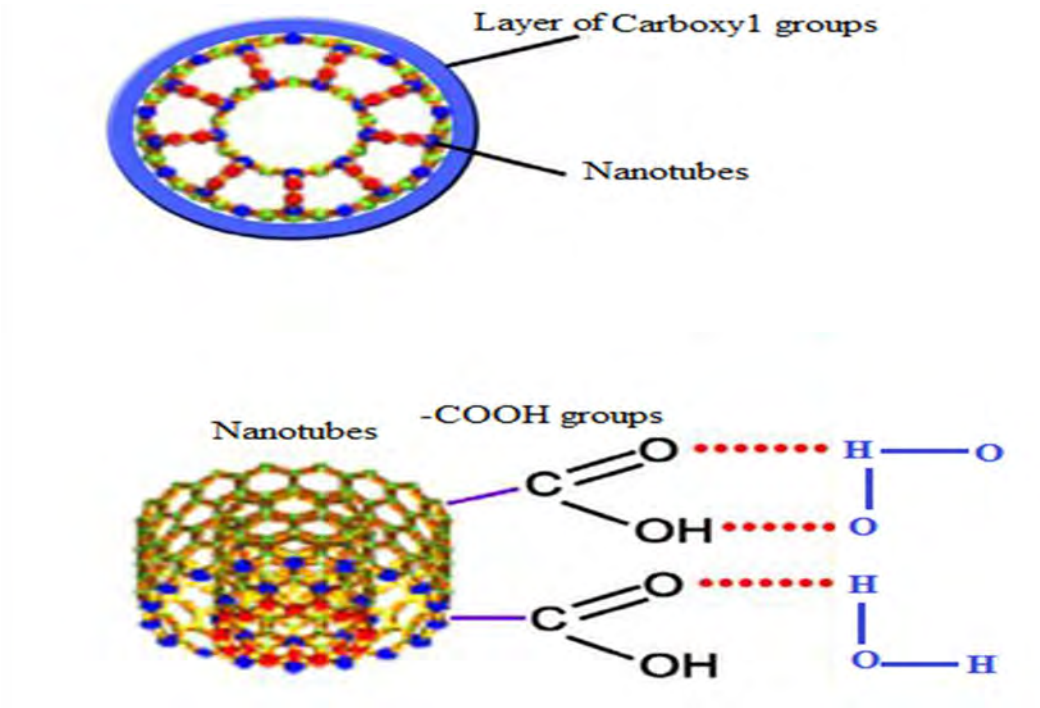

Figure 2.13 Possible interaction between COOH-MWCNTs and molecules structure of water during cement hydration process(Passant 2015).

Hamzaoui et al.(Hamzaoui et al. 2012) studied the effect of pre-prepared carbon nanotubes suspensions (varying from 0.01 to 0.06 wt% by cement.) on mechanical properties and microstructure of mortar and concrete respectively. The authors concluded that the mortar nanocomposites reinforced with CNTs at an amount of 0.01 wt.% exhibit a 29% and 21% increase in flexural strength and compressive strength, respectively. The microstructural characterization of the modified materials suggests that CNT act as bridges between pores and micro and nano cracks leading to a reduction in porosity and in turn an increase of compressive strength.

Rashid et al. (Rashid et al. 2012)reported a comparison of the mechanical properties of cement paste reinforced with both surface-functionalized CNTs and unfunctionalized CNTs at concentrations of 0.1% and 0.2% by cement weight. They noted that acid treated nanofilaments had a negative impact on mechanical properties compared with plain cement paste, while in contrast the suspensions prepared with the help of a surfactant and sonicator were found to significantly improve the mechanical properties. The average ductility increased by up to 73%, flexural strength by 60%,

Young's modulus by 25%, and the modulus of toughness increased by 170%. The inferior mechanical performance of composites reinforced with treated CNT/Fs was attributed to the formation of ettringite crystals, formed due to the presence of sulphate ions.

Wang et al.(Wang et al. 2013) studied the mechanical properties of cement mortar reinforced with carbon nanofibres (CNFs) in concentrations of 0.05%, 0.075%, 0.1%, and 0.2% by weight of cement. CNTs were dispersed using a sonicator and methylcellulose (MC) in a ratio of MC to CNFs of 2:1. They reported that at 7 days, the flexural strength of each CNFs/cement composite was degraded and was lower than that of the plain mortar, which was attributed to the negative impact of methylcellulose on the early hydration process, generating excessive ettringite formation. After 28 days, the flexural strength significantly improved, up to 21% with 1% CNFs, as a result of the enhancement of interfacial interaction between CNTs and the matrix. However, the compressive strength was slightly lower than that of the plain samples, which was attributed to the negative impact of the methylcellulose on the cement hydration process.

Mendoza et al. (Mendoza et al. 2014) investigated the effect of combinations of silica nanoparticles (NS) on the re-agglomeration process of 0.25% of MWCNTs by cement weight, and mechanical strength within cement matrixes at early ages. The results indicate that the positive effect of MWCNTs depend on the amount of NS and hydration time. Combination with NS was found to improve formation of hydration products which can be attributed to the pozzolanic nature of NS.

Kim et al(Kim et al. 2014) focused on improving the effect of CNTs on mechanical properties (compressive strength and porosity) of cement composite containing micro silica. The CNTs in concentration of (0%, 0.15%, and 0.3% by weight of cement) and silica fume in amounts of 0%, 10%, 20%, and 30% by weight of cement were applied. The authors found that the dispersion nanotubes within the composite is improved with increase amount of silica fume (about 10–20%), the agglomerated CNTs intermixed with the particles of silica fume and mechanically broken to small bundles. While without silica fume, the compressive strength of the composite was found to

decrease which is due to the agglomerated CNTs acts to form pores and cracks resulting in decrease the composite strength. The addition of silica fume, up to 20%, was found to increase the relative compressive strength for composites containing 0.15 wt.% and 0.3 wt.% to 1.32 and 1.12 respectively, which was attributed to the combined effect of individual fibres and pozzolanic reactive of silica fume.

Danoglidis et al.(Danoglidis et al. 2016) determined the performance of cement mortars reinforced with 0.08, 0.1, 0.3 and 0.5 wt.% of well-dispersed MWCNTs. The impact on strength, stiffness, and toughening were evaluated. The results showed a significant increase in the strength and stiffness of all nano reinforced mixes. Addition of 0.1 wt.% MWCNTs to plain mortar increased nearly 1.9 times the flexural strength, and 1.7 times the first crack strength. Alongside the strength and stiffness, the values of the energy absorption capability were greatly improved over the plain mortar. In same year, these authors experimentally determined mechanical parameters for nanomodified Portland cement mortars, reinforced with well-dispersed MWCNTs and CNFs. The improvement of the modulus of elasticity and the fracture parameters of mortars reinforced with MWCNTs was 92.4%, and 86.7%, respectively, and with mortar reinforced with CNFs was 94.3%, and 105.9% respectively.

Tamimi et al.(Tamimi et al. 2016)studied the effect of incorporating silica fume with functionalized CNTs, at percentage of 0.15 wt.% of cement, in the cement mortar to enhance its mechanical properties. They reported that addition of silica fume at 15% increased the compressive strength by 13%. Moreover, compared with the control sample the flexural strength increased by 50% and 35% when using surface functionalized CNTs and no surface functionalized CNTs, respectively. The increase in flexural strength was related to the presence of carboxylic acid groups on the surfaces of carbon nanotubes that bring about a chemical interaction between the carboxylic acid and calcium silicate hydrate (C–S–H) or Ca(OH)2 hydration products.

From the above review, it can be summarized that almost all workers report an improvement in mechanical properties of cementitious composite with addition of nano filaments, which can be attributed to the characteristics of the CNT/Fs, dispersion methods, surfactant types, mix methods etc. While a few studies (i.e. Musso et

al(Musso et al. 2009), Rashid (Rashid et al. 2012)) found that functionalizing the nanofilaments had a negative impact on the mechanical properties, the reduction was attributed to hydrophilic functional groups having the ability to absorb water which hinders the hydration process.

2.5.2 Graphene (GO)

Relatively few studies have investigated the effect of graphene oxide as a reinforcing and filling agent, and its impact on mechanical strength and other performance characteristics.

Since 2012, Researchers at University of Monash, Australia, led by Dr Wenhui Duan, have developed a novel method for producing reinforced cementitious matrices with improved durability and strength by incorporation of graphene oxide (GO)(Samuel et al. 2014). Laboratory tests have shown that mixing 0.05% weight of cement of (GO) in the cement matrix led to improvements in flexural strength of between 41% and 59%, and compressive strength between 15% and 33%, and decreased the total composite porosity from 32.6% to 28.2%. This was attributed to the ability of GO to improve the degree of hydration of cement paste creating a more durable product.

Lv et al. (Lv et al. 2013) investigated the effect of graphene oxide (GO) on compressive, tensile and flexural strength of cement composites in addition to their microstructure. The concentration of GO was 0.03 wt. % of cement, and treated GO were dispersed in water using ultrasonication at 325W for 1 h, with polycarboxylate superplasticiser as a dispersion agent. The results show that this low amount of GO generated a remarkable increase in tensile strength (78.6%), flexural strength (60.7%) and compressive strength (38.9%) compared to samples without GO. It was reported that GO can regulate the cement hydration process and form flower-like and polyhedral crystals which dramatically increase material toughness.

Fakhim et al.(Fakhim et al. 2014) have measured the mechanical strength of cement nanocomposites containing 0.1–2wt% of in situ prepared graphene oxide and polycarboxylate superplasticiser (0.5wt% of cement), showing that 1.5 wt.% of GO was an optimal percentage causing a 48% improvement in tensile strength of the

cement mortar. Field emission scanning electron microscope (FE-SEM) images show well-dispersed GO platelets in the matrix, stretching across micro cracks, which can improve the composite resistance to carry applied stress.

Rhee et al.(Rhee et al. 2015) explored the enhancement of the compressive strength of cementitious mortar containing graphene sheets (GRH) derived from agricultural rice husk. Cement composites with fixed amounts of added nanomaterials at 0.8% by weight of cement, and silica fume at f 0%, 10%, and 30% by weight of cement were designed. The results show that the compressive strength of the composite containing 0.08% of GRH with higher specific surface areas and silica fume at 30%, increased by 80% (strength increased from 31.8 MPa of Plain to 57 MPa of GRH 0.8 wt.%, SF 30 wt.%). Of this 80% increment, silica fume contributes 28% and GRH contributes 52%.

Shang et al.(Shang et al. 2015) studied the effect of graphene sheets, and graphene oxide(GO) encapsulated silica fume (GOSF) on the rheological properties of cement pastes. The dosage of GO varied from 0.02% to 0.08% by weight of cement, and the replacement ratio of OPC with GOSF/SF was varied from 2% to 8% by weight. The results showed that the hydrophilic GO has a large surface area to absorb water molecules to its surface, reducing the free water content required for lubrication, which leads to a decrease of fluidity and an increase of the viscosity and yield stress of cement pastes. The fluidity of cement pastes is reduced with an increase in dosage of GO. Effects of GOSF (graphene sheets encapsulating SF) on the fluidity properties of cement pastes are higher than GO, which are due to the synergetic effects of the shape of SF and the surface activity of GO.

Li et al. (Li et al. 2016) explained a new mixing method using silica fume to pre-disperse GO nano sheets before mixing with cement. Dispersion efficiency of GO was examined through both scanning electron microscopy (SEM) images and compressive strength of the composite. The graphene sheets were found to re-agglomerate in the absence of silica fume, whereas the aggregated GO size was reduced by shear mixing and with sufficient amounts of silica fume. However, excess silica fume had a negative

effect on the compressive strength of the GO reinforced cement paste by preventing interactions between the GO and cement hydration products.

Despite the work reviewed above, studies are still needed to understand the various characteristics related to the durability of nano reinforced concrete including shrinkage behaviour (free and restrained), and mechanical characterization after exposure to various degradation conditions such as acid, freeze-thaw cycles, high temperature, chloride attack, etc. There is heavy reliance in previous studies on empirical investigations performed on cement at the laboratory scale, and further research needs to be carried out on mortars and concretes in field (realistic) scale structures. Moreover, the optimal type and effective concentration of carbon nano-additives (MWCNTs, F-MWCNTs, CNFs, and Graphene) as cement reinforcement agents still require theoretical and experimental investigation to verify their reinforcing efficiency through a cementitious composite.

In recent years, there has been a significant increase in the number of published papers in the area of carbon based nano-additives cementitious composites. For example, since December 2016 alone more than 40 research papers have been published on the use of carbon nanotubes, nanofibres and graphene oxide, to improve durability and mechanical strength of cement based composites. These include papers by (Liu et al. 2016, Lu et al. 2016, Sharma and Kothiyal 2016, Sharma and Kothiyal 2016, Tong et al. 2016, Hou et al. 2017, Luo et al. 2017, Shao et al. 2017, Wang et al. 2017, Wang et al. 2017, Zhu et al. 2017).(Danoglidis et al. 2016, Gdoutos et al. 2016, Nadiv et al. 2016, Tragazikis et al. 2016, Shao et al. 2017, Wang et al. 2017, Zhou et al. 2017). For future work, these papers could be a useful background to understand whether these show dramatically different results, or reinforce the findings of previous literature.

2.6 Practical Application of Carbon Nano Cementitious Composites

2.6.1 General

The excellent mechanical characteristics of carbon nanofibres (CNFs) nanotubes (CNTs), and graphene, are promising in enhancing properties such as strength, ductility, and toughness in cementitious composites. In civil engineering, carbon nano-additives are expected to have a wide range application in concrete structures(Sanchez and Sobolev 2010). Their applications can be classified into two approaches: structural and non-structural application. For structural applications, the unique structure of CNT/Fs and graphene sheets can provide stronger structural elements which can transfer the stress and prevent/delay the crack propagation within a composite. For non-structural application these materials may have application in self-sensing for measurements of strain, temperature, damage, self-heating (for de-icing), electromagnetic interference shielding, etc .(Ahmed Ibrahim 2011, Kim et al. 2014, Xu et al. 2015).

Although a great deal of research has been conducted in the nanocomposites area, significant technical issues still need to be solved prior to their practical large-scale structural application, over and above issues around their cost and availability (Maria et al. 2010, Metaxa et al. 2012). Homogenously dispersed carbon nano-additives are promising reinforcing agents at the nano scale however, that could provide effective strengthening layers and repair materials. The most important applications of CNTs/CNFs are likely to be based on their properties as reinforcement agents in composite materials, which can act to bridge across cracks at the nano scale resulting in crack growth hindrance at early hydration stages and reduced propagation of cracks to the micro scale, essentially creating a new generation of “crack-free materials”(Babak et al. 2013, Hanus and Harris 2013).

2.6.2 Crack-Free Cementitious Composites

While the most recently developed composites (i.e. high-performance fibre-reinforced cementitious composites (HPFRCC)) exhibit high mechanical strength, such composites are also extremely sensitive to early age crack formation as a result of high cementitious materials content(Carlswa 2002, Carlswärd 2006, Şahmaran and Li 2010). Cracking in concrete members is one of the most severe concerns, allows to diffusing of environmentally harmful species, thus resulting in a various of harmful chemical interactions though concrete materials. This may occur at various stages throughout the life of a structure(Tong et al. 2014). The formation of cracks, combined with the brittle nature of concrete materials, is primarily responsible for two damaging phenomena: reducing the strength and stiffness of the concrete structure, and accelerating the ingress of aggressive ions, leading to other types of concrete deterioration such as corrosion, alkali-silica reaction, and sulfate attack, and resulting in further cracking and disintegration. As a result, these cracks can dramatically reduce the long-term durability performance of concrete(Şahmaran and Li 2010).

The ability of CNTs and CNFs to control cracks at the nanoscale, induced by both flexure and shrinkage, has brought researchers closer to achieving a crack-free cement composite(Metaxa et al. 2012). Monteiro (Monteiro 2006) showed that radical enhancements in the durability of concrete to commonly known causes of deterioration can be achieved by control of the growth of microcracks that interlink the surface cracks with interior voids and microcracks. Parveen et al.(Parveen et al. 2013) explained that the although the use of microfibre reinforcements has led to significant improvement in the mechanical properties of cement-based materials by delaying the transformation of microcracks into macroforms, but they could not stop the crack growth. Therefore, the use of nano size particle or fibres is essential to prevent the transformation of nanocracks into microcracks.

Nano-additives cementitious composites therefore could produce materials that are more durable and longer lasting, contributing not only to the sustainability of the world's infrastructure, but also to a reduction in maintenance and repair costs, a

reduced environmental impact, and an overall improvement of the safety of structures constructed with concrete.

2.7 Summary

Despite extensive previous work, the areas below have been insufficiently addressed and so provide knowledge gaps for further study.

1. While the cost-effectiveness of dispersion techniques is not explicitly discussed in many previous studies, the need for repeatable, readily scalable and cost-effective techniques to generate effective dispersions of CNTs in fluids and matrices poses a tremendous hurdle that must be overcome prior to realizing wider applications of CNTs as, for example, reinforcement components in composites.
2. To date, a limited number of studies have investigated the effect of surfactant/polymers options that can practically be used with cementitious materials. Therefore, the effective type and concentration of surfactant that can practically be used to improve the dispersion of nano-additives and at the same time improve the properties of cementitious materials remains a subject of research that need to be extensively covered.
3. While the utilisation of ultrasonication in combination with surfactants, and use of mineral admixtures with the composite, have been studied in previous investigations, the use of ultrafine reactive admixtures (such as unidentified silica fume) has been relatively underexplored. This can be promising method to enhance significantly the dispersion degree of nano-additives and their reinforcing efficiency through a cementitious composite.
4. Despite the comprehensive works that have been reviewed above intensive studies are still required to understand the various characteristics related to durability of nano reinforced concrete including shrinkage behaviour (free and restrained), and mechanical characterization after exposure to various degradation conditions such as acid, freeze-thaw cycles, high temperature, chloride attack, etc. There is heavy reliance in previous studies on empirical investigations performed on cement at the laboratory scale, and further research needs to be carried out on mortars and

concretes in field (realistic) scale structures. Moreover, the optimal type and effective concentration of carbon nano-additives (MWCNTs, F-MWCNTs, CNFs, and Graphene) as cement reinforcement agents still require theoretical and experimental investigation to verify their reinforcing efficiency through a cementitious composite.

5. Nano-additives cementitious composites therefore could produce materials that are more durable and longer lasting, contributing not only to the sustainability of the world's infrastructure, but also to a reduction in maintenance and repair costs, a reduced environmental impact, and an overall improvement of the safety of structures constructed with concrete.

Points of 1-4 are targeted in the present research, which are necessary to define the real benefits and potential of crack-free composites produced with carbon nanomaterials, and to promote their uptake by the construction industry.

Chapter Three:

Materials and Experimental Procedures

3.1 Overview

This chapter describes the materials and methods used in this thesis for developing improved carbon based additives reinforced cementitious composites. It presents methods applied in: i) optimising a facile dispersion technique for de-agglomerating multiwall carbon nanotubes (MWCNTs) and its impact on performance of cementitious composites (for which results and discussion are presented in Chapter Four); ii) the impact of the proposed dispersion technique on dispersion of functionalised multiwall carbon nanotubes (F-MWCNTs), carbon nanofibres (CNFs), and few layer graphene sheets (FLGO)) and its impact on the mechanical properties of the developed cementitious composites (NRCC) based on these nano-additives for which results and discussion are presented in Chapter Five); iii) developing multiscale hybrid reinforced cementitious composites (MHRCC) (for which results and discussion are presented in Chapter Six); and iv) assessing the durability performance of NFCC and MHRCC (for which results and discussion are presented in Chapter Seven).

3.2 Materials

This section describes the properties of the materials used in this thesis.

3.2.1 Cementitious Raw Materials

3.2.1.1 Cement

Commercially available Ordinary Portland cement (Type I Portland cement, from Hanson Cement, UK) which satisfies the requirements of EN 197-1:2000(BSEN197-1:2000) (a European standard that was adopted as a British Standard) was utilized throughout this research. This is a widely commercially available cement used for making conventional concrete, and suitable for use in general concreting and cement-

related works. The chemical composition and physical properties of the cement as provided are listed in Table 3.1.

3.2.1.2 Microsilica

Microsilica is a by-product of the manufacture of silicon metals from ferro-silicon alloys in electric arc furnaces (Sorelli et al. 2008). Microsilica is supplied in numerous forms, such as undensified silica fume powder (which is extracted from the arc furnace filters directly), densified (which is compacted to increase the bulk density), and a slurry (which is mixed with water).

Undensified silica fume (USF) was obtained from Elkem Materials, Inc. EMS-940. Its chemical and physical properties are shown in Table 3.1. USF particles are usually grey in colour with an average diameter of 10μm, which is about 1/50-1/100 that of cement grains. The small particle size of USF fills the voids between cement particles, and improves packing and interfacial bonding.

The benefits of using microsilica include:

- Reducing the cost of the cementitious composite
- Controlling the rate of hydration.
- Reducing permeability due to its small particle size, improving strength in the hardened state and durability by creating a denser cement matrix.
- It can aid with dispersion and prevent re-agglomeration of nanotubes.

Table 3.1 Chemical properties of Ordinary Portland cement and microsilica.

Chemical properties			Physical properties		
Chemical analysis (%)	Cement	Microsilica	Type	Cement	Microsilica
SiO_2	>20	93.6	Specific gravity:	3.15	2.2
Al_2O_3	>6	1.3	Bulk density kg/m^3	1000-1250	130-430

Fe_2O_3	>6	0.9	Blaine fineness (cm^2/g)	3260	21,090
CaO	<50	0.5	Initial setting time (min)	119	-
MgO	<5	1	Final setting time (min)	210	-
SO_3	<3	0.4			
K_2O	<1	1.52			
Na_2O	<1	0.45			

3.2.2 Fine Gravel (Silica-Sand)

Commercially available silica sand with a maximum particle size of 0.5mm, and specific gravity of 2.63, was sourced from Sibelco in the UK and used in producing cementitious composites. Sand is used for making mortar and concrete. In cementitious composites, silica sand improves the compaction, maximises the bond strength, and promotes a good casting finish. The grain size distribution (as provided) is uniform, with 85-95% of the material between 150 to 300μm and only 5 to 12% smaller than 75μm.

3.2.3 Coarse Gravel

Coarse aggregate of crushed stone with sharp edges was sourced from Covers Timber and Builders Merchants-Brighton -UK and used in this study for making concrete. The maximum size of the coarse aggregate was 10mm and specific gravity was 2780 kg/m^3.

3.2.4 Microfibres

Microfibres were used as a reinforcement material in the cementitious systems to control cracking through bridging and load transfer across cracks, and to improve the mechanical strength and post cracking behaviour. Steel microfibres were used, with properties shown in Table 3.2.

Table 3.2 Properties of steel fibres.

Fibre type	Length (mm)	Diameter (mm)	Aspect ratio (L/D)	Fibre strength (MPa)	Density (Kg/m^3)	E (GPa)
Steel fibre	13	0.16	81.25	2250	7850	200

3.2.5 Carbon Nano-additives

In this research, four types of carbon-based nano-additives (three types of nanofilaments, and graphene sheets) were used as additions to cement mortar. Nanofilaments used were: i) commercially available multiwall carbon nanotubes (MWCNTs); ii) functionalised multiwall carbon nanotubes (F-MWCNTs); and iii) carbon nanofibres (CNFs). Few layer Graphene oxide (FLGO) was also used as a cement additive. MWCNTs, F-MWCNTs, and FLGO were purchased from Cheaptubes, Inc. (cat# sku-030102, Brattleboro, VT, USA), and CNFs were purchased from sigma Aldrich, Inc. FLUKA. The physical properties as provided by the suppliers are presented in Table 3.3. Photographs of 0.05g of each additive are shown in Figure 3.1

Table 3.3 Properties of nano and micro fibres.

Type	Diameter (nm)	Length (μm)	Purity (% carbon by mass)	Specific Surface Area m^2/g	Bulk Density (g/cm^3)	Aspect ratio L/D
MWCNTs	8-15	10-50	95	233	1.95	100-600
F-MWCNTs	8-15	10-50	95	233	1.95	100-600
CNFs	100	20-200	-	50-60	1.90	200-1000
FLGO	-	-	95	Size: (300-800) nm lateral dimensions	1.90	

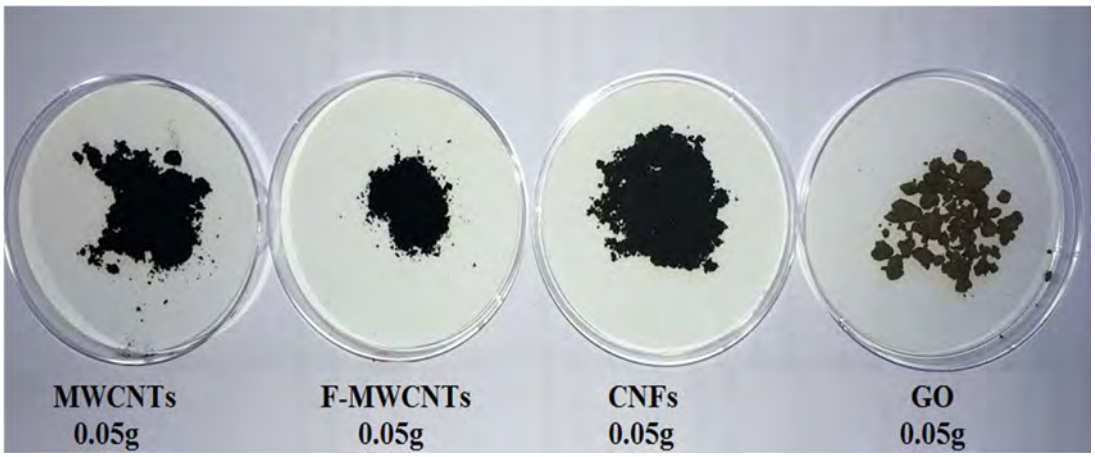

Figure 3.1 Photograph showing four types of carbon nano-additives used in this study: MWCNTs, F-MWCNTs, CNFs, and FLGO.

3.2.6 Surfactants/Dispersion Agents

In this study, three dispersion agents were investigated, namely: methylcellulose (MC), Polycarboxylate Ether (PCE), and Naphthalene Sulfonates Formaldehyde (NSF). Their chemical and physical properties are explained in Table 3.4.

MC is a kind of non-ionic surfactant (wetting agent) with excellent wettability, dispersibility and adhesion properties. Its use results in less bubbling during composite manufacture, and more compacted materials(Wang et al. 2014). Methylcellulose is available as a powder, which is dissolved in water prior to use. PCE and NSF are known as superplasticisers, which improve the workability of cement based composites. Nowadays, these are commonly used as dispersion agents to de-agglomerate nanofilaments in cementitious composites systems. The primary difference between NSF and PCE is that the latter is a third-generation of plasticizer that can maintain the initial setting characteristics of fresh cement mixture, an effect which is attributed to the structure and shape (comb-like) of side chains of PCE(Xiao-Lin et al. 2005).

3.3 Experimental Approach

The development of improved nanofilament reinforced cementitious composites (NRCC) and multiscale hybrid reinforced cementitious composite (MHRCC) formed the focus of the research in this thesis (Figure 3.2). Experimental testing followed a phased approach (the tests performed for each step are presented in Table 3.5.

Table 3.4 Properties of admixtures/surfactants used to disperse MWCNTs, and F-MWCNTs.

Properties	PCE	NSF	MC
Chemical Classification	Polycarboxylate	Naphthalene	Methylcellulose A, Methyl cellulose ether
Appearance and form	light low viscosity liquid	Dark brown low viscosity liquid	White to Off-White Powder
pH of 10% content	6.7	7-9	6-8
Bulk density g/ml	1.075	1.2	1.31 g/cm3
Ionic nature	Cationic	Cationic	Non-ionic
Solubility	Soluble in water	Soluble in water	Soluble in water
Solid content (mass %)	11.4	40-42	100

In the research on nanofilament reinforced cementitious composites (NRCC), composite fabrication began with dispersion of carbon nanotubes at three different dosages, using the ultrasonication technique as the main dispersion method. Obtaining sufficient dispersion is a major challenge in the use of carbon nanotubes in producing cementitious composites reinforced at nano scale. Therefore, an extensive experimental program was conducted to find the optimum dispersion conditions to produce cement paste with the best mechanical strength, targeting carbon nanotubes as the main nano-additive. This was carried out by testing different sonication intensities, different treatment durations, different types of surfactant/superplasticiser,

and the effect of supplementary cementitious materials (Undensified Microsilica). Then, the effect of the optimised dispersion technique on dispersion of the remaining types of nano-additives used in this research was examined. The tests carried out within the project are discussed in Chapters Four and Five.

In Chapter Six, the concept of tailoring properties to suit requirements and to offset the disadvantages of one component by the addition of another has been proposed through a hybrid system of nano and micro fibres. Cementitious composites reinforced using nanofilaments (carbon nanotubes/fibres) and micro-scale (steel fibres) fibres have been developed. Their mechanical properties in terms of compressive, tensile, and flexural strength, in addition to fracture toughness, were evaluated at various curing ages, along with their microstructure (using Scanning Electron Microscopy (SEM)). Multiwall carbon nanotubes (CNTs), and carbon nanofibres (CNFs), were used as the nanoscale additives at a dosage of 0.025% wt. of cement. One type of steel fibre at a volume fraction of 2% was used as the micro fibre additive.

Chapter Seven and Chapter Eight address one of the more promising applications of nanocomposites, in developing thin-layer repair/strengthening composites with reduced susceptibility to shrinkage and cracking (i.e. free crack composite). In chapter Seven, the durability performance of nanofilament reinforced cementitious composites and multiscale hybrid reinforced cementitious composites based on carbon nanotubes and carbon nanofibres (the proposed nanofilament composites in previous chapters) in term of shrinkage behaviour and sulfuric acid ingression resistance were addressed. This part of the experimental work involved investigation of drying shrinkage, end-restrained, and base-restrained shrinkage, in addition to the composites' resistance to aggressive ions. In chapter Eight, the performance of MHRCC-CNF was investigated as a thin layer to repair/strengthen large scale RC beams, to simulate the performance of nanocomposites in real structural elements. Flexural behaviour under monotonic flexure loading was investigated. Test results were analysed based on cracking behaviour, strain distribution across the depth of the repair/strengthening composite, vertical mid span deflection, ductility, and ultimate flexural load and failure mode.

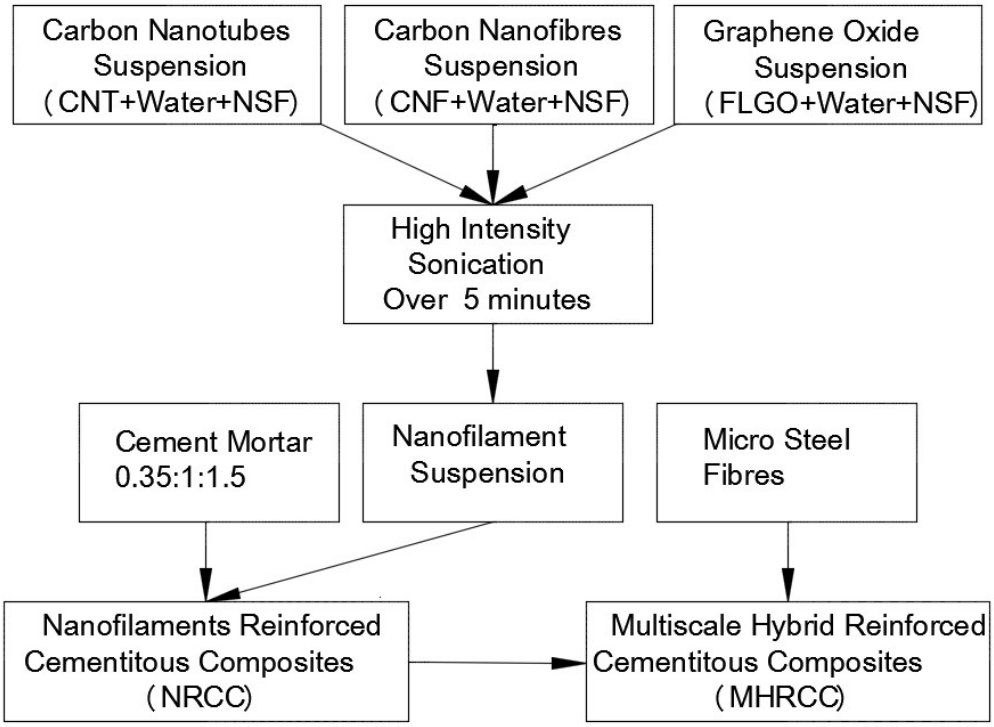

Figure 3.2 Experimental approach in the design of nano-additives cementitious composite.

Table3.5 Tests Performed on a Chapter by Chapter basis.

Chapter	Analysis	Tests Performed
Chapter Four: Dispersion Optimisation	1-Effect of Ultrasonication - Intensities - Treatment Duration - Concentration Characterisation - Dispersion Level	Visual Inspection Optical Microscopy UV-Vis Spectroscopy Transmission Electron Microscopy (TEM)
	Mechanical Characterisation	Compressive Strength Direct Tensile Strength
	Microstructure Characterisation	Scanning Electron Microscopy (SEM)
	2-Effect of Surfactants on - Dispersion of nanotubes	UV-Vis spectroscopy

	- Stability of nanotubes suspension	
	Mechanical Characterisation and Microstructure	Compressive Strength Fluidity
	3- Effect of Micro Silica	TEM
	- Mechanical Performance	Compressive Strength Porosity SEM
Chapter Five: Develop Nanofilament Reinforced Cementitious Composites	Dispersion Characterisation of Nano-additives: - Stability - Concentration	UV-Vis spectroscopy
	Characterisation of nanofilaments of "As Supplied": - MWCNTs - F-MWCNTs - CNFs - FLGO	TEM
	Characterization of Nano-additives Cementitious Composites	Compressive strength Flexural Strength Tensile Strength Flexural Toughness Workability Porosity and density Measurement SEM TEM
Chapter Six: Develop Multiscale Hybrid Reinforced Cementitious Composites	Mechanical Behaviour of Produced Composites	Compressive strength Flexural Strength Tensile Strength Energy Absorption Under Flexural Loading
	Composite Microstructures	SEM
	Shrinkage Performance	Free Drying Shrinkage

Chapter Seven Durability Performance: Shrinkage Behaviour and Sulfuric Acid Resistance		Restrained shrinkage Base- Restrained Shrinkage End- Restrained Shrinkage SEM
	Sulfuric Acid Attack - Microstructure Characterisation	Crushing Load Weight Loss Visual Inspection SEM
Chapter Eight Multiscale Hybrid nanocomposites in Repairing/ Strengthening RC Concrete	RC large Scale Beams: - Mechanical Properties and Shrinkage behaviour	Compressive Strength Tensile Strength Free shrinkage
	RC large Scale Beams: - Load-Deflection Curves	Cracking Behaviour Ductility Ratios Ultimate Strength

3.4. Methodology of Chapter Four: Dispersion Experimental Program

This section explains the experiments and methods followed in Chapter Four, it is described over three phases as follows:

3.4.1. Phase I: Ultrasonication-Assisted Dispersion of Carbon Nanotubes

3.4.1.1 Suspension preparation

Nanofilament suspensions were normally prepared by firstly mixing a nanofilament (weighed using an Ohaus Adventurer SL Analytical Balance, accurate to 0.1 mg) and surfactant in tap water. Next the suspension was sonicated with a 750 W 20KHz ultrasonic system (Model 705 Sonic Dismembrator) with a 19mm macro probe.

3.4.1.2 Energy Delivered Through Ultrasonication

The sonication technique has been commonly used to exfoliate bundled CNTs into single tubes in low viscosity liquids such as water, acetone and ethanol (Chen et al. 2014). The dispersion mechanism can be summarised as follows: In the sonicator, electrical energy is delivered to the converter and transformed into mechanical waves. The energy of ultrasound wave induces rapidly collapsing cavitations bubbles which act to provide a highly localised shear force exceeding the tensile strength of the nanotubes, and thus can act to detach individual CNTs from bundles (Yan and Eugene 2012).

The energy could be set to the required level using an amplitude controller. Intensity is expressed by the energy delivered (Joule) per unit time (min) by the area of the probe (cm^2). Intensity has a direct relationship with the amplitude settings: the low amplitude setting delivers a low intensity sonication, and the high amplitude setting delivers a high intensity sonication.

In this study, following previous authors' studies, high intensity sonication over short time periods was adopted as the optimal dispersion method, in which the delivered energy (the required plateau energy) to the solution ranges between (388-458)J/ml per min(Liew et al. 2016). The delivered energy to the solution ranges between (20-86) J/ml, (52-125) J/ml, and (388-458) J/ml per min of Low, Moderate, and High intensity sonication respectively. These energies (under a certain intensity) varies slightly from treatment to treatment as it is influenced by the solution viscosity, solution temperature, the exact position of the probe, etc (Chen et al. 2014, Bo et al. 2015). High sonication intensity was found to dramatically increase the suspension temperature over longer sonication periods. Thus, to avoid the expected overheating and structural damage that may occur in the nanotubes, the treatment duration was set at a short duration (i.e. 5 minutes) and at every minute the sonication was automatically paused for 20 minutes. In this study, all experiments were performed in triplicate and the results reported here are the means of the three trials.

The dispersion optimisation phase consists of three stages:

First stage: Investigates the effect of sonication intensity on dispersion of carbon nanotubes in water (using Ultraviolet–visible spectroscopy-Uv-vis). The

ultrasonication treatment followed immersion of the ultrasonic probe into the suspension. Low, moderate, and high intensities sonication was separately employed to examine the effect of various intensities on dispersion of agglomerated multiwall carbon nanotubes (three different percentages were examined) in water.

Three groups of MWCNTs suspensions were prepared. Groups A and B each consisted of 12 suspensions of 0.01%, 0.025%, 0.05% MWCNTs. These suspensions were sonicated with low and moderate intensities over a duration of 10, 20, 30, and 40 minutes. Group-C, consisting of 6 suspensions of 0.01%, 0.025%, 0.05% MWCNTs, were sonicated under high intensity sonication over a duration of 3, and 5 minutes (Table3.6). The temperature of the suspensions during sonication was monitored to avoid overheating.

Amplitude settings of 20%, 50% and 100% were used to represent low, moderate, and high intensity sonication, respectively. Low and moderate intensities were run over four different sonication times, 10, 20, 30, and 40 minutes, and high intensities were run over 3, and 5 minutes.

Second stage: Suspensions of groups A, B, and C were mixed with cement paste ingredients (mix design is presented in Table7.7) to investigate the effect of the dispersion methods used on nanotubes/cement paste mechanical performance. Using these suspension groups, a total of thirty mixes of cement specimens were prepared. For comparison, reference samples of plain cement paste (PC), and cement paste containing undispersed nanotubes (T1, T2, and T3), were also prepared. Under each group, samples are labelled as "CT-1 (3, 5, 10, 20, 30, 40), CT-2 (3,5, 10, 20, 30, 40), CT-3 (3,5, 10, 20, 30, 40) , first letter "C" represents the cement paste, second letter "T" refers to "MWCNTs", the numbers "1", "2", and "3" refer to the dosages of MWCNTs of 0.01%, 0.025%, and 0.05% by cement weight, respectively, and the fourth symbol "3", "5", "10", "20", "30", "40", indicates the sonication time in minutes. Details of the experiments are summarised in Table3.6. Mixing procedures were carried out in the following sequence: Dry ingredients (cement, and sand) were mixed together for 2 minutes using a Hobart mixer. The remaining mixing water and superplasticiser were added during this initial 2 minutes mixing. The nanofilaments

suspension was then added and mixed for a further 4 minutes. Next, the paste was cast and vibrated for compaction in stainless steel cubic moulds (25 x 25 x 25) mm, and wooden dog-bone moulds for the characterization of compressive and tensile strength tests, respectively. All specimens were de-moulded after one day from the casting then cured in water until testing. For each mix, four cubes were tested after 3 and 28 days of curing, and three dog-bone specimens were tested after 28 days.

Table 3.6 Sonication intensities and treatment duration.

Group	ID	MWCNT %wt.	SP/MWCNT	Sonication Intensity	Sonication Time (min)
A	CT-1	0.010	1.0	Low	10,20, 30, 40
	CT-2	0.025	2.5		10,20, 30, 40
	CT-3	0.050	5.0		10,20, 30, 40
B	CT-1	0.010	1.0	Moderate	10,20, 30, 40
	CT-2	0.025	2.5		10,20, 30, 40
	CT-3	0.050	5.0		10,20, 30, 40
C	CT-1	0.010	1.0	High	3, 5
	CT-2	0.025	2.5		3, 5
	CT-3	0.050	5.0		3, 5

Table 3.7 Mix design proportions of Phase-I.

Mixture ID	Cement	Water	Sand	MWCNTs %	Superplasticiser PCE: MWCNTs
CO	1	0.35	1.5	-	0.08 by cement weight
CT-1 CT-2 CT-3	1	0.35	1.5	0.01 0.025 0.05	1:8

The third stage. In the above stages (first and second stage) the amount of water used with the ultrasonication treatment was fixed at a volume of 100 ml. To verify the effect of water volume of dispersion of nanotubes, stage 3 examined whether the volume of dispersion water affected the efficiency of the proposed dispersion method, and also determined the effective nanotubes to volume ratio that led to a higher dispersion level

and concentration of individual nanotubes. High intensity sonication over 5 minutes was used this experiment. Eight nanotube suspensions of 0.025 % wt. were dispersed in 25ml, 50ml, 100ml, 150ml, 250, 500ml, 750ml, and 1000ml volumes of water. Figure3.3 shows the varying volumes of water used in the experiments.

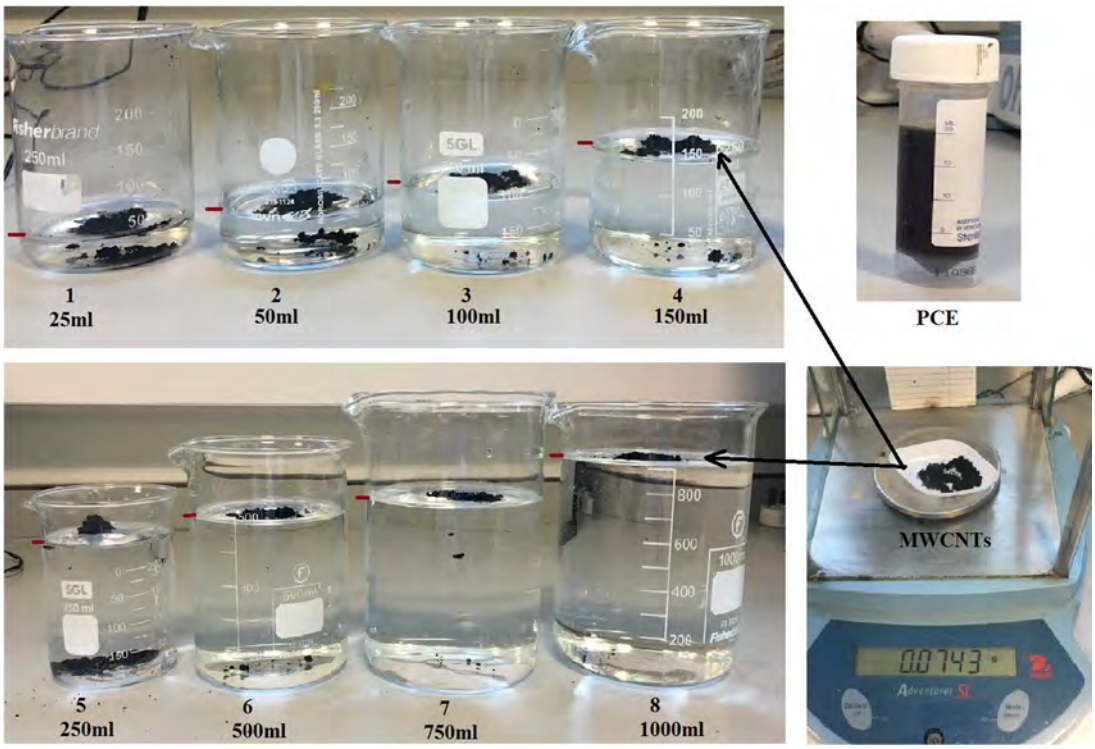

Figure 3.3 Experiment details to verify the effect of different volumes of water on dispersion of multiwall carbon nanotubes.

3.4.2 Phase II: Effect of Surfactants

Generally, surfactants are classified in accordance to their surface charge characteristics. The surfactants used in this research are cationic surfactants (PCE, and NSF) which form a positive charge when dissolved in water, and non-ionic– surfactants (MS) with no net surface charge.

The main aim of using dispersion agents (i.e. surfactants/superplasticiser) is to facilitate the dispersion to individual nanotubes in aqueous media. Each nanotube, in principle, is covered by the surfactant molecules in which the hydrocarbon chains of

surfactants interact with the CNT surface while the hydrophilic heads orient toward water for dissolution. It is important to note that the final configuration can be described as a cylindrical micelle with a nanotube in the centre(Oxana V. et al. 2013). This mechanism increases the nanotube wettability, and dispersibility in water. Although many surfactants can be used for dispersing nanotubes in water, some of those are incompatible when added to cement mixtures as they can retard/prevent hydration processes, entrap substantial air in the paste, or undergo reactions with water-reducing admixtures, resulting in re-agglomeration (Collins 2011).

In this phase, experiments to optimise the appropriate type and concentration of surfactant have been carried out using one concentration of nanotubes (0.025%) by cement weight. Experiments were divided into two stages:

- **First stage:** Determination of optimal type of surfactant and concentration leading to the highest dispersion of nanotubes in water. Three series of nanotubes suspensions have been dispersed in combination with different surfactants, and in different concentrations. With each surfactant (i.e. PCE, NSF, and MC), nine suspensions of nanotubes were prepared at various concentrations (nanotubes-to surfactant ratio of 1:2, 1:4, 1:6, 1:8, 1:10, 1:12, 1:14, 1:16, and 1:20).
- **Second Stage:** During this stage experiments were carried out to assess surfactant compatibility with cement paste. With each surfactant, the optimal concentration that led to a higher dispersion of nanotubes was used to prepare nanotubes suspensions for addition to cement paste. Properties of the nanofilament composites (mix design is presented in Table 3.8) such as compressive strength and workability have been used as composite performance criteria to demonstrate the compatibility of the surfactant used and its effect on the efficiency of MWCNTs dispersion within the composites. Six cement paste mixtures were prepared using the same procedures as in Phase I. The paste was used to test the workability, then cast and vibrated for compaction in stainless steel cubic moulds (25 x 25 x 25)mm. For each mix, four cubical specimens were tested after 3, 7, and 28 days of curing. Mixtures containing only PCE, NSF, and MC, were labelled as PC-PCE, PC-NSF, PC-MC respectively, and mixtures prepared with nanotubes suspension were labelled as CT-PCE, CT-NSF, and CT-MC.

Table 3.8 Mix design proportion of Phase-II.

Mixture ID	Cement	Water	Sand	MWCNTs	Superplasticiser /Surfactant PCE, NSF, MC: MWCNTs
PC	1	0.35	1.5	-	PCE at 0.08% by cement
PC-PCE PC-NSF PC-NSF	1	0.35	1.5	-	1:2, 1:4, 1:6, 1:8, 1:10, 1:12, 1:14, 1:16, and 1:20
CT-NSF CT-PCE CT-MC	1	0.35	1.5	0.025	1:2, 1:4, 1:6, 1:8, 1:10, 1:12, 1:14, 1:16, and 1:20

3.4.3 Phase III: Effect of Undensified Microsilica

In this phase, the dispersion technique has been extended to include use of pozzolanic admixtures (i.e. Undensified Microsilica). Mineral admixtures have been found to aid with improving the dispersion of carbon nanotubes, and improving the bond with the surrounding matrix within the composites, as due to its fine particle size USF acts as a physical barrier and contributes to the prevention of re-agglomeration of MWCNTs through the composite.

Experiments were carried out to: i) investigate the effect of undensified silica fume (in three replacement percentages of 5%, 10%, and 15% replacement by cement weight) on the compressive strengths and porosity of nanotube/cementitious composite.; ii) examine the synergistic effect of USF and MWCNTs on the microstructure of cementitious composites; and iii) understand the mechanisms of USF in preventing re-agglomeration of MWCNTs within the cement composite. The interaction of silica fume with calcium hydroxide and with Portland cement was studied using microscopy-based techniques. In this phase nanotubes were added at a set percentage

of 0.025% by cement weight. Table 3.9 showing the mix proportions used in this phase.

Eight mixtures including PC and CT-2 were prepared using the same procedure as in Phase I (except the micro silica was added with the dry ingredients). The prepared mortar was cast and vibrated for compaction in stainless steel cubic moulds of (50 x 50 x 50) mm. With each mixture, a cubic specimen of (100x100x100) mm was cast. This sample was used to core out 4 cylindrical specimens, these cores of 30mm (diameter) and 80mm (height) were used for porosity measurements. All specimens were de-moulded after one day following casting then cured in a water tank until testing. Specimens have been labelled as (PC+5%SF), (PC+10%SF), and (PC+15%SF), (CT2+5%SF), CT2+10%SF), and (CT2+15%SF).

Table 3.9 Mix design proportion of Phase-III.

Mixture ID	Cement	Water	Sand	Silica fume	MWCNTs	Superplasticiser NSF,
PC	1	0.35	1.5	-	-	0.08%
PC+5%SF PC+10%SF PC+15%SF	1	0.35	1.5	0.05 0.1 0.15	-	0.08%
CT+5%SF CT+10%SF CT+15%SF	1	0.35	1.5	0.05 0.1 0.15	0.025	1:10*

*MWCNTs:NSF=1:10

3.4.4 Dispersion Characterization

3.4.4.1 In liquid

Ultraviolet–visible spectroscopy (Uv-vis), optical microscope, and transmission electron microscope (TEM) has been employed to quantify the dispersion of the

nanofilaments in water. Each device is shown in Figure 3.4. The dispersion state on a micrometre scale was examined using polarization optical microscopy (Amplival Pol. D, Carl Zeiss, Tena, German). The extent of nanotube dispersion in water relative to the variations in the duration of sonication, intensity of sonication, and surfactant concentration was evaluated using ultraviolet–visible spectroscopy (UV–vis spectroscopy UV-20401PC). The morphology of nanofilaments was examined using Transmission Electron Microscopy (TEM) (Hitachi-7100 Transmission Electron Microscope (TEM) operated at 125 kV), and Scanning Electron Microscopy (SEM) (using a Zeiss model LEO 1455VP). Drops of diluted suspension were placed on a grid prior to imaging and allowed to dry in air.

3.4.4.1.1 Ultraviolet–visible Spectroscopy (Uv-vis)

Ultraviolet-visible spectroscopy (UV-vis) is a spectroscopic technique in which the absorption of electromagnetic radiation in the ultraviolet-visible region is recorded. UV-vis absorption spectra were recorded using a UV-visible spectrophotometer (shown in Figure 3.4a) at a scan rate of 60nm/min over the range 300–800nm, with a matched pair of glass cuvettes, 1 cm in optical path length, placed in a thermostatic cell holder.

UV-vis spectra have been used as follows:

- The recorded absorbance for different suspensions can be used for comparison between the dispersion methods. The higher the dispersion levels of MWCNTs in water were observed, the higher the absorbance values were recorded. After sonication treatment on nanofilament suspensions, samples were removed and diluted by a factor of 100, resulting in nanofilaments contents that were suitable for UV–vis measurements. For all experimental studies the absorption was measured alongside a reference sample. Normally the corresponding pure surfactant diluted by the same factor is used as a reference during the characterization of MWCNTs-surfactant dispersions.
- Concentration of the dispersed nanotubes in water can be determined by applying the Beer-Lambert law to the recorded absorbance. Quantitative UV-vis which is

used to determine the concentration of an analyte can absorb in the determined wavelength region. The Beer-Lambert law (Eq.3.1), which gives a linear relationship between absorbance and concentration for dilute solutions, is used. A calibration plot was generated by measuring the absorbance of a series of solutions with different known concentrations, thereby the concentration of the target analyte can be determined from the plot. The absorbance of a suspension can be related to the molar concentration (c) and the sample thickness (l) by the Beer-Lambert law, via the molar extinction co-efficient (ε).

$$A = \varepsilon cl \qquad \text{(Eq. 3.1)}$$

- Stability through centrifugation-based method. Centrifugation is one of the methods of investigating the sedimentation behaviour of MWCNTs in water, and is used here to indirectly assess the stability of dispersion. Good particle dispersion is related to a low sedimentation rate. For this, MWCNT suspensions were subjected to centrifugation at 3,000 rpm for 10 min. The suspension stability was examined using Uv-vis spectra recorded before and after centrifugation.

  Dispersion stability indexes (X_{st}) were obtained using absorbance values at a wavelength of 500nm (as described by Eq. 3.2). The lower the index values obtained from each surfactant, the more stable the individual nanotubes in the suspension

  $$X_{st} = (At_0 - At_c)/At_c \qquad \text{(Eq.3.2)}$$

  Where At_0= absorbance directly after sonication treatment of 10 minutes, and At_c= absorbance value after centrifugation.

3.4.4.1.2 Optical Microscopy Measurements

Suspensions containing a known weight fraction of MWCNTs were prepared by adding nanotubes to the aqueous solution without and with surfactant, respectively. Before and after ultrasonication treatment, a drop of the suspension was carefully sucked up with a burette and dipped on a slide to settle, then the suspension was examined with a polarization optical microscope (shown in Figure 3.4b).

3.4.4.1.3 Transmission Electron Microscopy (TEM)

TEM is a microscopic technique in which a beam of electrons is transmitted through an ultra-thin specimen which interacts with the specimen when it passes through to form the sample image. The image is enlarged and focused onto an imaging device, such as a fluorescent screen located on a layer of photographic film and obtained by a sensor (CMOS sensor). The assessment of the morphology of nano-additives is based on determining their characteristics using a transmission electron microscope equipped with a camera (Gatan OneView 4K) CMOS optimized for both sensitivity and speed (shown in Figure 3.4c).

TEM can yield information such as nanotubes dimensions (diameter and length), distribution and morphology. The produced images can be also used to judge whether good dispersion or agglomeration has been achieved in the sample. Sample preparation for TEM analysis was done by taking one drop of the prepared solution after dilution in water, which was then put onto a carbon film on a 3mm grid of copper.

Figure 3.4 a) Ultraviolet-visible spectroscopy model (UV-2401PC), b) polarization optical microscope (Amplival Pol. D, Carl Zeiss, Tena, German), and c), Transmission electron microscope (TEM).

3.4.4.2 In Cementitious Composites: Mechanical and Microstructural Characterisation

Investigating the mechanical properties of nanofilament reinforced cementitious composites is a practical (proxy) method for evaluating the dispersions and performance of nanofilaments as reinforcement agents in the matrix. Improved mechanical properties are due to the effectiveness of well dispersed nanofilaments though the cement matrix. Poor dispersion, as discussed in the literature (see Chapter Two, Section 2.4.1), leads to a decrease in the mechanical properties.

The mechanical strength has been investigated during the following:

- Experiments of Phase I include compressive strength and direct tensile strength.
- Experiments of Phase II include compressive strength and workability.
- Experiments of Phase III include compressive strength and porosity.

3.4.4.2.1 Compressive Strength

Compression testing is a standard method used to determine material capacity to withstand an applied load before failing. The compressive strength tests were performed according to ASTM C39(ASTMC39/C39M-17) produced nanofilament composites have been tested after various ages of curing, using a hydraulic Mechanical Testing System (MTS). The compressive strength of each specimen was computed by dividing the maximum load to failure by its average cross sectional area. Compressive strength tests were performed on between 3-5 replicates of each specimen type under a constant compressive load rate, shown in Table 3.10.

Table 3.10 Cubic specimen's dimensions and the load rate used.

Specimens Dimensions			Compressive load (kN)	Load rate (kN/s)	Note
Length (mm)	Width (mm)	High (mm)			
25	25	25	25	0.188	Used with experiments of Phase-I, and Phase-II
50	50	50	45	0.75	Used with experiments of Phase-III, and Chapter5
100	100	100	180	3	Used with experiments of Chapter Six

3.4.4.2.2 Direct Tensile Strength Test

The assessment of the tensile strength of cementitious composites with and without nanofilaments was carried out through a direct tensile test (using dog-bone shaped specimens). Although the direct tension test is difficult to conduct for many reasons such as i) it can be difficult to control loading eccentricities (which could lead to a combined loading state i.e. tension and bending), and ii) it may be difficult to control the sample alignment with the machine loading direction (mis-alignment results in error in the calculated tensile stress), the briquette tension test method (described in AASHTO T132(AASHTOT132 2000)) was used for investigating the effect of nanofilaments on composites' tensile strength. Figure 3.5 shows the conventional test method for composite uniaxial tension testing using dog-bone shaped specimens. The geometry of the dog-bone, its cross-sectional area and use of steel auto alignment grips minimized the secondary stresses generated by the holding devices and the above eccentricities. The specimens were 76mm long, and 25.4mm square at their neck with enlarged ends.

To obtain increased understanding of the performance of carbon nanotubes incorporated cementitious composites, under monotonic direct-tensile load, direct tensile tests were carried out after 28 curing days using a universal testing machine (Instron 6300) under displacement control at rate of 0.005 mm/s. The tensile force is transferred to the specimen by the frictional force between the grips and the specimen.

Three specimens were tested for each mixture. The tensile stress σ_t was calculated from the following equation (Eq.3.3):

$$\sigma t = \frac{T}{A} \qquad \text{(Eq. 3.3)}$$

Where T: is the tensile load obtained from the load cell, and A is the cross sectional area of the specimens

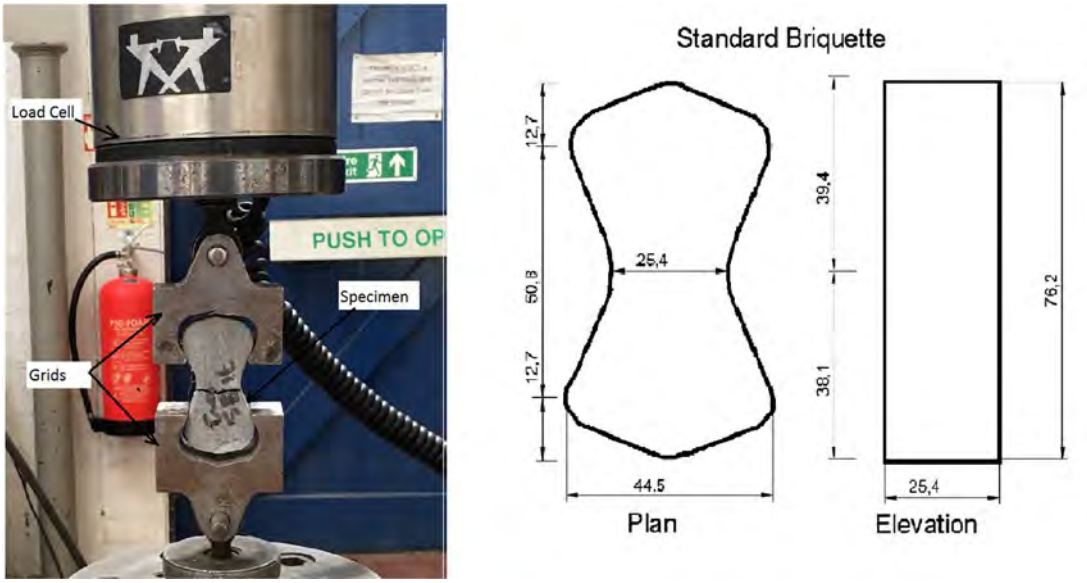

Figure 3.5 Direct tensile strength tests using dog-bone shape specimen.

3.4.4.2.3 Workability (Fluidity)

The flow of fresh nanofilament reinforced cementitious composite and cement mortar was tested by using a standard flow table test in accordance to ASTMC230/230m-14(ASTMC230/C230M-14) (Şahin and Köksal 2011) using a 254 mm flow table (Figure 3.6). The flow mould was in the form of a frustum shape with the bottom base being 100 mm wide and a top surface of 70 mm in diameter. The height of the mould was 50.8 mm. The fresh mixture was placed in a flow mould in two layers. Each layer was compacted with a standard hard rubber tamper 20 times and then levelled to create a smooth top surface. After the top surface of the cementitious material was levelled the flow mould was removed and the flow table was dropped 25 times in 20 seconds. The initial and final diameters were recorded to calculate the mixture flow. The flow is defined as the increase in diameter divided by the original diameter multiplied by 100.

Figure 3.6 Flow table apparatus.

3.4.4.2.4 Porosity Measurements

Porosity measurements of carbon nanofilaments cementitious composites were carried out using the method developed by Khan et al.(Mohammad Iqbal 2007), and Wilson et al(Wilson et al. 1999). The test was carried out for all mixtures using cylindrical cores of 80mm length and 30mm diameter, four for each mix. The specimens were chose in cylinder shape to increase the vacuumed surface area (under the porosity test) which can lead to accurate results on the behaviour of nano-additives through the cementitious composite. Due to the relatively small size of the available desiccator in the lab, a small size of the specimen (cylinder of 80mm length and 30mm diameter) were fixed over all the mixtures which can be tested in one time (to avoid the variant in the test environment). The test procedure was as follows: prior to testing, the samples were taken out of the curing tank then dried in an oven at a temperature of 105±5 ^{o}C for approximately 24 hours then weighed. The samples were then kept in a vacuum desiccator under 1bar of vacuum, for 24 hours. The desiccator was then filled with distilled water so that samples were fully submerged. Then the samples were kept under vacuum for 24 hours and allowed to equilibrate for the next 24 hours. The specimens were then weighed in air and water. The amount of water penetrating the sample is a measure of the porosity and is calculated as follows (Eq.3.4):

$$P = \frac{B - A}{B - C} \text{ x100} \qquad \text{(Eq. 3.4)}$$

Where: P is porosity (%); A is oven-dry weight; B is saturated surface dry weight; C is saturated submerged weight.

3.4.4.2.5 Microstructure Analysis using Scanning Electron Microscopy (SEM)

Scanning Electron Microscopy (SEM) (Zeiss; model of LEO 1455VP) was used to observe the microstructure of composite. The microstructural analysis of nanofilament specimens was done using qualitative imaging techniques to understand the effect of the dispersion method on the tested specimens and their obtained mechanical properties. SEM images of fractured surfaces were taken after sputtering the surface with gold as a conductive material to increase the image resolution and reduce charging effects. Images at scales between 50nm and 200nm were used to investigate

the dispersion of the nanofilaments at the nano-level. The image scales were selected to provide sufficient resolution for quantification of particle/filament size, thickness etc.

3.4.5 Summary of Dispersion Experiments

This chapter has provided a brief introduction of the characterization techniques employed in this work to assess nano-additive suspensions including optical microscopy, UV-Vis spectroscopy, and mechanical tests on the nanotubes/composites including compressive and direct tensile strengths. Employment of these techniques with respect to the aims and objectives of this thesis is discussed in Chapters Four and Five.

3.5 Methods and Experiments of Chapter Five

3.5.1 Overview

The dispersion technique proposed in Chapter Four involves three experiments phases, with the first and second phases providing a suspension with high concentrations of individual nanotubes. In the third phase, re-agglomeration of dispersed nanotubes into a composite, and improved bonding of nanotubes with the surrounding matrix, were achieved by incorporating 10% of undensified silica fume (USF) (as a cement replacement). Methods to examine the impact of the proposed dispersion technique on the dispersion of the remaining types of nanofilaments used within this research (i.e. functionalised multiwall carbon nanotubes (MWCNTs), carbon nanofibres (CNFs), and few layer graphene sheets (FLGO)) are described in the sections below.

Aqueous dispersions were assessed using Scanning Electron Microscopy (SEM)/Transmission Electron Microscope (TEM) and Optical Microscopy, and Ultraviolet–visible spectroscopy (Uv-vis). The interaction between nanofilaments. and USF was also assessed through TEM imaging. Mechanical performance of the

nanofilament reinforced cementitious composites based on MWCNTs, F-MWCNTs, CNFs, and FLGO were studied through compressive strength, direct and indirect (splitting) tensile strength, flexural strength, and porosity and density measurement. Relationships between the compressive strength- flexural strength, and compressive strength-tensile strengths were derived. The microstructure of the hardened composite was investigated through high resolution SEM.

3.5.2 Dispersion Characterisation of Nanofilaments and Graphene Suspensions

3.5.2.1 Nanofilaments Suspension Characterisation

An additive percentage of 0.025 % wt. (by cement weight) has been selected for the experiments of chapter Five. Nano-additives suspensions were prepared by mixing the ingredients below:

1- Nanofilaments of (F-MWCNTs, CNF) and FLGO at percentage of 0.025% by cement weight, equivalent to 0.0741 mg/l.
2- 500ml water (see Chapter Four, Section 4.2.2.3)
3- Surfactant: nano-additive ratio of 10:1 (see Chapter Four, Section 4.3.2.1).

The resulting mixtures were treated by applying high intensity-sonication with a sonication duration of 5 minutes (sonication set-up is shown in Figure 3.7). With each type of nanofilament two sets of suspensions were prepared.

- The first suspension set of F-MWCNTs, CNF, and FLGO was used for visual examination. The dispersion state of nano-additives before and after addition of NSF, and then after ultrasonication, were observed on a bulk scale through visual examination over 30 minutes (images were taken after 10 minutes of sonication and then after 20 minutes).

- The second set was used for stability and concentration evaluation, respectively. The methods used are explained in (Section 3.4.4.1.1). Stability over time was investigated by measuring the absorbance using Uv-vis spectrometry over various durations. After sonication, three samples were taken from each suspension and

diluted by a factor of 100, then the absorbance was recorded at durations of: t=0 min, after 30 min, 180 min, 1440 min (3 days), and 10080 min (7 days). Dispersion stability indexes (X_{st}) were obtained using absorbance values at a wavelength of 500nm and applying (Eq.3.2).

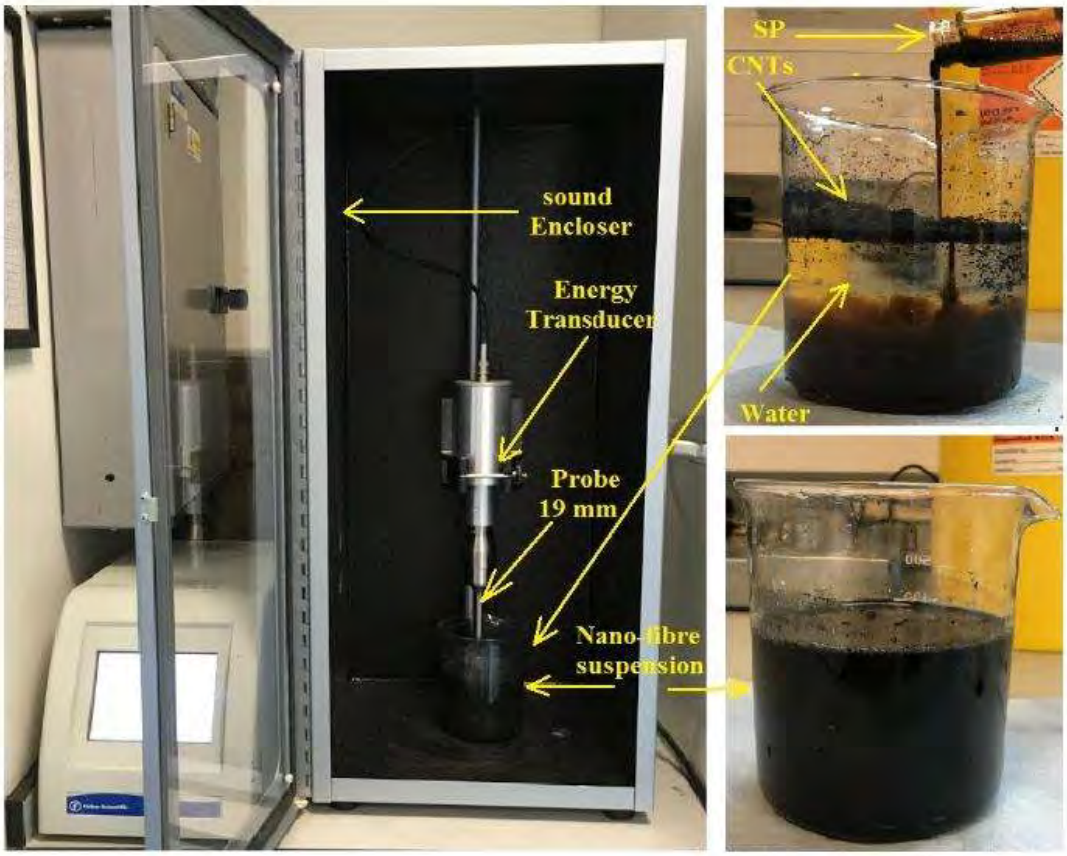

Figure3.7 Sonicator used in the dispersion of carbon nano-additives suspensions.

3.5.3 Nano-Additives Reinforced Cementitious Composites Characterisation

3.5.3.1 Composite Preparation

After dispersion, five batches of nano-additives reinforced cementitious composites based on MWCNTs, F- MWCNTs, CNFs, and FLGO were prepared and labelled as "NRCC-CT," "NRCC-CT_f," "NRCC-CF", and "NRCC-GO", respectively. A

reference specimen of plain cementitious paste, labelled as PC, was used as a control for comparison. The mix proportions for NRCC are shown in Table 3.11.

Mixing procedures were carried out in the following sequence: all dry ingredients (cement, micro silica, and sand) were mixed together for 2 minutes using a high shear mixer Zyklos (Pan Mixer ZZ 75 HE) (Carsten 2010). The remaining mixing water and superplasticiser were added during this initial 2 minutes mixing. The nanofilaments suspension was then added and mixed for a further 4 min (Carsten 2010, Peyvandi et al. 2013). The mixture was cast and vibrated for compaction in: i) cubic moulds of 50mmx50mmx50mm for compressive strength testing in accordance to ASTMC109(C109M-16a); ii) cylindrical moulds of 100 mm diameter and 200mm height for splitting tensile strength testing in accordance with ASTM C496 (C496M-11); and iii) a prism bar mould of 40mmx40mmx160mm for toughness measurement. Cores of 30 mm (diameter) and 80 mm (height) were used for porosity measurements following the method developed by Wilson et al. and Khan (Wilson et al. 1999, Mohammad Iqbal 2007) All specimens were de-moulded one day following casting and then cured in a water tank until testing.

Table 3.11 Mix design proportions of chapter Five.

Mixture ID	Cement	Water	Sand	Silica fume USF	Nanofilaments	Nanofilaments: NSF Superplasticiser
PC	1	0.35	1.5	0.1	-	0.08Wt.% by cement weight
NRCC-CNT	1	0.35	1.5	0.1	0.025% CNTs	1:10
NRCC-CNT_f	1	0.35	1.5	0.1	0.025% F-MWCNTs	1:10
NRCC-CNF	1	0.35	1.5	0.1	0.025% CNF	1:10

NRCC-GO	1	0.35	1.5	0.1	0.025% FLGO	1:10

3.5.3.2 Mechanical Strength Characterisation

Test details for cubic specimens of 50x50x50 mm for compressive strength, and cores of 30 mm (diameter) and 80 mm (height) for porosity measurements, are given in Sections 3.4.4.2.1, and 3.4.4.2.4, respectively. Test set-up is shown in Figure 3.8.

3.5.3.2.1 Tensile Strength

Direct and splitting tensile tests are direct and indirect methods used in this study to determine the tensile strength of a composite.

Direct tensile testing can provide a uniaxial and approximately real tensile strength of cement-based composites. Unlike metals it is difficult to obtain direct tensile strengths for cementitious composites due to their brittleness, and no standard test method has been adopted by ASTM to provide a direct measurement of tensile strength for a cementitious composite. The direct tensile testing method adopted here is discussed in section 3.4.4.2.2. Splitting tensile tests were also performed, according to the standard test method for splitting tensile strength of cylindrical concrete specimens(C496M-11). The cylinders were tested using a hydraulic mechanical testing system (MTS) at a constant compressive strength rate of 0.75 kN/s.

The splitting tensile strength (horizontal stress along the vertical diameter) is calculated through the following equation (Eq.3.5):

$$f_{sp} = \frac{2\mathrm{p}}{\pi \mathrm{dl}} \qquad (\mathrm{Eq.}\ 3.5)$$

Where:

f_{sp}: splitting strength (N/mm^2)

P : maximum applied load(N)

d: diameter of cylinder (mm)

L: length of cylinder (mm)

In the cylinder splitting test, two horizontal linear variable differential transformer (LVDTs) are used to measure the horizontal deformation under vertical applied load, which can be an indication to the resistance to crack propagation. For strain measurement, two LVDTs were fixed on two faces of the specimens using high strength glue.

3.5.3.2.2 Flexural Strength

The Flexural Strength was tested on prisms of 40x40x160mm. The prisms were tested under centre-point loading at a displacement rate of 0.18 mm/min and span of 120 mm using an Instron Testing Machine (Intron Model 8630). The deflection was measured using two LVDTs.

The load-deflection curves were analysed to obtain the material toughness in accordance with JSCE-SF4 Japan Society of Civil Engineering, Standard for Flexural Strength and Flexural Toughness.

The Flexural Toughness Factor (FT_δ) is calculated using Eq.3.6.

$$FT_\delta = (T_{b\delta} \times l)/(\delta \times b \times h3) \qquad \text{(Eq.3.6)}$$

Where FT_δ = Flexural Toughness Factor at a beam displacement of δ, Tb_δ = Area under the load-versus-deflection plot up to a deflection of δ, l = Span length, and b width and h= depth of the beam.

Figure 3.8 Test set-up of a) compressive strength, b) flexural strength, and c) splitting tensile strength tests.

3.6 Methods and Experiments of Chapter Six

3.6.1 Overview

In this section, methods and tests explored the behaviour of multiscale hybrid nanofilament reinforced cementitious composites based on carbon nanotubes (MHRCC-CNT), and based on carbon nanofibres ((MHRCC-CNF). A hybrid system was obtained by combining filaments at the nanoscale with microfibres. Multiwall carbon nanotubes (MWCNT), and carbon nanofibres (CNF) at a dosage of 0.025 wt.% were used as nanoscale filaments. Steel fibres at a volume fraction of 2% were used as the micro fibre additive. The mechanical properties were evaluated at various curing ages, along with sample microstructure.

Experimental Details

3.6.1.1 Mixture Preparation

Multiscale hybrid reinforced cementitious mixtures were prepared as follows: All dry ingredients (cement, microsilica, and sand) were first mixed for 2 minutes in a high shear mixer (Zyklos Pan Mixer ZZ 75 HE), then during a further 2minutes water and NSF were added (the remaining quantity). Micro fibres (for hybrid-fibre mixtures) were gradually added and mixing continued for another 2 minutes. The nanofilament suspension was then added and mixed for a further 4 minutes. The mixing procedure is illustrated schematically in Figure 3.9. The prepared mixes were poured, in accordance to ASTM C192 (C192M-13a)into wooden dog-bone shaped moulds, and plastic moulds for compressive and flexural tests, with dimensions (100x100x100) mm in accordance to BS EN12390-3: 2009 (BS-EN12390-3 2009), and 100mmx 100 mm x 500 mm in accordance to ASTM C1609(C1609M-12), respectively. Mix design and mixture labelling is shown in Table 3.12

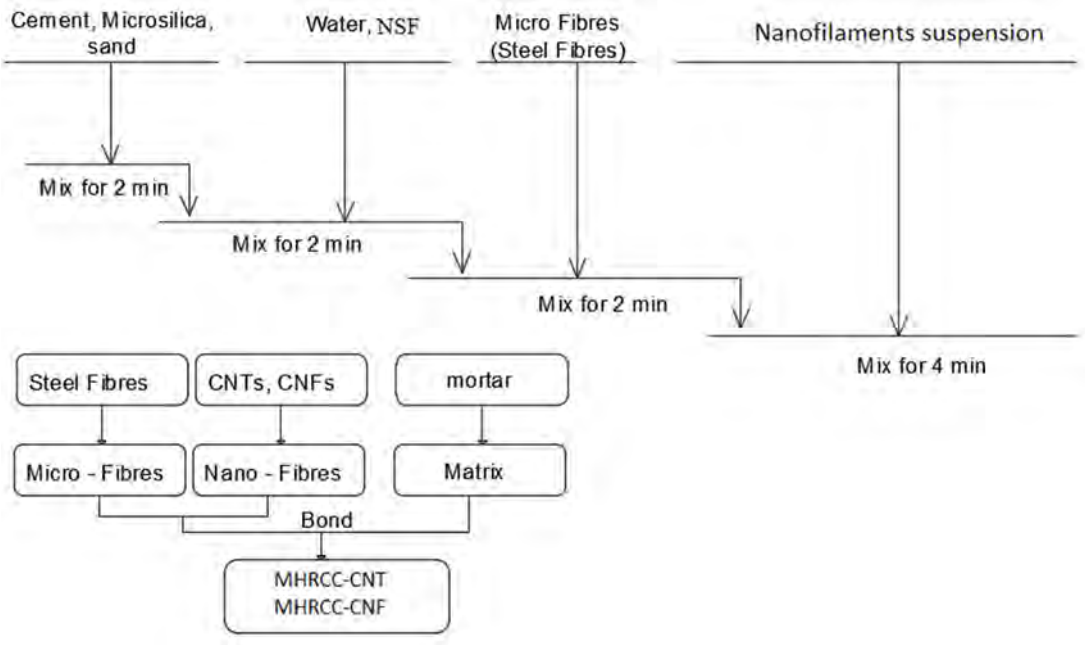

Figure 3.9 Schematic mixing procedure for multiscale hybrid reinforced cementitious composites.

Table 3.12 Mix design proportions of Chapter Six.

Mixture ID	C	W	Sand	USF	CNT/Fs	Microfibres %Vf	Nanofilaments: NSF Superplasticiser
FRC	1	0.35	1.5	0.1	-	2%	0.08Wt.% by cement weight
MHRCC-CNT	1	0.35	1.5	0.1	0.025% CNTs	2%	1:10
MHRCC-CNF	1	0.35	1.5	0.1	0.025% CNF	2%	1:10

3.6.1.2 Mechanical Strength Characterisation

Generally, understanding the development of mechanical properties during the early ages of concrete maturity is a key to fundamental materials science-based predictions of early age deterioration (Grasley et al., 2005 and Lura, (2003). Therefore, mechanical properties of multiscale hybrid reinforced cementitious composites were measured at early ages and at later ages, to assess changes in mechanical properties over curing time.

The following mechanical tests were performed to provide time-dependent material parameters for hardening composites:

Compressive Strength Tests: This test was performed on 100mmx100mmx100mm, at three different ages (3, 28, and 90 days), following the methods described in Section 3.6.1.1. Three specimens were examined for each test under a constant compressive load rate of 3 kN/s.

Tensile Strength Test: Dog bone-shaped specimens, and 100mm×200mm cylindrical specimens of three different ages (3, 28, and 90 days) were used to determine the direct

and indirect tensile strength (Figure 3.10). Details of splitting tensile tests are given in Section 3.6.1.1. An Instron testing machine was used to perform direct tensile tests at a constant displacement rate of 0.18 mm/min, following the ASTM standard D638. Linear Variable Differential Transformers (LVDTs) were attached near the grips connected to the specimen. The average elongation was obtained from the two LVDTs placed on opposite sides of the specimen. LVDTs were used to detect elongation during the test, and to understand the behaviour of the composites under monotonic direct-tensile loading.

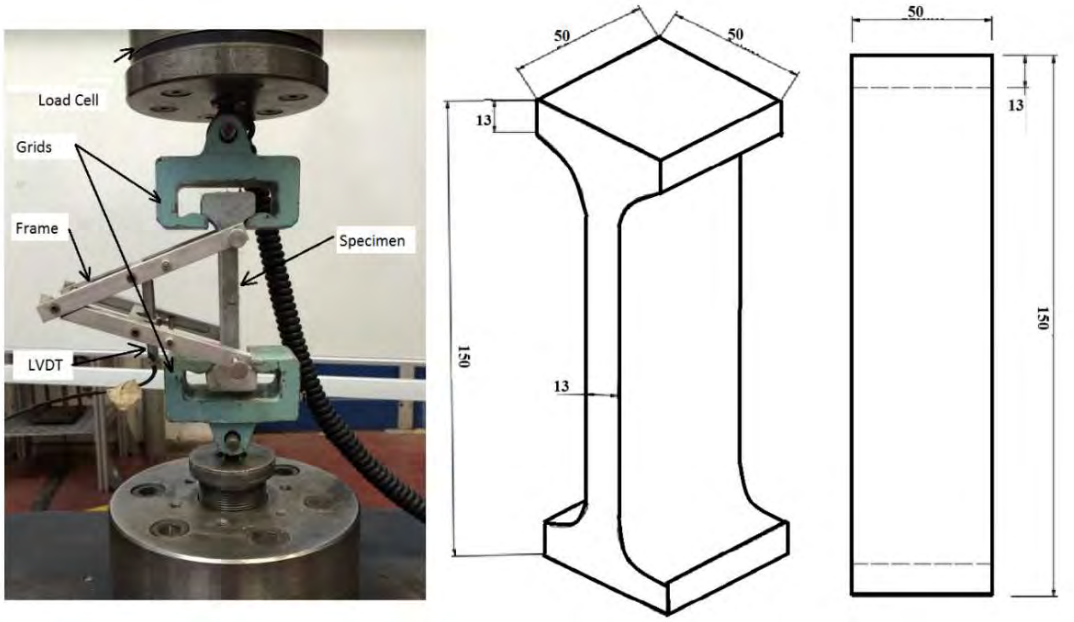

Figure 3.10 Test set-up tests for dog bone specimens, including supports, grids, and LVDT with the frame.

Flexural Strength: Four-point bending tests were performed with the aim of characterising the ultimate flexural strengths, post-cracking behaviour, and fracture energy of the fibre composites (Baughman RH and AA 2002). For the flexural strength test, beams of 100x100x500mm were tested under four-point loading at a loading rate of 0.24 mm/min. LVDTs were fixed on both sides of the set-up to measure the vertical deformation at mid cross-section of the specimen, as shown in Figure3.11. The

flexural strength was calculated based on the average results of three specimens, in accordance to ASTM C1609.

Maximum flexural strength (f) was calculated by substituting experimental test data into Eq.3.7

$$f = (P\ L)/bd^2 \qquad \text{(Eq. 3.7)}$$

(Four-point loading test)

Where;

f: Flexural strength in MPa.

P: Load in N.

L: Span length in mm.

b and d = breadth and depth (in mm) of the beam, respectively.

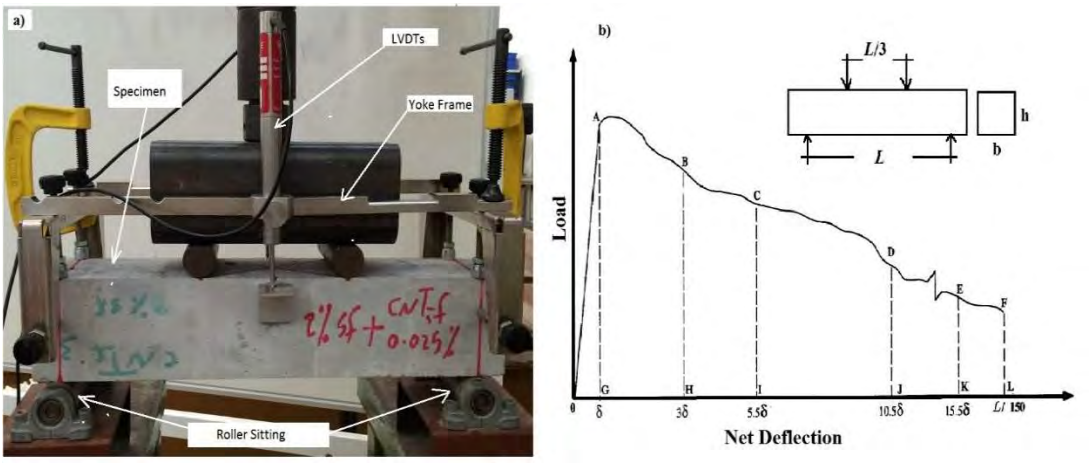

Figure 3.11 Test set-up of beams under four points loading.

Energy Absorption using JSCE SF-4 Standard Test Method: Due to the difficulties of accurately identifying the exact location of the first crack point on the load deflection curve in accordance to ASTM C1081, the load-deflection curves were analysed in accordance to JSCE-SF4. The Flexural toughness factor (FT_δ) is calculated using Eq.3.8 (Nemkumar and Jean-François 1995).

$$FT_{\delta} = (T_{b\delta} \times l)/(\delta \times b \times h3) \quad \text{(Eq.3.8)}$$

Where FT_{δ} = Flexural Toughness Factor at a beam displacement of δ, $T_{b\delta}$ = Area under the load-versus-deflection plot up to a deflection of δ, l = Span length, and b width and h= depth of the beam.

In this method, the area under the load deflection curve up to a deflection of (span/150) is obtained and results obtained from this test method yield an absolute toughness value. A flexural toughness factor is calculated which has a unit of stress(MPa) (Yurtseven 2004). This factor can be considered as the post crack residual strength of the material when loaded to a deflection of (span/150). Determination of the first crack point is not a concern in this test method. In addition, stability problems encountered right after the first crack do not affect the obtained results significantly as beams are deflected too far out from the first crack point. However, results of this test method are highly dependent on specimen size and geometry. The (span/150) deflection chosen in this test method is often criticized for being much greater than acceptable serviceability limits. In addition, this test method does not distinguish between the pre and post crack behaviour, which may be very important in some applications.

3.7 Methods and Experiments of Chapter Seven

3.7.1 Overview

Several methods have been used in the past to assess shrinkage of concrete and resulting cracking such as free drying shrinkage and restrained shrinkage. In this study, these tests have been used to demonstrate the effects of nanofilaments as regards the control of cracking, and shrinkage cracking for repair/strengthening applications. Nanofilament reinforced cementitious composites, and multiscale hybrid reinforced

cementitious composites (based on carbon nanotubes and carbon nanofibres), were examined.

3.7.2 Experiment Details

3.7.2.1 Free Drying Shrinkage

Free drying shrinkage tests were performed in accordance to ASTM C157(ASTMC157 2014) (the standard test method for length change of hardened hydraulic-cement mortar and concrete). Free Drying Shrinkage of nanofilament reinforced cementitious composites was conducted on specimens at different geometries.

For the first geometry, in accordance to ASTM C157, for each mix three specimens of 75x75x285mm were cast, and shrinkage measurements were conducted using Free drying shrinkage apparatus (as shown in Figure 3.12). The test begins on the day of specimens demoulding with shrinkage determined at various ages up to 180 days.

A second set of specimens of 40x60x400mm were used to monitor the free drying shrinkage on specimens of similar geometry to those used with end-restrained shrinkage tests.

Data were collected using demecs targeting points and a mountable strain gauge (as shown in Figure 3.13). The four sets of demecs were evenly spaced and glued to the specimens, three on top and one on one side of the beam. A 10mm clearance centre-to-centre was provided, and demecs buttons were fixed to the top and side of the specimens in the corresponding positions. Placing demecs on both sides allowed a certain redundancy, enabling measurement of the strain at a specific level, even if a demec point was lost over time. The strain was measured from both sides of the beam and the average of the two values was calculated.

Figure 3.12 Set-up for evaluating free drying shrinkage.

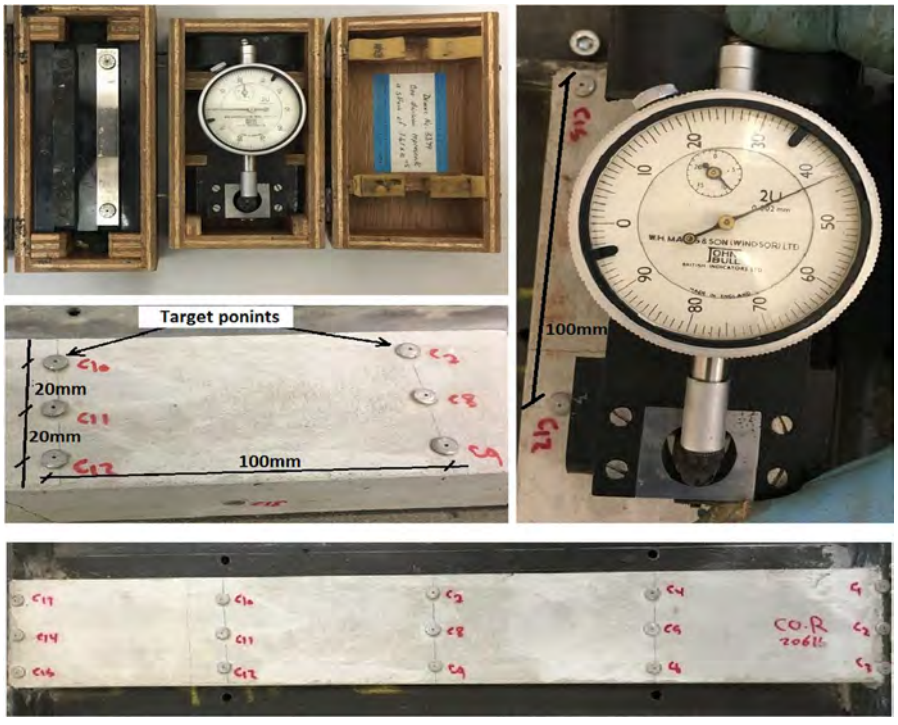

Figure 3.13 Set-up for evaluating free drying shrinkage of prism bars showing demecs targeting points and mountable shrinkage strain apparatus.

3.7.1.2 Restrained Shrinkage

Restrained shrinkage is one of the main causes of premature failure of patch material. It is neither design nor construction related, and it is unavoidable for any repair and strengthening techniques. In the present research two types of test methods (cracks tendency tests methods) were adopted to simulate the effect of restrained shrinkage, an end-restrained and a base-restrained set-up.

Overlays were cast on a substrate, which is the most suitable technique to simulate base restraining under real overlay conditions. The end-restrained set-up offers a direct evaluation of the effect of (for instance) the type of nanofilament used to reinforce a cementitious composite.

A ring test is the most popular restrained test method in which the shrinkage of an external concrete ring is restrained by an inner steel ring. This method however was not available in the laboratory in which this research was performed, so a modified end restrained test was instead employed.

3.7.1.2.1 Base-Restrained Shrinkage

The base-restrained tests consisted of (out-stretched) overlay strips of 30x100x500 mm cast on a large concrete beam (100x100x500 mm), see Figure 3.17. The procedures of repair and strengthening of tensile zone of the beams as following:

- Concrete substrate beams were produced approximately three months in advance to minimise the remaining shrinkage, i.e. to maximise the differential shrinkage between overlay and substrate.
- One of the beam surfaces was modified/ roughened using an air needle gun (an effective tool to remove several millimetres from the concrete surface).
- After surface preparation and cleaning, the surface was positioned upwards and the wooden moulds plates were re-positioned on the beam substrate.
- The concrete internal surface was kept wet, i.e., in the saturated condition. This action was adopted to avoid the excessive absorption of water by the surface to be repaired.

- Two deformed reinforcement bars (10mm in diameter) were placed on the prepared surface prior to casting. These bars are providing restraint and act as stress risers at the overlay which accelerates microcracks growth at high stress intensities. Stress risers are responsible for initiating cracks from which failure results.
- The prepared overlay composite mixture (method explained in Chapter Five) was manually placed into the moulds in one layer and compacted by vibration.
- Figure 3.14 shows the procedure of preparing the substrate surface, cleaning the surface, and reconstructed the beams by applying a repair/strengthening layer.

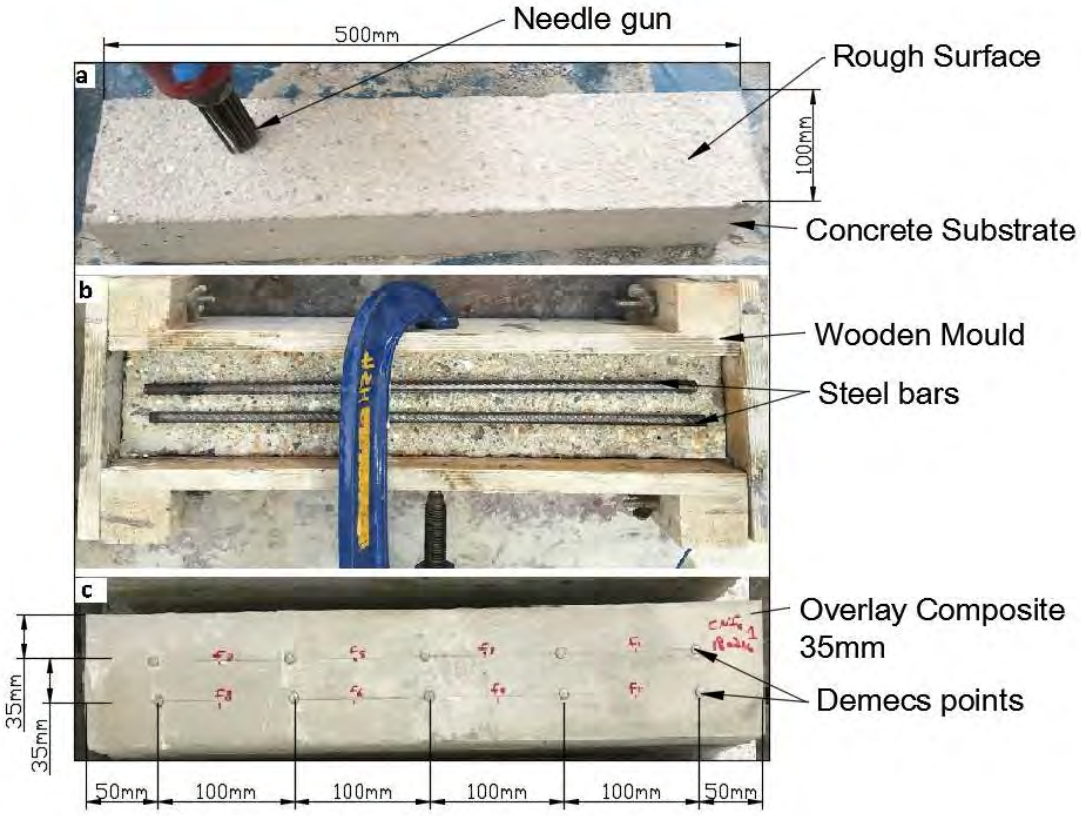

Figure 3.14 Base-restrained test set up. Photographs a, b, and c show the substrate preparation, applying the overlay nano-additives composite, and applying demecs targeting points.

3.7.1.2.2 End-Restrained Shrinkage

The influence of the overlay properties on cracking is then examined by exposing thin specimens to an end-restrained condition, for which a new test method is proposed.

An advantage of the end-restrained type of set-up is that it facilitates a direct evaluation of the effect of the nanofilament used. In other words, it represents a pure axial load case, not disturbed by the occurrence of bond stresses along the interface to the substructure.

This test method was employed in Kovler (1994) and developed by Jonas(Jonas 2006). In this study 60x40x400mm of NRCC based on carbon nanotubes and carbon nanofibres in addition to PC specimens were fastened between two end grips. In this study a "new" set-up was modified as shown in Figure 5.15, consisting of a Rectangular Hollow Section (RHS) (RHS of 120x80X8) mm, giving a smooth and slippery surface to ensure that restraint would only develop at the ends of the specimen. L-shaped supports of steel (40x40mm of 4mm thickness) were secured to the flange by means of bolts at 500mm. The bolts, which had a very tight fit, were fastened prior to each test. An 8-mm thick steel plate of 150mm length with smooth surfaces was further manufactured. Just prior to placing the nanofilaments composite, the plate was loosely positioned directly at the oiled and smooth surface of the upper flange to allow for easy removal after hardening. Forms were then fastened along the sides before the mixture was placed. The restraint was achieved through three 125mm threaded bars at each L-shaped support extending approximately 75mm in to the composite.

Directly after casting, the surface was covered by plastic foil to allow for a curing period of 24 hours. The test was then initiated by removing the cover and the form sides. The plate underneath the composite was gently removed to ensure that no restraint would be generated along the bottom of the specimen. Two sets of target points for deformation measurements were evenly distributed and glued to the surface at an individual distance of 100 mm. A total of four measuring distances were obtained along the specimen. For some of the tests additional target points were positioned at one of the L-shaped supports. The process of testing was initiated after one day of curing, For each mix, two specimens were tested simultaneously in the test frame, one for restrained and one for free shrinkage measurement. The free shrinkage test was used to give information on the rate and magnitude of free deformation of the material used.

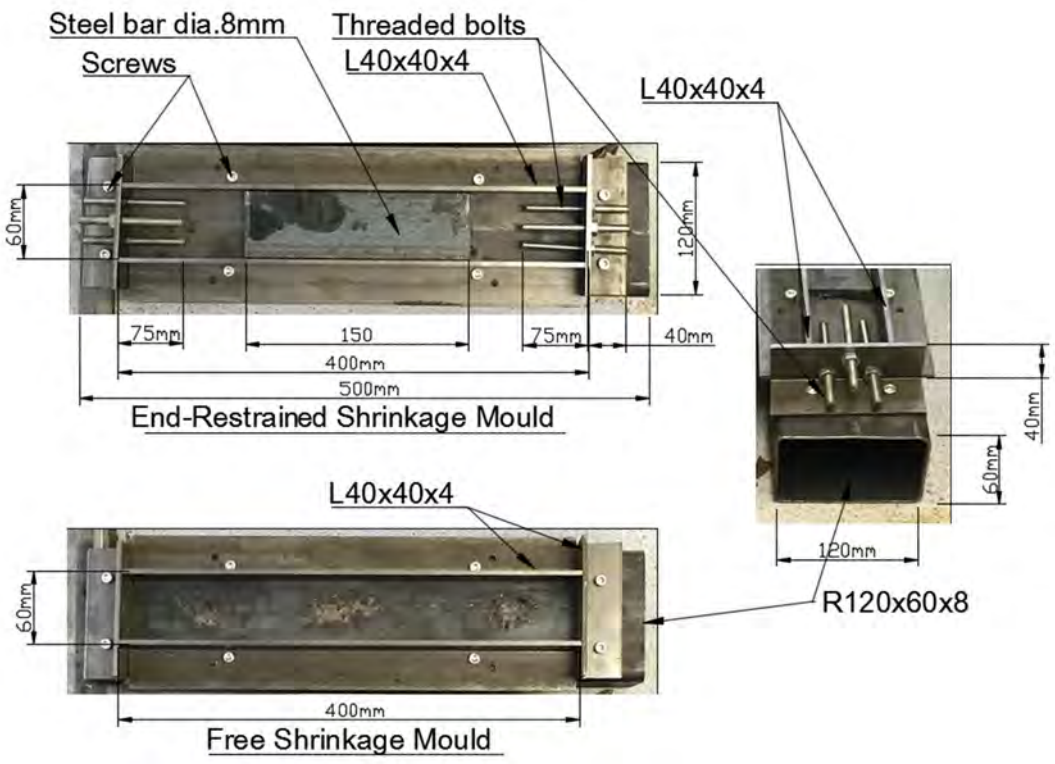

Figure 3.15 End-restrained test set up.

3.7.2 Sulfuric Acid Resistance Experiment Details

This test was conducted on cementitious composites containing nanofilaments (i.e CNT, and CNF) to understand the composite's behaviour under an acidic environment.

Sulfuric acid solutions-The test cubic specimens were immersed in jars filled with equal quantities of 5% sulfuric acid solutions (pH =1). This concentration of sulfuric acid is representative of that found in acidic environments (e.g. sewers) that are in the process of deterioration. The pH levels of the acid solutions were monitored at an average interval of one week with a portable pH meter. The periodic testing of the acid

solutions along with the use of small test cubic specimens provided an accelerated evaluation of the acid resistance of the concrete mixes.

Measurements of the test Cubic Specimens-Test were performed after 90days of immersion in the acid. The test specimens were removed from the acid, washed with fresh water several times, and oven-dried for 24 hr. Upon removal from the oven, the three test specimens of each mix were weighed and then tested under compression.

Scanning electron microscope (SEM) examination For the SEM examination of each specimen type, small fractured specimens, approximately 6mm thick x 12mm long x 6mm high, were prepared from one of the test specimens that had been marked for microscopic examination. A typical specimen, as mounted on a stud, is shown in Figure3.16. To obtain clear photomicrographs (and avoid sample charging), the top surface of the fractured specimens was rendered conductive with a sputtered layer of carbon. Photomicrographs were taken of specimens with and without nanofilaments.

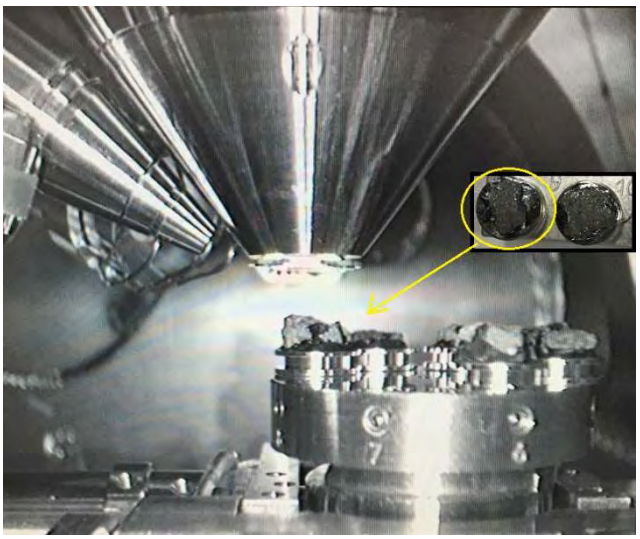

Figure 3.16 SEM specimen as mounted on studs in the electron beam.

Chapter Four:

Dispersion of MWCNTs for Cementitious Application: Effect of Sonication Intensity, Surfactants, and Mineral Admixtures

4.1 Introduction

When producing cementitious/CNTs composites with improved mechanical performance, there are four key areas and two main challenges that need to be addressed and understood (Figure 4.1). The key areas are i) the properties and effects of the MWCNTs used in the nano composite fabrication, ii) the properties and effects of the surfactants used in the dispersion process, iii) the effect of the dispersion method used on the integrity/structure of nanotubes, and iv) the orientation of nanotubes within the composites. The two main challenges are: i) optimising effective dispersion techniques for carbon nanotubes in water, and maintaining this dispersion level and preventing re-agglomeration within the composites; and ii) enhancing the bond strength of nanotubes with the surrounding matrix. In this chapter, the properties of nanotubes and surfactants, and achieving a novel and effective dispersion of the nanotubes will be addressed (the remaining factors would be recommended for future study).

As the reinforcing efficiency is proportional to the amount of dispersed nanotubes in the composites(Chen 2016), in this chapter different methods have been employed to optimise a novel dispersion technique that leads to a higher sustained concentration of individual nanotubes in water and consequently significant reinforcing efficiency throughout a cementitious composite.

This chapter presents the outcomes of the dispersion method testing described in (Chapter Three, Section 3.4). Specifically, this chapter presents:

1- Optimisation of the effect of sonication conditions on the dispersion of nanotubes in water and in cementitious composites. The study was conducted using three different sonication intensities and various treatment times, and the

relationship between the concentrations of nanotubes (individually dispersed) with the sonication intensity and treatment duration (phase I).

2- Optimisation of the effectiveness of surfactants in aiding the dispersion of nanotubes in water and their compatibility with the cement, (phase II).

3- Optimisation of the effect of microsilica in preventing the re-agglomeration of nanotubes through the cementitious composite and improving the bond with the surrounding matrix, (phase III).

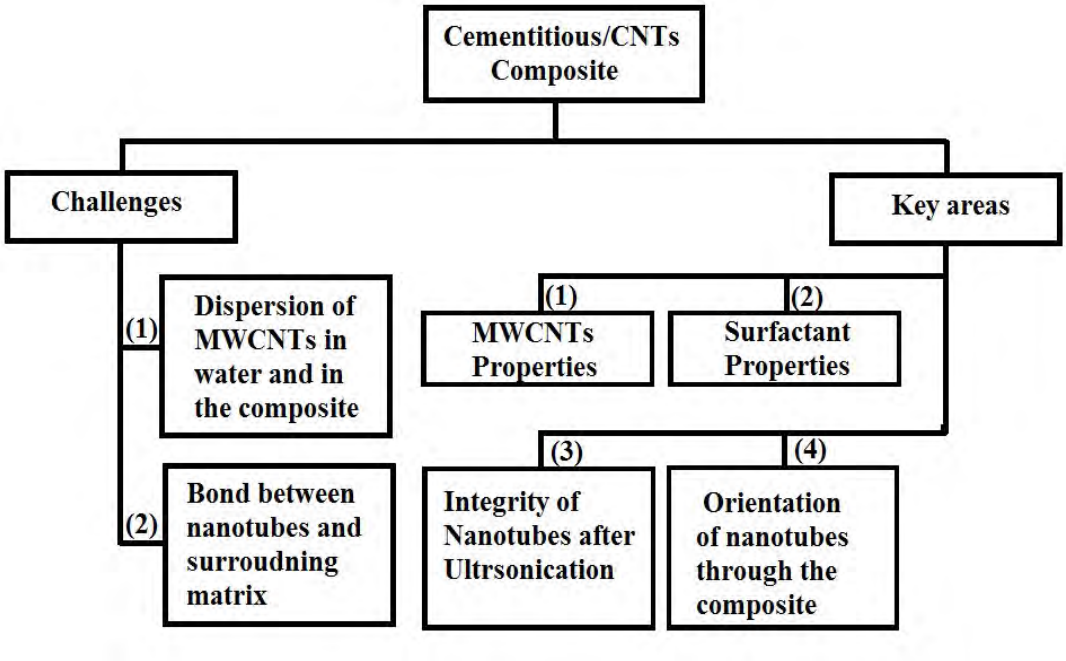

Figure 4.1 A schematic diagram showing the challenges affecting the positive performance of MWCNTs through cementitious composites, and the key areas that need to be investigated to understand micro-structural development in cementitious/CNT composites.

4.2 Phase I: Effects of Sonication Intensities and Duration

4.2.1 Overview

Although the ultrasonic technique has been proven as an emerging and effective method for dispersing agglomerated nanotubes for a wide range of applications (see Chapter Two, Section 2.4.1.2), to date producing an effective dispersion method for

cementitious application has been a challenging task (Maria et al. 2010). This section presents the results of experiments (Chapter Three Section 3.4.1) to optimise effective sonication intensities and durations. The results will be analysed and discussed as follows:

- Effect of sonicator intensities (Low, Moderate, and High intensity sonication) and treatment duration in combination with surfactant on the dispersion levels of carbon nanotubes in water. The results were derived via optical microscope measurements, UV-Vis spectroscopy, concentration characterisation, visual examination, and TEM.
- In this study, following the previous author's study, the delivered energy to the solution ranges between (20-86) J/ml, (52-125) J/ml, and (388-458) J/ml per min of Low, Moderate, and High intensity sonication respectively. The energy delivered (under a certain intensity) usually varies from treatment to other due to its influence by the solution viscosity, solution temperature, position of the probe, etc(Santos 2008, Fusion 2017).
- Effect of the proposed technique on performance of carbon nanotubes in different concentrations throughout a cementitious composite. These results were derived using compressive and direct tensile strength tests.
- Effect of varying water quantity on dispersion level and concentration of nanotubes (via UV-Vis spectroscopy).

4.2.2 Results and Discussion:

4.2.2.1 Dispersion Mechanism Using Ultrasonication- First Stage

The sonication waves delivered to the suspension were found to break down the interaction force (Van der Waal forces) between the agglomerated nanotubes, and separate them to an individual level in the aqueous solutions. Dispersion via sonication treatment is based on the induced energy (which varies and depends on the sonicator settings) causing micro and nano cavitation (i.e. vacuum-bubbles) to be formed among the solution molecules (Maria et al. 2010, Yan and Eugene 2012). These bubbles collapse violently when they touch the nanotubes surfaces. The collapsed bubbles will

cause a large pressure force that will pull the tubes/fibres away into the solution; hence, the CNTs become separated from each other in the liquid(Oxana V. et al. 2013). The intensity of the produced bubble depends on the amount of energy introduced to the solution and sonication time which subsequently affects the dispersion states. An excessive amount of applied energy/produced bubbles may break (i.e. shorten) the nanotubes. The effect of ultrasonication intensities on the integrity of nanotubes is partly discussed here, but forms an area which requires further investigation in future work.

During the separation process the dispersion agent (i.e. surfactant) molecules can easily adsorb onto the outer surfaces of nanotubes, and then prevent the re-aggregation of the nanotube. The mechanism of dispersion is known as the unzipping process (shown in Figure 4.2) and can be summarised as follows:

- Ultrasonication delivers a high shear force which acts to open gaps at the ends of the nanotubes bundles (Figure 4.2 b).
- Gaps between the neighboured tubes become new sites where surfactant molecules can be adsorbed on the outer surfaces, preventing re-aggregation (Figure 4.2c).
- With continuation of sonication, the opening-up of the tubes proceeds further, and will continuously allow surfactant muscles to adsorb up along the opened sections of the gap until a nanotube can be completely separated from the bundle (Figure 4.2d).

The amphiphilic nature of the dispersion agent (surfactant/polymer) simplifies the dispersion process, as their molecules adsorb at interfaces generating a repulsive force, and enhancing the tube surface wettability. These properties play an important role in the dispersibility and stabilization of nanotubes in water.

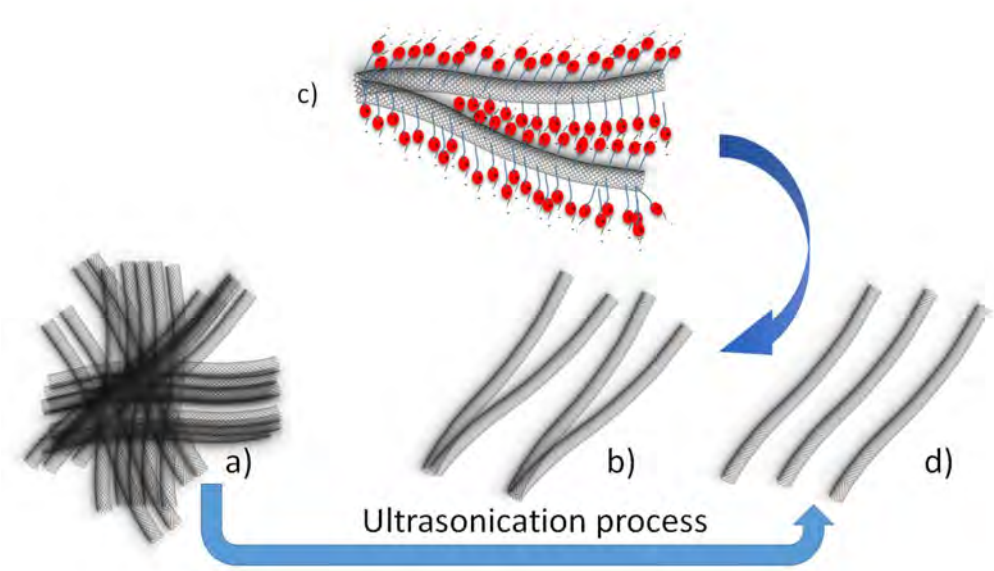

Figure 4.2 Schematic figure showing MWCNT unzipping mechanism using ultrasonication and surfactant-based superplasticiser. a) Agglomeration of MWNCNTs, b) and c) subsequent surfactant "unzipping" mechanism with sonication. (b) Stabilization of smaller bundles due to (c) adsorption of surfactant on the surfaces of the carbon nanotubes. d) individual MWCNTs.

4.2.2.1.1 Optical Microscope Measurements

Optical microscope images (shown in Figures 4.3) were conducted to examine the behaviour of nanotubes at the microscale. For these tests three nanotube suspensions were prepared (Figure 4.3 a, d, and g). In the first suspension, MWCNTs at 0.025% by cement weight (i.e. 8.7 mg/l) in 100 ml of water were mixed manually for two minutes. After agitation ceased images were taken at low magnification of X20, and X40, as shown in Figure 4.3b, and Figure4.3c, respectively. These images show large and dense clusters of carbon nanotubes at the micro-scale. In the second suspension (Figure 4.3 e, and f) a superplasticiser (PCE) in a ratio of 1:4 (MWCNTs-to-PCE) was added to the suspension, and manually mixed for two minutes. Although it was possible to achieve dark (i.e. apparently dispersed) suspensions after manually shaking for a few minutes, CNTs suspensions were not stable and only an initial (temporary) dispersion was achieved. After agitation was stopped, nanotubes rapidly re-agglomerated and sedimented at the bottom of the beaker. The re-agglomeration

mechanism can be attributed to the high Van der Waals interaction force between the nanotubes which creates a large and relatively heavy cluster which then rapidly settles to the bottom of the container. In the third suspensions, a stable and homogenised suspension was achieved after treatment via sonication in combination with surfactant (Figures 4.3 h, and i). Due to their extremely small diameter, individual CNTs are invisible under conventional optical microscopy. CNTs suspensions can be characterised using spectroscopy however, and the morphology of individual nanotubes was examined through TEM images.

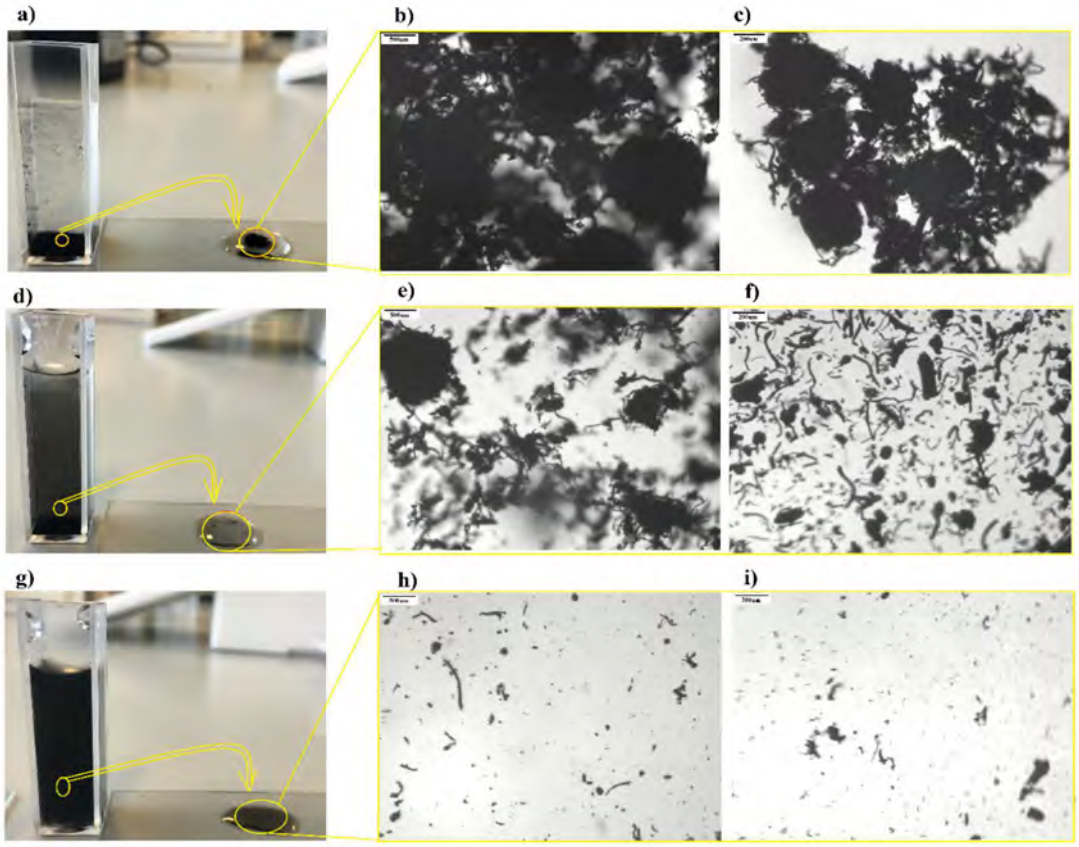

Figure 4.3 Photographic images showing nanotubes in the suspension a) before the addition of superplasticiser (PCE), and d, g,) after addition of PCE. The optical microscope images show MWCNTs suspensions: b& c) show large agglomerations of MWCNTs in suspension without PCE and sonication treatment, e& f) show relatively small clusters of nanotubes in suspensions containing PCE, and h, & i) showing the suspension treated using sonication in combination with PCE.

4.2.2.1.2 UV-Vis spectroscopy:

- Sonication Intensities and Treatment Durations

The effect of ultrasonication intensities (i.e. Low, Moderate, and High intensity sonication), and treatment durations (3, 5, 10, 20, 30, 40) min were qualitatively investigated via the recorded UV–Vis absorbance spectra. Spectra of thirty-three suspensions of MWCNTs with dosages of 0.01%, 0.025%, 0.05% wt. by cement weight (which are equivalent to 0.28mg/l, 0.714 mg/l, and 1.428 mg/l respectively), were recorded and shown in Figures 4.4, Figure 4.5, and Figures 4.6, respectively. Absorption by the sonicated suspensions was clearly observable in the UV-vis wavelength range between (350-800) nm, thus 500nm was selected as the characteristic absorption wavelength. This wavelength is virtually unaffected by ambient conditions of nanotubes as reported by(Rastogi 2008) . With each intensive sonication, the corresponding absorbance of the suspensions was plotted as a function of the sonication time, represented in Figure 4.7. The experimental outcomes can be summarised as follows:

- Absorbance values steadily increased with increasing nanotube concentrations in the suspension.
- At all sonication intensities, absorbance values for the first treatment interval were relatively low compared to the values given by longer treatment durations.
- After 20 minutes of treatment, the absorbance values of suspensions sonicated under condition of low and moderate internists were relatively similar.
- A short treatment duration (i.e. 5 min) at high sonication intensity resulted in higher absorbance values compared to longer treatments at low and moderate sonication intensity.

It is well known that higher absorbance values reflect higher concentrations of well dispersed nanotubes in the suspensions, (Yonghui Liu 2010). Lower absorbance values show that the majority of the nanotubes remain in an agglomerated state and the applied energy is not enough to begin the exfoliation process.

The UV-vis spectra show that absorbance values are highly dependent on the ultrasonic treatment conditions (i.e., sonicator setting and treatment duration). Use of high sonication intensity gave a dramatic increase in absorbance (i.e. an increase in

the concentration of individual MWCNTs) after sonication for 5 minutes for all examined concentrations of added MWCNTs.

Overall, high intensity sonication gave the highest degree of dispersion of MWCNTs in water. Use of lower sonication intensities required longer time periods to generate effective dispersions. After 20 minutes of treatment duration under low and moderate sonication intensities the absorbance gradually increased, although some agglomerated nanotubes in the suspension were still visible. The absorbance was significantly increased at around 40 min of treatment duration, with no appreciable settling/sedimentation for at least several hours. Given these extended treatment durations for effective dispersion at lower sonication intensities, a minimum sonication time of 5 min over a high sonication intensity (of 100% amplitude) was adopted as a facile method for dispersion of the nanotubes for civil engineering application, with less time and energy consumed.

Although the absorbance values tend to increase when treatment duration increased, the treatments in this study were stopped at 40 minutes with low and moderate intensity sonication, and at 5 minutes with high intensity sonication, to avoid a) impact of increasing suspension temperature, and b) the physical breakage of the tubes. The effect of rising suspension temperature as a result of high sonication intensity on the performance of nanotubes through the cementitious composites should be investigated in future work.

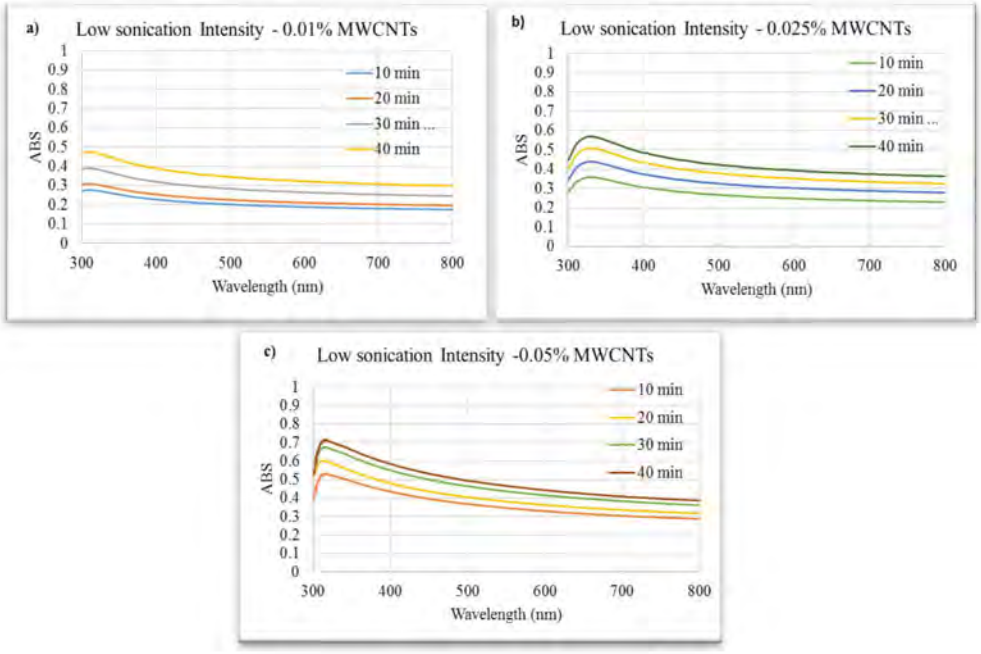

Figure 4.4 UV-visible spectra of aqueous suspensions with different concentration of MWCNTs subjected to Low sonication intensity. (a), (b), and (c) represent the absorbance of MWCNTs at 0.01%, 0.025%, 0.05%, respectively.

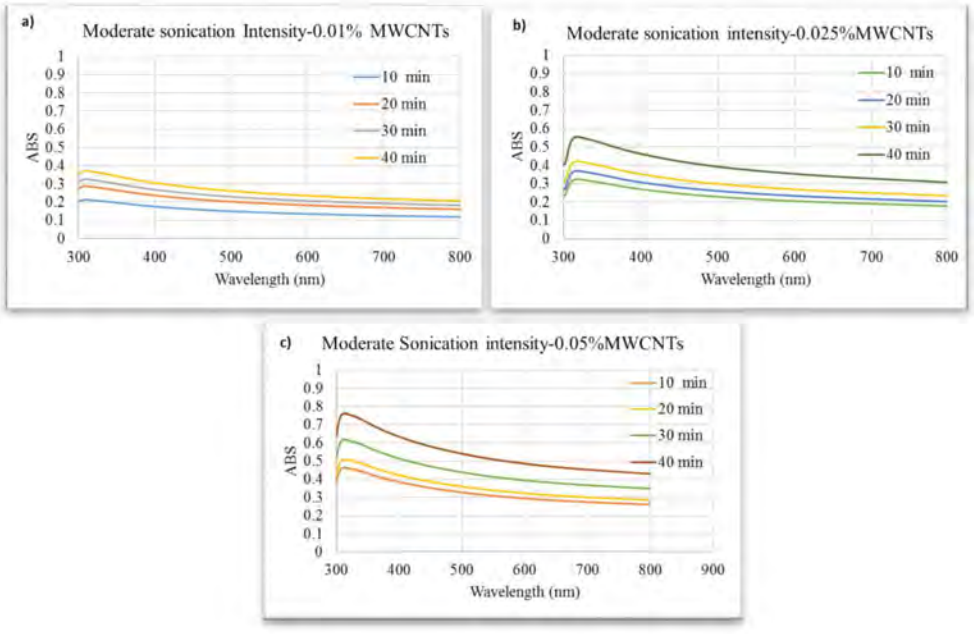

Figure 4.5 UV-visible spectra of aqueous suspensions with different concentration of MWCNTs subjected to moderate sonication intensity. (a), (b), and (c) represent the absorbance of MWCNTs at 0.01%, 0.025%, 0.05%, respectively.

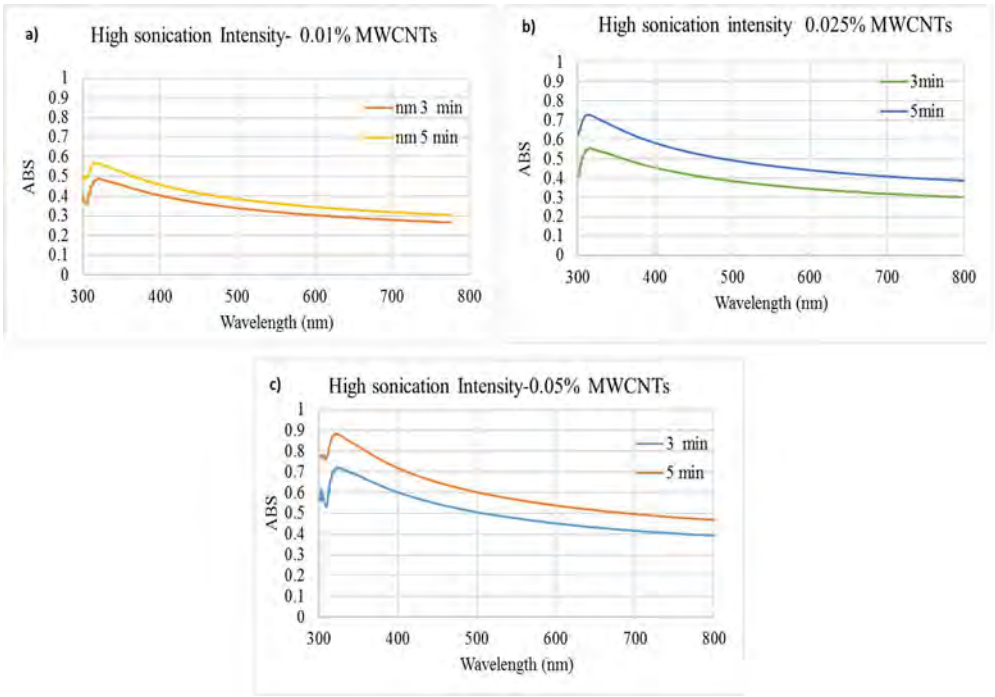

Figure 4.6 UV-visible spectra of aqueous suspensions with different concentration of MWCNTs subjected to high sonication intensity. (a), (b), and (c) represent the absorbance(ABS) of MWCNTs at 0.01%, 0.025%, 0.05%, respectively.

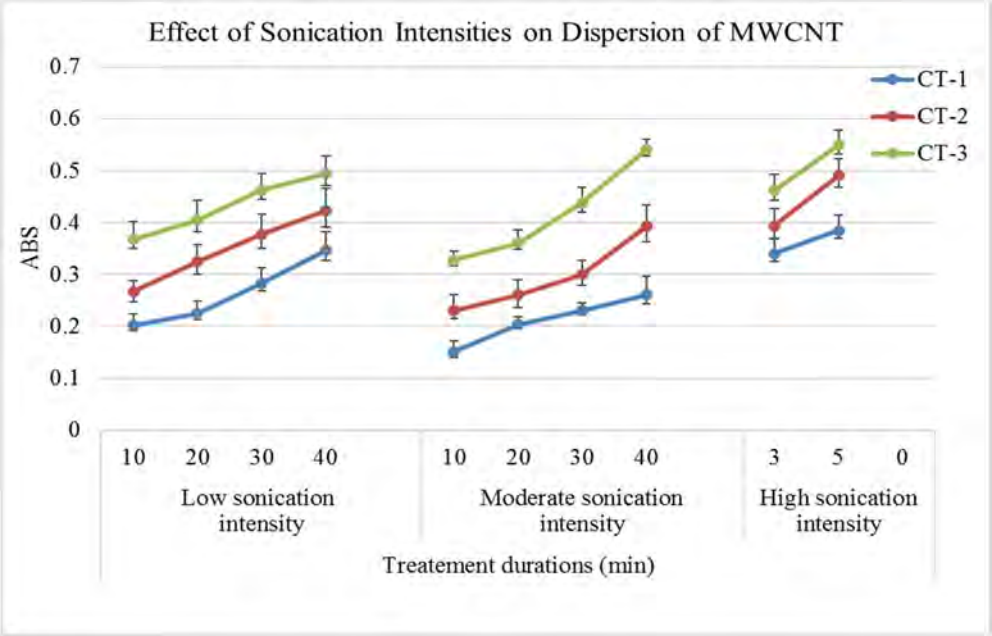

Figure 4.7 Absorbance of MWCNTs suspension treated using different sonication conditions (i.e. moderate and high intensity), absorbance values (ABS) were recorded at 500nm for different sonication durations.

- Concentration of Dispersed CNTs

UV-Vis absorbance data were also used to evaluate the concentration of individually dispersed nanotubes in the solution. The dispersion assessment is critically dependant on the existence of a linear relationship between absorbance at a certain wavelength and concentration of dispersed, suspended MWCNTs.

Data confirmed that a linear relationship between absorption values and nanotubes concentration was present for three suspensions of nanotubes (0.28mg/l, 0.71mg/l and 1.43mg/l) at different concentrations, following Beer's law (Bo et al. 2015). Concentrations showed in Figure 4.8a, Figure 4.9a, and Figure 4.10a represent the last six solution which were prepared by diluted the starting MWCNT suspensions (0.28mg/l, 0.714mg/l, 1.43mg/l) by certain factors in Figure 4.8a the dilution factors were 1:1, 1:2, 1:4, 1:8, 1:16, and 1:32, and in Figure 4.9a the dilution factors were 1:1, 1:2, and1:1.25, and then 1:1, 1:2, 1:4, 1:8, 1:16, 1:32, and in Figure 4.10a the dilution factors were 1:1, 1:2, 1:2, and 1:1.25, and then:1, 1:2, 1:4, 1:8, 1:16, 1:32. Inset images shown in (b) represent the UV–vis spectra of MWCNTs of the prepared

concentrations of carbon nanotubes in PCE surfactant aqueous solution. The recorded absorptions decreased with decreasing MWCNTs concentration in aqueous solutions, and a linear relationship between absorption and concentration, following Beer's law, could be observed between 300nm to 800nm in the inset images (c).

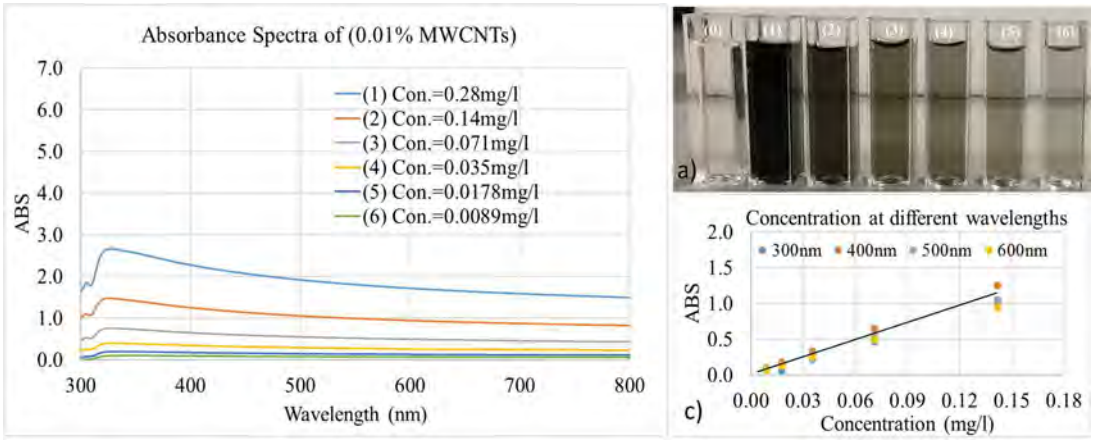

Figures 4.8 a) Optical micrograph of 0.01%MWCNTs suspensions at different concentrations: (1) 0.28 mg/L (starting MWCNT solution), (2) 0.14 mg/L, (3) 0.071 mg/L, (4) 0.035 mg/L, (5) 0.0178 mg/L, and (6) 0.0089 mg/L (b) recorded UV-vis spectra at wavelengths 300nm-800nm. (c) absorption as a function of concentration of the MWCNTs suspensions conducted at the wavelength of (300, 400, 500, and 600) nm.

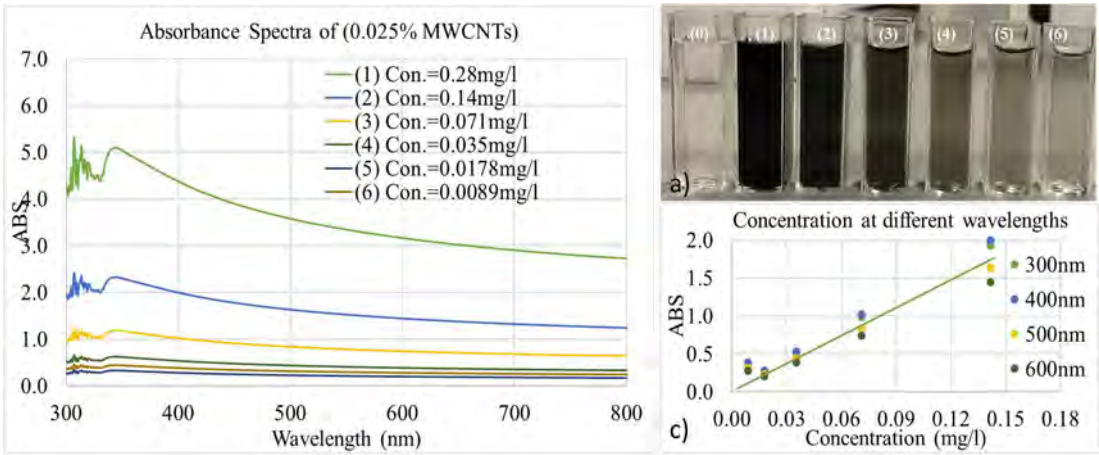

Figures 4.9a) Optical micrograph of the 0.025%MWCNTs suspensions at different concentrations: (1) 0.285 mg/L (starting MWCNT solution), (2) 0.143 mg/L, (3) 0.0714 mg/L, (4) 0.035 mg/L, (5) 0.0179 mg/L, and (6) 0.0089 mg/L (b) recorded UV-

vis spectra at wavelength 300nm-800nm. (c) absorption as a function of concentration of the MWCNTs suspensions conducted at the wavelength of (300, 400, 500, and 600).

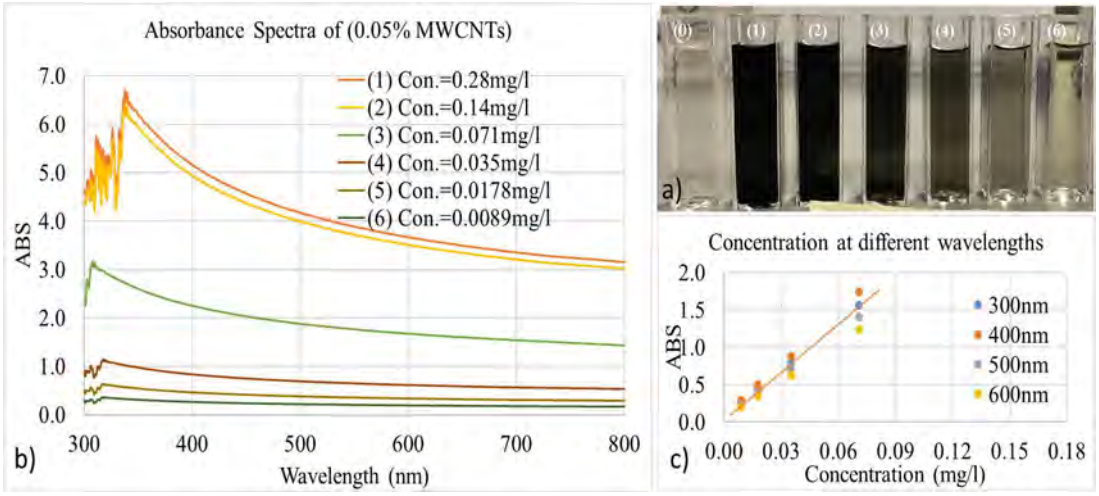

Figures 4.10 a) Optical micrograph of the 0.05%MWCNTs suspensions at different concentrations: (1) 0.285 mg/L (starting MWCNT solution), (2) 0.143 mg/L, (3) 0.0714 mg/L, (4) 0.035 mg/L, (5) 0.0179 mg/L, and (6) 0.0089 mg/L (b) recorded UV-vis spectra at wavelength 300nm-800nm. (c) absorption as a function of concentration of the MWCNTs suspensions conducted at the wavelength of (300, 400, 500, and 600).

The obtained results revealed that the increased addition of nanotubes up to 1.428 mg/l could affected the efficiency of the proposed technique in the dispersion of nanotubes to the individual level. For example, at an absorbance value of 1, the concentration of individual nanotubes in a suspension of 0.01% (Figure 4.9) was 1.2 mg/l, and in the second suspension at 0.025% (Figure 4.10) was about 1.1mg/l, while in the third suspension at 0.05% (Figure 4.11) this was about 0.05 mg/l. This result indicates that suspension of low ratios of nanotubes (between 0.01%-0.25%) gives a higher concentration of individual nanotubes. Thus, while absorption spectroscopy can be used as an effective investigation tool for monitoring the dispersion state of nanotubes in suspension, it is essentially a semi-quantitative tool requiring concentration-dependent calibration.

4.2.2.1.3 Visual Examination

Two sets of aqueous MWCNTs suspensions were prepared for visual examination of sedimentation following ultrasonication and surfactant treatment. Visual observations of sedimentation were taken over 1–3 days and initial conclusions were drawn as to the most effective dispersion method on suspension stability.

The first set was treated with the addition of surfactant (PCE) and manually mixed for 2 min. After cessation of mixing, photographs (Figures 4.11a) were taken over one hour (immediately after cessation of mixing, and then after each 20-minute settling time). The second set of suspensions underwent 5 min of high-intensity ultrasonic treatment, then clear glass vials were filled with the suspension and allowed to settle for one hour (for comparison with set one) at which intervals photographs (Figures 4.11b) were taken. With only manual mixing and PCE addition, large clusters of nanotubes were suspended with the first 20 minutes prior to their agglomeration and settling at the bottom of the glass vials. After sonication (set two), a more homogeneous suspension was obtained, with photographs taken after one hour showing that the MWCNTs suspension had remained stable for all of the examined durations.

Compared to the suspension without sonication treatment, it can be argued that a high sonication intensity over a short time period, combined with use of PCE, is sufficient to generate a coating of PCE on the nanotubes. This induces electrostatic repulsion and counterbalances the Van der Waals attractive force, and leads to a more homogenous and stable suspension. As a high intensity ultrasonic wave passes through the solution, it rapidly generates a large number of cavitation bubbles which then collapse, and enhance surfactant penetration between the tubes/fibres.

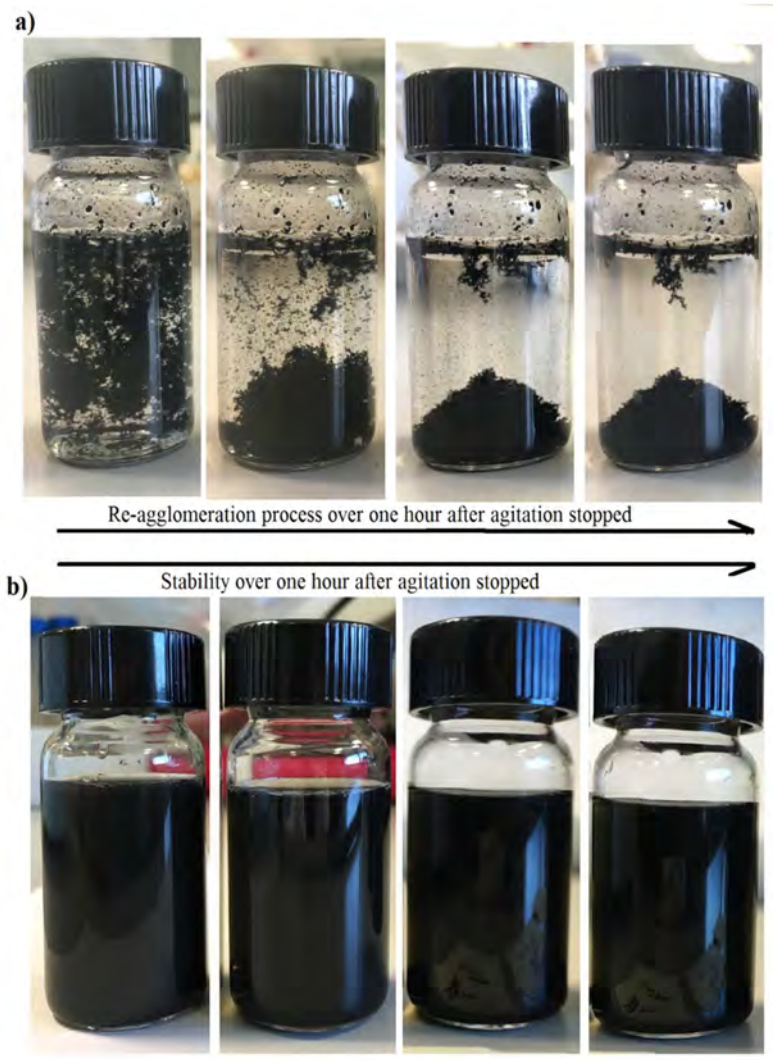

Figures 4.11 Micrographs of MWCNTs dispersions in water in the presence of PCE surfactant prepared by means of a) a manual shaking for 2 minutes and b) a high-intensity probe type sonication process for 5 min. The photographs were taken immediately after treatment and then after 20 minute intervals.

4.2.2.1.5 Transmission Electron Microscopy (TEM)

Figures 4.12 (a, and b) show low and high magnification TEM images of carbon nanotubes manually mixed with the presence of PCE. Without ultrasonication treatment, most of the carbon nanotubes appear as clusters on the TEM grid with average clusters diameters of about 500-1000 nm, and no individual tubes can be observed, which is attributed to the strong tube-tube interaction forces, and the hydrophobic nature of the tubes, which make the use of only surfactant insufficient to create the required repulsive force to disperse them to an individual tubes level.

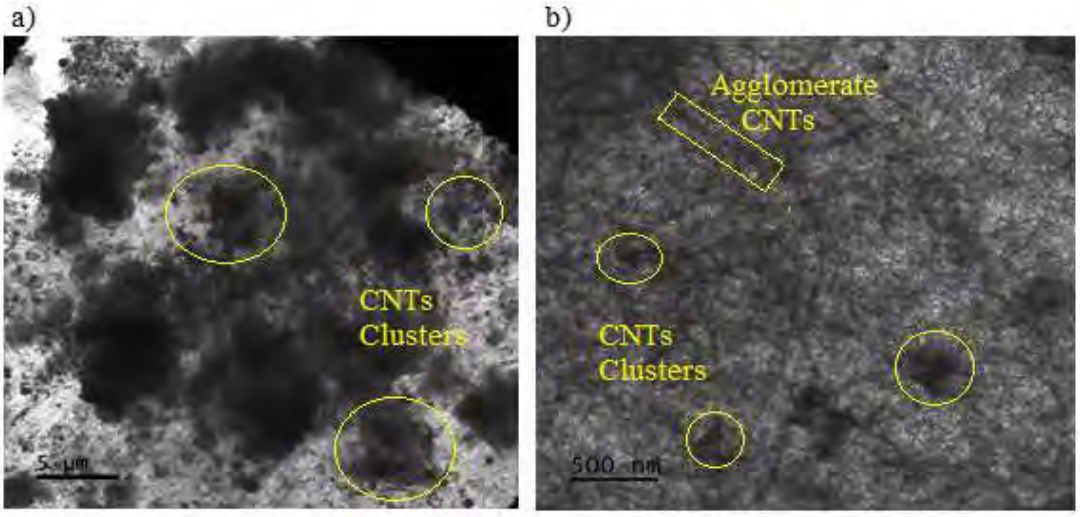

Figure 4.12 TEM images showing nanotubes suspensions treated via manually shaking over 2 minutes, a) low magnification image showing large clusters of nanotubes, b) high magnification image showing clusters and bundles of nanotubes.

High magnification images (Figure13a-f) show the morphology and nanotubes characterisation following dispersal via high sonication intensity over a short time duration. The images show:

- Ultrasonication at high intensity over even very short time intervals (i.e. 5 minutes) was found to produce suspensions with high concentrations of individual dispersed nanotubes, Figure (13a-b).

- A layer of PCE can be observed on the outer surface of nanotubes in varying thicknesses ranging from 5nm-15nm.
- Few bundles of nanotubes with average diameters (50-100) nm can be observed, Figure (13c-f).
- Individual nanotubes can be observed with diameters in the range of (25-50) nm, the tube thickness increases with increasing thickness of the observed PCE layer on the walls of nanotubes, Figure (13c-f).
- The PCE adsorbs onto the nanotube surfaces and creates repulsive forces, which dominate over attractive Van der Waals forces between the carbon nanotubes. This balance of repulsive and attractive forces creates a thermodynamically stable dispersion, which might even result in the separation of nanotubes from the bundles into individual tubes. Figure (13c-e).

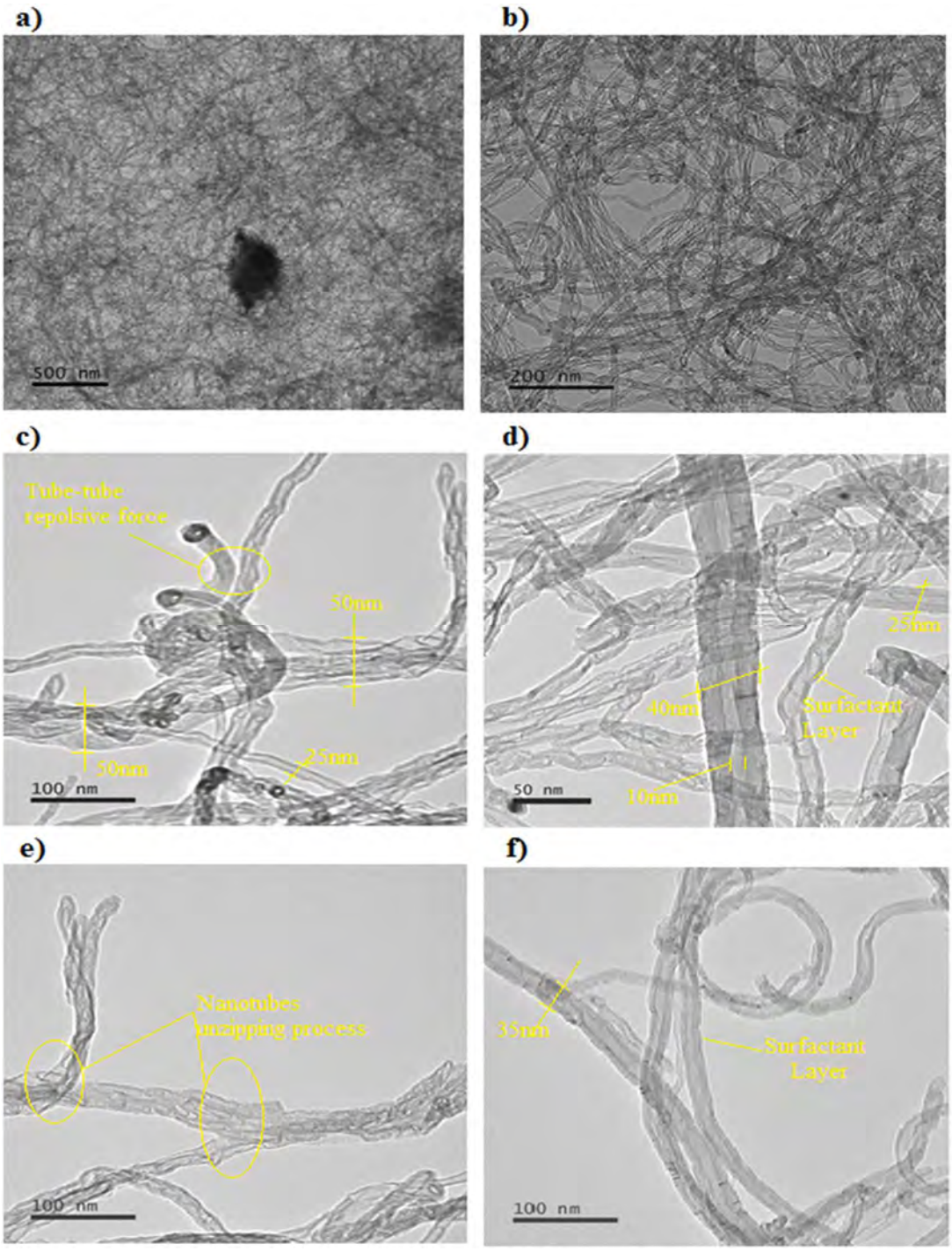

Figure 4.13 TEM images showing the dispersion status of nanotubes suspensions dispersed via high sonication intensity over 5 minutes (images a, and b), and the geometry of the nanotubes and the dispersion mechanism with the presence of PCE (images c-f).

4.2.2.2 Mechanical Characterisation and Microstructural analysis: Second Stage

Compressive strength and direct tensile strength tests were conducted on cementitious/CNTs composites to investigate the efficiency of nanotubes dispersal via different sonication intensities (Low, Moderate, and High). Three different dosages of MWCNTs were examined (0.01, 0.025, and 0.05) wt.%, labelled CT-1, CT-2, and CT-3 respectively.

4.2.2.2.1 Compressive Strength

The obtained results of compressive strength of nanotubes cementitious composites at 3 days and 28 days are summarised in Table 4.1, and Table 4.2, and presented in Figure 4.14, and Figures 4.15, respectively. The compressive strength as function of sonication intensity, treatment duration, and nanotube concentration was presented in the graphs of (a, b, and c), which represent the effect of low, moderate, and high intensity sonication, respectively. Moreover, graph (d) shows the improvement in compressive strength of CT-1, CT-2, and CT-3 relative to a control mix (PC) as a function of sonication intensities and treatment duration.

The results revealed that the agglomerated CNTs (added without dispersion) led to marginal improvements in compressive strength at early age, at a maximum of 16% improvement at 0.05 wt.% CNT concentration. These results can be attributed to the "filler effect" of agglomerated nanotubes which potentially contribute in refining large structural pores at early age and so enhance the density. At 28 days, the nanotube effect on compressive strength was diminished, which can be attributed to the significant increases in packing density from generated hydration products, which mask the filling effect of nanotubes.

At early age, compressive strength (3 day), the results indicate that when the nanotube suspensions were dispersed via low sonication intensity over four different treatment durations (10, 20, 30, 40) minutes, the effect of nanotubes in enhancing the compressive strength ranged between (10% - 20%), (16 %- 26%), and (14% - 23%), at 0.01, 0.025, and 0.05 wt.% MWCNT dosage (i.e. CT-1, CT-2, and CT-3)

respectively. When increasing the sonication intensity to a moderate level (over the same sonication durations), a significant improvement in compressive strength was obtained, with the improvements for the same concentrations of nanotubes (CT-1, CT-2, and CT-3) ranging between (14% - 42%), (25 %- 45%), and (21% - 46%), respectively. High sonication intensity over short times (i.e. 3 and 5 minutes), gave a higher improvement in compressive strengths i.e.; CT-1, CT-2, and CT-3 showed improvements of (27% - 49%), (38 %- 53%), and (34% - 47%) respectively.

At 28 day, the enhancement in compressive strength for all the examined nanotubes suspensions ranged between (13%-16%), (15%-18%), (12%-15%), and (28%), (33%), (36%), and, (25%-36%), (42%), and (41%) when low, moderate, and high intensity sonication was applied in the dispersion process.

Evidently, the addition of low amounts of MWCNTs dispersed using different dispersion techniques led to varying improvements in compressive strength. This revealed that compressive strength could be influenced by the sonication intensity applied to the suspensions through the dispersion process. The strength was found to increase with increasing concentration of well dispersed nanotubes, rather than with the starting addition dosage. At higher sonication intensity and/or long treatment durations, higher concentrations of individual nanotubes were obtained. These results are in good agreement with previous findings (see Chapter Two, Section 2.5.1).

The resulting higher strength is believed to be due to the physical contribution of well dispersed carbon nanotubes which act to fill in-between the composite structural pores which then reduce the porosity of the matrix, and contribute to denser cement composites. Also, nanotube (bundles or individual) bridging effects can improve the material's ability to delay micro-crack formation and enhance the load bearing capacity of the cement matrix (Li et al 2005, Han 2011) by bridging across neighbouring hydration products.

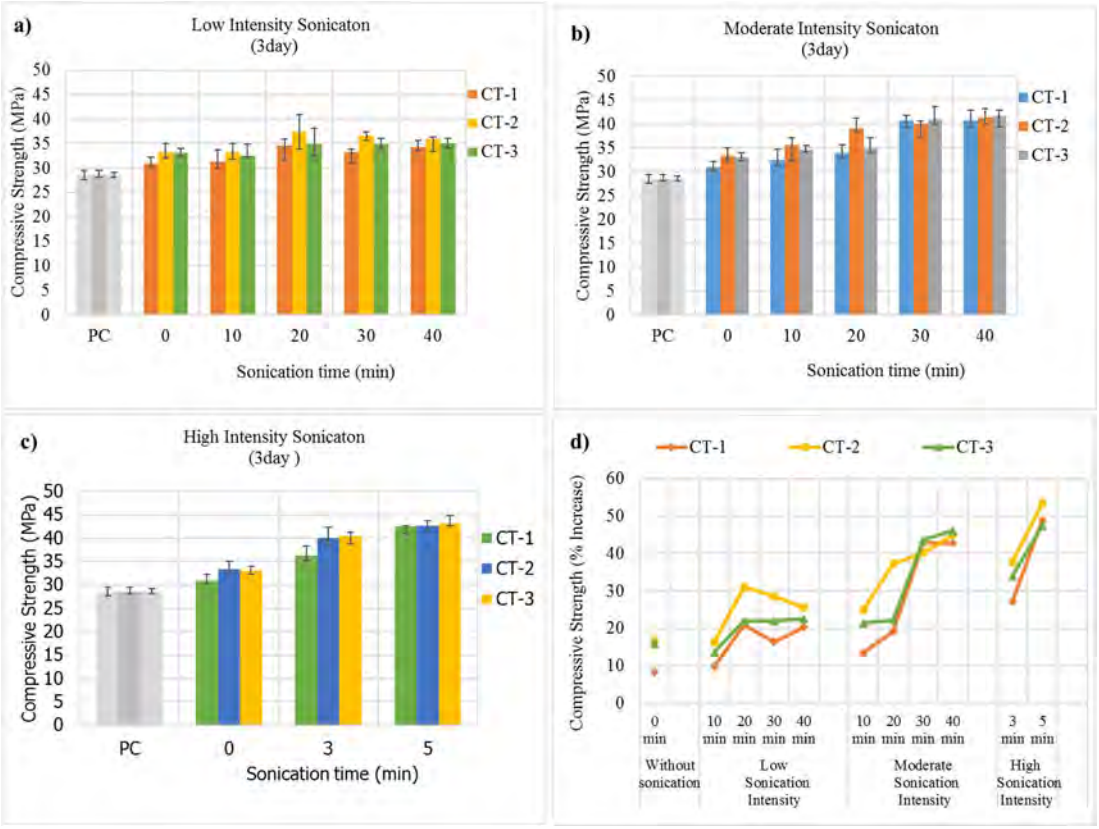

Figure 4.14 3 days' compressive strength of nano cementitious composites containing three dosages of MWCNTs (CT-1, CT-2, CT-3) dispersed using a) low sonication intensity over (10, 20, 30, and 40) minutes, b) moderate sonication intensity over (10, 20, 30, and 40) minutes, c) high sonication intensity over (3, and 5) minutes, (error bars represent values within one standard deviation of the mean), and d) relative improvement in compressive strength compared to control mix.

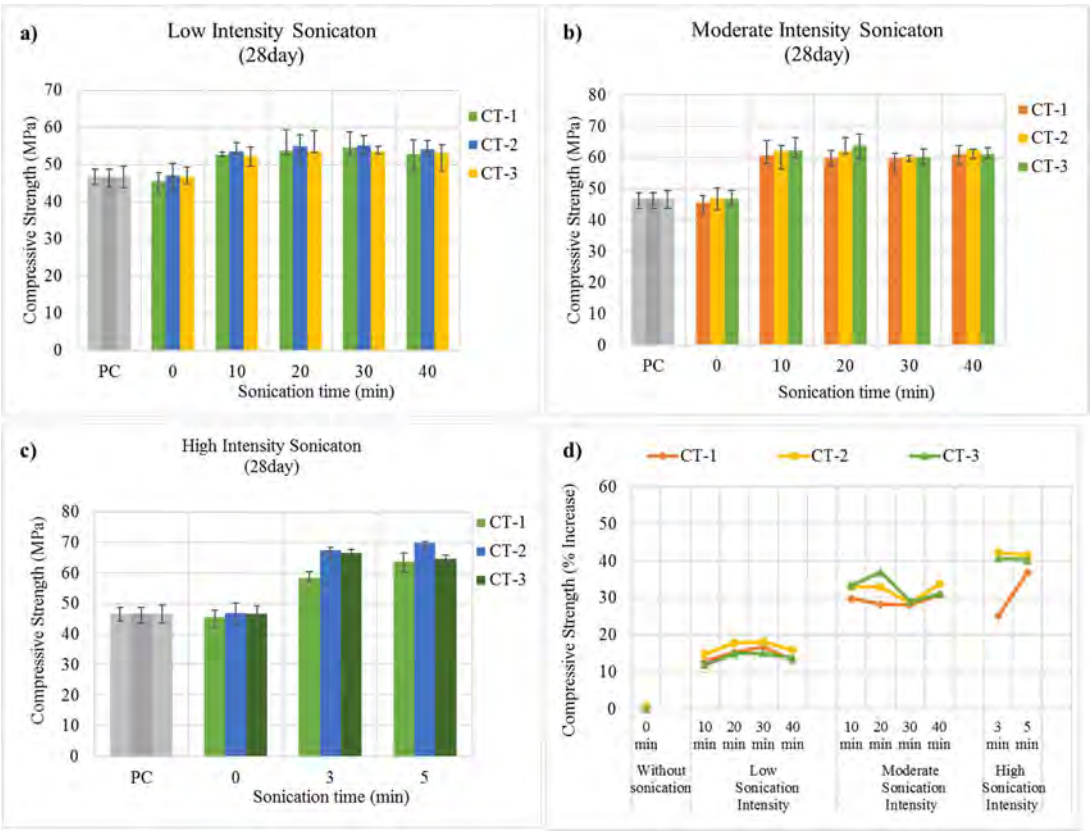

Figure 4.15 28 days' compressive strength of cementitious nanocomposites containing three dosages of MWCNTs (CT-1, CT-2, CT-3) dispersed using a) low sonication intensity over (10, 20, 30, and40) minutes, b) moderate sonication intensity over (10, 20, 30, and 40) minutes, c) high sonication intensity over (3, and 5) minutes, (error bars represent values within one standard deviation of the mean), and d) relative improvement in compressive strength compared to control mix.

Table 4.1 Compressive strength of nano cementitious composites after 3 and 28 days of curing containing three dosages of MWCNTs (CT-1, CT-2, and CT-3) dispersed under various sonication conditions.

Mix ID	Treatment Duration	Sonication Conditions	Compressive strength After 3 days		Compressive strength After 28 days	
			Mean (MPa)	S. D	Mean (MPa)	S. D
control	-	-	28.56	0.83	46.63	2.58
CT-1	10	Low intensity	31.37	1.97	52.61	0.66
CT-1	20		34.52	3.16	53.80	5.36
CT-1	30		33.25	0.94	54.45	3.66
CT-1	40		34.35	2.07	52.79	4.45
CT-2	10		33.22	2.18	53.57	2.35
CT-2	20		37.41	3.16	54.94	4.94
CT-2	30		36.71	1.88	55.10	2.76
CT-2	40		35.84	1.02	54.12	3.74
CT-3	10		32.45	1.69	52.24	2.50
CT-3	20		34.83	3.09	53.63	2.80
CT-3	30		34.83	1.81	53.66	2.51
CT-3	40		34.99	0.79	53.09	4.00
CT-1	10	Moderate intensity	32.41	3.01	60.56	5.44
CT-1	20		34.02	1.50	59.83	2.20
CT-1	30		40.79	2.36	59.71	1.53
CT-1	40		40.76	5.03	61.04	2.68
CT-2	10		35.68	0.90	62.04	3.54
CT-2	20		39.21	1.98	61.98	3.11
CT-2	30		40.04	2.26	60.06	3.81

CT-2	40		41.40	1.19	62.40	2.90
CT-3	10		34.65	1.37	62.20	2.26
CT-3	20		34.91	1.80	63.88	4.26
CT-3	30		41.01	0.81	60.20	2.23
CT-3	40		41.71	3.30	61.09	1.32
CT-1	3	High intensity	36.33	1.82	58.33	2.54
CT-1	5		32.21	0.93	63.83	2.62
CT-2	3		39.35	1.10	66.33	0.89
CT-2	5		43.78	1.52	65.97	3.48
CT-3	3		38.24	2.08	65.64	1.17
CT-3	5		42.09	0.98	65.39	0.64

4.2.2.2.2 Direct Tensile Strength

The direct tensile strength was found to be significantly influenced by the addition of nanotubes, and by the sonication intensity used in the dispersion process as summarised in Table 4.2 and Table 4.3. The results revealed that the agglomerated CNTs (added without dispersion) had a limited influence on the direct tensile strength. This behaviour is in agreement with many published literature. Figures 4.16 presents the obtained results of the direst tensile testing, inset (a), (b), and (c) show the effect of low, moderate, and high intensity sonication, respectively, and (d) shows the improvement in tensile strength of specimens containing three different dosages of carbon nanotubes (CT-1, CT-2, and CT-3) relative to the control mix PC.

Nanotubes suspensions of CT-1, CT-2, and CT-3 treated via low intensity sonication over four different treatment durations (10, 20, 30, 40) minutes were found to enhance the tensile strength of the composites by (11-27)%, (24-41)%, and (22-45)%, although improvements with increasing treatment time were variable. Treatment via moderate sonication intensity led to greater enhancements ranging between (42-68) %, (70-84) %, and (59-77) %, respectively, while high sonication intensity over short times (i.e.

3 and 5 minutes) led to significant improvement of (29-83) %, (35-86) %, and (42-87) %, respectively, as shown in insets (d). Greater sonication durations at moderate and high sonication intensities resulted in greater improvements in tensile strength.

These results indicated that high sonication intensity over a short time period (up to 5 min) gave a higher concentration of well dispersed nanotubes which significantly improved tensile strength. Individually dispersed nanotubes can bridge across nanocracks and therefore guarantee higher load-transfer under tension. At a nano level, individual nanotubes arrest cement hydration products and prevent initiation of cracks, leading to higher mechanical strengths.

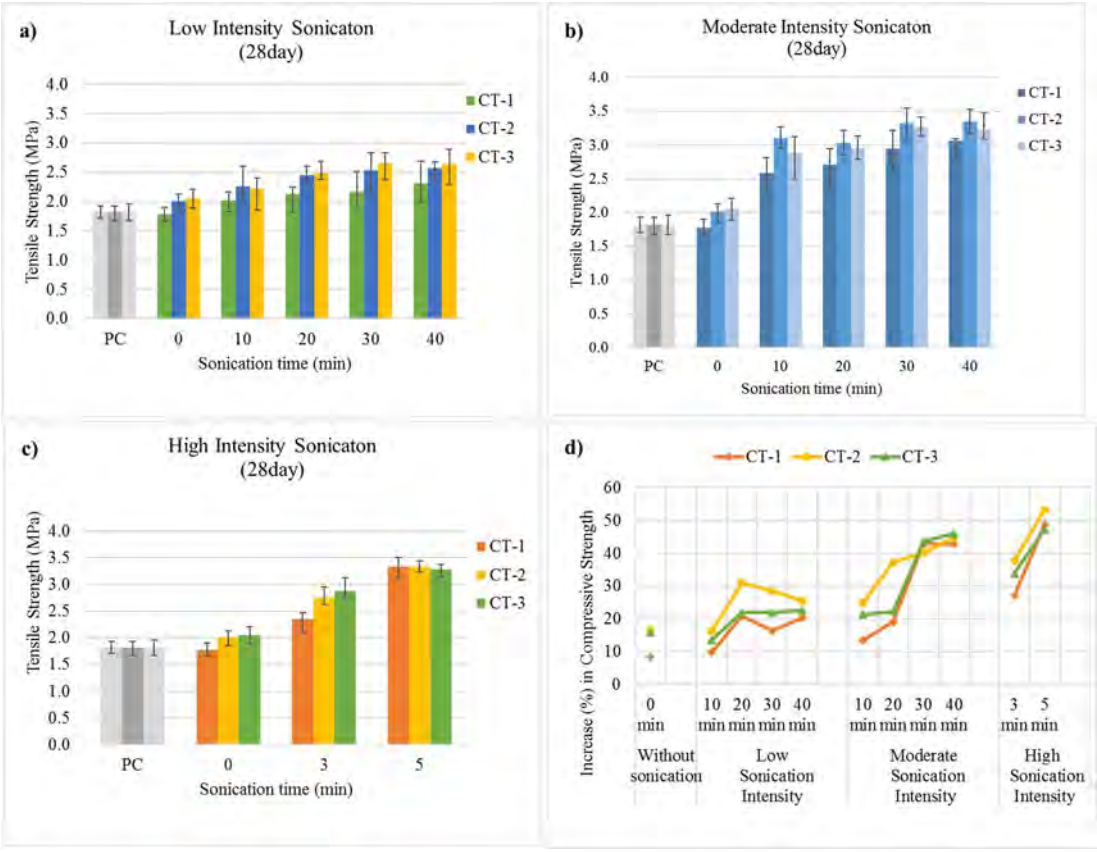

Figure 4.16 28 days' direct tensile strength of cementitious nanocomposites containing three dosages of MWCNTs (CT-1, CT-2, CT-3) dispersed using, a) low sonication intensity over (10, 20, 30, and 40) minutes, b) moderate sonication intensity over (10, 20, 30, and 40) minutes, c) high sonication intensity over (3, and 5) minutes, (error

bars represent values within one standard deviation of the mean), and d) relative improvement in tensile strength compared to control mix.

Table 4.2 Mechanical strength of cementitious nanocomposites composites after 3 and 28 days of curing containing three dosages of MWCNTs (T1, T2, and T3) without dispersion.

Mix ID	Compressive Strength				Tensile Strength	
	After 3 days		After 28 days		After 28 days	
	Mean	S.D	Mean	S.D	Mean	S.D
T1	30.94	1.11	45.52	3.67	2.13	0.11
T2	33.31	1.48	47.02	4.05	2.17	0.13
T3	33.08	0.83	46.70	4.03	2.37	0.24

Table 4.3 Direct tensile strength of cementitious nanocomposites after 28d of curing containing three dosages of MWCNTs (CT-1, CT-2, and CT-3).

Mix ID	Treatment Duration	Sonication Conditions	Tensile strength After 28 days	
			Mean (MPa)	S. D
CO	-	-	1.82	0.13
CT-1	10	Low intensity	2.02	0.46
CT-1	20		2.13	0.08
CT-1	30		2.16	0.72
CT-1	40		2.31	0.18
CT-2	10		2.26	0.52
CT-2	20		2.45	0.20
CT-2	30		2.53	0.26

CT-2	40		2.57	0.21
CT-3	10		2.23	0.38
CT-3	20		2.48	0.18
CT-3	30		2.65	0.30
CT-3	40		2.64	0.20
CT-1	10	Moderate intensity	2.59	0.41
CT-1	20		2.71	0.16
CT-1	30		2.95	0.54
CT-1	40		3.06	0.76
CT-2	10		3.10	0.41
CT-2	20		3.03	0.40
CT-2	30		3.32	0.23
CT-2	40		3.35	0.23
CT-3	10		2.89	0.32
CT-3	20		2.95	0.20
CT-3	30		3.26	0.36
CT-3	40		3.23	1.61
CT-1	3	High intensity	2.35	0.10
CT-1	5		3.33	0.12
CT-2	3		2.46	0.24
CT-2	5		3.39	0.21
CT-3	3		2.58	0.21
CT-3	5		3.41	0.10

4.2.2.2.3 Scanning Electron Microscopy (SEM)

Scanning electron microscopy (SEM) images were employed to observe the microstructure of the hardened cementitious composite containing 0.025% MWCNTs after curing for 28 days. Figure 4.17 shows typical images of a fractured surface (samples were collected from the fracture surface of dog-bone specimens after failure), showing that the nanotubes have been individually dispersed and uniformly distributed over the detected area, although some agglomeration of CNTs was also noticed (Figure 4.17a). As noted previously, these nanotubes act as a nano reinforcing agent, bridging the cement hydration products, and delaying/preventing nano crack formation.

Furthermore, embedded CNTs also act to fill the pores between the hydration products (i.e. calcium silicate hydrate (C–S–H), calcium hydroxide (CH) and calcium sulfoaluminate hydrate (ettringite)). The filler action results in a denser microstructure which enhances the composite strength compared to the reference matrix. These observations are in good agreement with past SEM investigations (Konsta-Gdoutos et al. 2010, Nochaiya et al 2011, Morsy et al. 2011, and Zou et al 2015).

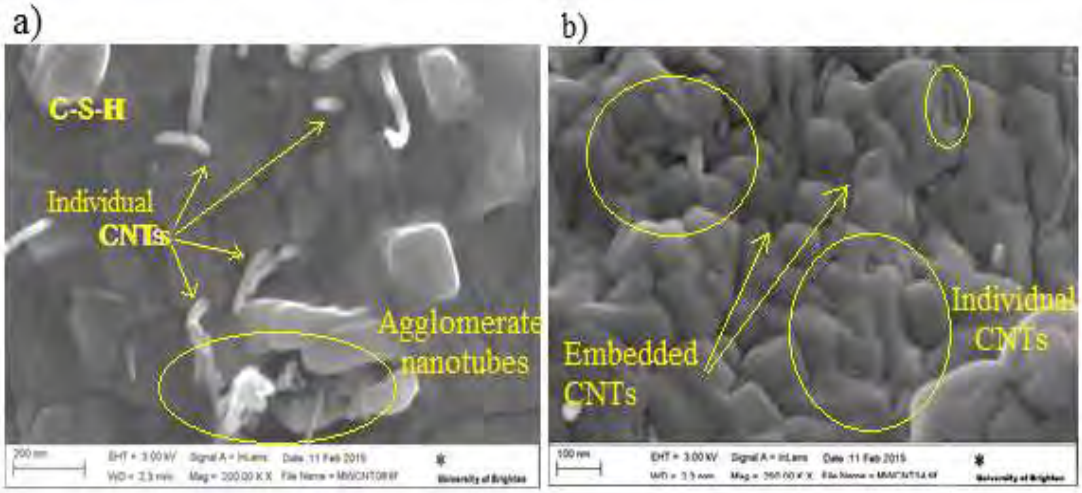

Figure 4.17 Typical SEM micrographs of the cement/CNFs composites.

4.2.2.3 Effects of Water Volume on Sonication Intensity: Third Stage

Water volume is one of the parameters that affects the intensity of sonication (energy delivered to the suspension). The energy delivered is uniformly distributed over the total volume water volume causing micro and nano cavitations (vacuum-bubbles) to be formed among the solution molecules. A large volume of cavitations creates, at first, in a small fraction of water that in the immediate vicinity of the ultrasound probe, then the cavitations will separate to the whole water volume. Hence, the ultrasonic intensity depends entirely on the design and location of the probe.

Optimisation experiments for obtaining maximum cavitation intensity using the ultrasonic probe were developed using a simple and fast experimental method. Different volumes of suspension containing a set amount of nanotubes (0.025 wt.%) mixed with different volumes of water (seven different volumes) and treated under high intensity sonication for 5 minutes. Recorded absorbance at wavelength of 500nm show that the efficiency of the sonication method was relatively uniform for volumes between 100ml and 250ml (Figure 4.18). Higher absorbance values resulted when nanotubes were dispersed in a volume of 500ml. In this sense, higher absorbance' values mean a more intense cavitation delivered that led to higher faction of individual nanotubes in the water volume. At higher water volumes, lower absorbance values were observed. Studies on the critical paraments for efficient sonication reviled that the ultrasound intensity diminishes with an increase in the distance from the source (sonic probe). A higher possibility of re-agglomeration after ultrasonication when the nanotubes dispersed in a relative small water volume, small tube-tubes distances increase the effects of Van der Waals force interactions that increase their tendency to agglomerate(Clésia C. et al. 2001, Tyson et al. 2011).

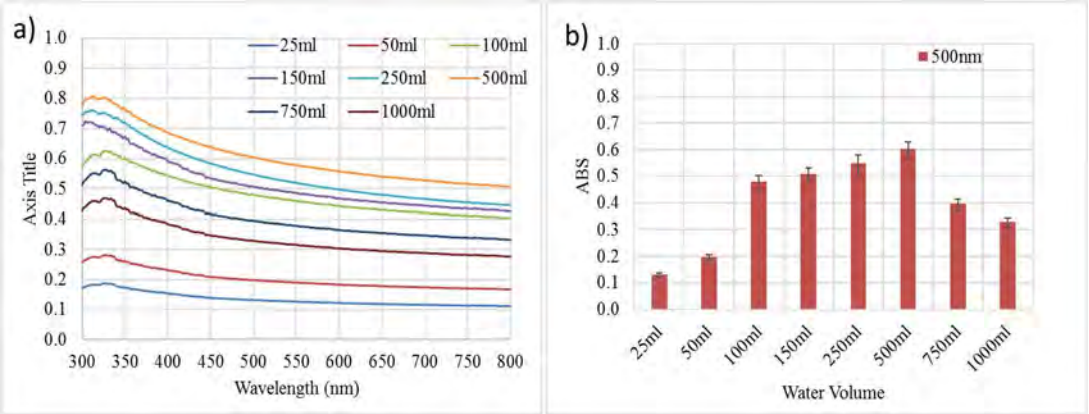

Figure 4.18 a) Showing Uv-vis spectra of nanotubes dispersed in eight different volumes of water, and b) absorbance at a wavelength of 500nm.

4.3 Phase II: Effect of Surfactants

4.3.1 Overview

Applying a surfactant as a dispersion agent significant aids the dispersion of nanotubes in water. Although a large number of studies in the literature have addressed the effect of surfactant/polymers on dispersion efficiency (Liu 2012). The exact mechanism of dispersion, and the optimum type and concentration, of surfactants used in the nanotubes dispersion process for cementitious composites is poorly understood, and still subject to research. Due to the wide range of surfactants/polymers tested, and the variation in their properties, the results from different works frequently cannot be compared. This makes it difficult to select effective surfactants based on previous studies and accurately predict their dispersing effect.

In general, efficient dispersion of nanotubes requires that the used dispersants have 1) an anchoring part (backbone) that attaches to the CNT surface, and 2) a stabilizing part that interacts favourably with water. Surfactants, due to their amphiphilic structure, adsorb at the interfaces of agglomerated nanotubes, modifying properties such as surface tension, wettability and surface charge at the interface. This thesis tests

and optimises surfactants that lead to higher level of individual nanotubes and at the same time compatible with the cement hydration process. A limited number of works in the published literature have investigated the effect of different surfactants in dispersing carbon nanotubes for cementitious application. In this chapter, three different dispersion agents have been investigated for non-covalently functionalized nanotubes, and optimised to produce an effective dispersion agent that incompatible with cement hydration. Naphthalene, polycarboxylate ether based superplasticisers, and methylcellulose have been examined to investigate their effect on the dispersion of carbon nanotubes suspensions in water. Then their compatibility with cementitious composites have been also examined. The effect of concentration of the proposed surfactant on the dispersibility of CNT in water was then investigated.

4.3.2 Dispersion Mechanism Using Surfactants: : First Stage

The fundamental properties of a surfactants are classified based on their tendency to adsorb at the nanotubes surfaces, interface the deriving forces, and on their surfactant molecules. The stronger tendency to adsorb at the outer nanotubes surfaces, the better dispersion ability and leading to higher fraction of individual nanotubes. The surfactant lowers the interfacial tension between the neighbouring tubes, thus when the tubes are covered by surfactant molecules the amount of the force required to expand the interfaces is reduced. The denser the surfactant packing at the interfaces, the larger the reduction in the surface tension. Adsorption at the nanotube surface is controlled by the chemical structure of the surfactant (chemical structures of PCE and MC are schematically represented in Figures4.19).

The amphiphilic nature of the surfactant molecule is critical to its interaction with the surface of the nanotubes and the aqueous medium. The hydrophilic part of the surfactant molecule is referred to as the head group and the hydrophobic part is the tail (Figure 4.20). Tails physically interact through Van der Waals forces with the wall of the carbon nanotubes and the hydrophilic heads remain free in the water. Therefore, hydrophobic and hydrophilic groups determine the extent of interactions with both the surface of the nanotubes and the surrounding media (water and/or the composite when they are added to the cementitious mixture). The tails (hydrophobic part) are either

linear or branched and the head is usually attached at one end of an alky1 chain. The length of the chain varies in according to the number of carbon atoms (depending on surfactant type), i.e. either relatively short-chain surfactants like C8, or C10 (low viscosity), or longer-chain C14 or above (higher viscosity) (Yonghui Liu 2010, Ghorabi 2012). The effect of the degree of chain branching, chain length, and position of the polar groups on surfactant dispersion efficiency are important parameters that are recommended for future study.

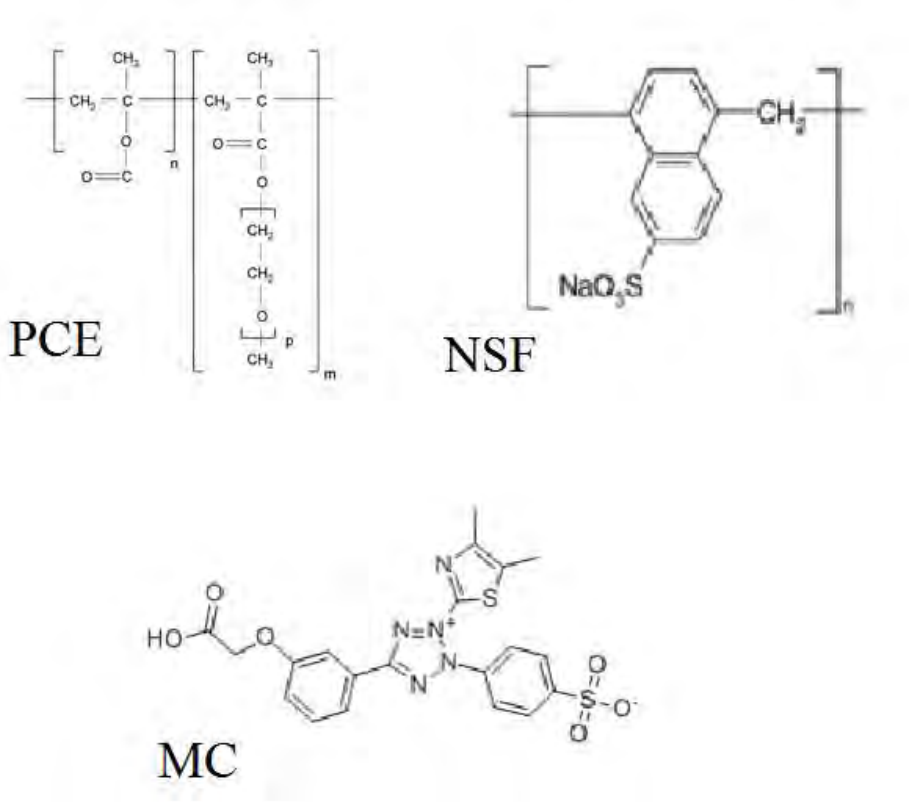

Figure 4.19 PCE, NS, and MC chemical structure: n=anionic carboxylic group, p=PEO unit (polyethylene oxide), m = side chain.(Kong 2016, Shu 2016)

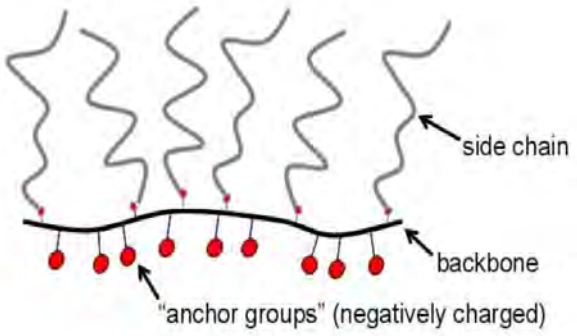

Figure 4.20 Schematic of the molecular structure of the surfactant, showing the comb-like shape of the superplasticiser which consists of a negatively charged backbone and a series of side chains.

The strength of surfactant-nanotube interactions is affected by the attachment model. Currently, there are several models that describe adsorption of surfactant molecules onto CNTs, as depicted in Figure4.21: a) Hemimicelle adsorption of surfactants onto nanotubes; b) encapsulation of a CNT inside a cylindrical micelle of surfactants; c) helical adsorption of surfactant molecules around the nanotubes; and d) random adsorption of surfactants onto the tube surface. Detailed interpretations of the experimental results are often difficult since direct evidence of the adsorbed structures is not trivial to obtain, and different experiments have led to contradictory conclusions. The polymer-wrapping model has been suggested as giving the strongest polymer-nanotube interactions, as in this model the polymer coats the nanotubes forming a helical structure in close contact with the nanotube surface(Maria et al. 2010).

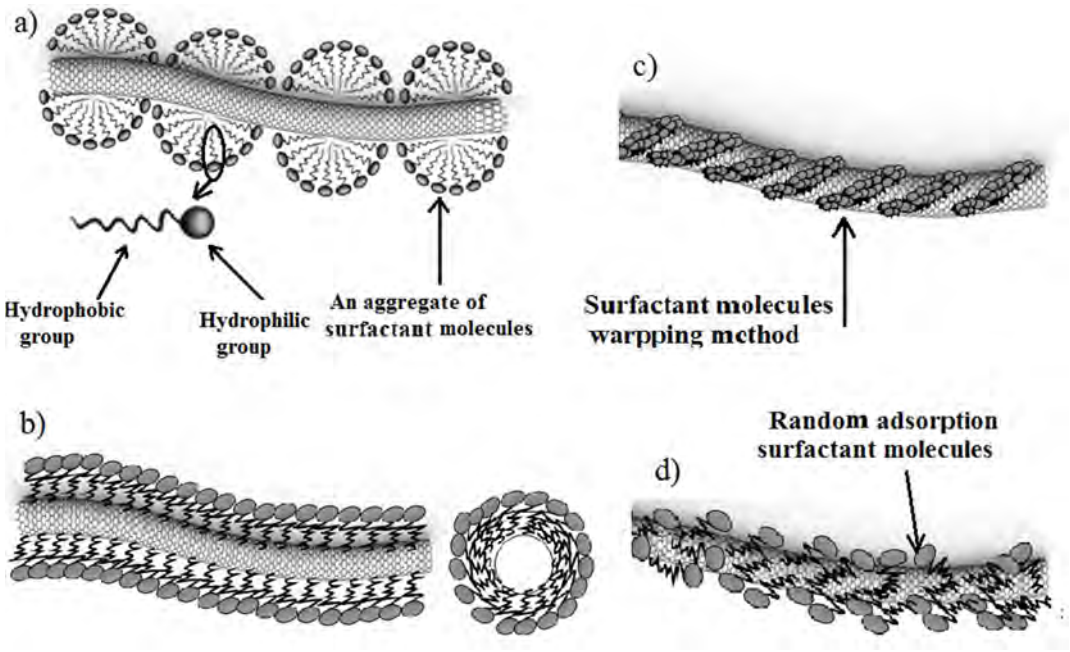

Figure 4.21 Mechanism by which the dispersion agent aids dispersion of carbon nanotubes, a) Hemimicelle adsorption of surfactants onto CNT, b) Nanotubes encapsulated in a cylindrical surfactant micelle (both cross section and side-view), c) helical wrapping structure of surfactant over the tube surface, and d) random adsorption of surfactant molecules.(Junrong et al. 2007, Liew et al. 2016)

The comb-like molecular structure of polycarboxylate ether (PCE) (known as an effective water reducing agent for use in cement suspensions) consist of two segments that can facilitate the dispersion of nanotubes in water. One segment (i.e. backbones) of the polymer interacts with the nanotube surface, whereas the other segment (i.e. side chain) interacts with the water. The effect of backbone and side chain lengths of the PCE on dispersion of agglomerated nanotubes needs to be determined in further study (Kong 2016). A schematic illustration of the structure of PCE is given in Figure4.19.

The backbone is considered to drive adsorption mainly through electrostatic interactions with surfaces while the side chains are chosen to be non-adsorbing and induce steric hindrance among adsorbed layers. Backbone chemistry, backbone length, number of side chains, length of side chains and charge density have a significant impact on the dispersion of carbon nanotubes, in addition to their direct

influence on water reduction, workability, rheology, strength development, air entrainment and adsorption speed.

Since the sufficient adsorption of PCE onto the surface of nanotubes walls (as similar as to cement particles) is a prerequisite for dispersion, the improvement of the dispersing performance of PCE molecules is influenced significantly by its chemical structure, nevertheless, it could be improved by optimising effective adsorption process, and concentration used (Ferrari et al. 2012, Shu 2016). The effect of the chemical structure of the surfactant, such as PCE, and NSF, in aiding nanotube dispersion under ultrasonication could usefully be investigated in future work.

4.3.2.1 Effect of Surfactant type on Dispersion of CNTs

4.3.2.1.1 Visual Characterisation

Visual comparison of the effectiveness of surfactants (i.e. in this study PCE, NSF, and MC) in the dispersion and stabilisation of CNTs was used as a preliminary test. Photographs of CNTs in water containing different types of surfactant are shown in Figure 4.22. Figure4.22a (no surfactant) clearly shows that CNTs settle at the bottom of the flask, and evidences that MWCNT suspensions without surfactant exhibited aggregation, where most of the MWCNTs sedimented after a very short time. Figures 4.22b-c shows three nano suspensions containing PCE, NSF, and MC before sonication, immediately after sonication, and 3hr, 6 hr and then 3 days after sonication treatment. Visual inspection of all suspensions did not indicate any difference between their effects at early treatment ages. After sonication and agitation stopped, the suspensions became purely black and remained stable over a reasonable period, indicating that the nanotubes (individual and the relatively small amount of bundled nanotubes) remained effectively suspended in the aqueous media.

Nanotubes in PCE and MS suspensions did not settle at all during the duration of the experiment. After 3 hours, however, nanotubes in the NSF suspension began to settle, and by three days after treatment nanotubes had agglomerated in large bundles and settled on the bottom of the glass bottle (Figure4.22 c and d). The reason for rapid settlement of NSF dispersed nanotubes can be attributed to the destabilization of the

colloidal system initiated by the relatively heavy NSF molecules (Ferrari 1997). The relatively low molecular weight of PCE and MS are giving stable colloids for a longer time, providing sufficient steric hindrances to maintain the suspension. The effect of different molecular weights of PCE, NSF, and MC on dispersion, and adsorption on the nanotubes outer walls, needs to be investigated in future work.

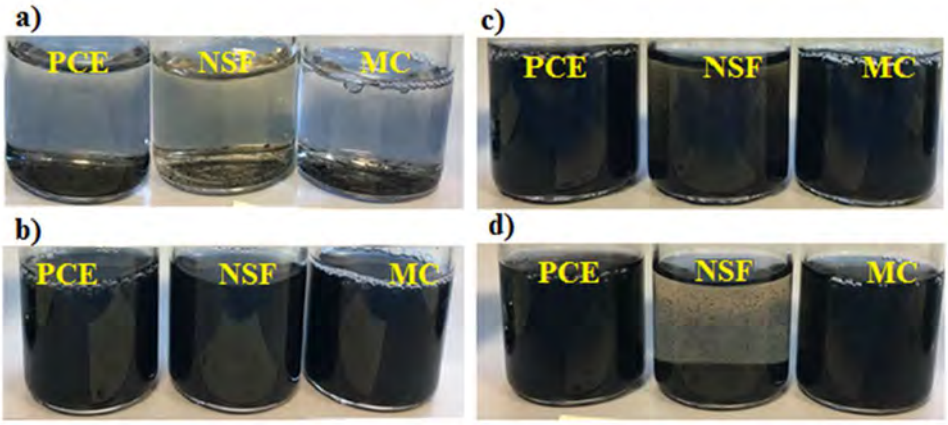

Figure 4.22 Photographs of nanotubes suspension containing PCE, NSF, and MC as dispersion agents: a) before sonication, b) immediately after sonication, c) and d) after sonication by 6hr, and 3 days respectively.

4.3.2.1.2 UV-vis Absorbance

Surfactant effectiveness and efficiency for adsorption at the tube surfaces for surface tension reduction can be assessed using UV-Vis absorbance. As noted above, the higher the obtained absorbance, the higher the number of individual nanotubes in the suspension, which provides a proxy measure for the effectiveness of surfactant action. UV–vis absorption spectroscopy of the nanotubes suspensions containing different type, and concentrations of surfactants was carried out. The absorbance spectra of only surfactant solutions are used as a baseline correction for experimental analysis, and the Uv-vis absorbance was chosen at the wavelength of 500nm as reported in many previous studies (Rastogi 2008). With each surfactant (i.e. PCE, NSF, and MC), spectra of nine suspensions of different concentrations (nanotubes-to surfactant of 1:2, 1:4, 1:6, 1:8, 1:10, 1:12, 1:14, 1:16, and1:20) were used to examine the following.

- Most effective surfactant type in dispersing the agglomerated nanotubes in water.
- The optimum surfactant concentration that lead to highest absorption values.

The results, as shown in Figure 4.23, revealed varying adsorption of surfactant molecules on the nanotube surfaces. This phenomenon is generally related to the molecular behaviour of the surfactant used (i.e. its molecular structure). Effective adsorption is a prerequisite to the de-bundling mechanism which has been postulated to occur through an "unzipping" process of the nanotubes bundles during ultrasonic agitation. Molecules of NSF and PCE have long side chains in their structure and they are believed to adsorb more strongly to the surface of nanotubes, therefore they lead to suspensions with higher concentrations of individual nanotubes. Up to a certain level, the absorbance values increase with increasing concentration of the added surfactant, which can be attributed to an increase of the surfactant molecules adsorbed on the tubes surface until a saturated level is reached. The percentages of the used surfactant that lead to higher absorption were found to begin from 1:6 (nanotubes-to-surfactant), and reached a saturated (or maximum) level at 1:10 for PCE, MC, and 1:12 for NSF. Superplasticiser based surfactants (PCE, and NSF) have approximately the same dispersion effectiveness, while the MC has less dispersion ability, in agreement with literature studies (Chapter Three, Section 2.5.1).

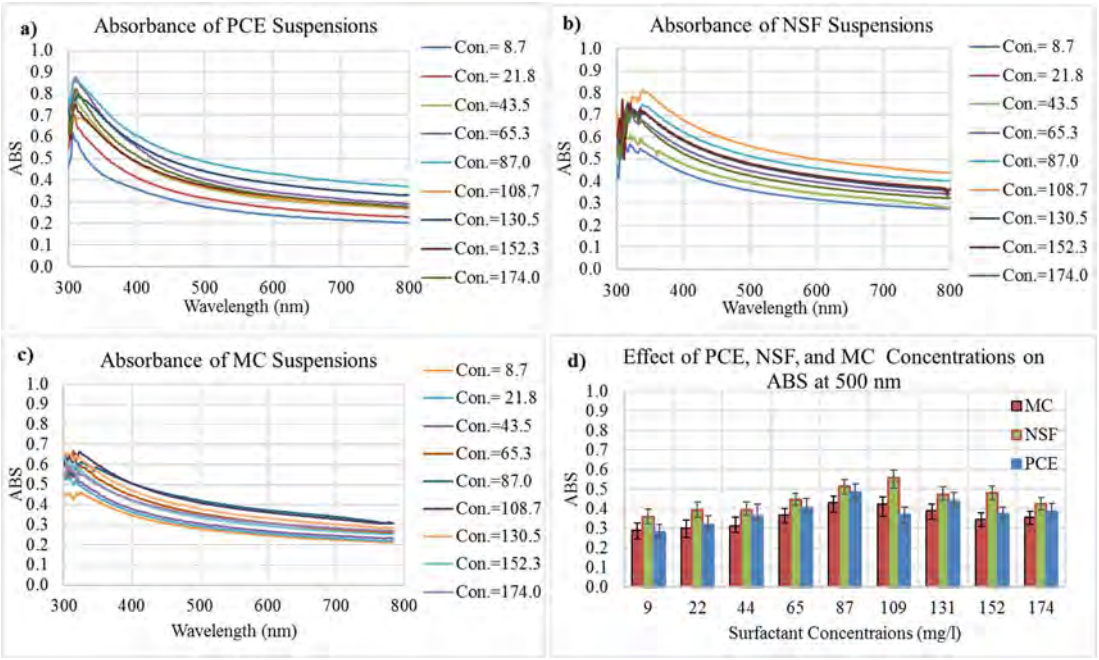

Figure 4.23 UV-vis spectra of nanotube suspensions containing nine different concentrations of a) PCE, b) NSF, c) MC. d) shows absorbance as a function to the surfactant concentrations at a wavelength of 500nm.

The adsorption of surfactant molecules on the surface of suspended nanotubes was examined by high magnification TEM images. Figure4.24 (a, and b), and Figure 4.24(c, and d) show nanotubes treated in the presence of NSF in a ratio of 1:4, and 1:10 respectively. The tubes appear as partially coated with the NSF, and a random organization of the surfactant molecules on the tube surface can be clearly observed. The thickness of the layer ranged between (5-15 nm), which can be attributed to the relatively low added ratio of the NSF (1:4). In contrast, at higher addition ratio (1:10) the tubes appear (as shown in Figure4.24c, and d) as larger and totally coated with the surfactant molecules, and the thickness of the adsorbed layer appears greater than in the images of (a, and b), with an average diameter of 15nm. This could be a reason behind higher concentrations of surfactant stabilizing suspensions of CNTs for longer periods, but effectively reaching a "plateau" in performance at ratios around 1:10.

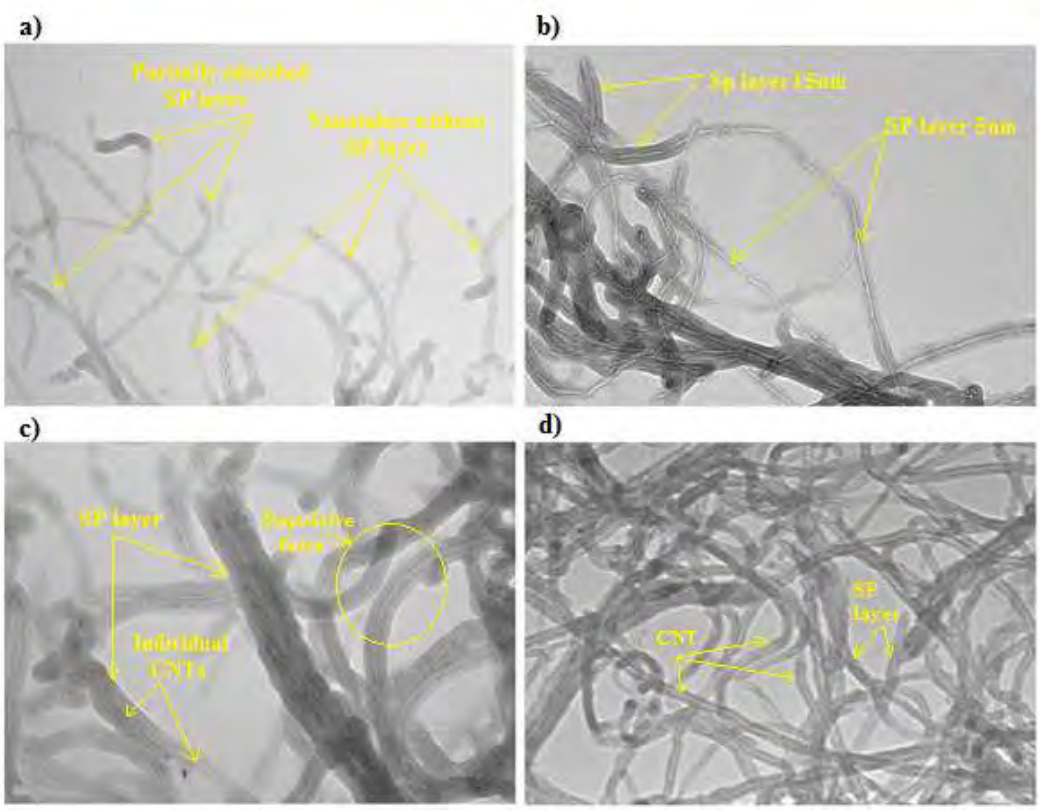

Figure 4.24 Typical TEM images showing the effect of different concentrations of NSF, on the adsorption behaviour of NSF molecules on nanotubes surfaces, a, and b) the addition ratio is 1:4 (nanotubes to surfactant), and (b, and c) the addition ratio is 1:10.

4. 3.2.2 Effect of Surfactant on Stability of Dispersed Nanotubes

The suspension stability in aqueous solutions was studied with the help of Uv-vis spectra that were recorded before and after subjection to centrifugation. The stabilization effect of the surfactant could be attributed to electrostatic repulsion among the hydrophilic head group against Van der Waals attractive forces between neighboring nanotubes surfaces. Stable dispersions of nanotubes were obtained in the presence of surfactant, although different types and concentrations of nanotubes are significantly affect the stability of dispersed nanotubes in aqueous solutions.

To farther test effect of surfactant on suspension stability, the absorbance was obtained immediately after sonication by 10 minutes and after centrifugation. The absorbance

at a wavelength of 500nm was obtained and plotted as a function of the concentrations of the surfactant to generate curves describing the change of concentration of nanotubes in suspension from which inferences about tube stability in suspension were made. The results are shown in Figure4.25. It is evident that MWCNT suspensions with low surfactant to nanotubes ratios (less 1:8) exhibited obvious higher difference in the absorbance before and after centrifugation. For suspensions with 1:8, 1:10, 1:12 nanotubes to surfactant ratios the absorbance remained uniform after centrifugation (Figure 4.25a-c), so the suspension with higher concentrations was relatively stable.

From the absorbance values at a wavelength of 500nm, dispersion stability indexes (X_{st}) were obtained (as described by Eq.4.1) to reflect the effect of different concentrations on the dispersion stability over time after sonication treatment. The lower the index values obtained from each surfactant, the more stable were the individual nanotubes in the suspension (Table 4.3)

$$X_{st} = (At_0 - At_c)/At_0 \qquad \text{(Eq.4.1)}$$

Where At_0= absorbance directly after sonication treatment by 10 minutes, and At_c= absorbance value after centrifugation.

Figure 4.25.d shows stability indexes of nanotubes suspensions containing PCE, NSF and MC at all the nine examined concentrations. Generally, all the examined surfactants/concentrations decreased surface tension, and overcame Van der Waals interactions between MWCNTs. The stability indexes indicate that the surfactants tested (i.e. PCE, NSF, MC) are effective dispersants for nanotubes in aqueous solution, and that reasonable surfactant content can improve stability of the dispersed nanotubes. Although use of MC led to relatively low absorbance values (i.e. concentrations of individual nanotubes), the stability indexes revealed that MC with higher addition concentrations (above 1:6) can produce stable suspensions, and can withstand re-agglomeration because of the centrifugation action. On the other hand, the lower stability indexes obtained from nanotubes suspensions containing PCE in

the range of 1:8-to 1:12, revealed that these percentages of PCE were sufficient to produce stable suspensions with higher fraction of individual nanotubes.

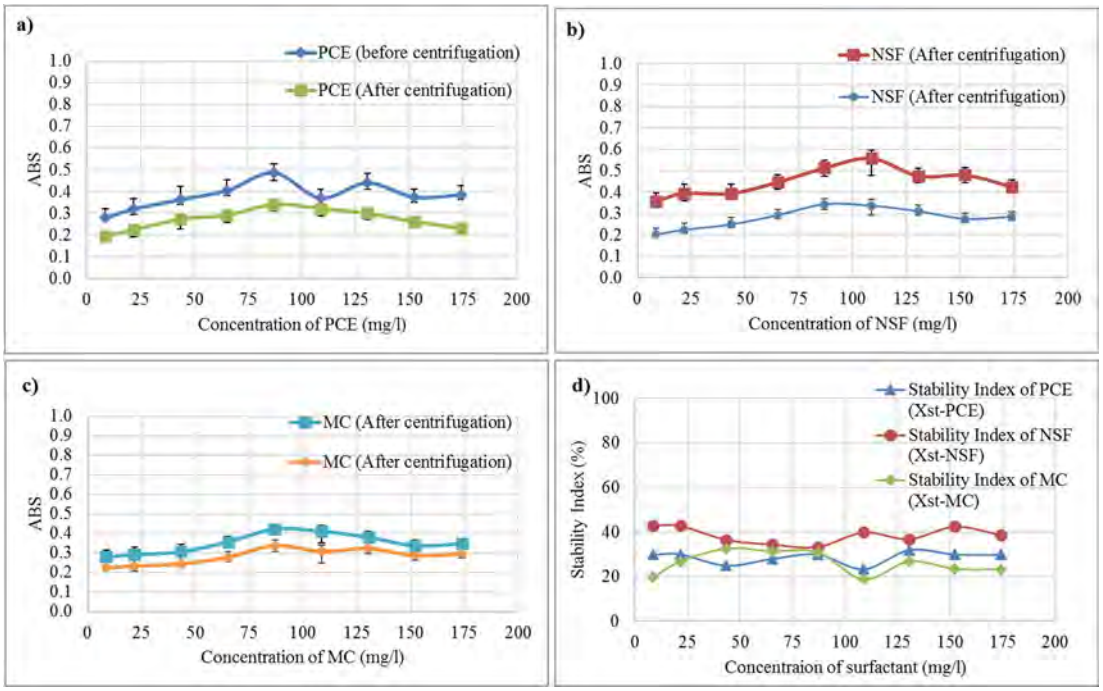

Figure 4.25 Absorbance at a wavelength of 500nm as a function of the concentrations of added surfactant before and after centrifugation: a) PCE, b) NSF, d) MC. d) shows the stability indexes (%) of nanotubes-PCE/NSF/MC suspensions, and represent the ability of added surfactant/concentration to help disperse nanotubes and withstand subsequent re-agglomeration.

Overall, the above results indicate that the sonication technique (i.e. high sonication intensity over a short time) is sufficient to produce an efficient coating layer of superplasticiser adsorbed on the nanotubes/fibres which can induce electrostatic repulsion and counterbalance the Van der Waals attractions force.

Table 4.4 Stability indexes of nanotubes dispersed in different concentrations of PCE, NSF, and MC as a dispersion agent.

MWCNTs: Surfactant	Stability Index of PCE Xst-PCE	Stability Index of NSF Xst-NSF	Stability Index of MC Xst-MC
1:2	30	43	20
1:4	30	43	27
1:6	25	37	33
1:8	28	34	31
1:10	30	33	31
1:12	23	40	19
1:14	32	37	27
1:16	30	43	24
1:20	30	39	23

4.3.3 Compatibility of Surfactants with Cement/CNTs Composites: Second Stage

Cement/CNTs composite properties such as compressive strength, and fluidity, have been chosen in this phase as composite performance criteria to demonstrate the compatibility of the surfactant used and their effect on the efficiency of MWCNTs performance within the composites.

4.3.3.1 Compressive Strength

Compressive strength test results of cement composites containing nanotubes dispersed with different surfactants (PCE, NSF, and MC) are presented in Figure 4.25 at 3, 7, and 28 days after curing. Three control mixes were fabricated for this study: PCE and NSF were added to control mixes PC-PCE, and PC-NSF, respectively, to maintain the mixture workability. These control mixes were used for comparison with cement/CNTs composites containing PCE and cement/CNTs composites containing MC, and cement/CNTs composites containing NSF respectively.

It is observed that the use of surfactant-based superplasticisers (either PCE, or NSF) in the dispersion of nanotubes resulted in a distinct improvement of the composite

strength compared to the reference mix. The strength of specimens containing MWCNTs dispersed using PCE, and NSF were improved by 53%, 39%, 42%, and 40%, 23%, 31%, at 3,7,28 days, respectively (Figure4.26d). Although the non-ionic surfactant (MC) has successfully dispersed the nanotubes in the water, a significant reduction in the compressive strength of the specimens containing these suspensions was observed (Figure4.26c). This can be attributed to the incompatible effect of the agent (MC) with cement hydration, leading to a delay in the cement hydration process. These surfactants can increase the amount of entrapped air in cement paste to a level that has been seen in the fresh mix. In addition, these types of surfactant undergo reaction with water-reducing admixtures, which might retard hydration and cause re-agglomeration (Frank et al. 2012). As reported in many studies, compatibility between surfactants and the cement matrix is an important issue that affects the mechanical properties. Surfactants, containing polyethylene oxide side chains, work similarly to polycarboxylate-based superplasticisers, which can disperse cement particles, modify the fluidity of mortar, reduce porosity and improve microstructure density then mechanical strength. (Parveen et al. 2015)

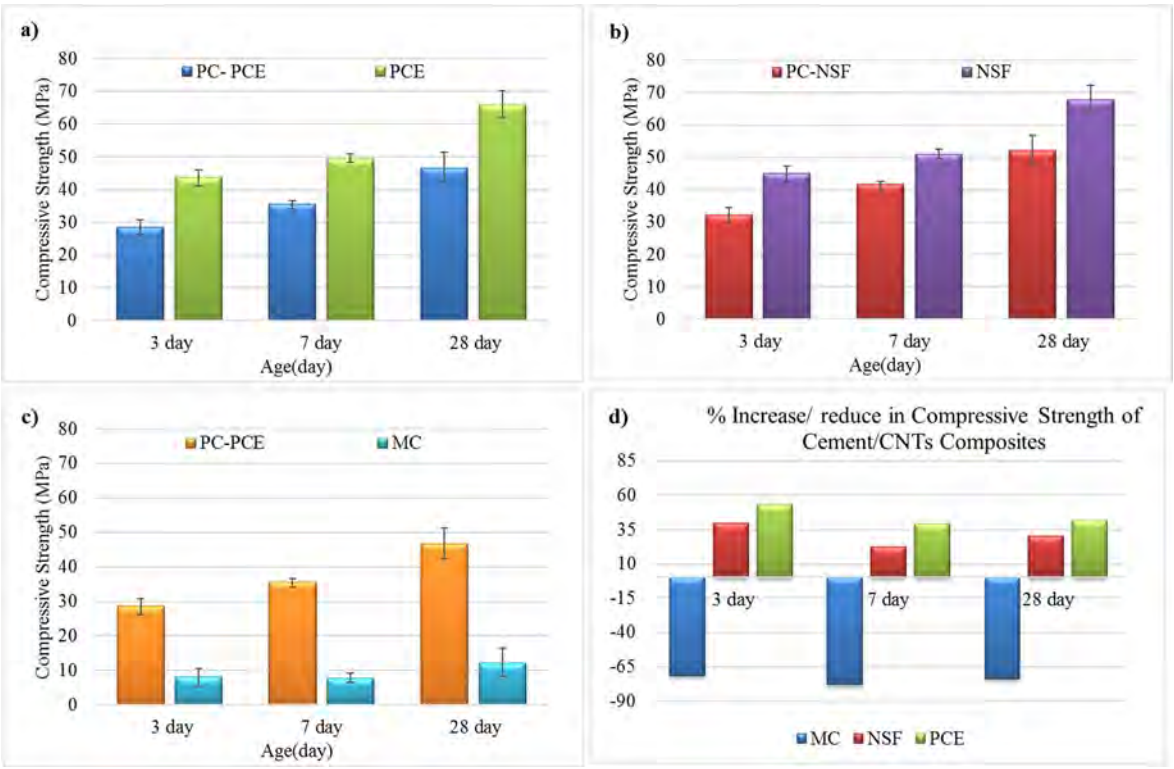

Figure 4.26 Compressive strength of cementitious composites containing MWCNTs dispersed using, a) PCE as a dispersion agent, b) NSF as dispersion agent, c) MC as dispersion agent, and d) the relative improvement/reduction in the compressive strength compared to the control mixes.

4.3.3.2 Fluidity of Fresh Nano Composites

The effects of surfactant, and nanotubes-surfactants, on the flow of the composites were examined to understand the effect of the added surfactant/nanotubes on the mixture behaviour. Compared to the control paste (without superplasticiser), addition of surfactant-based superplasticiser (PCE, and NSF) in ratio of 0.4% by cement weight (based on manufacturer's recommendation- in terms of MWCNT-to surfactant, this ratio is equal to 1:10), led to an increase in the mixture average flow values from 185mm to 200mm, and 205mm respectively (as shown in Figure 4.27). In CNTs/mixtures, flow values show that both PCE and NSF led to approximately the

same flow increment, i.e. meaning that the adsorbed surfactant on the tubes also acts to improve the workability when added to the mixture.

Flow values were found to be significantly higher (215mm) in the case of paste containing nanotubes dispersed with non-ionic agents (MC). These differences in flow are attributed to the hydrophobic and hydrophilic nature of these agents contributing to a reduction in the viscosity of the mix and at the same time to the formation of a large volume of stable air bubbles (El-Sayed et al. 2014). Generally, the effect of surfactants on the dispersion of nanotubes and workability is dependent on the composition, the type, and the concentration of surfactants (Rastogi 2008, Fan et al. 2012). All examined mixtures provide higher workability, which is further increased when functionalised nanotubes are used.

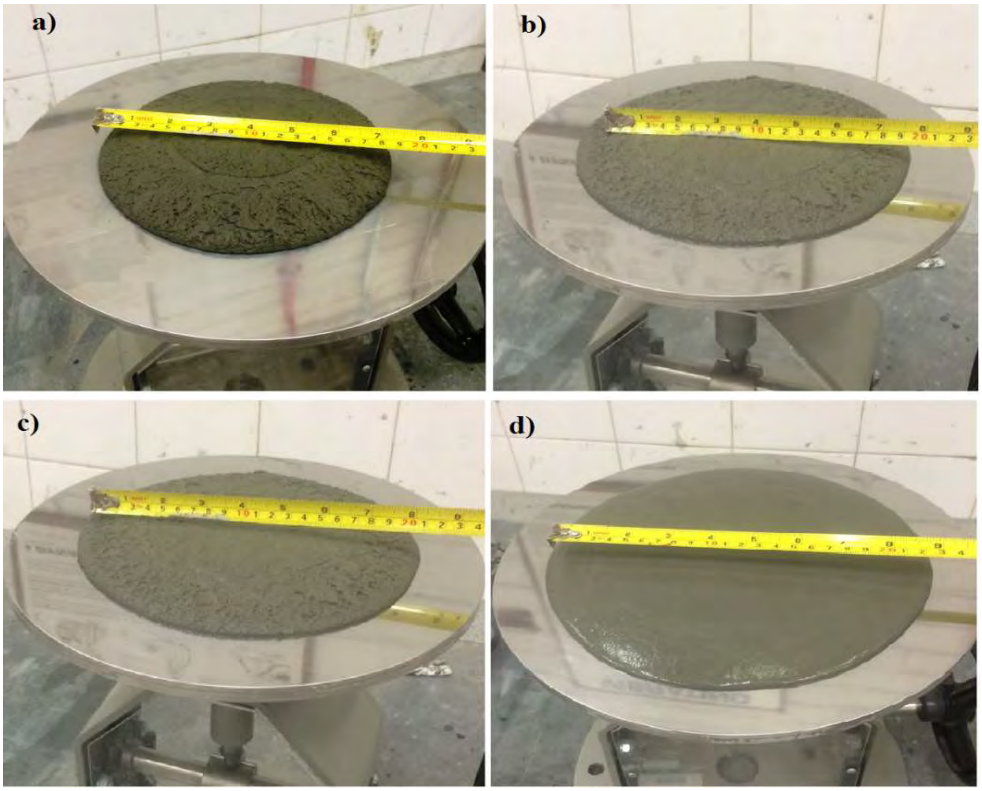

Figure 4.27 The flow behaviour of pastes containing different types of surfactants at concentration ratio of 1:10: a) Flow of control mix, b) Flow of paste containing nanotubes dispersed using NSF (which was slightly higher than that of paste containing PCE), c) Flow of paste containing CNTs dispersed using MC.

4.4 Phase III. Effect of Micro Silica

4.4.1 Overview

In Phase I and Phase II a novel dispersion technique was optimised to generate a CNT/suspension with a high concentration of individual nanotubes, which is stable for a reasonable duration, and which is compatible with the cement hydration process. This technique includes high sonication (via a sonic probe) over a short time period in combination with a surfactant i.e. superplasticiser based Naphthalene Sulfonates Formaldehyde (NSF) (an effective dispersion agent to disperse nanotubes in water) (Geng Ying et al. 2005).

However, this dispersion technique could not ensure prevention of the re-agglomeration of carbon nanotubes, and does not guarantee a good dispersion within the cementitious composite. Immediately after mixing the nano-suspension with the cement mixture ingredients, cement hydration products consume the aqueous media (water and NSF) and cause the nanotubes (that are available in the fresh mixture voids) to re-agglomerate in large bundles. This behaviour necessitates the use of physiochemical barrier that can improve the dispersion stability in the composite, thus preserving the nanomaterial dispersion up to the composite stage.

In this Phase, work on novel dispersion techniques has been extended to include using a pozzolanic admixture with extremely fine particles (i.e. Undensified microsilica, USF) to lessen and/or prevent the re-agglomeration of nanotubes through the composite. The current experimental study was undertaken to optimise the effective incorporation percentage.

The Experiments include:

- Characterisation of particle size distribution and the morphology of USF.
- Interaction between USF and MWCNTs.
- Characterisation of the mechanical strengths of the composite with the addition of different percentages of USF (as a cement replacement).

4.4.2 USF Particle Characterisation

A comprehensive understanding of the behaviour of the cementitious ingredients, cement and USF, is necessary to determine their effect on improving the dispersion of nanotubes through the composite. Undensified silica fume has been characterised in two phases; first in the dry state, and second in the wet state after adding water with manual mixing. The characterisation was carried out using optical microscopy and transmission electron microscopy.

Dry phase: Undensified silica fume is a fine lightweight powder that possesses spherical particle shape with varying size. Under optical microscopy, the USF was seen to have a wide range of particle sizes ranging from below the limit of resolution of the microscope up to a few millimetres. Images show that larger clusters were agglomerates of thousands of individual silica spheres. For comparison, cement grains in a powder state were also examined. Figure 4.28 shows selected micrographs for cement, and USF at a magnification of x40. The images revealed that the surface texture of cement particles were extremely rough, and the particles were angular in shape. In contrast, USF particles are spherically shaped with a very smooth surface texture. USF showed very fine particles with diameters in the range of a few microns.

W**et phase:** TEM provided a high magnification image which revealed accurate information about the USF after manual mixing with water, such as surface texture, particle size distribution, and particle sizes. Figure 4.29 shows that silica particles have extremely fine diameters in the wet phase, from a few nanometres upwards. Dry silica fume powder exhibits a much larger particle size (average particle size ca. 0.15 μm) as during collection, cooling and bagging, the primary particles form larger agglomerates (not aggregates), and these agglomerates are easily dispersed into very small particles after adding water. Moreover, the surface texture is extremely smooth - in transmitted light the detected silica particle appeared clear, extremely fine-grained, smooth texture.

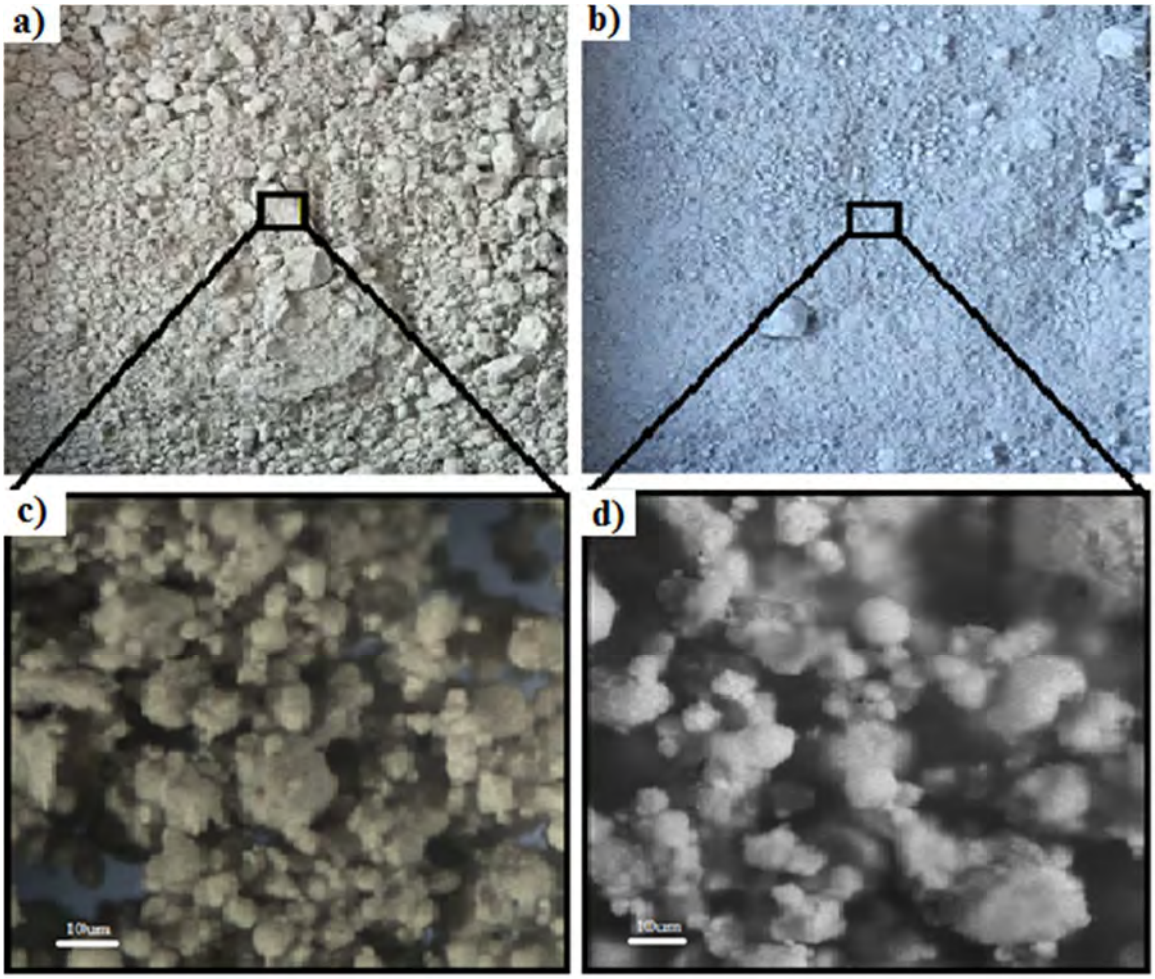

Figure 4.28 Photographs of a) cement, b) Microsilica, and Optical micrograph images showing particles size distribution and shapes in individual and agglomerated phases of c) cement, d) Microsilica.

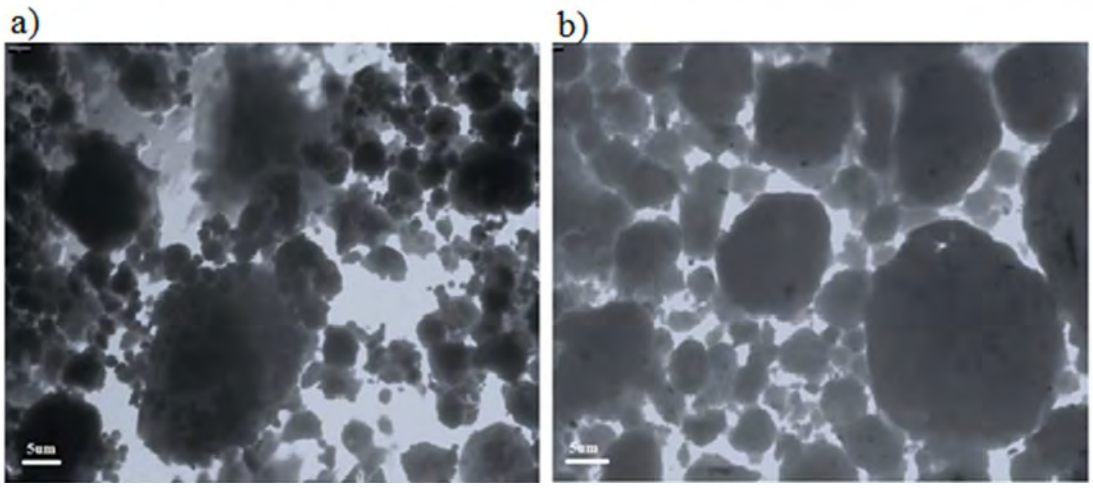

Figure 4.29 Optical microscopes images at different magnifications of a) 10000x, b) 30000X of USF spheres particles.

4.4.3 Interaction between USF and MWCNTs

Due to its pozzolanic activity, USF is extensively used to enhance the engineering properties of cementitious composites. In this study, it was also used at the same time to enhance the dispersibility of the nanotubes. On a molecular level, these spherical particles have sizes which are similar to the diameters of nanotubes, and move freely in between the nanotubes, and thus act to provide a superior barrier leading to better mechanical properties. This makes silica fume particles an ideal physical barrier, and prevents re-agglomeration as a result of the strong interaction force between CNTs.

To better understand the mechanism of silica fume particles in preventing the re-agglomeration of nanotubes throughout a composite, a suspension of nanotubes and silica fume was prepared. TEM images were taken to investigate the interaction mechanism between nanotubes and silica fume particles. Figures.4.30 shows different high magnification TEM images that illustrate the effect of USF inenhancing the dispersion of MWCTs in the composite, and preventing their possibility to re-agglomerate due to drying and/or free movement mechanisms. The smooth and relatively small size of USF particles (ca. 200 times smaller than anhydrous cement particles) disrupts the tube-tube interaction (van-der Waals indication force) that accelerates CNTs in re-agglomerating in the composite. Superplasticiser available in the fresh mixture (adsorbed on the surface of CNTs, USF, and cement grains) may act

to link the smaller particles of USF in between the nanotubes. Presence of USF in between individual nanotubes during the wet mixing process reduces the effectiveness of Van der Waals forces and leads to permanent separation of nanotubes in the composite.

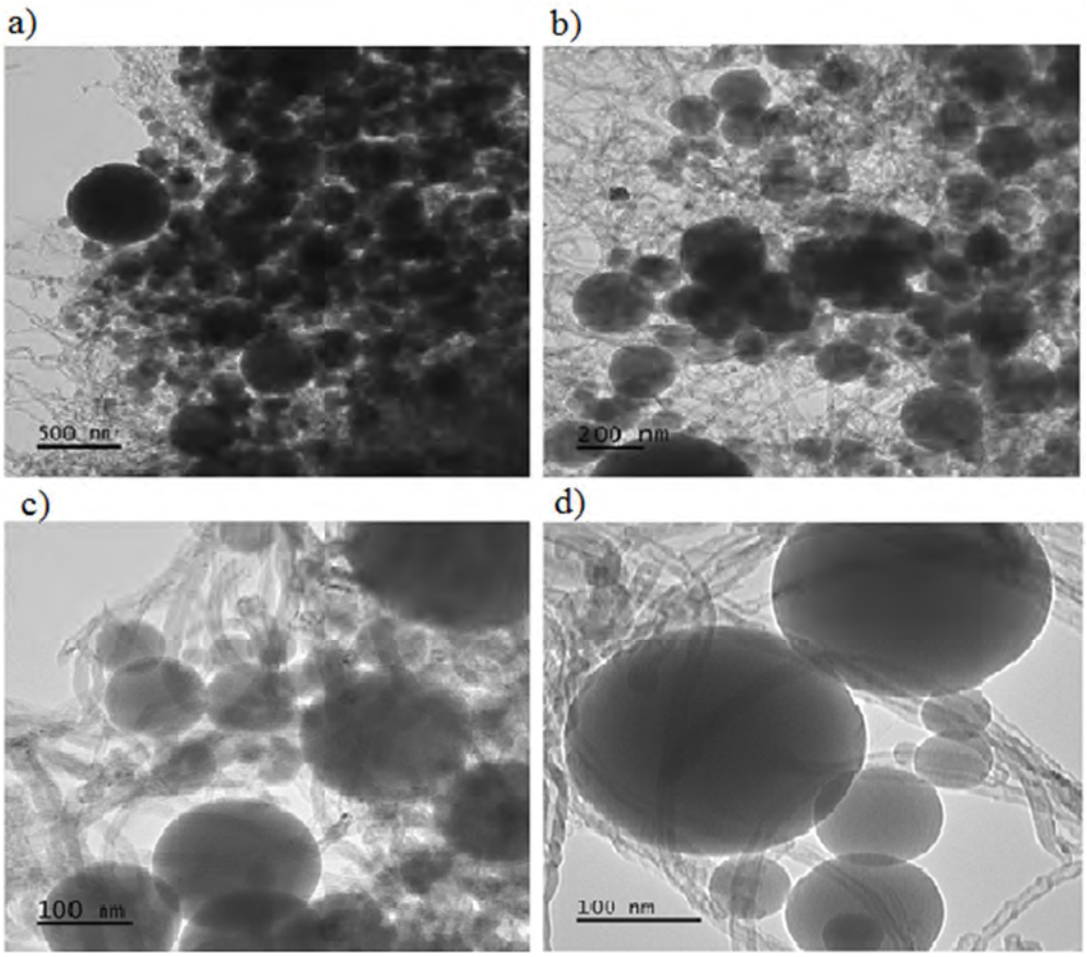

Figure 4.30 TEM images of a typical sample containing MWCNTs and USF after manual mixing. The images were taken at different magnifications of a) 30k, b) 50k, c) 80k, and d) 100k.

4.4.4 Mechanical Performance

Since silica fume is a very reactive pozzolanic material, it typically has strong influence on the mechanical properties of a cementitious composite. Silica fume reacts with the formed calcium hydroxide (which is soluble in water and has low strength affecting the quality of composite) to form additional binder material known as

"calcium silicate hydrate", which is very similar to the calcium silicate hydrate formed from Portland cement. This product is responsible for most of the engineering properties in cement. At the time, their presence in combination with nanotubes can lead to improve the dispersion and/or prevent the re-agglomeration of nanotubes within the composites. This will lead to subsequent improvement in the mechanical strength of the nanocomposites. The effect of silica fume on the performance of nano cementitious composites, therefore, was investigated in term of compressive strength , and porosity measurement.

4.4.4.1 Compressive Strength

Compressive strength results as a function of the extent of hydration are presented in Figures 4.31. It is found that all compressive strengths of composites containing only MWCNTs (CT-2) were higher than those of the control sample (PC) i.e. compressive strength increased by 21%, and 17% at 3 and 28 days respectively. Composite strengths increased further with incorporation of USF and MWCNTs. For example, percentages of 5%, 10%, 15% and 0.025% (i.e. CT-2) of silica fume and MWCNT content in the mixture led to increases in compressive strength of 28%, 41%, and 45%, and 38%, 50%, and 59% after 3 and 28 days, Figure 4.31 a-b, respectively.

To understand the synergistic effect of addition of different percentages of USF (i.e. 5%, 10%, 15%) on enhancing the performance of MWCNTs throughout the composite, a comparison to a composite containing only MWCNTs was made. By increasing the USF content, the strength gains of the nanocomposites were increased by 9%, 20%, 24%, and 14%, 24%, and 34% after 3 and 28 days respectively.

The pozzolanic reaction of microsilica leads to an enhancement of the mechanical strength of the composite (Inna 2013, Peyvandi et al. 2013). Therefore, incorporating both silica fume and MWCNT leads to a greater potential for improving the composite mechanical strength by enhancing the dispersion of nanotubes and preventing their re-agglomeration. USF is dispersed into very small particles after mixing, due to its unpacked and hydrophilic form. Smaller particle sizes (around 10nm diameter) of USF were found to fill in-between the individually dispersed nanotubes, giving a composite

with improved packing density (Arteaga-Arcos et al. 2013) and preventing re-agglomeration of the nanotubes to, as shown schematically in Figure 4.31. Moreover, the densification of the matrix due to the addition of USF can enhance the bond between the nanotubes and the surrounding matrix thereby increasing mechanical strengths (Peyvandi et al. 2013). The combination of USF and MWCNTs has been shown to significantly improve the strength of the material, although the relative dominance of the three potential mechanisms by which USF operates cannot be discriminated based on the present data, i.e.:

- USF particles fill into pores and in between the nanotubes, which densify and reinforce the hydrating gel structure.
- The pozzolanic reactions occurring between the silica-rich USF particles and cement hydration products lead to formation of Calcium Silicate Hydrate, which also acts as link improving the bond between the nanotube and surrounding matrix
- USF act as nucleation sites within the cementitious mixture, accelerating the hydration process

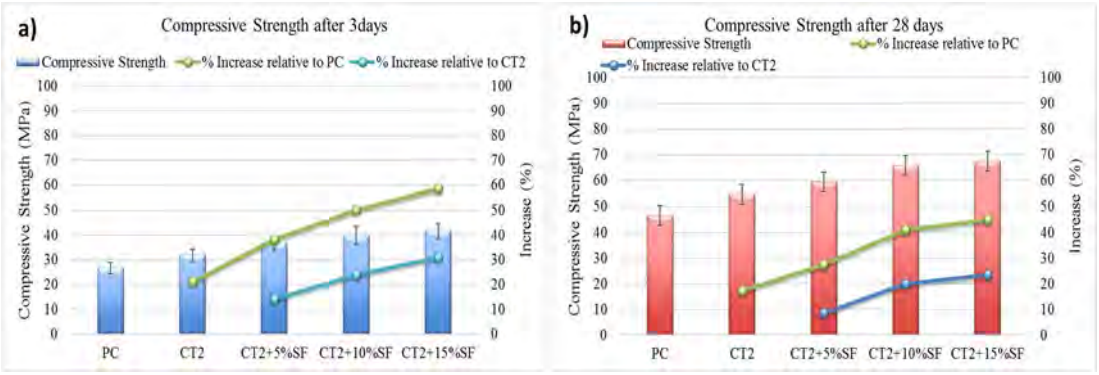

Figure 4.31 Compressive Strength graph of the control mix (PC), a composite with only MWCNTs (CT2), and composites containing MWCNTs and three percentages of USF (i.e. CT2+5%SF), CT2+10%SF), (CT2+15%SF), a) after 3 days, b) after 28 days.

4.4.4.2 Porosity

Porosity values for the Portland cement mortar (PC), specimens containing USFs (i.e. 5%, 10%, 15%) as a replacement for cement, and specimens containing 0.025% MWCNTs and USFs after 28 days curing are shown in Figure 4.32. Compared to PC, addition of 5%, 10%, 15% of USF led to a decrease in the porosity of the hardened composites by 13%, 18%, 25% respectively. In nanocomposite specimens addition of only 0.025% of MWCNTs resulted in a decrease of composite porosity by 17%. The incorporation of both MWCNTs and USF led to further significant decreases in the composite porosity, i.e. porosity is decreased by 24%, 32%, and 28% when USF is added in percentages of 5%, 10%, 15% respectively.

This reduction in porosity can be attributed to the synergistic effect of individual nanotubes and silica particles filling pores between hydration products and bridging nano/micro capillary pores. Optimising the porosity of nanotube cementitious composites is vital since porosity significantly impacts the mechanical performance, as crack propagation begins at the pores and the nanotube are essential in refining the pore structures(Samuel et al. 2014).

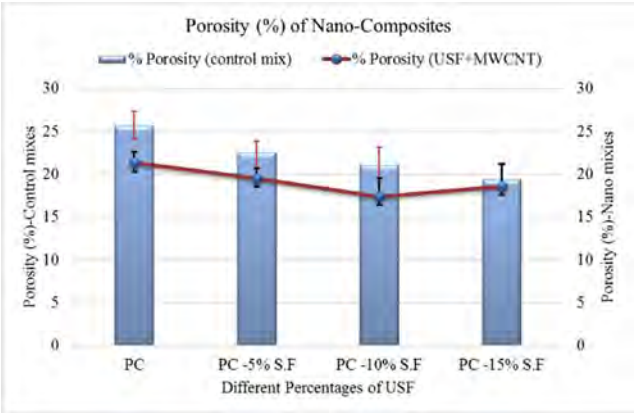

Figure 4.32 Porosity (%) of control mix (PC), and composites containing MWCNTs and three percentages of USF ((CT2+5%SF), CT2+10%SF), and (CT2+15%SF)).

4.4.5 Microstructure

Scanning electron microscopy images were used to study the microstructure of two different nano composites in addition to the control mix, i.e.; i) cement mortar sample (PC) without the addition of USF and MWCNT, ii) composites containing MWCNTs, and iii) composites containing MWCNTs and USF.

1- Figure 4.33 shows typical images of the fracture surface of the PC sample, a) showing the structural voids, visible micro cracks within the composite, and the main cement hydration products (CH, and calcium silicate hydrates (C–S–H) gels). b) showing the needle–like ettringite crystals (calcium sulfoaluminate), and the sheet-like habit of calcium hydroxide ($Ca(OH)_2$).

2- In a composite without silica fume, typical SEM images show large areas of agglomerated nanotubes located in the composite structural voids. One such agglomeration is shown in Figure4.34. This revealed that even when a good dispersion of MWCNTs in water is achieved, small and large clusters of nanotube agglomerates occur within the final composites. This can be attributed to the strong van dar Waal interaction force between the nanotubes leading to re-agglomeration during sample curing. The schematic diagram in Figure 4.35 explains the effect of silica particles in keeping the nanotubes individually dispersed through the composites. Figure 4.35 a) and b) illustrate the mixture in the fresh phase, and Figure 4.35 c) and d) the composite in the hardened phase. a) and c) represent composites without the addition of USF as in the hardened phase (d) the nanotubes return to a re-agglomerated state in the composite voids.

   To date the reasons behind the re-agglomeration of CNTs after adding well dispersed suspensions are not totally understood. Some researchers have attributed this phenomenon to the effect of drying/evaporation on dispersion and the free movement of CNTs in the fresh composite. When the suspension is mixed with the cementitious materials, the large amount of cement adsorbs the water rapidly, and in this case the nanotubes can move towards each other and form bundles as a result of Van der Waals forces (as the mixture in this

case is still in a fresh, wet, phase). Other theories are based on free movement, as the re-agglomeration of CNTs in fresh cement paste is possible in that most cement grains and the spacing between them are much larger than CNTs.

3- To investigate the effect of USF on dispersion of nanotubes throughout the composite, typical SEM images of the nano composite containing 0.025% wt. of MWCNTs and 10% USF after 28 days were obtained. Because of the pozzolanic reactivity nature of USF, it is difficult to distinguish silica particles throughout the composites. Silica fume reacts with the free $Ca(OH)_2$ to form an addition C-S-H gel.

The observed nanotubes were individually embedded in the composite and predominantly distributed (in almost all of the examined areas) as shown in Figure 4.36. Composite nanocracks reinforced by nanotubes were also observed, as nanotubes are randomly dispersed throughout the hydrated cement products reinforcing in between the C–S–H crystals, extending from cracks. During the early hydration process, the availability of extremely fine silica particles plays a major role in preventing neighbouring nanotubes from re-agglomerating. The images confirm their ability in preventing the re-agglomeration of nanotubes as the result of the strong van der Waal's interaction force. Moreover, the presence of USF shows a beneficial interaction of nanotubes with the host matrix, with hydration products present around the surface of the tubes. The resulting enhanced bond strength consequently enhances load transfer efficiency between the cement matrix and the nano reinforcements, and their effective bridging across voids and cracks, improving the composite mechanical performance.

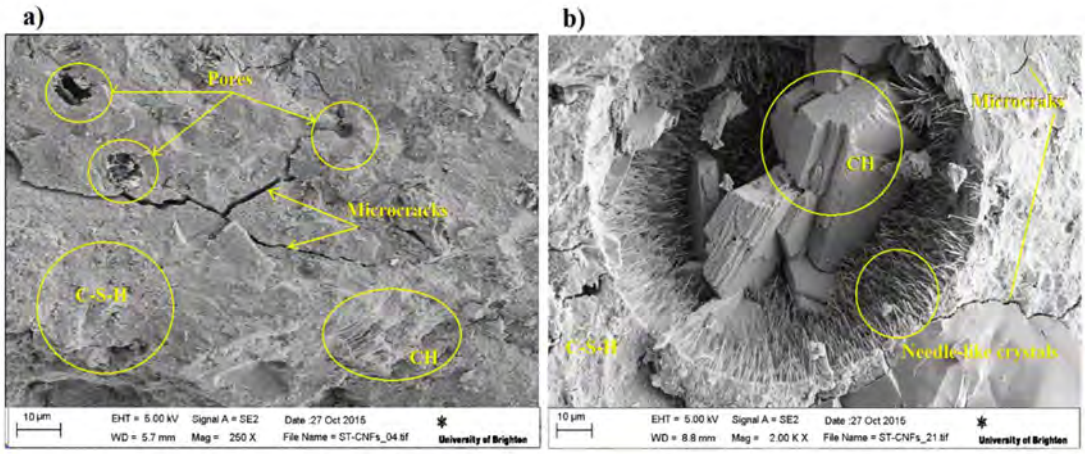

Figure4.33 SEM images of microstructure of cement paste after 28 days showing a) structural voids, visible micro cracks within the composite, and the main cement hydration products CH, and C–S–H. b) showing the shape of the hydration products, in this case the needle-like crystals of ettringite.

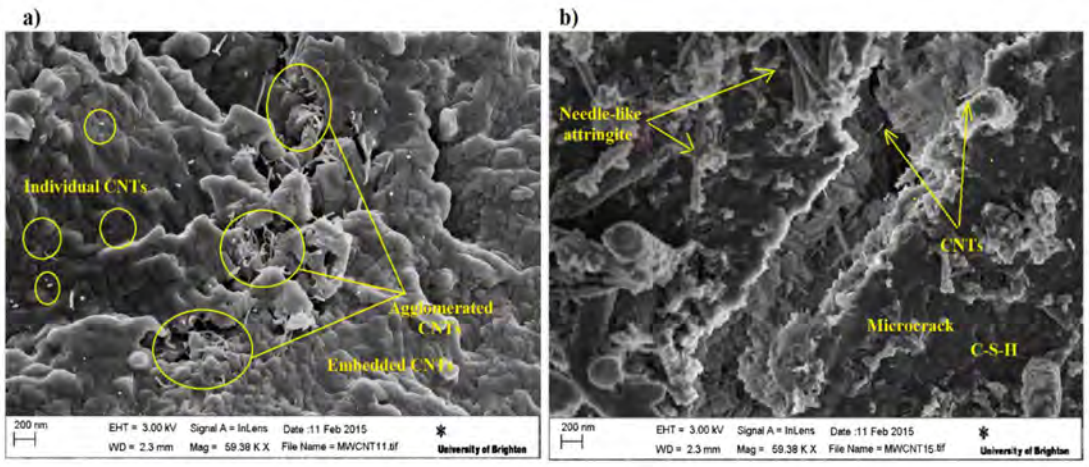

Figure 4.34 SEM images of cement composite containing only MWCNTs, a) showing the agglomeration of MWCNTs in the structural voids, b) the availability of a few individual nanotubes bridging the initiated microcracks.

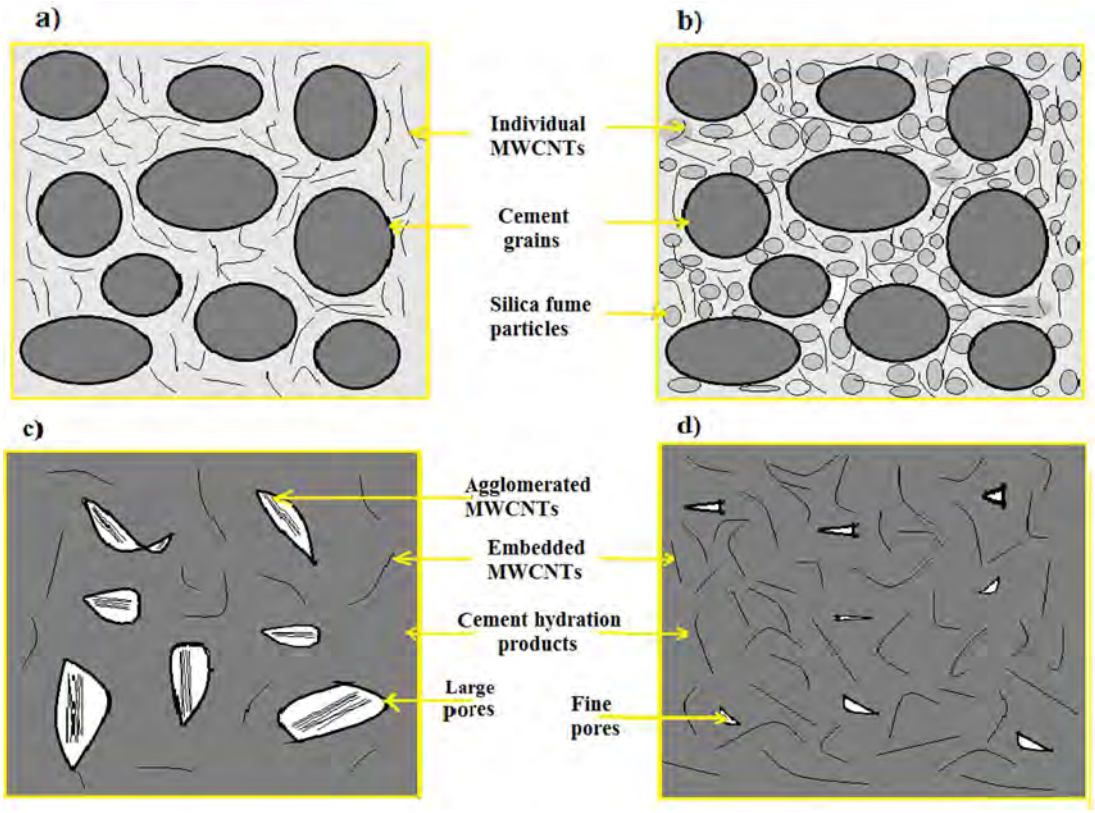

Figure 4.35 Schematic diagram showing the effect of silica fume in preventing the re-agglomeration of MWCNTs, a) and b) show MWCNTs-mixtures with and without USF in the fresh phase, c) and d) show MWCNTs-mixture with and without USF in the hardened phase

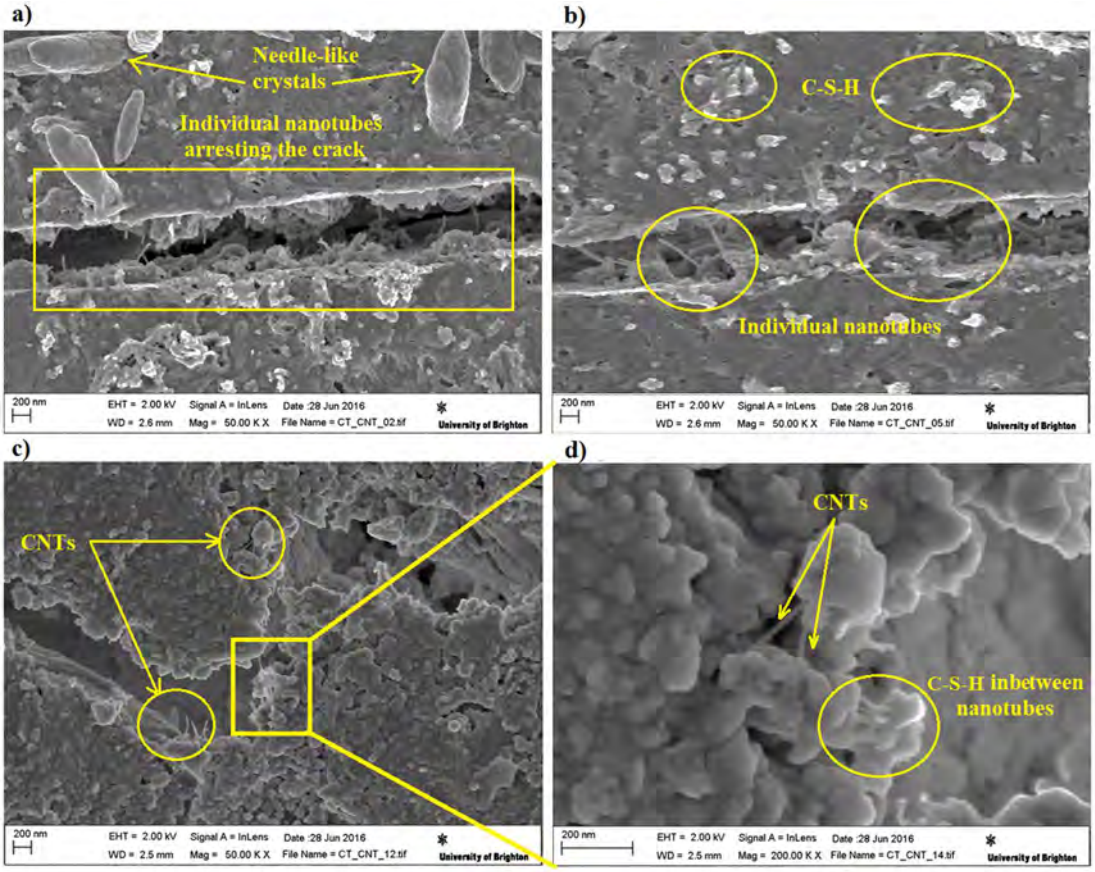

Figure 4.36 SEM of cementitious composite containing MWCNTs and USF. The availability of extremely fine USF plays a major role in preventing nanotubes from re-agglomerating, and maintains dispersed high dispersion of nanotubes through the composites.

4.4.6 Summary

This chapter (over three phases) has studied the influence of ultrasonication, surfactant, and mineral admixtures in optimising a novel method for dispersion of carbon nanotubes for improved performance cementitious composites.

- Phase I. The effect of ultrasonication intensities (using a sonic probe) on the dispersion of nanotubes (in different concentrations) for cementitious composites has been optimised. The study was conducted through three different sonication intensities and various treatment times, and the relationship between the

concentration of nanotubes (individually dispersed) and the sonication intensity and treatment duration was assessed. The results indicated that high sonication intensity applied over a short time (up to 5 min) using 0.025% of MWCNTs gave a high concentration of well dispersed nanotubes in water, which subsequently significantly improved the mechanical strengths of cement composites.

- Phase II optimised the effectiveness of surfactant type and concentration on the dispersion and stability of nanotubes in water, and their compatibility with the cement. For this study three different surfactants have been investigated in different concentrations. The main outcomes were, i) the results revealed that the percentages of the used surfactant which led to higher concentrations of individual nanotubes began at a 1:6 ratio (nanotubes- to- surfactant) and reached a saturated level at 1:10 for PCE, MC, and to 1:12 for NSF. ii) stability indexes indicated that surfactants (i.e. PCE, NSF, MC) are effective dispersants for nanotubes in aqueous solution, and that reasonable surfactant content can improve stability of the dispersed nanotubes. Although use of MC led to relatively low absorbance values (i.e. concentration of individual nanotubes), the stability indexes revealed the MC with higher addition concentrations (above 1:6) can produce stable suspensions, and has the ability to withstand re-agglomeration as a result of centrifugation. On the other hand, the lower stability indexes obtained of nanotubes suspensions containing PCE in the range of 1:8-to 1:12, revealed that these percentages of PCE were sufficient to produce stable suspensions with higher fraction of individual nanotubes. iii) the results on mechanical strength of cementitious composites containing CNTs-surfactant based superplasticisers (either PCE, or NSF) in a ratio of 1:10 (MWCNTs-to surfactant) showed a distinct improvement in composite strength compared to the reference mix, maintaining an acceptable mixture workability.
    - Phase III. In this phase, the work on novel dispersion techniques has been extended to include use of a pozzolanic admixture with extremely fine pozzolanic materials (i.e. Undensified microsilica) to improve and/or prevent the re-agglomeration of nanotubes through the composite. The results revealed that the USF particles fill in pores and in between the nanotubes, which densify and reinforce the hydrating gel structure. In addition, the pozzolanic reactions

occur between the silica-rich(SiO_2) USF particles and cement hydration products leading to formation of additional Calcium Silicate Hydrate gel which also contribute with improving the bond between the nanotube and surrounding matrix.

Chapter Five:

The Effect of High Intensity Sonication on the Dispersion of Carbon Nanofilaments and Graphene oxide, and its Impact on the Mechanical Performance of Cementitious Composites

5.1 Overview

Generally, poor dispersion of carbon nano-additives is the major challenge involved in fabricating cementitious nanocomposites, because relatively strong Van der Waals' forces cause agglomeration of the nano-additives and their subsequent uneven distribution in the composite material (Sanchez and Sobolev 2010, Yazdanbakhsh et al. 2012). Having shown the effectiveness of high intensity sonication treatment over short time periods for dispersing MWCNTs (Chapter Four), this chapter examines the effectiveness of this method on alternative nano-reinforcing agents, specifically examining the effect of high intensity, short duration sonication treatment on i) the dispersion efficiency of functionalized multiwall carbon nanotubes F-MWCNTs, carbon nanofibres CNFs, and few layer graphene oxide (FLGO) in water, and ii) their reinforcing efficiency in cementitious composites. Results for MWCNTs (Chapter Four) are presented for comparison.

The proportion of nano-additives used was set at 0.025% by weight of cement (the optimal percentage according to the investigation in Chapter Four phase I). Aqueous dispersions were assessed using Scanning Electron Microscopy (SEM)/Transmission Electron Microscope (TEM) and optical microscopy, and Ultraviolet–visible spectroscopy (Uv-vis). Mechanical strength tests (compressive strength, direct and indirect tensile strengths, and flexural strength), workability, and porosity and density measurements were used to evaluate the structural properties of the composites.

5.2 Results and Discussion

5.2.1 Characterisation of Dispersed of Nano-additives

Application of high intensity sonication over 5 minutes' duration in combination with NSF (1:10, nano-to-surfactant ratio), was the method followed to facilitate the dispersion of the nano-additives (F-MWCNTs, CNFs, and FLGO) prior to their incorporation into cementitious composites. This had the aim of reducing their hydrophilic properties, improving dispersion, and increasing the concentration of individual nanotubes/fibres/graphene sheets in the suspensions.

Three sets of suspensions for each nano-additive were prepared ((1) CNFs, (2) F-MWCNTs, and (3) F LGO). In each set, two suspensions were prepared for visual examination, and stability and concentration evaluation, respectively. The first and second suspensions from each additive were prepared by adding a nano-additive and manually mixing in water (with and without NSF, respectively) to visually examine the effect of functional groups and/or NSF on the dispersion of the nano-additive in water. After cessation of mixing photographs were taken after 10, and then after 20 minutes settling time.

Figure 5.1 showing the behaviour of the nano-additives in water and in the presence of carboxyl functional groups and/or surfactant NSF over 20 minutes of treatment duration. They give an indication of the degree of dispersion, and the importance of using a sonicator in the dispersion process. The CNF suspension quickly settled to the bottom of the container (even before the time of the first photograph), F-MWCNTs, and FLGO appeared in relatively large clusters which were suspended during the examination period (Figure5.1 a1-d1). Carboxy1 groups and/or NSF in the F-MWCNTs and FLGO suspensions were found to partially help in the dispersion, and dispersion stability, of the added nano materials, although the presence of carboxy1 dispersant groups, and/ or NSF surfactant agent, do not effectively act in the absence of high shear force (delivered by sonicator), as shown in Figure 5.1 (a2-e2, and c2-f2).

After sonication (third suspensions), more homogeneous suspensions were obtained (Figure 5.1 d3-f3), with photographs showing that the CNFs, F-MWCNTs, and FLGO suspensions remained stable for several hours (longer with functionalised nanotubes and graphene), then the nano-additives gradually re-agglomerated and settled due to the high Van der Waals interaction forces. The synergistic effect of functionalised nanotubes and NSF was found to form the longest lasting suspensions, which can be attributed to hydroxyl functional groups on the walls of the tubes hindering their re-agglomeration, leading to a more stable suspension.

Compared to the suspension without sonication treatment, it can be argued that a high sonication intensity over a short time period, combined with use of surfactant/functional groups, is sufficient to generate a coating of NSF on the nanotubes/Fibres/graphene sheets. The availability of functional groups on the tubes/sheets in combination with surfactant molecules induces electrostatic repulsion and counterbalances the Van der Waals attractive force (Yazdanbakhsh et al. 2012), and leads to a more homogenous and stable suspension. As a high intensity ultrasonic wave passes through the solution, it rapidly generates a large number of cavitation bubbles which then collapse, and enhances surfactant penetration between the tubes/fibres and graphene sheets.

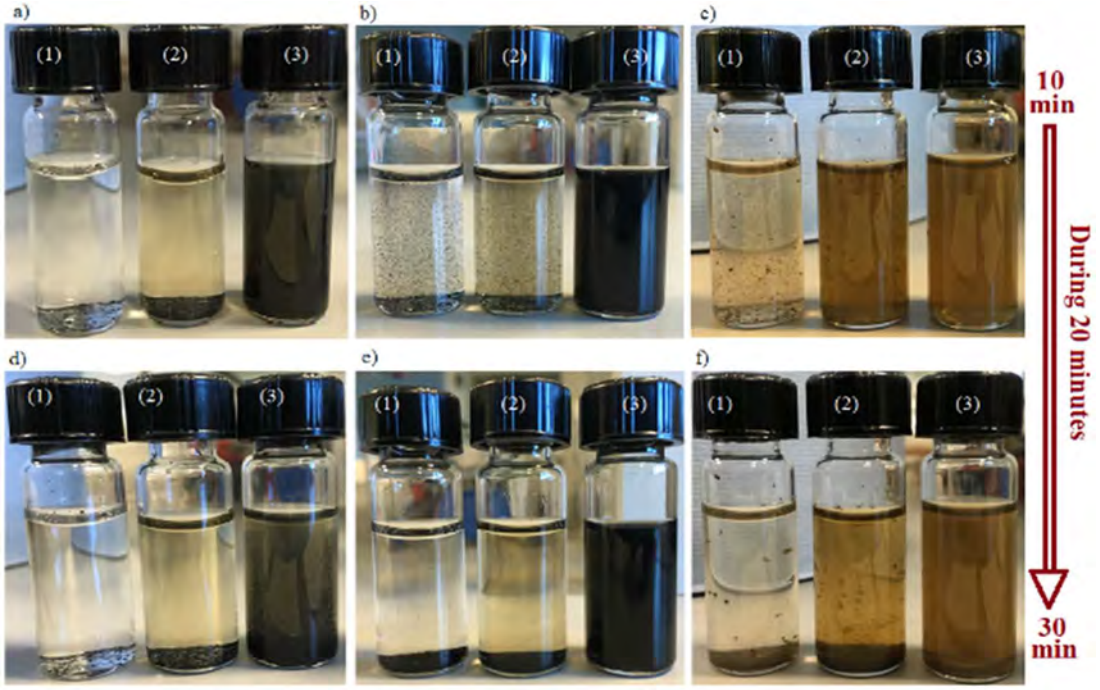

Figure 5.1 Photographs of CNFs, F-MWCNTs, and FLGO suspensions. (1), (2), and (3) show photographs after mixing with: water; water and NSF; and water and NSF in combination with sonication. a), b), c) show photographs of CNTs, F-MWCNTs, and FLGO suspensions, respectively after 10 minutes settling time, and photographs d), e), and f) show the same suspensions after 30 minutes.

Uv-vis spectra of nano-additives suspensions were measured after sonication treatment (at t= 0 min, 30 min, 180 min, 1440 min, and 10080 min) as shown in Figure5.2 (a-c). High intensity sonication was found to deliver the highest energy to the suspension, resulting in highest absorbance values (i.e. highest dispersed concentrations). From the absorbance values at a wavelength of 500nm, a dispersion stability index (X_{st}) was calculated (as described by Eq. 5.1) to reflect the effect of high-intensity sonication on the dispersion stability over time after sonication treatment.

$$X_{st}= (At_0 - At_n)/At_0 \qquad \text{(Eq.5.1)}$$

Where At_0= absorbance directly after sonication treatment and At_n= absorbance values after t= 30 min, t= 180 min, t= 1440 min, and t= 10080 min.

The dispersion stability index for CNFs, F-MWCNTs, and FLGO suspensions was plotted as a function of time after sonication treatment, as shown in Figure 5.2d. Compared to those at t=0 the indices revealed that suspensions that were sonicated for 5 minutes remain stable for a few hours, and after three hours the nanofibres started to re-agglomerate and settled at the bottom of the glass vials. The process of re-agglomeration was slower when there was a higher availability of hydroxyl functional groups on the tubes and graphene sheets.

UV-Vis spectroscopy data and the visual inspection therefore indicated that short period, high-intensity sonication, in combination with NSF, delivered the required energy to produce a higher concentration of individual particles, which was stable for a longer time period. The stability of CNFs was found to be the lowest, and F-MWCNTs the highest, among the examined nano-additives. The lower surface areas of CNFs (per unit weight) compared to higher surface area of carbon nanotubes (Ahmed Ibrahim 2011), resulted in less adsorbed surfactant on their outer surfaces, and subsequently less repulsive force created in the suspension which is responsible for stabilizing the individual CNFs suspensions. The larger hydrophilic surfactant head group available on functionalised carbon nanotubes surfaces created a stronger and longer ranging repulsive tube/tube force, which responsible for reducing the re-agglomeration rate. The longer range originates directly from the hydroxyl functional group and the adsorbed surfactant layer (NSF).

F- MWCNTs, and FLGO suspensions remained homogenous and stable for longer duration, due to (as discussed above) the presence of functional groups on the surface of the carbon nanotubes and graphene sheets, respectively. In particular, the apparent weak tube-tube/sheet-sheet interaction forces after treatment can be attributed to the synergistic effect of the carboxyl functional groups, NSF, and the sonication technique, which facilitate an unzipping process derived by the energy delivered form the sonicator(Song et al. 2013, Parveen et al. 2015).

Although the dispersion degree of nanotubes/fibres and graphene sheets depends on the amount of energy supplied via the sonicator, and feasibly increasing the energy could improve dispersion characteristics, the energy delivered using the proposed

technique will be employed over the rest of the research experiments. This method is scalable, and can be used to rapidly reach a desired dispersion plateau, and so has good potential for practical construction application. Moreover, it also reduces the probability of damaging/breaking the CNTs which could occur if longer-duration, higher intensity sonication was used.

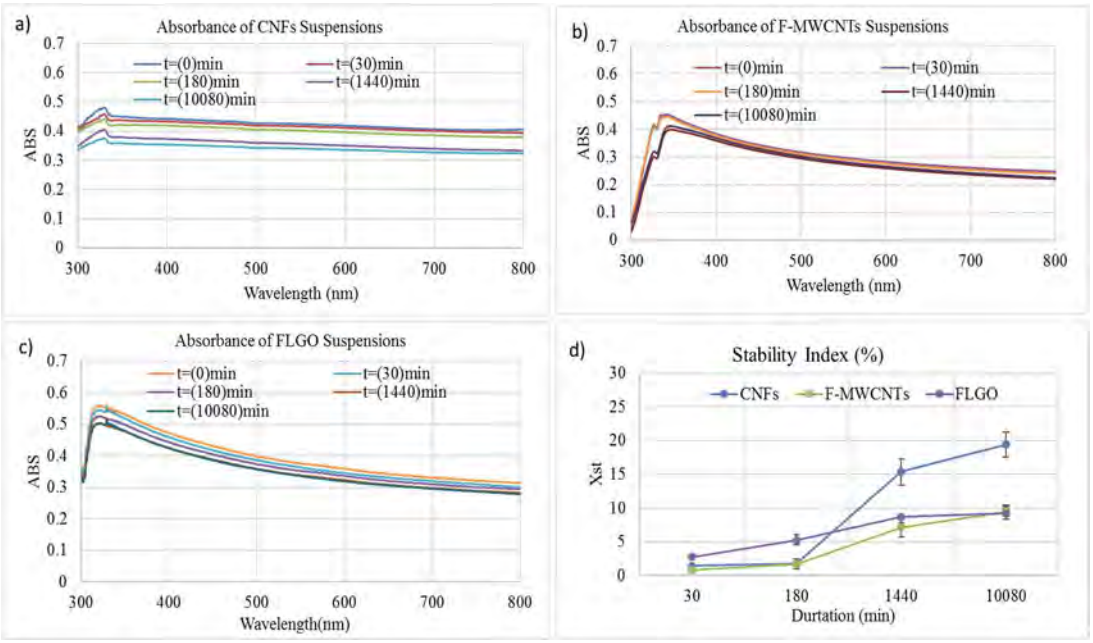

Figure 5.2 UV-Vis absorbance spectra recorded after different periods of sonication for a) suspensions, b) F-MWCNTs suspensions, c) FLGO suspensions. d) shows the dispersion stability indices of the treated suspensions.

Recorded absorption values at wavelength of 500nm were also employed to determine the concentration of; individual functionalised nanotubes, nanofibres, and graphene sheets. The absorbance at a wavelength of 500nm was converted into concentration using an extinction coefficient determined through a dilution series (as shown below). This is possible due to the fact that stable suspensions were shown to obey the Beer–Lambert's Law, with a well-defined extinction coefficient (Marsh 2007). The absorption represents the amount of individual nano-tubes/fibres/graphene sheets in the suspensions. Inset (a) in Figures 5.3, Figures 5.4, and Figures 5.5 shows three photographs of CNFs, F-MWCNTs, and FLGO suspensions, respectively, at different concentrations of 3.5, 1.75, 0.88, 0.44, 0.22, 0.11 mg/l. These suspensions were obtained by diluting the starting suspensions at concentration of (3.5) mg/l with NSF

and water, which were also used for calibration. A linear relationship between absorption values and nanotubes/fibres/graphene concentration was present for the three suspensions, in accordance with Beer's law (Bo et al. 2015). Insets (b) represent the UV–vis spectra of the prepared concentrations of nanotubes/fibres and graphene sheets in NSF surfactant aqueous solution. The recorded absorptions decreased with decreasing concentration of nano particles in aqueous solutions, and a linear relationship between them, following Beer's law, could be observed between 300nm to 800nm (the linearity in in figure Figures 5.3, Figures 5.4, and Figures 5.5 were validated up to the concentration of 0.5mg/l, 2.0mg/l, and 1.75 mg/l respectively).

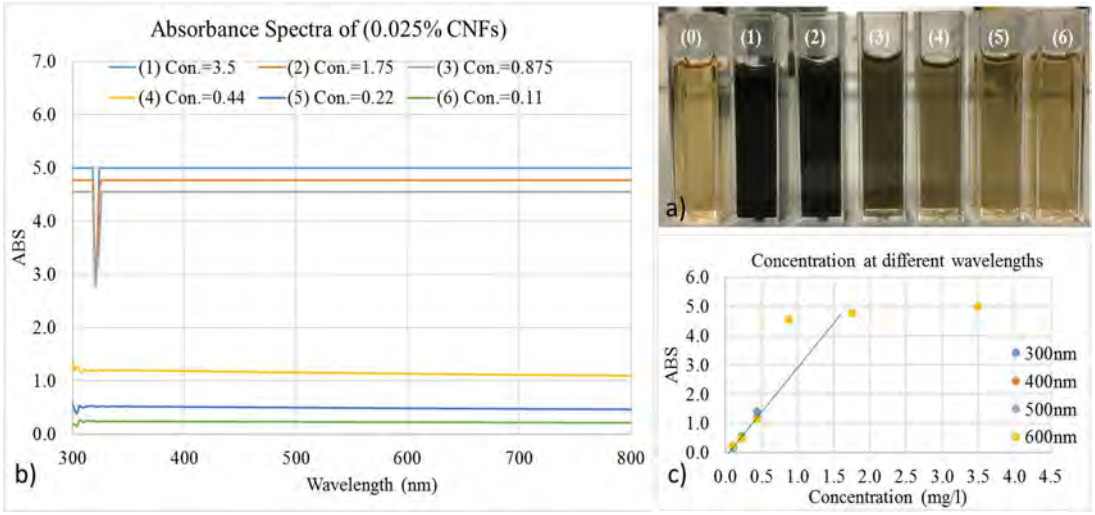

Figure 5.3 a) Optical micrograph of the 0.025%CNFs suspensions at different concentrations: (1) 3.5 mg/L (starting MWCNT solution), (2) 1.75 mg/L, (3) 0.875 mg/L, (4) 0.44 mg/L, (5) 0.22 mg/L, and (6) 0.11 mg/L in the presence of NSF superplasticiser (10:1 NSF-to-MWCNTs). (b) Recorded UV-vis spectra of CNFs at different concentrations. (c) Absorption as a function of concentration of the CNFs suspensions conducted at the wavelength of (300, 400, 500, and 600nm).

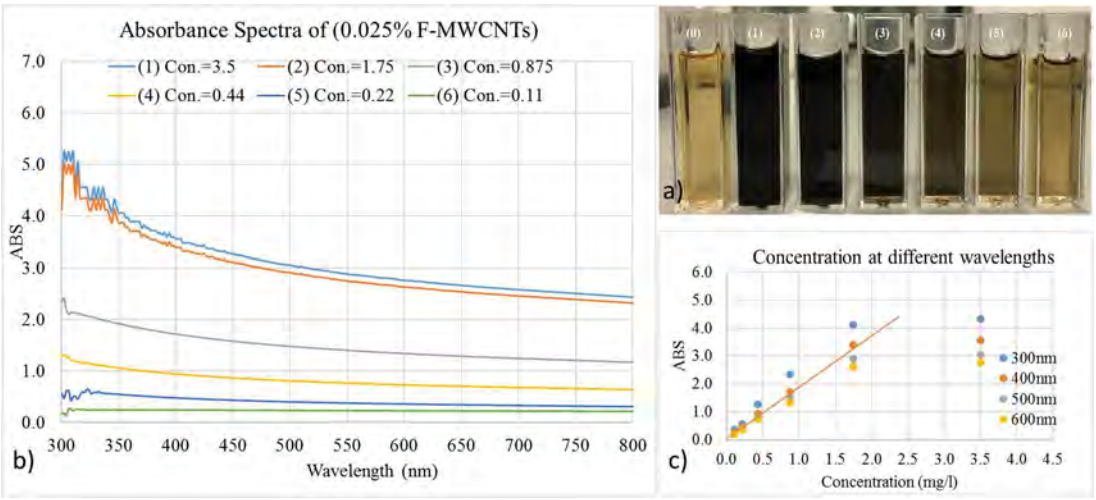

Figure 5.4 a) Optical micrograph of the 0.025%F-MWCNTs suspensions at different concentrations: (1) 3.5 mg/L (starting MWCNT solution), (2) 1.75 mg/L, (3) 0.875 mg/L, (4) 0.44 mg/L, (5) 0.22 mg/L, and (6) 0.11 mg/L in the presence of NSF superplasticiser (10:1 NSF-to-MWCNTs). (b) Recorded UV-vis spectra of F-MWCNTs at different concentrations. (c) Absorption as a function of concentration of the F-MWCNTs suspensions conducted at the wavelength of (300, 400, 500, and 600).

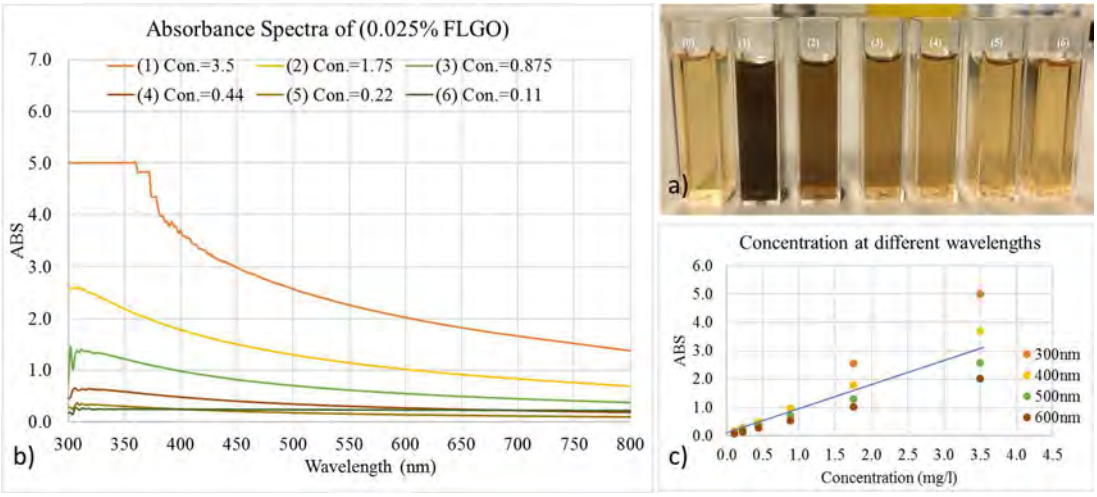

Figure 5.4 a) Optical micrograph of the 0.025%FLGO suspensions at different concentrations: (1) 3.5 mg/L (starting MWCNT solution), (2) 1.75 mg/L, (3) 0.875 mg/L, (4) 0.44 mg/L, (5) 0.22 mg/L, and (6) 0.11 mg/L in the presence of NSF superplasticiser (10:1 NSF-to-MWCNTs). (b) Recorded UV-vis spectra of FLGO at different concentrations. (c) Absorption as a function of the concentration of the FLGO suspensions conducted at the wavelength of (300, 400, 500, and 600).

5.2.1.1 Transmission Election Microscopy Characterisation

TEM images of the carbon nanofibres, functionalised carbon nanotubes and few layer graphene oxide, before and after sonication treatment, are shown in Figures 5.5, Figures 5.6, and Figures 5.7, respectively.

5.2.1.1.1 As-Supplied CNFs

As-Supplied nanofibres (CNFs) suspensions without ultrasonication treatment were in the form of agglomerates, Figure5.5 (a-b) show that most of the nanofibres are present as clusters, and no individual fibres can be observed. The sonication treatment using the proposed technique combined with NSF was effective at breaking up the agglomerates and dispersing the CNFs, and abundant individual nanofibres could be observed following treatment, in addition to smaller bundles (with an average size of 500nm). Figure 5.5 (b-f) show the average diameter (with the adsorbed layer of NSF), and length distribution of the CNFs after sonication treatment. The resulting individual nanofibres range in size from 150 to 200nm, with the majority of the CNFs having lengths in the range 20um to 50um. Although dispersion using ultrasonication will inevitably reduce the length of CNFs (Tyson et al. 2011), high sonication intensity over short time periods has been found here to be less damaging (the measured sizes after dispersion remained in the same range as the as supplied CNTs, (see Chapter Three, Table 3.1)). Retaining a relatively high aspect ratio for the CNFs during their dispersion in the cementitious composites is essential if they are to act as an effective reinforcing agent, since the improvement in the composite mechanical strength will be proportional to the fraction of embedded CNFs with less damage (Parveen et al. 2013).

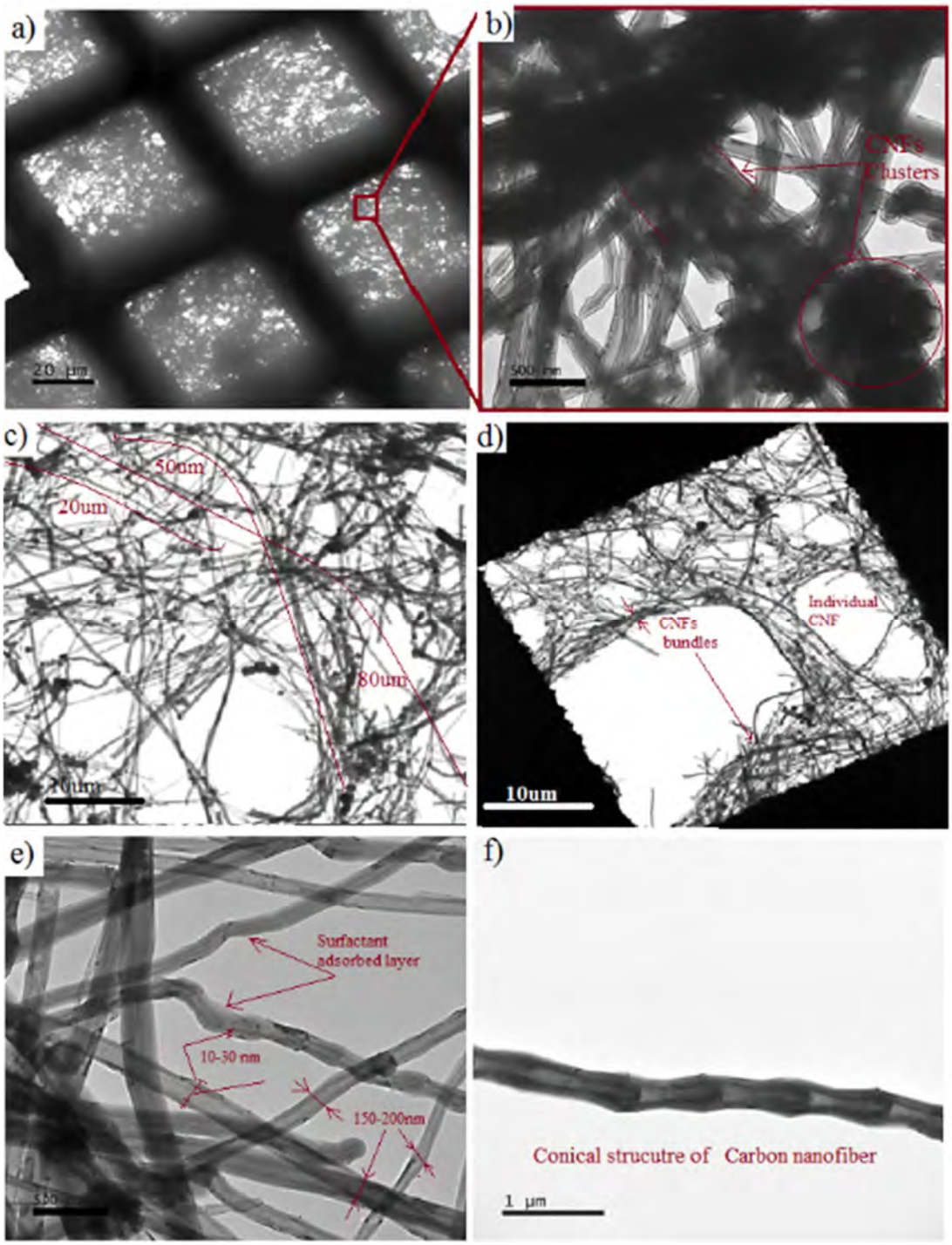

Figure 5.5 TEM images of carbon fibre suspensions, a-b) showing the agglomeration of nanofibres on the grid during the test, c-d) represent bundles and individual nanofibres at progressively higher magnification, and e-f) show diameters of individual nanofibres.

5.2.1.1.2 As-Supplied F-MWCNTs

Chemical modification of the surface properties of MWCNTs is one of the methods that has been attempted to improve the dispersion of nanotubes in water. Chemical functionalization is based on grafting the covalent bond of hydroxyl functional groups (-COOH) onto the carbon form of the nanotubes. These groups can be generated at the ends or at the sidewalls of nanotubes, which have many defects(Chunyu Li 2003). Functionalization methods can be achieved via a wide range of methods such as oxidative damage to the nanotube framework by strong acids, in particular, treatment of CNTs with strong acid such as HNO_3, H_2SO_4 or a mixture of them, which leave holes functionalized with oxygenated functional groups(Barick and Tripathy 2011). Figures 5.6 show the dispersibility of functionalised nanotubes before and after sonication treatment. F-MWCNTs in the suspension before sonication remained in large clusters, revealing that the availability of functional groups alone was not enough to obtain individual dispersed nanotubes (Figure 5.6a). Figures 5.6 (b-d) show images of the suspensions after sonication, differences in the structure of functionalised nanotubes were observed, nanotubes appeared to be defected and shorter compared to that of “as received” nanotubes. This could be attributed to the pre- functionalisation process and ultrasonication treatment in this study(Peng-Cheng et al. 2010, In-Yup Jeon1 2011). The diameter of nanotubes has also been increased after ultrasonication as compared to the “as-supplied” functionalised MWCNTs which possibly relates the introducing of surfactant layer. Moreover, structural damage and shortening the tubes by the functionalization (acidic oxidation process) and ultrasonication are probably due to the action of intensive energy delivered to the suspension (shear force) on the defect areas (the bond areas with -COOH), leading to rapid shortening of the tubes and widening of the defect zones.

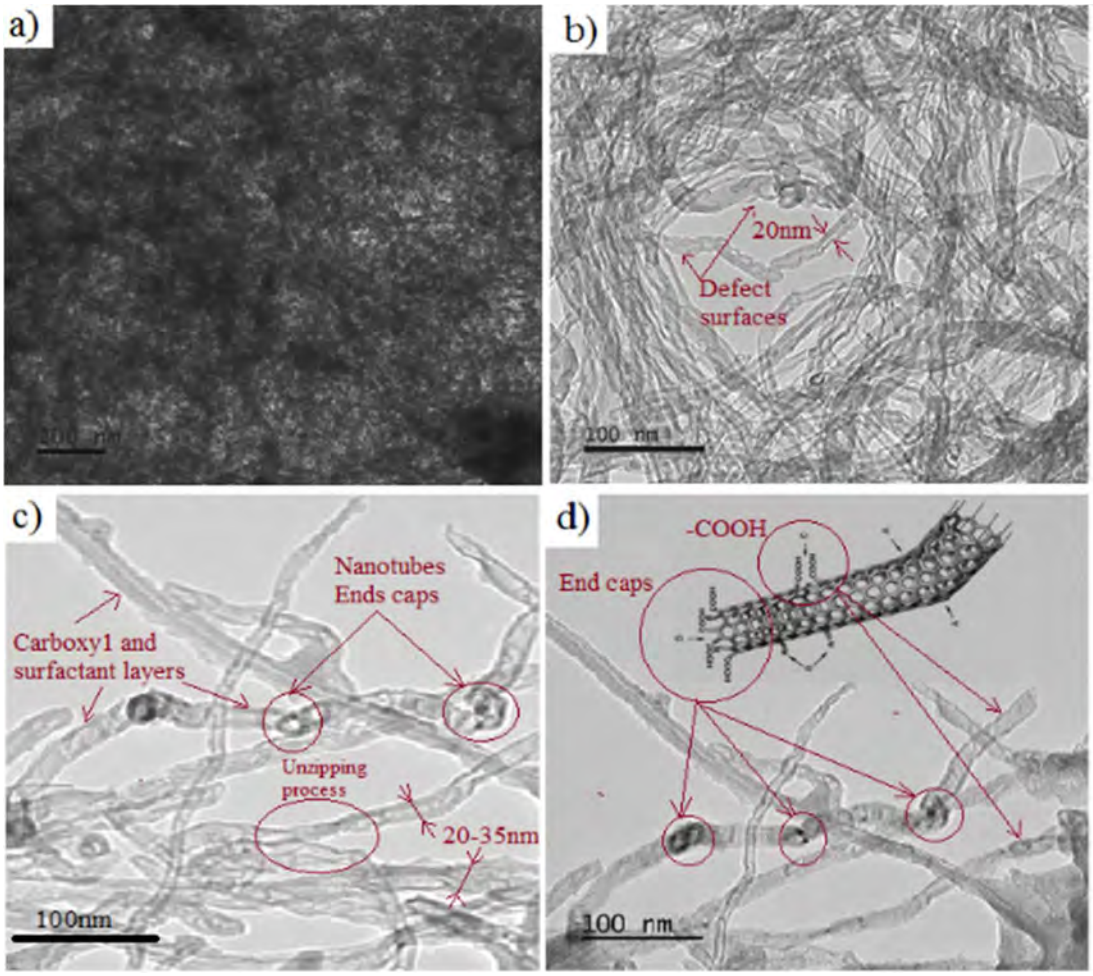

Figure 5.6 TEM images of hydroxyl functionalised MWCNTs a) nanotubes suspension manually mixed for 2 minutes, b-d) showing the nanotubes suspensions after sonication treatment, the morphology of functionalised nanotubes, and the geometry of nanotubes, and the thickness of the adsorption layers.

5.2.1.1.3 As-Supplied FLGO

TEM images of the as-supplied graphene oxide suspension (manually shaken for 2minutes) show a number of graphene sheet-like transparencies over the investigated area of about 100 μ m×100μm (scale bar: 20μm) and 20μm×20μm (scale bar: 5μm), Figures 5.7 a, and b, respectively. The observed dark areas show thick stacking of graphene layers. After sonication treatment, the prevalence of higher transparency areas indicates the presence of much thinner films of single-to-few layers graphene oxide (as shown in Figure 5.7 c-d).

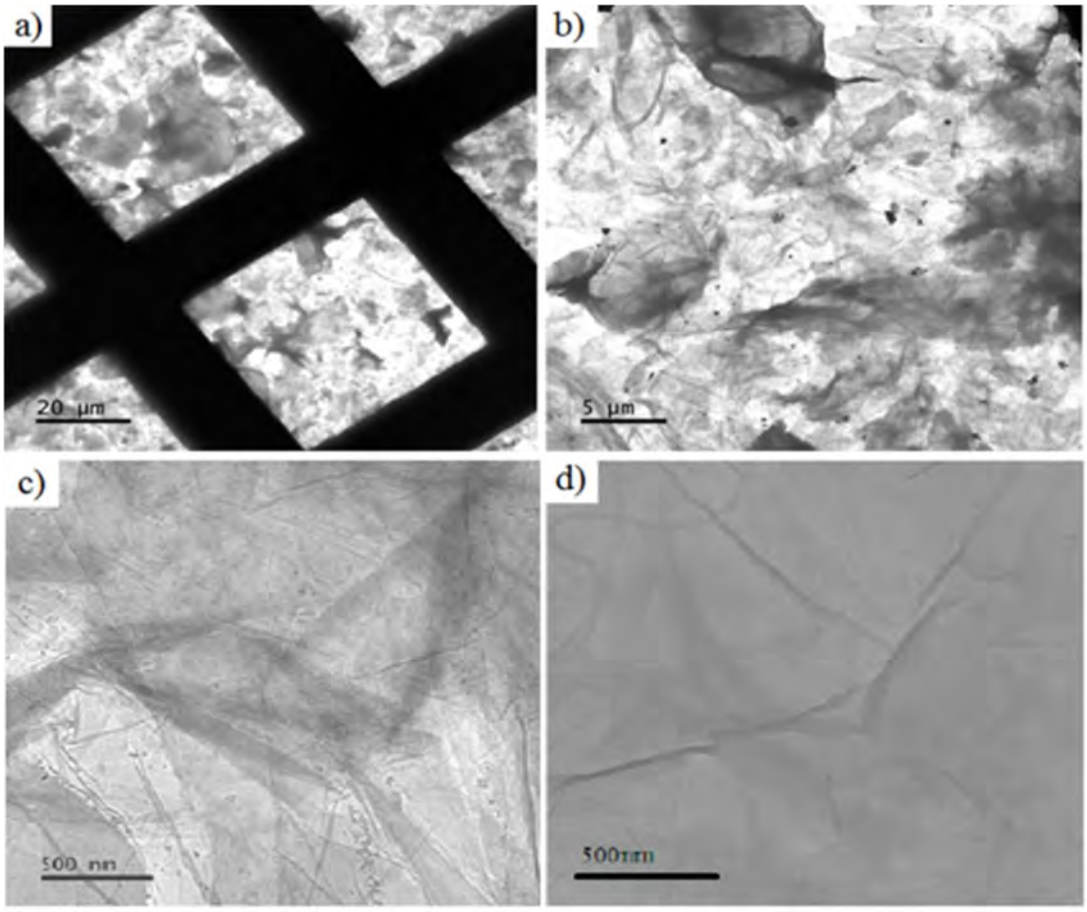

Figure 5.7 TEM images of few layer graphene oxide. a) suspension before ultrasonication with graphene and surfactant in water, and manually shaken for two minutes, b) suspension after ultrasonication.

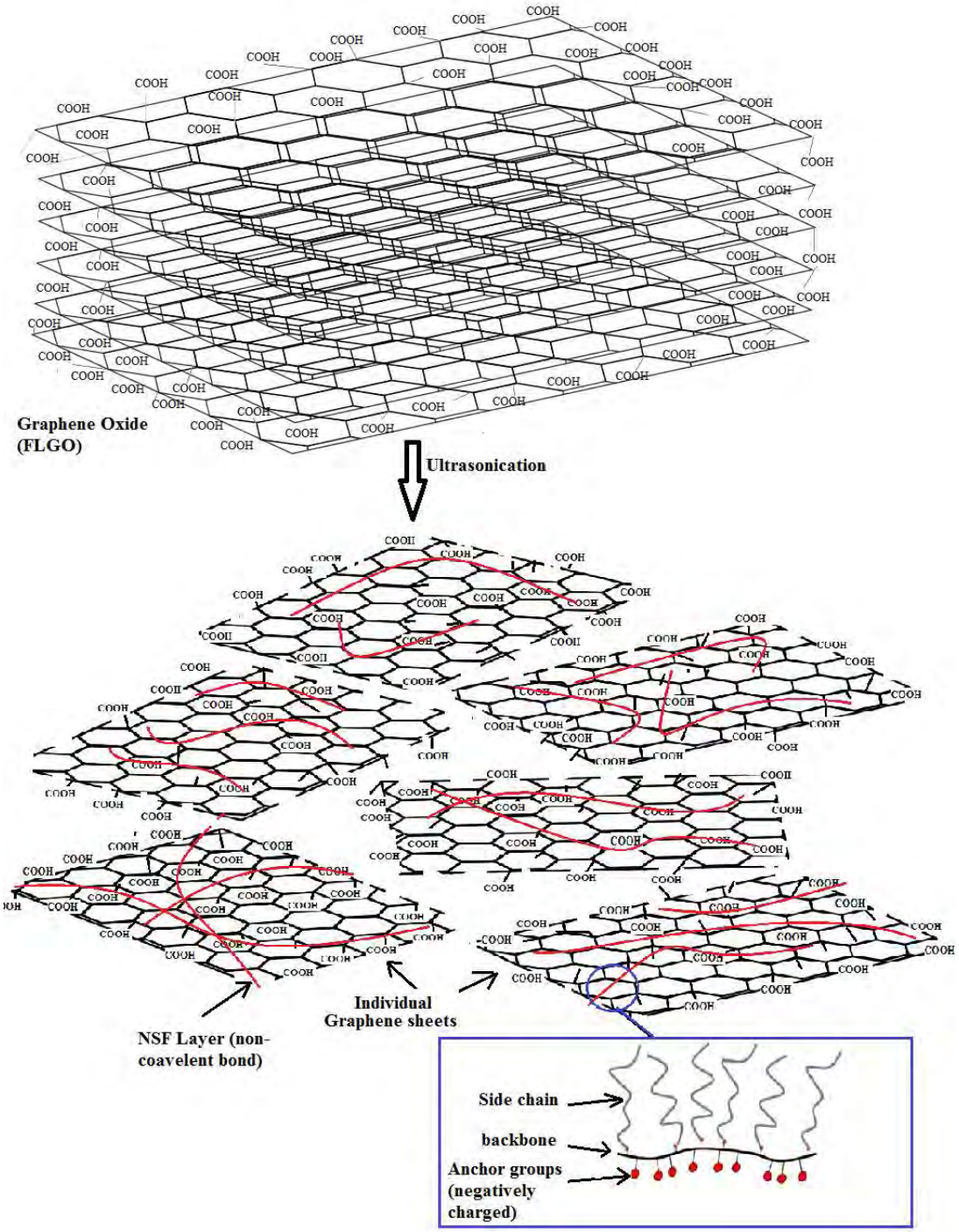

Figure 5.8 Schematic diagram for dispersion of FLGO through the ultrasonication process.

Given the structure of FLGO and the observed TEM images, a schematic diagram (Figure 5.8) is proposed to summarise the exfoliation process of agglomerated graphene sheets. When the functionalized graphene sheets and the surfactant were mixed together, the dispersion is generally accomplished by the chemical modification (covalent bond of hydroxy1 groups) of the graphene sheets and through non-covalent functionalization with a dispersant (red lines), both modifications together enhanced significantly the repulsive force in-between the nano-scale sheets. In other words, under ultrasonic treatment, the grafted graphene sheets were a result of the synergistic effect of both carboxy1 groups and the surfactant which increased the interlayer space. Thus, the TEM micrographs confirm that high intensity sonication applied over short time periods produces graphene exfoliation with fewer graphene layers.

5.2.2 Characterization of Nano-additives Reinforced Cementitious Composites (NRCC)

Composite materials produced using the optimal dispersion method were further characterized in term of their mechanical performance following nano-additives (i.e CNFs, MWCNTs, F-MWCNTs, and FLGO) incorporation. Details of the mixture proportions by weight are given in Table 3.11. Workability and Porosity and density measurements are firstly presented, followed by the hardened cementitious composite strengths (in term of; compressive strength, direct and indirect tensile strengths, and flexural strength), toughness behaviour, and relationship between the mechanical strength properties**.** For comparison, MWCNTs/composites compressive and direct tensile strengths results are also presented (these results were presented in chapter four phase II). Although there are no standard test methods have been adopted by ASTM to provide direct measurement of tensile strength of cement composites, direct tensile strength (via dog-bone shaped specimens) has been used here to provide a uniaxial and approximate real tensile strength of cementitious composites containing nano-additives. Finally, the microstructure characterisation is presented.

5.2.2.1 Workability

In this study, flow properties (an indicator of workability) of fresh mixtures of the produced nano-additives cementitious composite were evaluated based on flow table results. The workability of mixtures containing MWCNTs and CNFs was slightly lower than mixtures without nano-additives (i.e. control mixtures). The finding indicates that the addition of low amounts of carbon nanotubes/fibres did not impact (i.e. only slightly reduced) the workability. The rheological properties were enhanced (flow value of 110%) for mixtures containing functionalised carbon nanotubes (F-MWCNTs), and few layer graphene oxide(FLGO) which can be attributed to an increased wettability caused by the functional groups (-COOH) present on the tube walls/sheets.

5.2.2.2 Porosity and Density Measurement.

Porosity and density determinations of cementitious composite (with and without nano-additives) were carried out on a range of core specimens and compressive cubes at 28 days to evaluate the effect of carbon nanotubes/fibres and graphene sheets on physical properties. Values for the control mortar and composites containing nano-additives after 28 days curing are shown in Figure 5.9a. At 28 days, it is evident that the incorporation of nanotubes/fibres had filled internal pores and reduced composite porosity. Addition of 0.025% F-MWCNTs, MWCNTs, CNFs, and FLGO resulted in a decrease of composite porosity by 17%, 21%, 26%, and 21%, respectively, compared to the mixture without nano-additives. This reduction in porosity can be attributed to the effect of individual nano tubes/fibres filling pores between hydration products and bridging nano/micro capillary pores. Optimising the porosity of nano-additives cementitious composites is vital since porosity significantly impacts the mechanical performance, as crack propagation begins at the pores and the nano-additives are essential in refining the pore structures(Samuel et al. 2014).

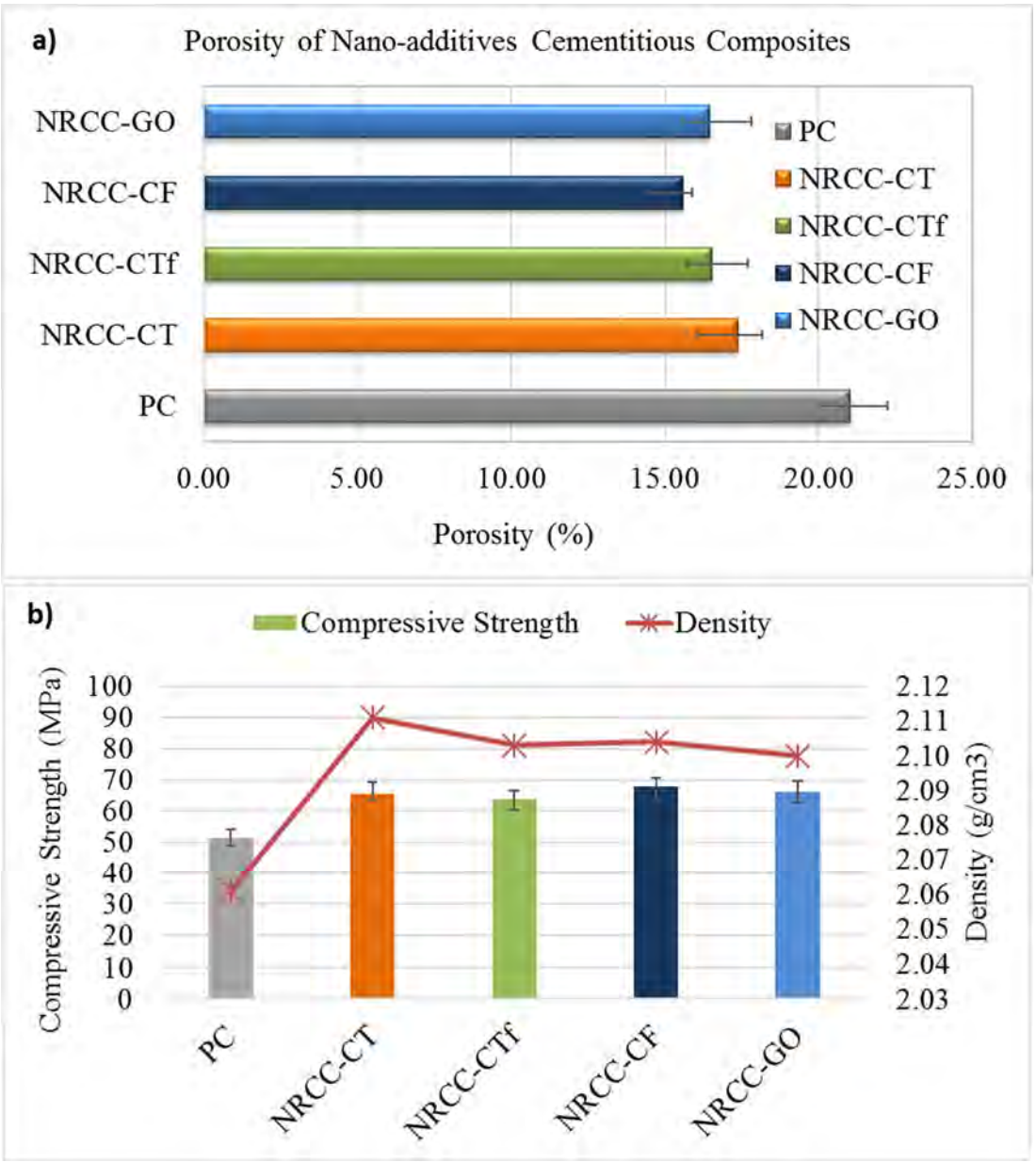

Figure 5.9 a, and b are graphs show Porosity (%) and density (g.cm-3) results for cementitious composite specimens containing MWCNTs, F-MWCNTs, CNFs, and FLGO in addition to control specimens (PC) after 28 days curing.

In principle, addition of these materials slightly affects the density of the cementitious composites, the average density measured on control specimens was 2.06 g/cm^3 with a standard deviation of 0.35, and addition of MWCNTs, F-MWCNTs, CNF, and FLGO slightly increased the density up to 2.12g/cm^3 with a standard deviation of 0.27. This increase however was not statistically significant. The improved packing density

is attributed to the refining of structural composite pores resulted with the addition of nano-additives. Above Figures5.9b shows the correlation between the 28-compressive strength and the recorded density, this confirms that while there was no distinct effect of nano materials on the density, they do enhance the mechanical strength of the material.

5.2.2.3 Mechanical strengths

The obtained results and variations observed in the compressive strength, tensile strength, and flexural strength are presented in terms of percentage changes with respect to the reference mix (PC) of each nano-additive specimen on day 3, 28, and 90. All results are presented in Figures 5.10.

Inclusion of nano-tubes/fibres/graphene sheets generally improves the composites' mechanical strengths and the obtained results are as follows:

1- **Compressive strength:** Improvement in the compressive strength of the mixtures containing MWCNTs (NRCC-CT), F-MWCNTs(NRCC-CTf), CNFs (NRCC-CF), and FLGO(NRCC-GO) at 3, 28, and 90 days was: 30%, 35%, 38%, 33%; 28%, 24%, 32%, 29%; and 11%, 15%, 20%, 17% compared to the control mix (as shown in Figure5.10a).

2- **Flexural Strength:** It is apparent that there is a distinct variation in improvement in flexural strength, depending on the nano-additive used. MWCNTs, and F-MWCNTs led to moderate improvement ranging between 6% and 17%. CNFs lead to a maximum of 32% improvement after 90 days, while using FLGO led to a significant improvement i.e after 3, 28, and 90 days' improvement of 77%, 52%, 68% (Figure 5.10b).

3- **Tensile Strength:** as shown in Figure 5.10c and Figure 5.10d the improvement in direct tensile strength from addition of MWCNTs, F-MWCNTs, CNFs, and FLGO was 37%, 18%, 18%, 56%; 29%, 16%, 19%, 52%; and 42%, 19%, 16%, 51% after 3, 28, and 90 days, respectively. The results show that addition of nanotubes/fibres or graphene sheets obviously increases the direct tensile strength. A significant

improvement was obtained in splitting (indirect) tensile strength which was generally higher than that obtained with direct tensile tests. A 42%, 35%, 38%; 50%, 45%, 47%; and 75%, 38%, 38%, 52% after 3, 28, and 90 days, increase in the splitting tensile strength was observed with NRCC-CT, F- NRCC-CTf, and NRCC-GO (due to the high cost of the graphene material, this test was not carried out with graphene).

The effectiveness of using the same added percentage of the nanotubes/fibres/graphene sheets in increasing the cementitious composite compressive, flexural, direct and splitting tensile strength was in in the order of; CNFs> F-MWCNTs=FLGo> MWCNTs, FLGO> CNFs> F-MWCNTs> MWCNTs, and FLGO> CNFs> F-MWCNTs> MWCNTs, respectively. Furthermore, at early age (i.e. after 3 days curing), the strength enhancement is distinctly higher than at 28 days, while the strengths at 28 days were little different (lower) from the strengths at age of 90.

Both direct and indirect tensile strength tests have been carried out to determine the tensile stress of control mortar (PC) and composite of NRCC-CT, NRCC-CTf, NRCC-CF, and NRCC-GO. A significant difference in the tensile strength results obtained from two methods can be noticed. Splitting tensile strength was higher than the obtained strength for direct tensile strength, which agrees with previous studies (Sarfarazi et al. 2016), and can be attributed to a high stress gradient along the crack plane. It is interesting to note that the difference between the splitting and direct tensile strengths is about 37%, 52%, 74%, 60% of PC, CT, CTf, and CF, respectively. The difference in the tensile strength of the two methods may therefore be partly governed by tensile stress distribution on the failure surface.

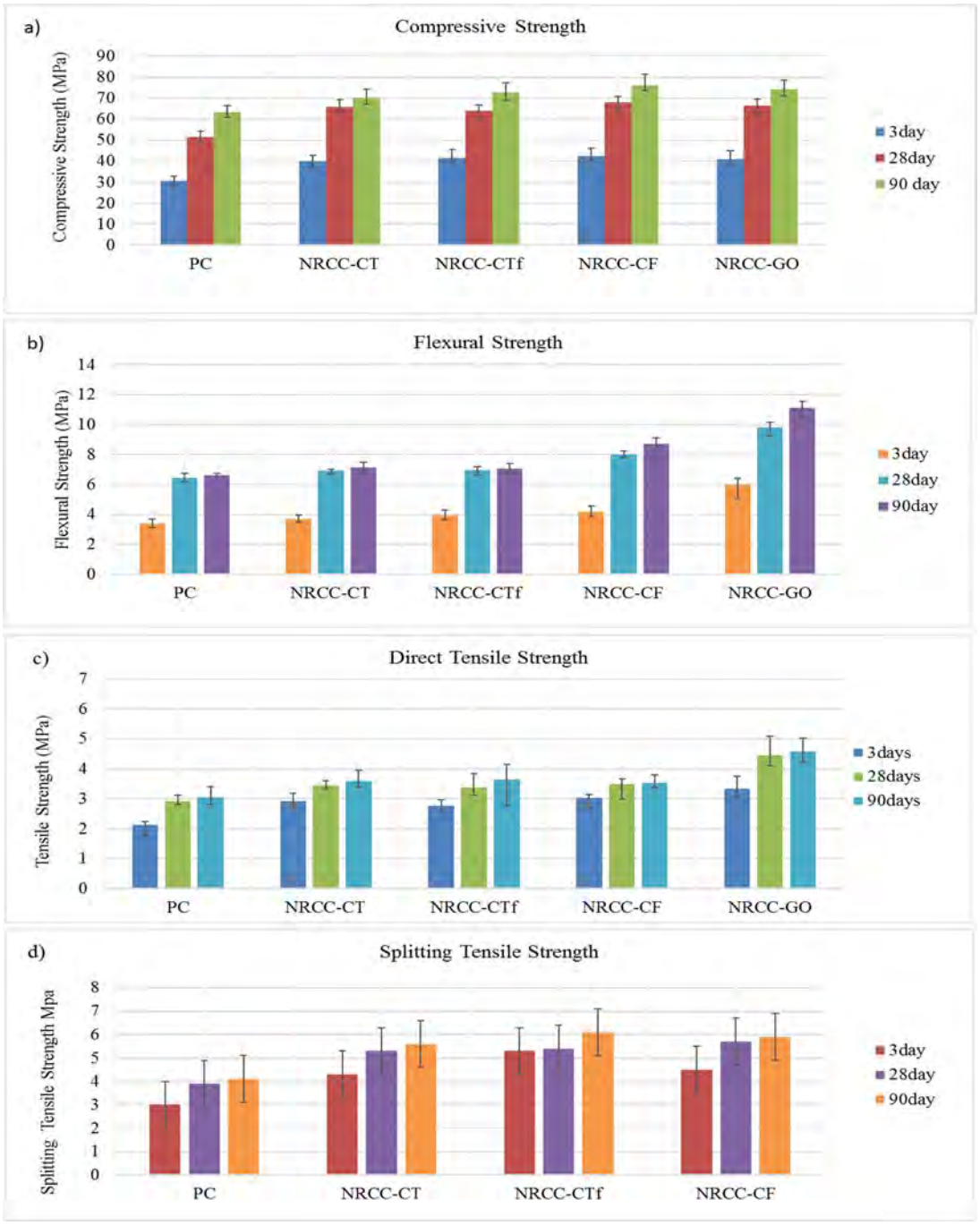

Figure 5.10 Graphs representing a) compressive strength, b) flexural strength, c) direct tensile strength, and d) splitting (indirect) tensile strengths of cementitious mixture (PC), and composite of NRCC-CT, NRCC-CTf, NRCC-CF, and NRCC-GO.

Generally, the significant improvement in splitting tensile strength over all the investigated tests of the composites can be attributed to the effective dispersion of the nano-additives. The well-dispersed and less defected nano particles can provide an effective nanofibres with high distribution states through the matrix, thus giving a higher arresting capacity with the cement hydration products. Poor dispersion has been found to play a crucial role in the mechanical performance of a material, which weakens rather than reinforces the composites, which leads either to no distinct improvement or a negative impact on the mechanical performance of the composites (Kim et al. 2012, Kerienė et al. 2013, Metaxa et al. 2013, Stynoski et al. 2015). Poorly dispersed nano-additives may become entangled into the hydration products, forming pores in between the bundles in the matrix. In addition, bundled tubes/fibres/sheets have too great a spacing to effectively control crack formation and propagation.

These results indicate that a very low content of nano-additives (0.025%) dispersed using the high intensity sonication method developed here is sufficient for improving the performance of cementitious composites reinforced with these additives, compared to a relatively higher content dispersed using complicated/longer methods as described in the literature.

5.2.2.4 Toughness Behaviour

The toughness of nano-additives reinforced cementitious composites was determined following three-point bending tests by calculating the area under the corresponding load–deflection curve, which is related to the energy absorption capacity of the material. The load–deflection curve was analysed according to the Japan Society of Civil Engineers (JSCE) method, which yields a flexural toughness factor, FT_{δ}.

Relationships between the load as a function of different deflection values and the obtained flexural toughness factor at various ages (3, 28, 90 days) are shown in Figure 5.11. Apparently the nano-additives inclusion does not prevent sudden and brittle failure when compared with the plain control mix. However, composites containing a nano-additive such as MWCNTs, F-MWCNTs, CNFs, FLGO were found to significantly increase the energy absorption (flexural toughness factor). Remarkable

increments of the flexural toughness factor can be seen in Table 5.1 with type of nano-additive (MWCNTs, F-MWCNTs, CNFs, and FLGO) added to the composite, and as a function of the recorded deflection up to failure (from 0.01mm to 0.045 mm at early age, and from 0.025mm to 1.25mm at 28 and 90 days). The high aspect ratio of nanotubes/fibres can successfully bridge nano cracks, and pulling out of these additives requires significantly more energy.

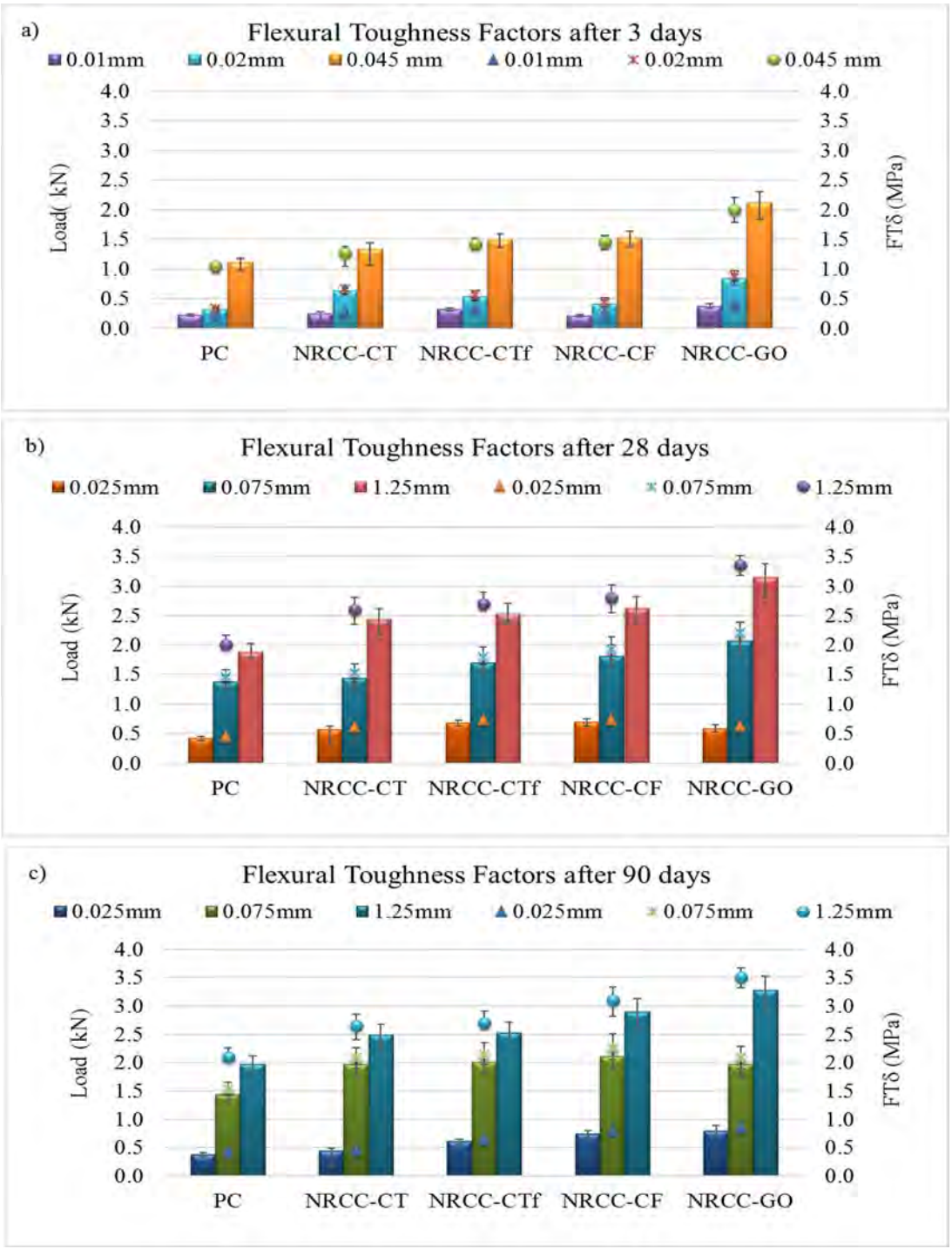

Figure 5.11 Relationship between the flexural load, and flexural toughness factor at different deflection values (from 0.01mm to 0.045 mm at early age, and from 0.025mm to 1.25mm at 28 and 90 days) for the reference PC and nano cementitious composites.

Table 5.1 Flexural toughness factors at 3, 28, 90 days for control and nano-additives reinforced cementitious composites of NRCC-CT, NRCC-CTf, NRCC-CF, and NRCC-GO.

Specimens designation	Nano-additives (%)	Flexural Toughness Factor MPa (3day)		Flexural Toughness Factor MPa (28day)		Flexural Toughness Factor MPa (90day)	
		Mean (MPa)	% Increase	Mean (MPa)	% Increase	Mean (MPa)	% Increase
PC	0	1.11	0	1.88	0	1.97	0
NRCC-CT	0.025	1.34	21	2.44	30	2.48	26
NRCC-CTf	0.025	1.50	35	2.53	35	2.53	29
NRCC-CF	0.025	1.63	48	2.63	40	2.91	48
NRCC-GO	0.025	2.11	90	3.14	68	3.28	67

5.2.3 Mechanical Strengths Relationships

In ACI318R-99, the relationship between flexural tensile strength f_f and compressive strength (fc) of ordinary Portland cement(OPC) is proposed as $f_f=0.62\ f_c^{0.5}$. The given relationship between splitting tensile strength f_{sp} and compressive strength f_c based on the ACI318-99 code is $f_{sp}=0.59\ f_c^{0.5}$. However, the relationship between tensile strength and compressive strength in nano cementitious composites is not yet defined. This relationship is examined here based on multiple regression analysis of test data.

5.2.3.1 Compressive Strength-Flexural Strength

In this work an investigation of the applicability of the existing relationship between the compressive strength and the flexural strength of cementitious composites

reinforced with different nano-additives is made by multiple regression analysis. The relationship proposed using multiple regression analysis is represented by $f_f = K\ f_c^s$. The values of slope (S) and intercept (K) obtained from experimental data are shown in Table 5.2. Figure 5.12 shows the regression equations based on the experimental results with, for comparison, the relationship from the predicted empirical regression equation using ACI-318R. The regression lines obtained (predicted, and from the experimental results) show that at early ages, a relatively consistent, within-estimate, relationship between the flexural strength and compressive strength was obtained (except for an overestimate with the FLGO composite) while a large deviation of the experiments results obtain from the predicted trend occurred with the 28 and 90-day test data (up to twofold with FLGO). The coefficient of determination (R2) is an indicator of the total variation in the dependent variable for the regression equation, and was found to be between 0.88-0.92. Most statisticians consider a R2 of 0.7 or higher for a reasonable model (although this depends on the number of data points). The results of the experimental and predicted flexural strengths, and the experiment to predict ratio were summarised in Table 5.2.

Similar to the factors affecting the compressive strength, the flexural strength of cementitious materials could be affected by the cement, and microsilica types and percentages, W/C ratio, curing time, specimen size and the testing method. In addition to these factors, flexural strength of nano-cementitious composite could be affected by the many other factors such as the types of the used nano-additives, concentrations, aspect ratios, and dispersion methods. Furthermore, the number of test data is important because the more test data may provide the better statistical validation for various factors. Although, the obtained equations as a function of their compressive strength using a relatively good number of experimental data, a further research is needed to verify the proportional relationship derived in this study, and to determine the effects of nano tubes/fibre/graphene sheets types, contents, numbers of test data, curing time and other factors. Thus, the derived relationship could be successfully used to represent the relationship between the flexural strength and compressive strength of cementitious composites containing different nano-additives dispersed based on the proposed method.

Table 5.2 Properties of regression equations of the relationship between compressive strength and flexural strength.

Mix	Slope, S	Intercept, K	Regression Equation	coefficient of determination
PC	0.96	0.128	$f_f(PC)= 0.128f_c^{0.96}$	R2= 0.89
NRCC-CT	0.94	0.154	$f_f(CT)= 0.154f_c^{0.94}$	R2= 0.88
NRCC-CTf	0.82	0.257	$f_f(CTf)= 0.267f_c^{0.82}$	R2= 0.85
NRCC-CF	1.1	0.110	$f_f(CF)= 0.11f_c^{1.10}$	R2= 0.92
NRCC-GO	1.1	0.134	$f_f(GO)= 0.134f_c^{1.10}$	R2= 0.89

Table 5.3 Summarizes the experimental results, predicted flexural strength as a function of the compressive strength, and the ratio of experimental/predicted strength of PC, NRCC-CT, NRCC-CTf, NRCC-CF, and NRCC-GO composites.

ID	Experimental flexural Strength (MPa)			Predicted flexural Strength (MPa) $f_f= 0.62fc^{0.5}$			Experimental /predicted ratio		
	3 day	28 day	90 day	3 day	28 day	90 day	3 day	28 day	90 day
PC	3.52	6.75	6.53	3.45	4.22	4.94	1.02	1.60	1.32
NRCC-CT	3.49	7.08	7.12	3.95	4.87	4.90	0.88	1.45	1.45
NRCC-CTf	3.99	7.30	7.12	3.89	4.89	5.24	1.03	1.49	1.36
NRCC-CF	4.36	7.99	8.72	3.83	5.09	5.39	1.14	1.57	1.62
NRCC-GO	6.16	8.72	10.35	3.98	5.17	5.17	1.55	1.69	2.00

*Values under predicted flexural strength

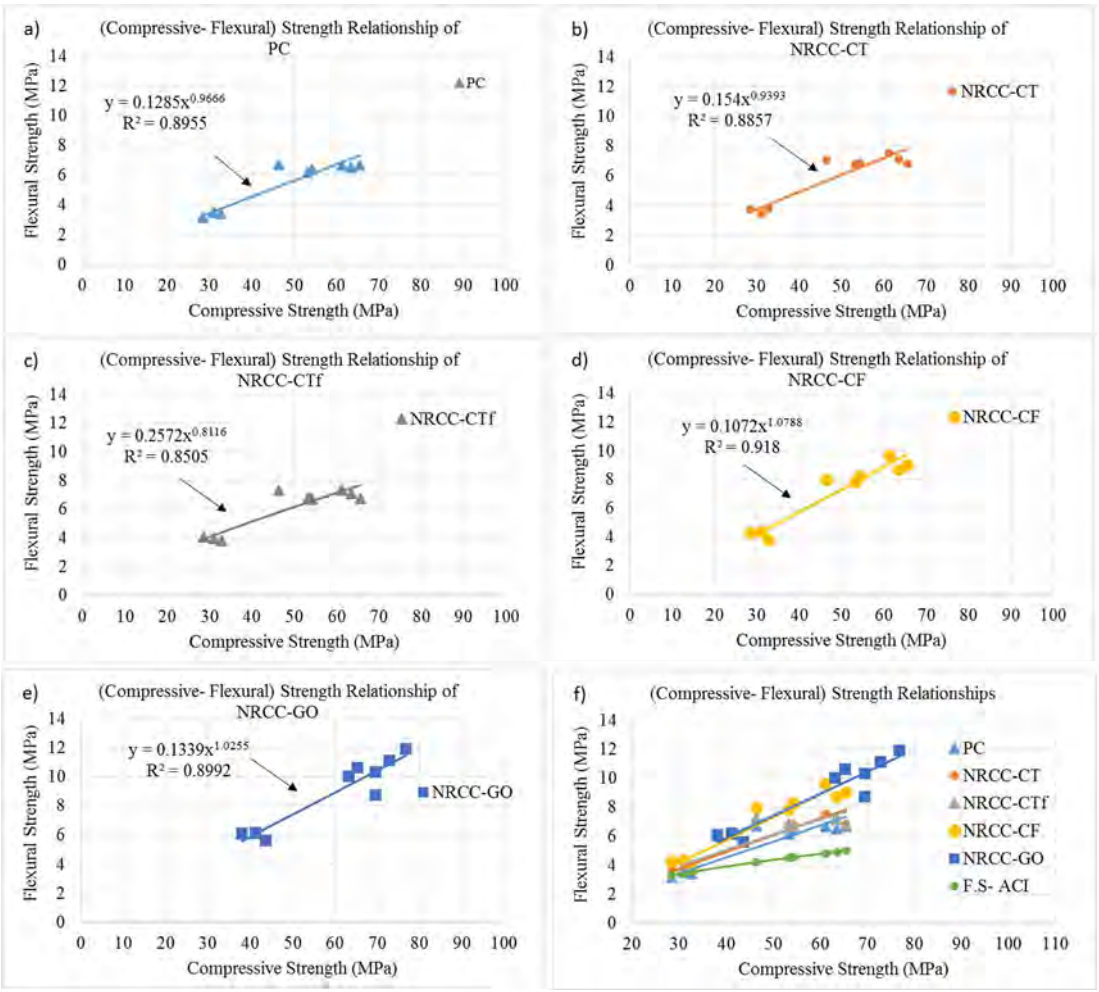

Figure 5.12 Graphs showing the experimental and predicted regression flexural strength equations for each nano-additive used in fabricating nano cementitious composites in addition to the control mix. The predicted equations are based on the equation of ACI 318R ($f_{td(PC)}= 0.62fc^{0.5}$).

5.2.3.2 Compressive Strength- (Direct and Splitting) Tensile strengths

Many researchers have found that the strength development pattern for tensile strength is similar to that of compressive strength, and depends on the strength of concrete, the type of curing, age and other factors.

Many empirical formulae are available for determining concrete splitting tensile strength ((fs_t) as a function of compressive strength and most researchers utilise a formula of the type:

$$f_{st} = K(f_c)^s \quad \text{(Eq.5.2)}$$

Where s is generally between 0.5 and 0.75.

The formulae as suggested by Iravani (Iravani 1996), ACI318-99, and CEB-PIP(MC 1993), respectively, are given below:

$f_{st} = 0.57\ f_c^{0.5}$ 50 MPa< f_c< 100 MPa (Eq. 5.3)

$f_{st} = 0.59\ f_c^{0.5}$ 21 MPa< f_c< 83 MPa (Eq. 5.4)

$f_{st} = 0.301\ f_c^{0.67}$ (Eq. 5.5)

The ACI equation (i.e. Eq.5.4) has been used in this study for comparison with the experimentally-derived equations, Table 5.4 summarizes the K and S values of all obtained experimental relationships. The development of splitting tensile strength of the nano composites with varying type of nano-additive in addition to the control mix are shown in Figure 5.13.

The experimental splitting strength of the control specimen (PC) was around 10% lower than the predicted value over all examined ages. The R-squared value (R2 = 0.953) shows that there is strong correlation between the criterion variable (flexural strength) and the predictor variables. From Figure 5.12, while the compressive-splitting strength relationships of NRCC-CT, NRCC-CTf, and NRCC-CF composites show the same linear trend, the experimental strengths of these composites were over the predicted strengths. For example, at 28 days (standard age) the experimental tensile strength of NRCC-CT, NRCC-CTf, and NRCC-CF composites was 4.97MPa, 5.86MPa, and 5.68MPa while the predicted tensile strength for same composites was about 4.3MPa, 4.7MPa, and 4.8MPa (Table 5.5).

Table 5.4 Properties of regression equations showing the relationship between compressive strength and splitting tensile strength, based on experimental data.

Mix	Slope, S	Intercept, K	Regression Equation	Coefficient of determination
PC	0.45	0.64	$f_{ts(PC)} = 0.64 f_c^{0.45}$	$R^2 = 0.92$
NRCC-CT	0.50	0.68	$f_{ts(CT)} = 0.5\, f_c^{0.50}$	$R^2 = 0.91$
NRCC-CTf	0.60	0.45	$f_{ts(CTf)} = 0.60 f_c^{0.60}$	$R^2 = 0.92$
NRCC-CF	0.45	0.85	$f_{ts(CF)} = 0.45 f_c^{0.45}$	$R^2 = 0.96$

Table 5.5 Experimental results, predicted splitting tensile strength as a function of the compressive strength, and the ratio of experimental/ predicted strength for PC, NRCC-CT, NRCC-CTf, and NRCC-CF composites.

ID	Experimental Splitting Tensile Strength (MPa)			Predicted Splitting Tensile Strength (MPa) $f_{sf} = 0.0.59 f_c^{0.5}$			Experimental /predicted ratio		
	3day	28day	90day	3day	28day	90day	3day	28day	90day
PC	2.93	3.83	3.98	3.3	4.2	4.4	0.89*	0.95*	0.85*
NRCC-CT	4.31	4.97	5.64	3.8	4.3	4.7	1.15	1.07	1.21
NRCC-CTf	5.17	5.68	6.32	3.7	4.7	5.0	1.40	1.22	1.27
NRCC-CF	4.53	5.81	6.00	3.83	4.8	5.1	1.18	1.20	1.17

*Values under predicted splitting strength

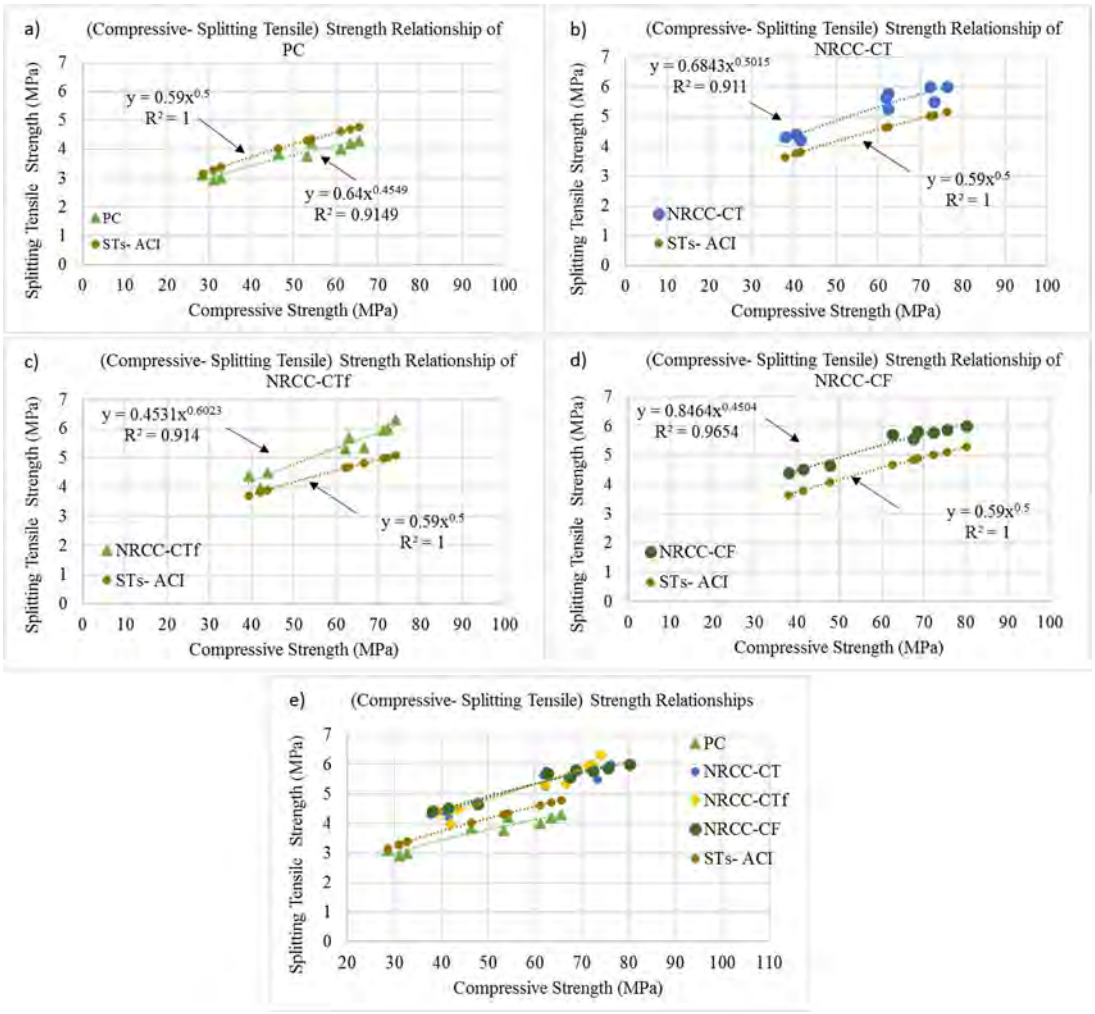

Figure 5.13 Graphs showing the experimental and predicted regression equations of compressive strength- splitting tensile strength of each nano-additive composites used in this study in addition to the control mix. Predicted equations are based on the equation of ACI 318R ($f_{td(PC)}= 0.59fc^{0.5}$).

Splitting strength was higher than the direct tensile strength for all the control and nano cementitious specimens: The splitting tensile strength of control and nano-additives reinforced cementitious composites of NRCC-CT, NRCC-CTf, and NRCC-CF was 37%, 62%, 63%, and 65% higher than of those direct tensile strengths. The obtained value (of difference between direct and indirect strength) of the control mixture is in good agreement with the literature(Khalaj and Nazari 2012, Mokhtar et al. 2017). The difference in the tensile strength between the two methods may therefore be partly governed by tensile stress distribution on the failure surface.

By regression, good correlations are found between the compressive strength and splitting strength and direct tensile strength as shown in Figure 5.14. From the equations summarised in Table 5.6, and as represented in Figure 5.14, both splitting tensile and direct strength can be predicted using the compressive strength values.

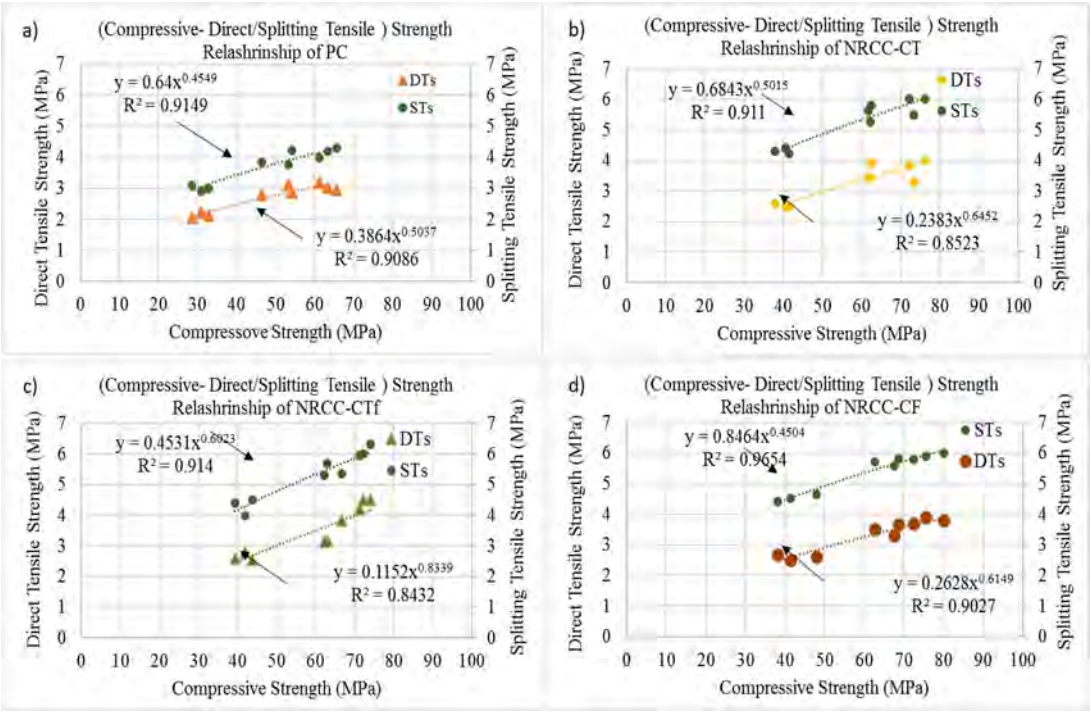

Figure 5.14 Graphs showing the regression equations of compressive strength, and direct tensile strength (DTs) and splitting tensile strengths (STs) of NRCC-CT, NRCC-CTf, and NRCC-CF, in addition to the control mix.

Table 5.6 Properties of regression equations of the relationship between compressive strength and direct tensile Strength.

Mix	Slope, S	Intercept, K	Regression Equation	coefficient of determination
PC	0.45	0.38	$f_{td(PC)}= 0.38f_c^{0.45}$	$R^2= 0.91$
NRCC-CT	0.5	0.40	$f_{td(CT)}= 0.40f_c^{0.5}$	$R^2= 0.81$
NRCC-CTf	0.81	0.12	$f_{td(CTf)}= 0.12f_c^{0.81}$	$R^2= 0.84$
NRCC-CF	0.61	0.27	$f_{td(CF)}= 0.27f_c^{0.61}$	$R^2= 0.91$

5.2.4 Microscope Characterisation

As discussed in Chapter Four, preventing the re-agglomeration of the nanotubes themselves can also play an important role in the improvement of mechanical properties of the composite. The addition of undensified microsilica (USF) is one of the main parameters of the proposed dispersion technique (explained in chapter four, Phase II), and this has proven to effectively enhance the performance of nanotubes through a cementitious composite. The synergistic effect of USF on preventing the re-agglomeration of CNF, F. MWCNTs, and FLGO through the composites was firstly studied through high magnification TEM images of particle suspensions. After, their hardened composites were investigated by SEM imaging.

5.2.4.1 TEM Investigations

Images in Figures 5.15, Figure 5.16, and Figure 5.17 show the interaction of small diameter silica particles with nanotubes, nanofibres, and graphene sheets. Similar to the observed trend of MWCNTs in chapter Four (phase II), USF can improve the dispersion of nanotubes/fibres and graphene sheets, and prevent their re-agglomeration (due to the strong attraction force between them). Figures 5.15 revealed that the large diameter of nanofibres (compared to the diameters of nanotubes) is almost similar to the diameter of most silica particles (in the range of 200nm (Figure 5.15a)). This could enhance the efficiency of silica particles, as a physical barrier, in

preventing the re-agglomeration of nanofibres through the composites. Moreover, the consistency in the diameters could result in denser composites with improved bond strength between nanofibres and the surrounding matrix. Although the TEM images in Figures 5.16 do not give direct evidence of the effect of the functional groups and surfactant molecules, or the presence of silica particles, in enhancing the interaction between the nanotubes and the surrounding matrix, these images show a high fraction of individual nanotubes, and less large voids. This is possibly due to the effect of silica particles together with nanotubes in enhancing the composite packing density, and preventing re-agglomeration. Figures 5.17 show that the silica parties (in the nano scale) were highly dispersed in the graphene sheets, and seems a contact with the between of them via the surfactant/functional groups that could help in keep the graphene sheets in the will dispersed level through the composites.

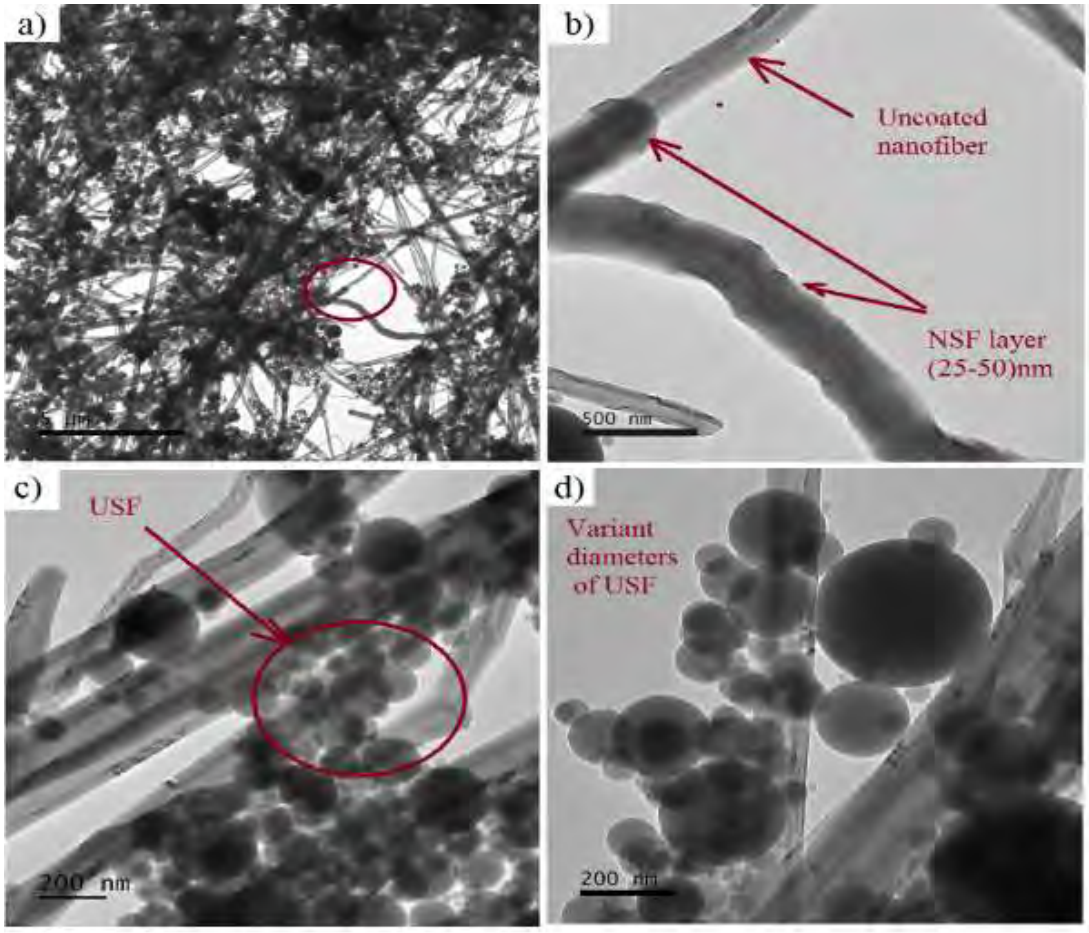

Figure 5.15 High resolution TEM images of the carbon nanofibers and USF suspension showing, a) Silica particles dispersed in between the nanofibres, with

similar diameters, b) surfactant molecules adsorbed on outer surfaces of nanofibres, and c) and d), action of silica particles in prevent the re-agglomeration and the distribution of the particles from smaller to larger in-between the neighbouring fibres.

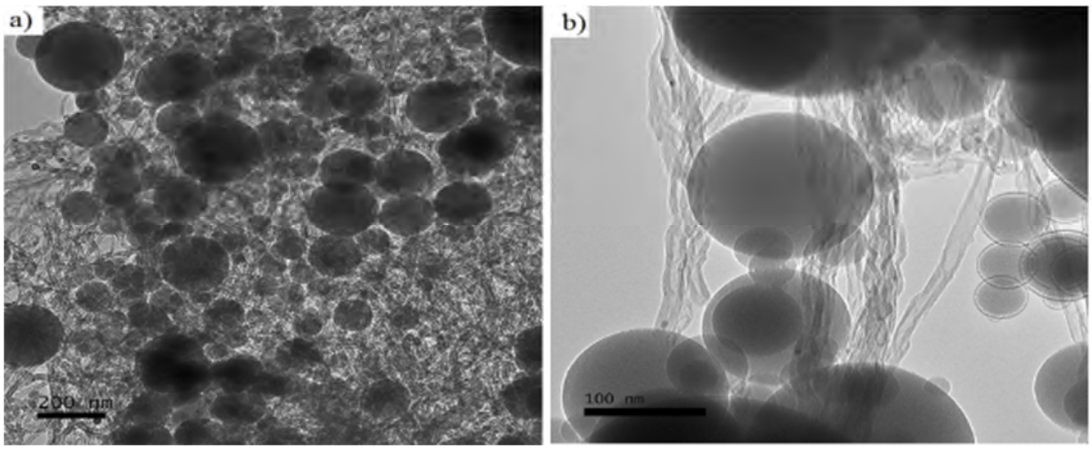

Figure 5.16 TEM images showing the functionalised nanotubes mixed with USF, showing the overall distribution of silica particles in between the nanotubes.

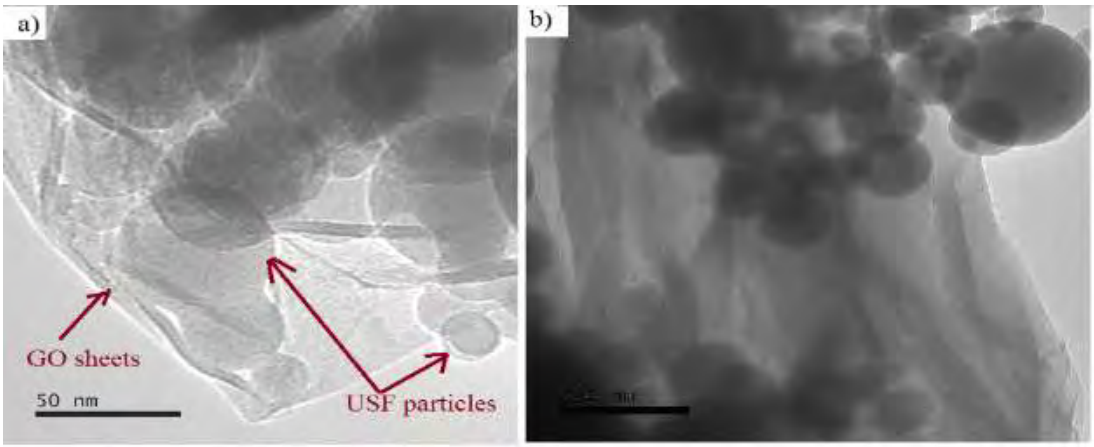

Figure 5.17 TEM images showing the functionalised few layer graphene oxide mixed with USF, showing the distribution of silica particles in between the graphene sheets.

5.2.4.2 SEM Investigations

Cementitious composites with carbon nano-additives (at dosages of 0.025%wt. by cement were imaged by SEM to investigate the relationship between the composites' mechanical strengths and their microstructural properties. Typical images of a fractured surface of the composites of F-MWCNTs, and CNF, samples were obtained from the fractured surface of dog-bone specimens of NRCC-CTf, and NRCC-CF, and respectively, are shown in Figures 5.18, Figures 5.19, respectively.

SEM imaging of nanotube/fibres composites (Figures 5.18, Figures 5.19) showed that nanotubes/fibres are predominantly uniformly distributed and individually embedded in the composite, in almost all the imaged areas, with an apparent absence of agglomerated nano particles in the composites. Bridging of cracks by the nanotubes/fibres was observed, while nanofibres can be clearly seen extending (Figure 5.18b, Figure 5.19b) from cracks following fracture due to their relatively large diameters compared to nanotubes. The embedded nature of these particles gives an indication of the strong interaction with the host matrix (hydration products). This improves bonding strength and consequently load transfer efficiency between the cement matrix and the nano reinforcements, and their bridging effect across voids and cracks.

From the images of nanotubes and nanofibres composites the following finding can be drawn.

- High-magnification images revealed that the observed diameters of nanotubes/fibres appear considerably larger than the diameters of those in the suspensions. Diameters of CNFs, and MWCNTs were around 500nm, as compared to 200nm, and around (50-100) nm, as compared to 25nm or less for the MWCNTs in suspension. Apparent large diameters on the fractured surfaces can be attributed to the attached/coated layer of cementitious hydration products (mainly calcium silicate hydration products originally from the chemical reaction of cement and USF with the solution (water and surfactant, and any functional groups) on the tubes/fibres surfaces).

- Nanotubes/fibres in the cementitious composites kept their original geometry and were not deformed due to the initiated pressure caused by hydration products formation.
- Surfaces of the observed nanotubes/fibres appear rough, which, along with the above observations, suggests that undensified microsilica and the finest cement grains from the matrix adhere strongly to the outer surface of the nanotubes and fibres with the aid of surfactant/functional groups.
- The observed completely de-bonded tubes/fibres from the matrix was probably due to the extra amount of solution adsorbed on the tubes/fibres. When the solution (mixing water and the surfactant) is consumed during the hydration process and/or evaporation, the composite gradually tends to dry and the fibres reduce their volume and separate from the matrix impairing their action as reinforcement.

Figure 5.18 SEM images of carbon nanotubes cementitious composites.

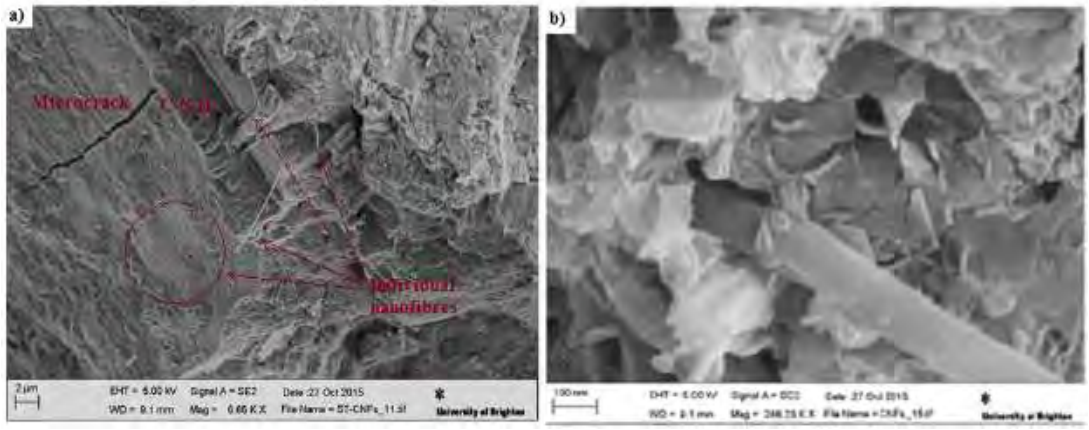

Figure 5.19 SEM images of carbon nanofibres cementitious composites.

5.3 Summary

In this chapter, the effect of an innovative dispersion technique on carbon nano-additives of F-MWCNTs, CNFs, and FLGO was investigated, as well as its effect on the mechanical performance of cementitious composites containing these nano-additives. Microscope images show a dramatic improvement in the dispersion state of nanotubes/fibres suspensions following combined use of superplasticiser and high intensity, short duration (5 minutes) sonication. High magnification TEM images generally show that bundle/clusters sizes of nano-additives became smaller after sonication, with an average bundle size ranging between 50 and 100 nm. Moreover, individual particles tend to have a larger diameter (compared to the original, as provided, material) of 25-30nm for MWCNTs and F-MWCNTs and 150nn-200nm for CNFs, reflecting the presence of an adsorbed layer of surfactant on the wall of the nanotubes/fibres.

Uv-vis absorbance data clearly show that the applied high sonication intensity has led to an increase in absorbance values which reflect an increase in concentration of suspended nano particles, due to the applied energy exceeding the binding interaction force (Van der Waals' interaction) between neighbouring nanotubes/fibres.

Mechanical strengths were significantly enhanced by the addition of carbon nano-additives. The origin of the ability of nano-additives to increase the strength gain can be attributed to:

- Physical contribution of dispersed nano-additives, wherein they act as a filler leading to higher densities compared to the density of PC. The addition of nano materials might also have helped to achieve a better packing, and minimise the composite void content giving higher densities.
- Nano reinforcing agents were acting to reinforce the cement hydration products (such as calcium silicate hydrates (C-S-H) and ettringite). Thus, the crack arresting ability of nanotubes/fibres is likely to help increase tensile resistance when the composite begins cracking, i.e. the fibres in the nanoscale increase crack arresting ability and delay nano cracks to microcracks' propagation, and then cracking at the macroscopic level.

- Dispersion techniques used may help to increase the coverage density of surfactant molecules on the surfaces of nanotubes/fibres, which may act as a cross-linker between the cement matrix and the nano-additives.
- The presence of nanotubes/fibres/ graphene sheets may also refrain the growth or propagation of internal cracks and help to transfer load. The distribution of nano-additives throughout the microstructure densifies the material and reinforces the hydration products, and acts as a nano strengthening agent, better distributing stresses at the micro scale.
- The availability of functional groups on F-MWCNTs, and graphene oxide which leads to a better dispersion level, and improves the bond between the nanotubes and the surrounding matrix ((Geng Ying et al. 2005). The surfactant molecules through non-covalent bond together hydroxy functional groups (covalent bond) are likely to be the cross-linking bridging between the sheets and surrounding matrix and playing a positive role in enhance the load transfer between the graphene sheets and the matrix, as it tends to enhance the mechanical interlocking coupled with chemical cross-linking type bonding.
- The geometry of CNFs compared to MWCNTs (i.e. their outer surfaces are conically shaped and angled with respect to the longitudinal fibre axis) can lead to improved bonding with the matrix, and bridging of cracks, improving the load carrying capacity(Metaxa et al. 2013). In addition their longer fibre length (around four times longer compared to MWCNTs) can lead to better capability in bridging cracks and thus improving the load carrying capacity.
- The possibility of nanotubes /fibres, or graphene sheets to form a homogenous inter-connecting entangled network of nanotubes in the matrix with some overlapping each other, the matrix is therefore restrained from failure until a fail in the bond or pullout/fracture in the tube/fibre/sheets occurs.

In the nano-additives reinforced cementitious composites tested, the addition of carbon nanotubes/fibres did not affect workability significantly. In the case of functionalised nanotubes the rheological properties are slightly enhanced which can

be attributed to the increased wettability caused by the presence of functional groups (-COOH) on the nanotube surface.

From the above it can be concluded that the suggested dispersion technical processing route (to disperse at 0.025% MWCNTs, F-MWCT, CNFs, and FLGO) represents a considerable advancement over previous methods. The technique of high-intensity sonication over short time intervals is an effective (and scalable) dispersion method, which can generate desired dispersion levels and be used to reproducibly manufacture structurally-enhanced cementitious composite materials.

Chapter Six:

Mechanical Performance of Novel Cement-Based Composites Prepared with Nanofilaments (NRCC), and Hybrid Nano-and Micro Fibres (MHRCC)

6.1 Introduction

To date, developments in fibre reinforced cementitious composites have extended to include the concept of fibre hybridisation, and high performance-high ductility fibre reinforced composites (Mohammed Alias Yusof 2013, Nemkumar Banthia*1 2013). The purpose of hybridization in composites is to tailor material properties to suit specific application requirements, to offset the potential disadvantages of one component by the addition of another, and to address the issue that fracturing in concrete is a multi-scale process requiring multiscale reinforcement agents.

In the past, the need for hybridisation comes from the fact that although conventional reinforcement agents such as reinforcement bars, macro fibres, and micro-fibres improve composite mechanical strength and ductility, reinforcing bars in particular arrest cracking at only specific sections and at a single scale. Micro/macro fibres reinforcements such as those applied in fibre reinforced concrete (FRC) ensure a random distribution of crack arresting zones within the composite, but in most cases the fibres act only at their specific dimensional scale. Composites with hybrid fibres can be produced by mixing fibres made from one material but having different geometries, properties, or different sizes. For example, small steel microfibres can be mixed with long macro steel fibres for bridging micro and microcracks respectively. The addition of fibres of different sizes leads to an improvement in the properties of the composites at both micro-and macro-levels-at micro-level, the fibres act to inhibit the initiation and growth of cracks(Balaguru 1992, Banthia and Sappakittipakorn 2007). (Metaxa et al. 2010, Han et al. 2011, Ahmed Sbia et al. 2014).

Limited attempts to date have been made in incorporating nanofibres in hybrid composite systems, so here the concept of hybridisation has been extended to incorporate nanoscale fibres into cementitious composites. Carbon based nano-

additives have been confirmed (in previous work in Chapter Two, and in this study in Chapter Three and Chapter Four) to significantly contribute to improving the mechanical performance of a cementitious composite, due to their action in filling nano pores and reinforcing cement hydration products, and in effectively bridging nano-cracks during loading and transferral of load (Ashour 2011, Hanus and Harris 2013, Siddique and Mehta 2014). Multi-scale hybrid reinforced cementitious composites with nano-additives could endow the composites with some superior mechanical properties, not least in multi-scale cracking inhibition. Use of hybrid fibre composites that exploit the synergistic effect of nano-and micro-additives can potentially lead to significant improvements in the mechanical performance, such as improving the tensile and flexural performance, and interfacial and fracture strength.

In this chapter, the performance of composites reinforced by addition of nanoscale (carbon nanotubes/fibres) and micro-scale (steel fibres) fibres has been investigated. The mechanical properties have been evaluated at various curing ages, along with their microstructure (using Scanning Electron Microscopy (SEM)). Two types of nano-additives that have been proposed in Chapter Four and Chapter Five (Multiwall carbon nanotubes (MWCNT), and carbon nanofibres (CNF)) are used. One type of steel fibre at a volume fraction of 2% used as the micro fibre additive.

6.2 Mechanical Behaviour of Produced Composites

Measurement of the mechanical properties of multiscale hybrid reinforced cementitious composites is an important stage in the identification of the general structural behaviour of the composite being produced. Since the hybridisation system deals with a new combination of nanotubes/fibres and micro steel fibre, it would be inaccurate if the commonly quoted standard values of individual (non-hybrid) composite properties were directly used to reflect the mechanical properties of the hybrid composite. Therefore, in this chapter, a comprehensive experimental investigation on the mechanical behaviour of i) control mixes (cement mortar (PC), and fibre reinforced composites based on micro steel fibre(FRC)), and ii) multiscale

hybrid reinforced cementitious composite mixes based on carbon nanotubes (MHRCC-CNT) and carbon nanofibres (MHRCC-CNF) is presented. For comparison, mechanical strengths of nanofilaments reinforced cementitious composites (NRCC) mixes based on carbon nanotubes (NRCC-CNT) and carbon nanofibres (NRCC-CNF), are grafted from Chapter Five.

Test procedures were carried out in accordance with the relevant BS EN, and ASTM Standards. The results obtained are discussed in detail and compared with some standard expressions for the prediction of a range of mechanical properties. The main conclusions are then summarised at the end of this chapter.

6.3 Results of Compressive, Flexural, Direct and Splitting Tensile Strengths

The test results of the mechanical strengths of the controls (PC, and FRC) and the hybrid composites of MHRCC-CNT, and MHRCC-CNF are summarized in Table 6.5, with results of NRCC-CNT, and NRCC-CNF materials also presented (investigated in Chapter Five) for comparison. Standard Deviations (SD) based on testing of triplicate samples are presented to confirm that the calculated inter-sample variations are not significant and do not affect the conclusions. According to the ASTM C348-14 and ASTM C349-14 specimens that resulted in strengths differing by more than 10% from the average value of all test specimens made from the same sample and tested at the same period were not considered when determining both flexural and compressive strength.

Combining carbon nanotubes/fibres with micron size steel fibres resulted in a considerable increase in composite strength. The sections below give details on strength gain derived from the hybrid fibre composites compared to both control samples of cement mortar (PC) and of fibre reinforced composites (FRC). A power regression analysis was used to obtain the relationships between the strengths of hybrid fibre composites and the curing age (day).

Table 6.1 Mechanical strength tests result for multiscale hybrid reinforced cementitious composites of MHRCC-CNT, MHRCC-CNF, in addition to control specimens (FRC), after 3, 28, 90 days.

Test	Age	FRC		MHRCC-CNT		MHRCC-CNF	
	day	Mean (MPa)	SD	Mean (MPa)	SD	Mean (MPa)	SD
Compressive Strength	3	43.3	0.20	49.3	1.10	48.3	2.56
	28	66.2	0.74	74.6	0.56	74.2	4.16
	90	77.2	0.26	89.2	0.40	92.0	3.75
Flexural Strength	3	7.8	0.20	9.3	1.10	11.0	1.50
	28	10.8	0.74	12.0	0.56	13.2	3.15
	90	11.0	0.26	12.2	0.40	14.2	2.50
Direct Tensile Strength	3	3.5	0.20	5.1	1.10	5.1	0.56
	28	4.8	0.74	6.7	0.56	6.9	1.39
	90	5.5	0.26	7.4	0.40	7.9	1.25
Splitting tensile Strength	3	6.4	0.30	8.4	1.65	9.0	1.57
	28	8.3	0.89	11.5	0.84	12.2	1.44
	90	9.9	0.40	12.9	1.20	14.4	1.12

6.3.1 Compressive strength (f_c):

Test results of compressive strength at 3, 28, and 90 days for multiscale hybrid reinforced cementitious composites of MHRCC-CNT, and MHRCC-CNF are presented in Figure 6.1. These results indicate that the hybrid system of MHRCC-CNT, and MHRCC-CNF, possessed higher compressive strength values compared to the controls. For example, compared to PC an improvement of 60%, 57%; 45%, 44%; and 41%, 45%, at 3, 28, and 90 days were observed, respectively. A lower improvement in compressive strength was observed compared to FRC, with 13%, 11%, and 15% improvement at 3, 28, 90 days respectively observed.

The marginal gain in compressive strength of hybrid composites could be attributed to the fact that the improvement in compressive strength is mainly affected by the mix design, and water/cement ratio that is followed to produce the composite. Improvement due to combined fibres is balanced between nano/microcracks bridged by multiscale fibres which leads to increase the composite load carrying capacity, and the voids created by presence of microfibre addition which leads to increasing the void content and formation of microcracks (microcracks are usually binging where the voids can be seen as defects) (Neves 2005Seong-Cheol 2015, Neves 2005).

The obtained regression equations (f_c) for each of the examined composites are summarized in Table 6.2. These equations are similar to the typical power regression equation (Eq.6.1), proposed in Chapter Five.

$$fc = K\, x^S \qquad \text{(Eq.6.1)}$$

Where: (x) is the age (day) where 3<x<90, K, and S are the regression coefficients.

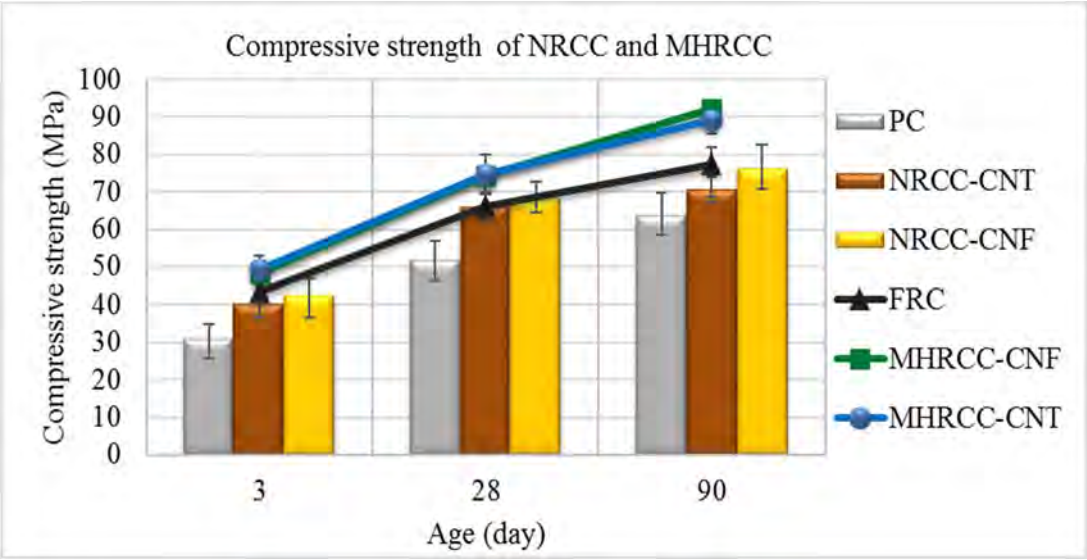

Figure 6.1 Compressive strength of NRCC mixes represented in bars, and MHRCC mixes represented in lines.

Table 6.2 Regression equations to predict the compressive strength as a function of composite age.

Composite ID	Regression Equation	Code: R^2
FRC	$fc_{frc} = 36.2\ x^{0.17}$	R^2=0.98
MHRCC-CNT	$fc_{hfc} = 40.8\ x^{0.17}$	R^2=1
MHRCC-CNF	$fc_{hfc} = 39.2\ x^{0.17}$	R^2=1

6.3.2 Direct and Splitting Tensile Strength:

Figure 6.2 shows the test results for MHRCC-CNT and MHRCC-CNF for dog-bone specimens (direct tensile strength) at various curing ages. Addition of nanofilaments (of nanotubes and nanofibres) in a hybrid system, significantly increased the direct tensile strength of the composites compared to PC, and FRC. Compared to PC an improvement of 139%, 139%; 130%, 136%; and 143%, 159%, at 3, 28, and 90 days was obtained, respectively. The hybrid system also led to an increase in strength over the FRC specimens of 46%, and 34%; 47%, 52%; and 45%, 43%, after 3, 28, and 90 days. These improvements confirm the positive synergistic effects between the nano-and-micro fibres.

Moreover, Figure 6.3 shows the tests result of MHRCC-CNT, MHRCC-CNF in cylindrical specimens (to illustrate splitting tensile strength) at various ages. Compared to (PC), the hybrid system with carbon nanotubes and nanofibres generated an improvement in splitting tensile strength of 178%, 199%; 195%, 214%; and 216%, 250%, at 3, 28, and 90 days, respectively. Compared to FRC, splitting tensile strength increased by 31%, 41%; 39%, 48%; and 37%, 54%, after 3, 28, and 90 days, respectively.

The improvements in splitting tensile strength may be related to an increase in the strength resulting from the synergistic effect of both nano-and -microfibres. An even distribution of fibres throughout the composite, multiscale reinforcement, and the nature of the bond between the fibres and the matrix are the main parameters

responsible for the improvement in strength. In the splitting test, the applied uniaxial load was distributed through the matrix by the fibres: the embedded fibres are responsible for withstanding the derived stress and absorbing the energy that could cause cracks and then failure. It can be seen that the concrete mix containing CNFs exhibited the highest tensile strength value for all test ages (early age, standard age, and late age). This behaviour is consistent with the measured direct tensile strengths of these mixes.

Regression equations which predict direct and splitting tensile strength (f_{dts}) are summarised in Table 6.3, and Table 6.4, and the test setup of dog-bone specimens and cylindrical specimens are shown in Figure 6.4 and Figure 6.5, respectively.

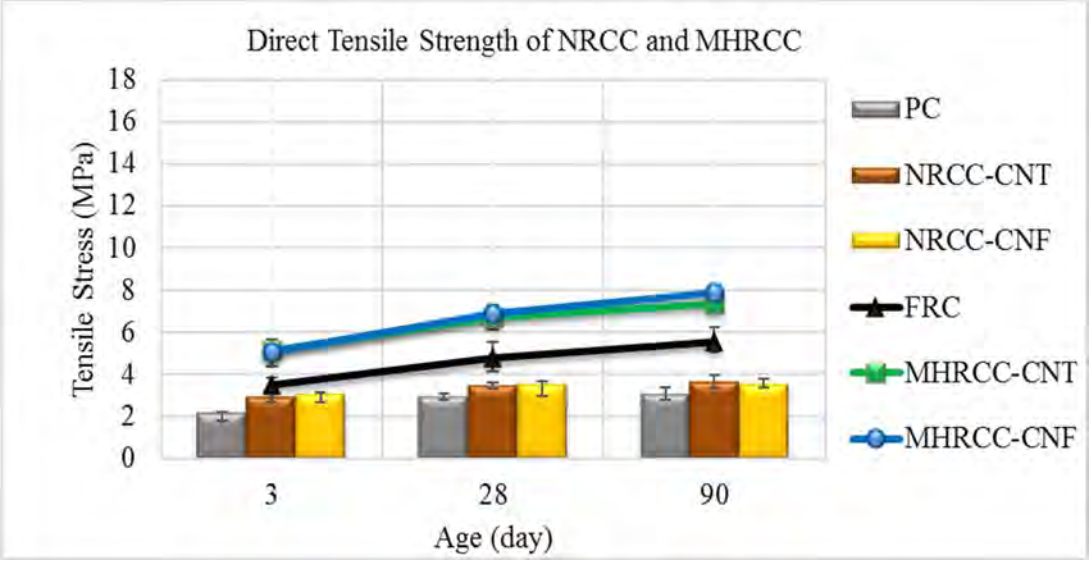

Figure 6.2 Direct tensile strength of NRCC mixes represented in bars, and MHRCC mixes represented in lines.

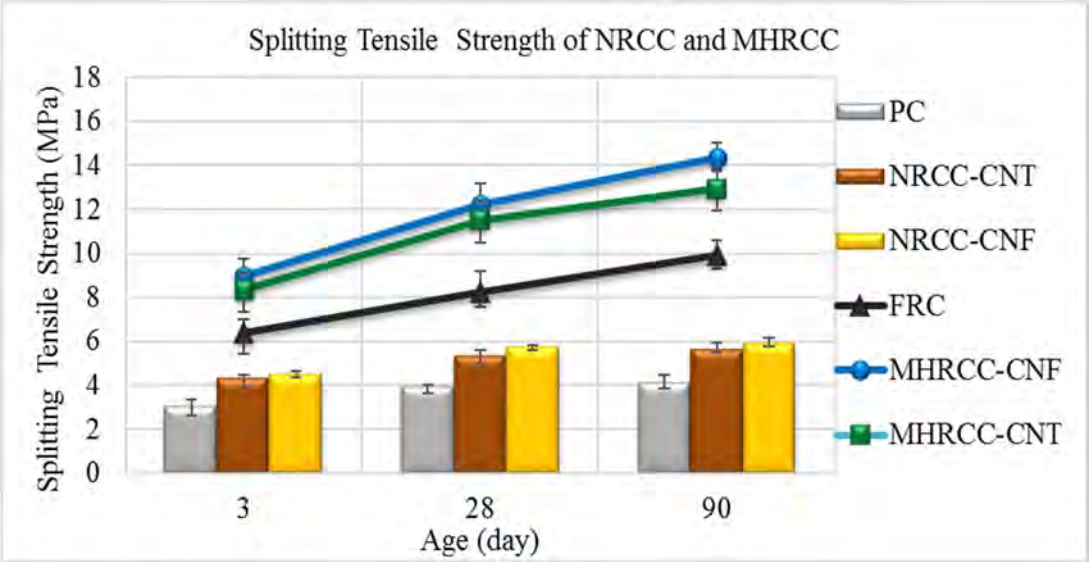

Figure 6.3 Splitting tensile strength of NRCC mixes represented in bars, and MHRCC mixes represented in lines.

Table 6.3 Regression equations to predict the direct tensile strength as a function of composite age.

Composite ID	Regression Equation	Code: R^2
FRC	$f_{dts} = 3.04\ x^{0.13}$	$R^2=1$
MHRCC-CNT	$f_{dts} = 4.56\ x^{0.11}$	$R^2=1$
MHRCC-CNF	$f_{dts} = 4.44\ x^{0.13}$	$R^2=1$

Table 6.4 Regression equations to predict the splitting tensile strength as a function of composite age.

Composite ID	Regression Equation	Code: R^2
FRC	$f_{sts} = 5.5\ x^{0.13}$	$R^2=1$
MHRCC-CNT	$f_{sts} = 7.3\ x^{0.13}$	$R^2=1$
MHRCC-CNF	$f_{sts} = 7.7\ x^{0.14}$	$R^2=1$

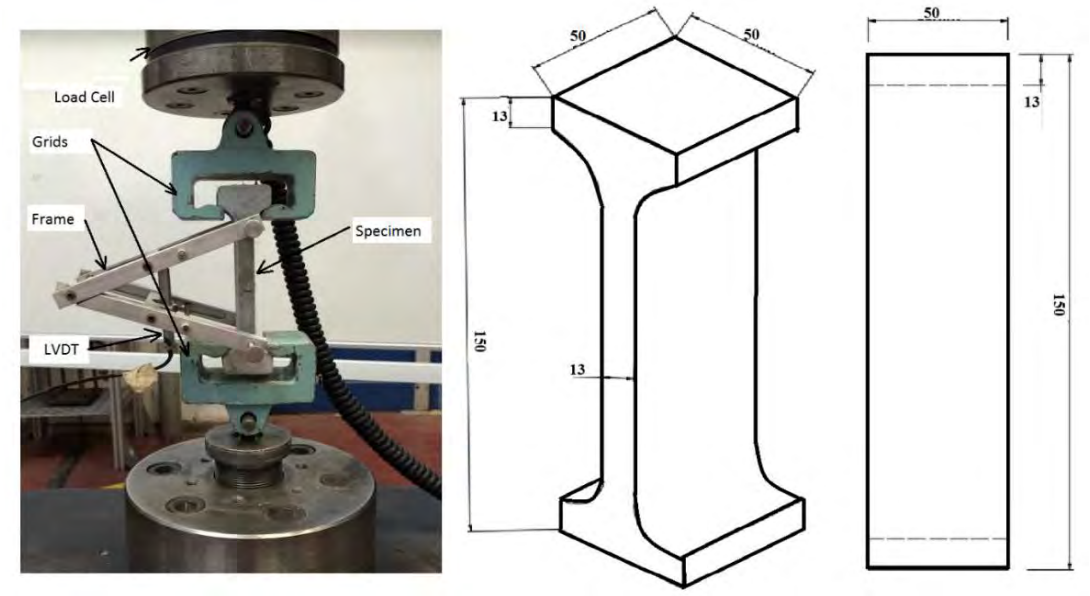

Figure 6.4 Test set-up for dog bone specimens, including supports, grids, and LVDT with the frame

Figure 6.5 Test set-up for cylinders under uniaxial load.

6.3.3 Flexural strength

Figure 6.6 shows the flexural strength behaviour of the hybrid composites at various ages. Compared to PC, the hybrid systems of MHRCC-CNT and MHRCC-CNF led to significant improvements in the flexural strength, of 177%, 226%; 86%,104%; and

84%, 114%, at 3, 28, and 90 days respectively. Compared to FRC, nanotubes and nanofibres combined with micro steel fibres generated an improvement in flexural strength of 19 %, 40 %; 11%, 23%, and 10%, 29 % after 3, 28, 90 days respectively.

Flexural strength was therefore significantly improved by the inclusion of fibres at the multiscale. The nanofilaments (nanotubes and nanofibres) were giving a higher probability of a micro crack being reinforced/ arrested, and the higher possibility of preventing the micro crack developing. Micro fibres are acting to improve energy absorption capacity, after crack initiation in the composite has occurred. The obtained regression equations to predict the flexural strength (f_{fs}) are summarised in Table 6.5. Figure 6.7 shows the test setup.

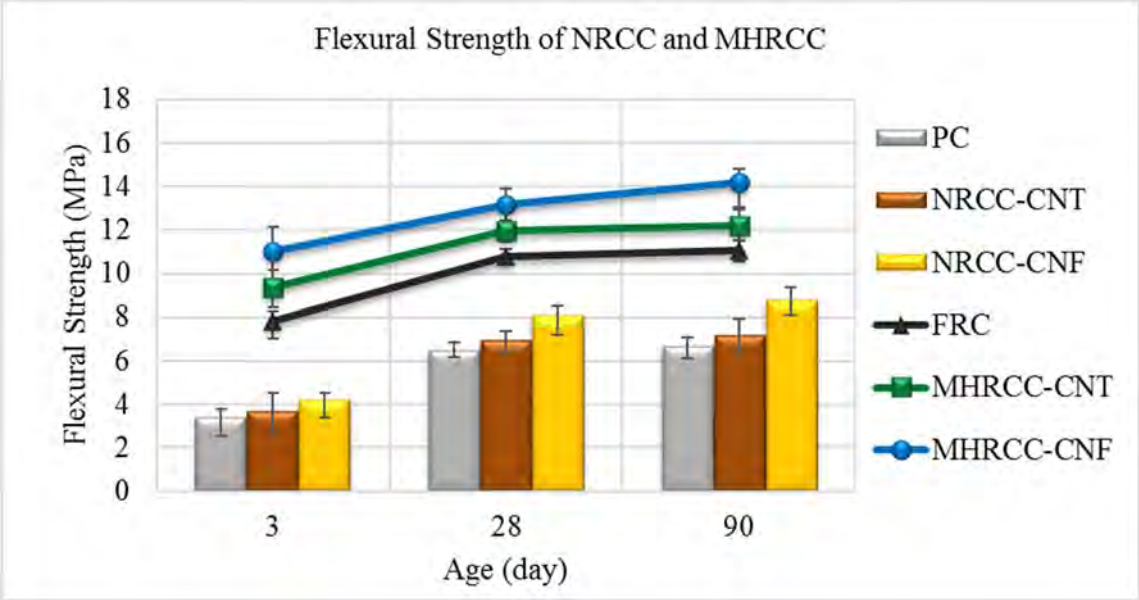

Figure 6.6 Flexural strength of NRCC mixes represented in bars, and MHRCC mixes represented by lines.

Table 6.5 Regression equations to predict the flexural strength as a function of composite age.

Composite ID	Regression Equation	Code: R^2
FRC	$f_{fs} = 7.1\ x^{0.11}$	R^2=0.92
MHRCC-CNT	$f_{fs} = 8.7\ x^{0.0.08}$	R^2=0.92
MHRCC-CNF	$f_{fs} = 10.1\ x^{0.07}$	R^2=1

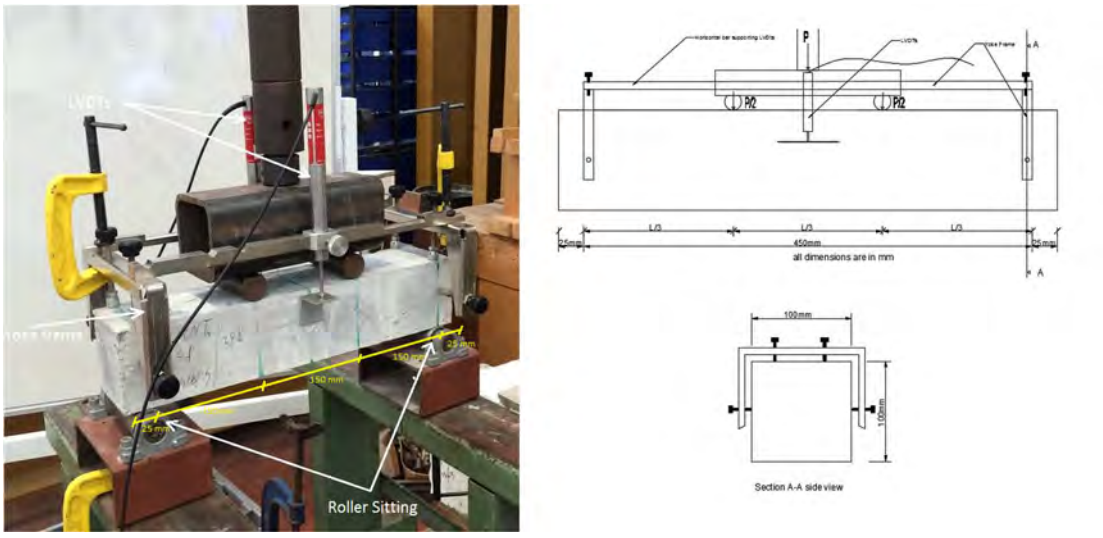

Figure 6.7 Test set-up of the beam under four-point loading.

6.3.4 Energy Absorption Under Flexural Loading

One of the most important parameters in the study of the behaviour of multiscale hybrid reinforced cementitious composites, especially up to reaching the peak load, is the energy required for crack initiation. Thus, in this study, adsorption energy represented by the Flexural Toughness Factor (FT_δ) has been used to study the resistance of hybrid fibre composites to cracking. Figure 6.8 (a, c, e) shows load–

deflection curves for FRC and MHRCC-CNT, MHRCC-CNF after 3, 28, and 90, days. The analyses were performed in accordance with the Japan Society of Civil Engineers (JSCE) method, and the obtained FT_{δ} (as explained in Chapter Three) are presented in Table 6.6. The combination of micro steel fibres and nanofilaments (CNT, and CNF) generates significant improvement in flexural toughness factors, up to failure (span/150, 3mm). Compared to FRC, the improvement was about 23%, 86%: 37%, 58 %: and 19%, 41%, after 3, 28, and 90 days, respectively. Using the nano-additives in combination with micro steel fibres seems to inhibit nano-cracks and restrict their growth within the composites, and improve the ability of the composites to carry greater loads before crack initiation, as there is a need for a greater amount of energy to produce the cracks.

Table 6.6 Flexural toughness factor of FRC and the hybrid fibre composite.

Specimens designation	Fibre addition %		Flexural Toughness Factor (3day)		Flexural Toughness Factor (28day)		Flexural Toughness Factor (90day)	
	Micro Fibres (by volume)	Nanofilaments (by weight)	Mean (MPa)	% Increase	Mean (MPa)	% Increase	Mean (MPa)	% Increase
FRC	2.0 %	0.0	5.5	0.0	7.8	0.0	7.8	0.0
MHRCC-CNT	2.0	0.025	6.7	23.3	9.3	18.9	9.3	18.9
MHRCC-CNF	2.0	0.025	10.1	85.8	11.0	41.1	11.0	41.1

To more fully understand the synergistic effect induced by nanofilenmts inclusion, particularly the effectiveness of nano-and micro fibre hybridization on the energy dissipated under bending load, flexural toughness factors were calculated and plotted for beam deflections (δ) of 0.5mm, 1mm and 2mm (Figure.6.8 (b, d, f)). Based on these data, the mechanism of nano-additives in improving the flexural strength is as follows:

1- During the first period of loading (deflection of 0.5mm) incorporation of nanotubes did not affect (increase) the absorbed energy compared to nanofibres composites. During all examined ages, the increase in the flexural toughness factor of MHRCC-CNT was about 10% compared to the flexural toughness factor (FT_{δ}) of FRC. The increases in MHRCC-CNF composites were about 30 %, 20%, and 25%. This can be attributed to the smooth surfaces of nanotubes (as supplied) compared to the deformed surfaces of nanofibres (CNF), i.e. the former may reduce the bond strength with the surrounding matrix. In combination with the high flexibility of the nanotubes, a frictional slip might occur (i.e. partial debonding) which can affect the efficiency of nanotubes to absorb/transfer the applied load to the composite. In this case, the majority of absorbed energy is due to the fully bonded micro fibres, as explained in the schematic diagram of Figure 6.9 (1-ABC). The factors that improve the bond of carbon fibres are their rougher surfaces, which is due to the nanofibres' surface morphology (i.e. conical outer surfaces) which increase the outer fibre surfaces areas, and their longer fibre length (up to 4 time longer than the nanotubes). These factors significantly increase the bond possibility of carbon nanofibres with the surrounding matrix.

2- Prior to crack localization, (deflection amount less than 1mm) the hybrid system exhibits a significant capacity to withstand bending, resulted in a higher amount of energy required to initiate the cracks compared to FRC (simply reinforced with steel fibres). The increase in the flexural toughness factors of MHRCC-CNT, and MHRCC-CNF was about 17%, 31%; 17%, 26%; and 15%, 23% compared to the FT_{δ} of FRC after 3, 28, and 90 days, respectively. The effectiveness is due to the positive effect of both nano and micro fibres, as schematically represented in the Figure 6.9 (2 BCDE).

3- At postcracking, i.e. at deflection of 2mm (where cracks are beginning to be initiated), after the first crack was formed, the composite reached its ultimate capacity to sustain an extra load. However, due to the combination of nano and microfibres, the composites show superior ability (higher adsorbing energy) to withstand the failure (collapse). Compared to FRC, the flexural toughness factors were increased by 20%, 45%; 18%, 34%; and 16%, 22% after 3, 28, and 90 days, respectively. Figure 6.9 (3-DEFG).

4- Up to a deflection of 3 mm, the obtained flexural toughness factor (FT_δ) results show that the nanotubes/fibres contribute to carry the load for longer period, leading to higher deflection before full, pull out, de-bonding and failure.
5- Up to failure, when the recorded deflection became more than 3mm, both nano and micro fibres were pulled out and lost their effectiveness in withstanding the applied load.
6- By bridging across cracks in nano and micro scale and reducing crack propagation, the hybrid fibres obviously affect the postpeak flexural softening response of the cementitious composites.
7- While nanofilaments reinforced cementitious composites (NRCC) (investigated in Chapter Five) show a drastic decrease in stress after the ultimate strength was reached, inclusion of multiscale fibres leads to ductile behaviour even after reaching ultimate tensile strength because of the multiple reinforcement and delay in crack propagation.

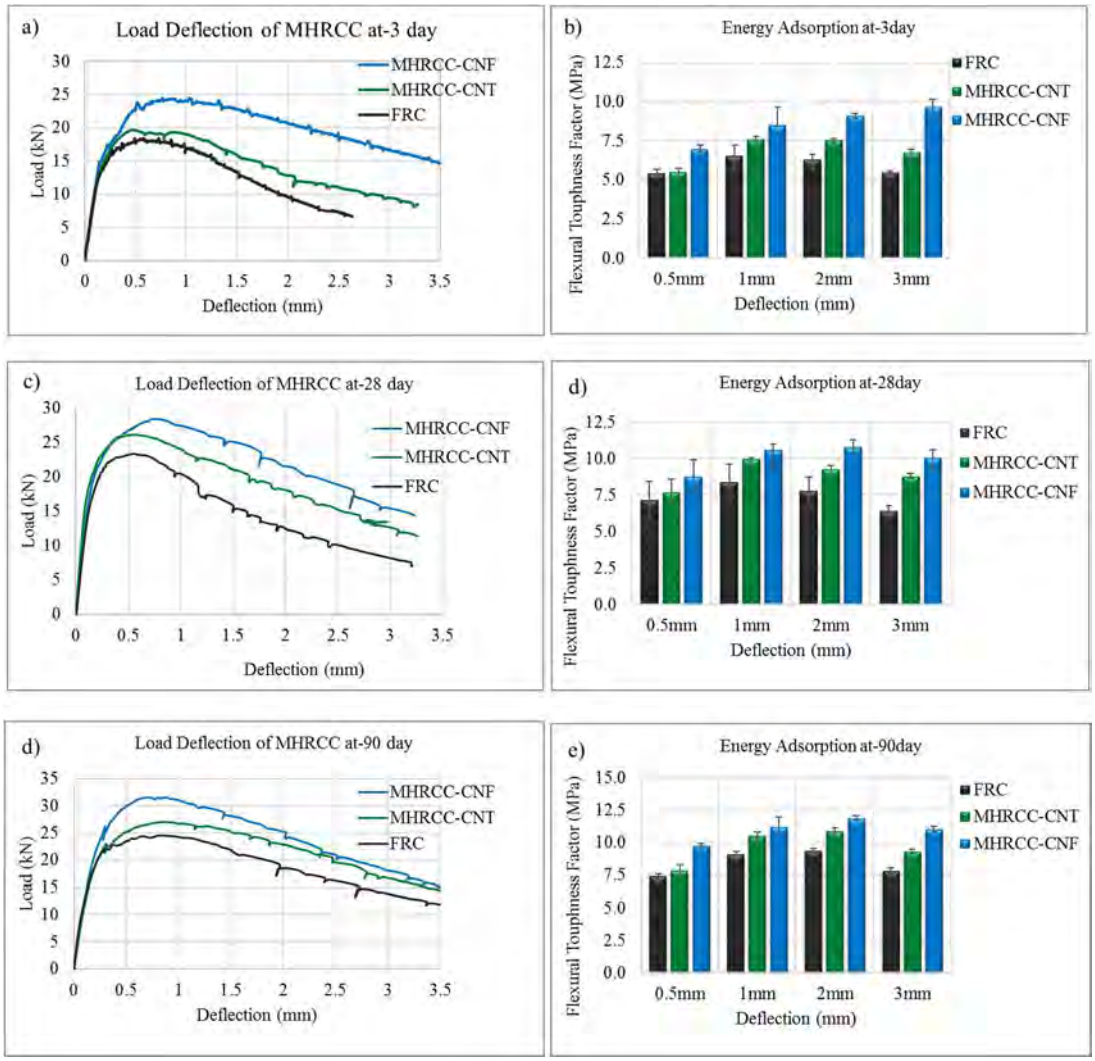

Figure 6.8 Represent the average load-deflection curves obtained from bending tests of FRC (control), and MHRCC-CNF and MHRCC-CNF. Graphs of (b, d, f) show flexural toughness factors (FT_δ in MPa) computed from curves in a, c, and e respectively.

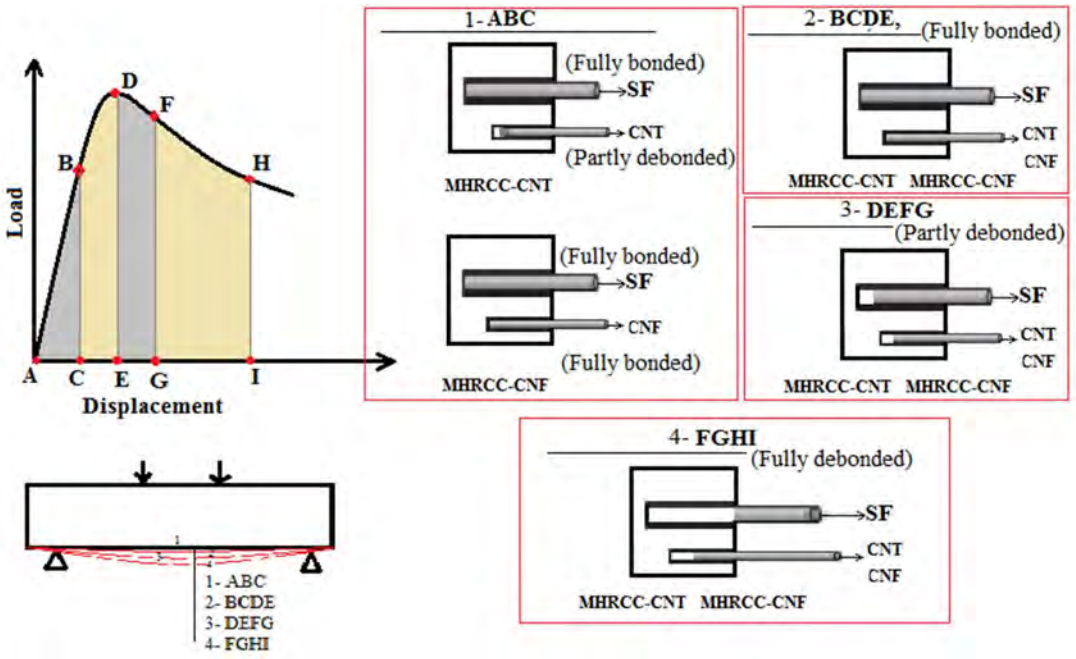

Figure 6.9 Synergistic effect of nano-and micro fibres on adsorbing energy before failure, deflection-Pullout relationship after 4 stages, 1(ABC) deflection about 0.5mm, 2(BCDE) deflection up to 1mm, 3(DEFG) deflection up to 2mm, and 4(FGHI) deflection up to failure (fully Pullout) 3mm.

6.3.5 Ductility Ratio

In order to better understand the effect on ductility of using hybrid nano and microfibres, the toughness ratio was calculated according to Eq.6.2. This is defined as the ratio of fracture energy factors of the cementitious composites with nano and micro fibres to those without fibres (plain mortar-PC), where both composites have similar matrix phases.

$$\text{Ductility ratio} = \frac{F_{T\delta}\ (\text{hybrid Fibre composite})}{F_{T\delta}\ (\text{control plain mortar})} \qquad \text{(Eq.6.2)}$$

Beside the increase in the compressive and tensile strengths due to the hybrid system, it has been observed (Figure6.10 and Table 6.7) a significant improvement in both the fracture energy and ductility ratio. The hybridisation of carbon nanofibres and micro steel fibres produces the most ductile material, where the fibres successfully and continuously carry and transfer the load from one scale to another. The increase in the dissipated energy reaches its highest values with addition of steel fibres at an early age. This can be attributed to the early pozzolanic reaction which increases the amount of C-S-H gel at early ages, and subsequently enhances the bond of the nano/micro fibres with the surrounding matrix.

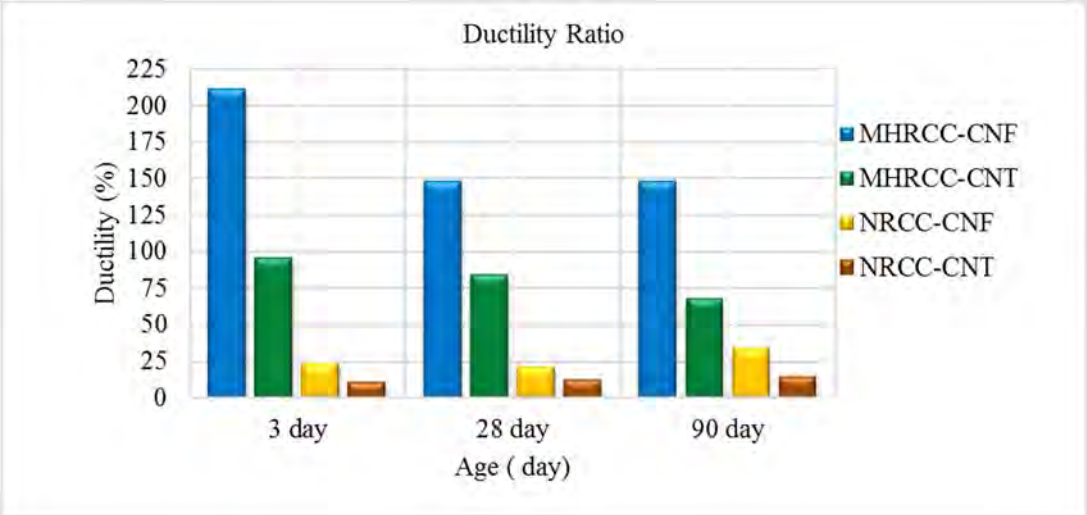

Figure 6.10 Ductility ratio of nanofilament reinforced cementitious composites and multiscale hybrid reinforced cementitious composites after 3,28, and 90 days.

Table 6.7 Ductility of nanofilament reinforced cementitious composites and multiscale hybrid reinforced cementitious composites after 3,28, and 90 days.

Ductility due to nanofilament in nanofilament reinforced cementitious composites			
ID	3 day	28 day	90 day
NRCC-CNT	11.47	12.85	15.02
NRCC-CNF	23.85	21.53	34.55
Ductility due to nanofilament in multiscale hybrid reinforced cementitious composites			
ID	3 day	28 day	90 day
MHRCC-CNT	95.7	16.56	16.56
MHRCC-CNF	354.0	97.09	97.09

6.3.6 Stress-Strain Relationship

The assessment of tensile stress–strain behaviour can help to quantify the contribution of each fibre reinforcing system to the overall composite tensile behaviour. The potential synergistic effect resulting from fibre hybridization may also be directly and explicitly quantified. Figure 6.11 and Figure 6.12 show the direct tensile stress versus the strain after 28 days for the control mixtures PC and FRC, and for mixtures of MHRCC-CNT, MHRCC-CNF. For clarity, the extreme curves were selected for all the composites over three of the four tested specimens for each composite. The ultimate value of the tensile stress was determined by computing the maximum registered tensile load during testing and the resulting strain recorded using LVDTs (Linear Variable Differential Transformers) for each specimen. The observed composite behaviour resulting from the mixing of two fibres at different scales corresponds approximately to (i) the effect of nanotube/fibres in controlling the crack formation and (ii) the micro steel fibre reinforcing the composite at larger scale. Different types of nanofilaments (due to geometrical properties or presence of functional groups from the surfactant which affect their interaction with the surrounding matrix) became activate at different stages of the tensile tests. The

obtained information can be explained during three stages, cracks initiation (inset figures), at peak, and after postcracking.

- In the first stage, up to the initiation of the first cracks, carbon nanotubes/fibres act as a nano reinforcement agent controlling the crack initiation, which plays a major role in enhancing durability (discussed in Chapter Seven). In the inset Figures, MHRCC-CNF composite show the highest first cracking stresses, reaching peak stresses of up to 5MPa. The subsequent gradual stress in the composite with MHRCC-CNT is a consequence of the bond of carbon tubes with surrounding matrix. The smooth nature of nanotubes' outer walls compared to the deformed (conical) shape of nanofibres, resulted in a less effective bond. Moreover, the length of nanofibres is about four time longer than the tubes, which resulted in a higher reinforcing efficiency.
- At the second stage, after the first cracking, the subsequent tensile stress of the hybrid fibre composite exhibits an increase up to a peak value with an increase in the ultimate strain of the composite. Up to the peak segment, the curve found to be affected by the addition of nanofilaments, thus it can be observed that an increase in composite strength increases the extent of curved portion in ascending branch and renders the drop in the descending part steeper for hybrid fibre composite. An increase in the slope of the descending part of the stress-strain curve is also observed when carbon nanotubes are used as a nano-additive. The bond strength between both fibres and the surrounding matrix act to increase of the hardened strain values. The strain values up to the peak were about twice as high as the recorded strain of FRC.
- After postcracking (the third stage) rapid tensile stress decay was seen in all curves. The similarity in behaviour between FRC and hybrid fibre composites after reaching the peak can be attributed to the crack restraining effect resulting from the nanofilaments being lost after microcracks are generated.
- It seems that the hybrid fibre composite is able to combine the features of each of the single-type fibre composites, increasing the stress after the first cracking. The composite performs better than only micro fibres at both cracking stages. Similar to the behaviour of nanotubes/fibres in nanofilaments reinforced cementitious

composites, the well dispersed distribution of nanotubes/fibres through the hybrid composite can be a major parameter in enhancing the synergy with the microfibres. Antte (Anette 2011) found that cracking stress was affected by the fibre-free areas in the material cross sections since they act as defects in the material. Fibre distribution and orientation have been found to depend on many factors, including: casting and placement technique, specimen size, fibre size, geometry and fibre content, and maximum aggregate size, Grünewald (Grünewald 2004) and Anette(Anette 2011) . Assessing the future impact of varying these parameters could be a useful area for future research.

These results indicate that with addition of nanoscale tubes/fibres, the composite specimens show higher resistance against bending deformation. This is due to the reinforcing efficiency of nanofilaments which can lead to absorption of greater amounts of energy by inhibiting cracking at nano scales, and thereby increase the energy needed to propagate the cracks. Although the hybridization of steel fibres and nanotubes/fibres did not demonstrate a multiple crack that can be observed by naked eye before the localisation of the single micro crack, the improved mechanical strength and toughness mechanism might be attributed to multiple cracking behaviour at a very small size (nano scale mutable cracking), which needs to be investigated in future studies.

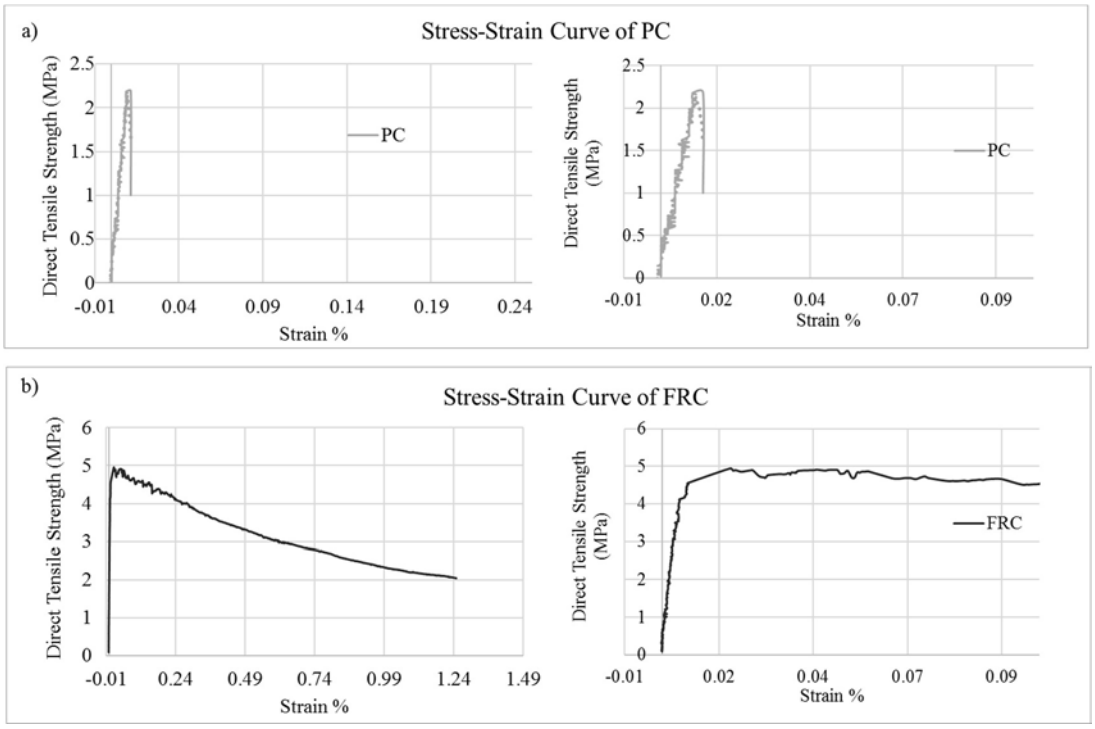

Figure 6.11 Stress-strain curves for control mixtures PC and FRC after 28 days.

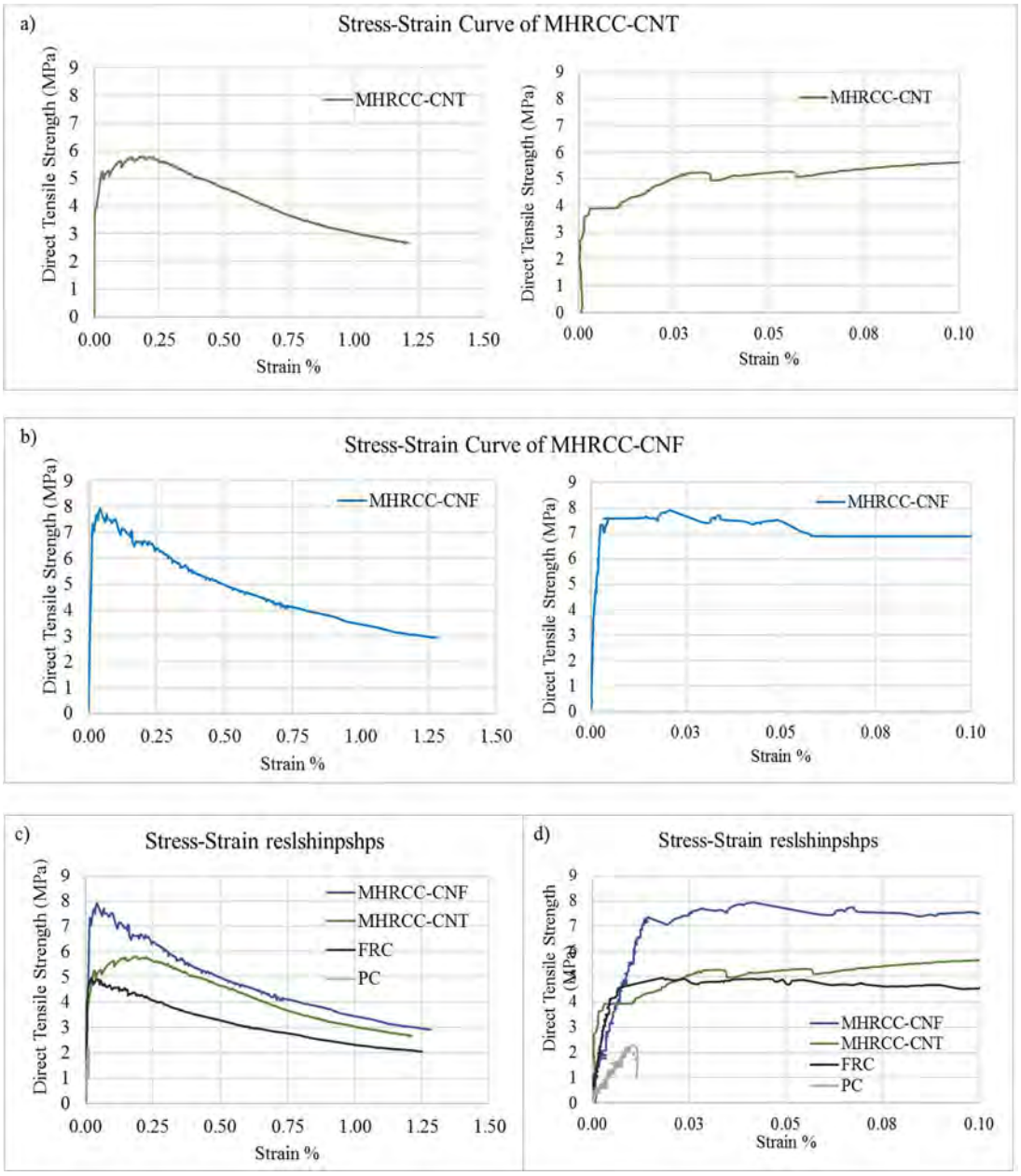

Figure 6.12 Stress-strain curves for hybrid fibre composites of MHRCC-CNT, and MHRCC-CNF after 28 days.

6.4 Predicting the Mechanical Strength of Hybrid Fibre Composites

6.4.1 Compressive Strength

The compressive strength data from the obtained test results on FRC, and predictions made using the equation proposed by Nataraja (Eq.6.3)(Nataraja et al. 1999) are presented in Figure 6.13 and reported by(Fakharifar et al. 2014, Lee et al. 2015). Based on this equation, a simple model to predict the compressive strength of multiscale hybrid reinforced cementitious composites ($f_{(hfc)}$) was derived based on following parameters:

(i) the model of Nataraja, to predict the compressive strength of FRC (Eq.6.3), in which the variables were plain compressive strength (f_{cp}), fibre volumetric ratio (V_f), and fibre aspect ratio (length l-to-diameter d) (ii) the power regression equations obtained based on the experimental results for nanofilaments reinforced cementitious composites. The compressive strength of control (PC), and nano tubes/fibres cementitious composites (obtained in Chapter Five) were used in this model.

i) Eq.6.3 shows the model of Nataraja 1995 which can be used to predict the compressive strength of FRC,

$$fc_{(frc)} = f_{cp} + 6.9133\ RI \qquad \text{(Eq.6.3) (Nataraja et al. 1999)}$$

$$RI = V_f(\ l_f/d_f)$$

Where:

f_{cp} = Experimental compressive strength of plain mortar (PC)

$V_{f,}$ = Volumatic fraction.

(lf, and df) = length and diameter of steel fibre

Comparison between the experimental and predicted strengths was made to examine the validity of this equation (Eq.6.3). Figure 6.13 shows an accurate correlation between the actual and predicted strength based on the compressive strength of the cement mortar (PC).

ii) Equations to predict the compressive strength of cement mortar (PC), and nano-additives of CNT, CNF can be represented by

$$fc = K\, x^{s} \quad \text{(Eq.6.4)}$$

Where (K) and (s) are, coefficients derived from the actual and predicted compressive strength of nano cementitious composite graph which has been investigated in Chapter Five (Figure 6.14). The values of these coefficients vary and depend on type of used nano-additives. K and S values are shown in Table 6.8

Hence from Eq. 6.3, and Eq.6.4, an equation to predict the compressive strength of the hybrid mixture and can be written as follows (Eq.6.5).

$$f_{(frc)} = K\, f_{cp}^{s} + 6.9133\ RI \quad \text{(Eq.6.5)}$$

As discussed in the previous section, the compressive behaviour of FRC is affected by the micro-fibre volumetric ratio, aspect ratio, and compressive strength of the plain mortar (f_{cp}). In this section, the formula (Eq.6.5) derived for representing the ultimate compressive behaviour of hybrid fibre composites ($f_{(frc)}$) is generated from the test results of FRC (Eq.6.3), and cementitious nanocomposites (Eq.6.4). Figure 6.15 and Table 6.9 represent the relationship between the test results and predictions made by the proposed models and the obtained results, respectively.

Table 6.8 Model coefficients obtained from the experimental results.

ID	coefficient K	coefficient S	Code: R^2
PC	0.93	1.10	0.98
CNT	2.1	0.82	0.82
CNF	1.5	0.89	0.93

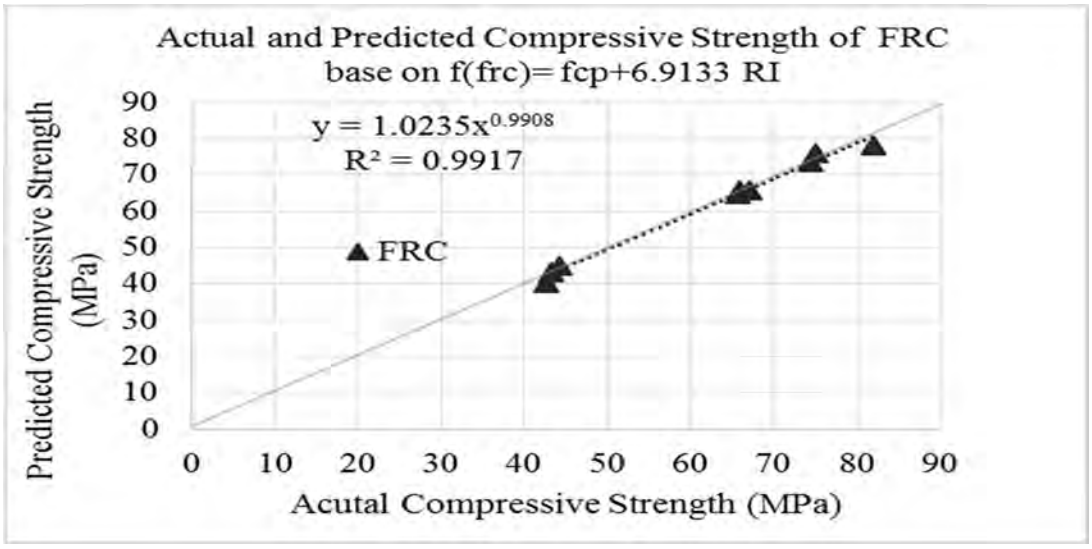

Figure 6.13 Actual and Predicted Compressive Strengths of FRC based on $f_{(frc)}$= f_{cp}+6.9133 RI.

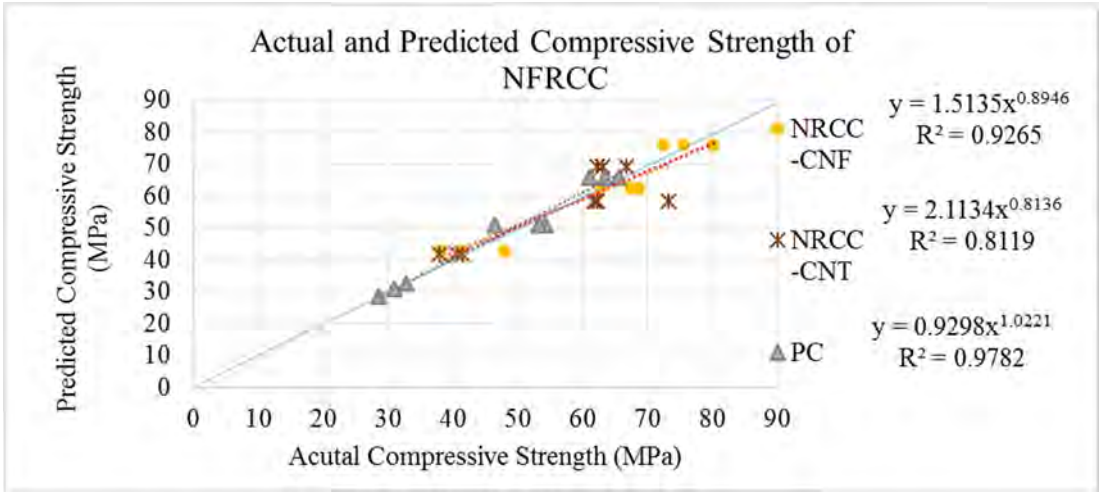

Figure 6.14 Actual and Predicted Compressive Strengths of PC and cementitious nanocomposites based on regression equations.

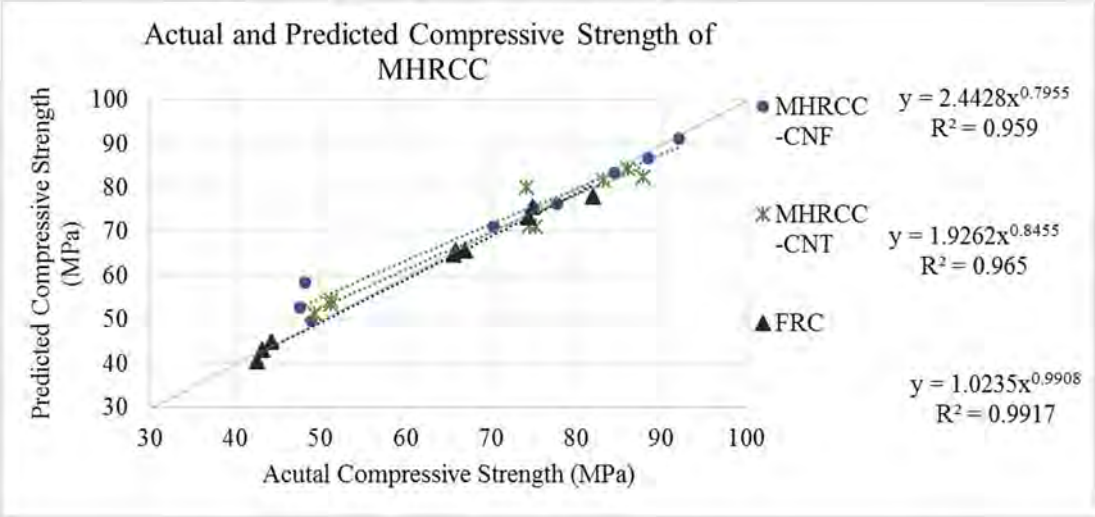

Figure 6.15 Actual and Predicted Compressive Strengths of PC and nanofilaments reinforced cementitious composites.

Table 6.9 Experimental and predicted compressive strengths of FRC and hybrid Fibre Composites.

Age (day)	FRC		MHRCC-CNT		MHRCC-CNF	
	Compressive Strength (MPa)		Compressive Strength (MPa)		Compressive Strength (MPa)	
	Experimental	Predicted	Experimental	Predicted	Experimental	Predicted
3	44.3	44.9	53.54	40.10	58.42	48.22
	43.2	43.0	51.26	48.80	52.74	47.62
	42.6	40.4	54.34	43.00	49.74	48.90
28	65.9	65.7	80.03	68.30	76.28	77.70
	67.0	65.7	71.09	66.30	75.34	75.00
	65.6	64.7	71.47	72.50	71.25	70.30
90	74.9	75.7	84.33	86.08	91.22	92.00
	82.0	77.9	81.65	83.22	86.66	88.50
	74.5	73.4	82.59	87.88	83.50	84.50

Hence, the obtained equations (shown in Figure 6.15) represent good predictions of the compressive behaviour of the hybrid composite of nanotubes and nanofibres. However, due to the limited ratios of micro and nanotubes/fibres that have been experimentally examined, this model is assumed to be applicable to a composite in which the steel fibres volumetric ratio is about 2%, and the addition percentage of nano-additives is 0.025% by cement weight

6.4.2 Tensile Strength

As explained in the previous sections, hybridisation plays an important role in the improvement of the tensile behaviour of the composite and causes an increase in the strength, delays crack propagation, and increases the cracking strain capacity. To further understand the tensile strength, a model was derived to obtain a close estimate of the true splitting tensile strength of hybrid nano and micro fibre composites based on experimental splitting tensile strengths obtained at various ages.

Several studies have been carried out investigating the relationship between the splitting tensile strength and the compressive strength of FRC. The available relationships are proposed by Musmar (Musmar 2013) which is based on several experimental data(Eq.6.6) as follows:

$$f_{sp=}((0.6+0.4(V_f \frac{l}{d}))\sqrt{0.78fc(fc_{(frc)})} \quad \text{(Eq.6.6)}$$

Where:

$f_{c(frc)}$: cylinder compressive strength of fibre reinforced (MPa)

f_{sp}: Splitting tensile strength (MPa)

$V_{f:}$ Volumetric ration of steel fibres

l & d: Steel fibre length and diameter respectively

Firstly, the equation was examined using the obtained results of splitting tensile strength of FRC (control mixture), in order to validate it with the experimental results. Figures 6.16, illustrate the experimental and predicted splitting tensile strengths values versus the experimental compressive strength according to Eq. 6.6. It indicates that the predicted values are acceptable and close to the observed values at later ages (90 day), but overestimate by 13 % at early ages (3 day).

This relatively close relationship encourages use of this equation to derive a model to predict the splitting tensile strength of the hybrid composites of MHRCC-CNT, and MHRCC-CNF, based on the obtained results on compressive strength.

The relationship between measured and predicted compressive strength was obtained (Eq.6.7, and Eq.6.8) by substituting the compressive strength in the equation with the predicted compressive strength obtained using regression analysis. The equation to predict the splitting tensile strength, therefore, can be written as follows:

$f_{sp=}$ $((0.6+0.4(V_f \frac{l}{d}))\sqrt{0.78fc}$

Where: fc =$fc_{(hyb)}$

MHRCC-CNT $fc_{(hyb.)}= 2.62\ f_{CT\text{-}SF}\ ^{\wedge}0.78$ (Eq.6.7)

MHRCC-CNF $fc_{(hyb.)}= 1.024\ f_{CF\text{-}SF}^{\wedge}0.99$ (Eq.6.8)

The obtained relationship of experimental and predicted splitting tensile strength based on the proposed equations is shown in Figure 6.17, and the data are shown in Table 6.10. The results revealed that the predicted tensile strength of MHRCC-CNT is close to the experimental results. Equations of MHRCC-CNT, however, tended to overestimate the strength at early age by about 12%, while it became very close at late ages. Equations for MHRCC-CNF were found to overestimate the splitting strength

by 10% at early ages, and the underestimation was higher at 3 days, being ca. 25%. Therefore, it may be concluded that these equations are most effective at early age and need to be modified to include (beside the experimental compressive strength) the influence of the bond and the tube/fibre aspect ratio and the geometry (which can be suggested for future work).

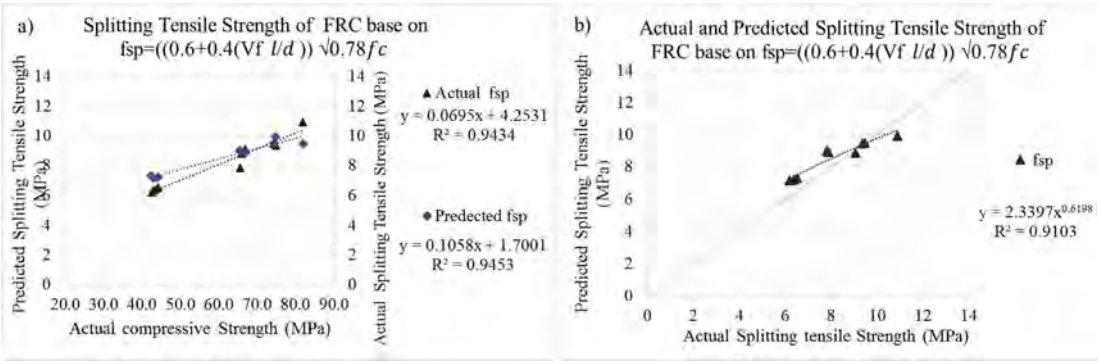

Figure 6.16 Splitting tensile strength of FRC, a) the relationship between the actual and predicted tensile strength as a function to the experimental compressive strength, and b) actual and predicted splitting tensile strength

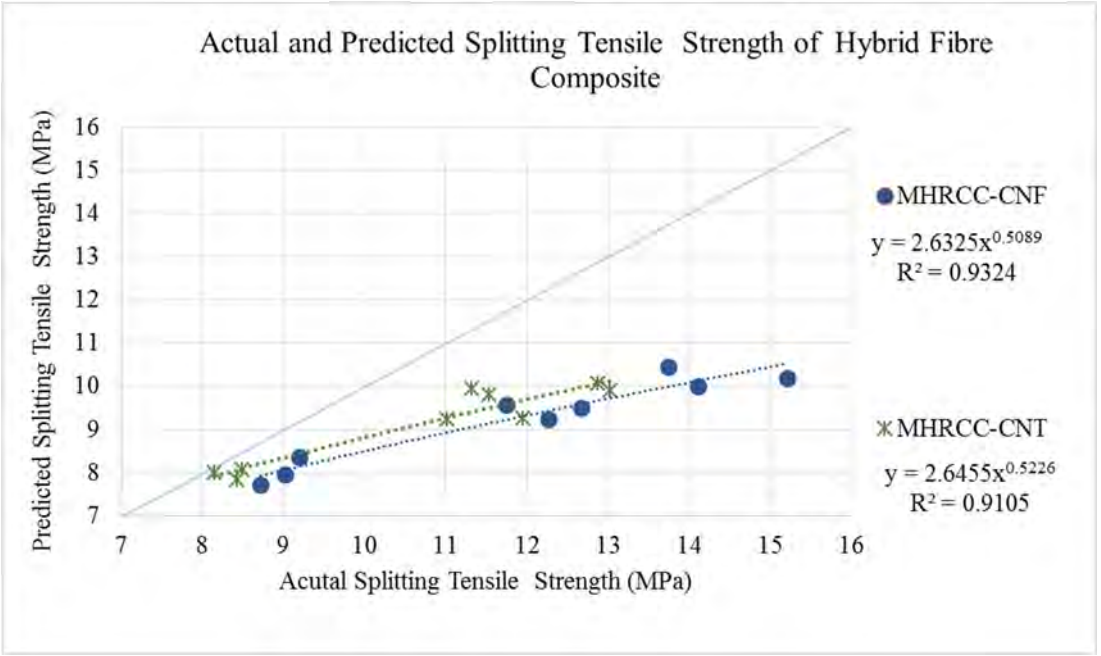

Figure6.17 The relationship between the actual and predicted tensile strength of MHRCC-CNT, and MHRCC-CNF.

Table 6.10 Experimental and predicted Splitting Tensile Strength of FRC and hybrid Fibre Composite.

Age day	Splitting Tensile Strength (MPa) of FRC		Splitting Tensile Strength (MPa) of MHRCC-CNT		Splitting Tensile Strength (MPa) of MHRCC-CNF	
	Experimental	Predicted	Experimental	Predicted	Experimental	Predicted
3	6.2	7.1	8.15	8.01	9.20	8.37
	6.5	7.3	8.42	7.84	9.02	7.95
	6.4	7.2	8.49	8.07	8.71	7.72
28	7.9	8.9	11.54	9.80	11.75	9.56
	7.8	9.0	11.02	9.23	12.67	9.51
	9.1	8.9	11.95	9.26	12.27	9.24
90	9.5	9.5	12.88	10.06	13.75	10.46
	9.4	9.4	13.02	9.90	15.21	10.19
	10.9	9.9	11.32	9.95	14.11	10.01

6.5 Composite Microstructures

Scanning electron microscopy (SEM) was performed on the fracture surface of dog-bone specimens (small size specimens of 25.4 x 20 x 7mm) before, and after tensile testing, to examine (a) composite microstructure, and (b) failure mechanisms. A uniform dispersion of fibres (both nano and/or micro) is essential to obtain composites with enhanced mechanical properties. Figurs.6.18 (a, b) show high-magnification SEM images of specimens containing CNT, and CNFs, indicating that the nanotubes/fibres are adequately dispersed (mostly nanotubes/fibres can be identified on the examined regions), and appear embedded into the hydration products, arresting the nanostructure.

These observations are in agreement with the investigations in Chapter Four and chapter Five, and with published literature (Cwirzen et al. 2009, Abu Al-Rub et al. 2012, Metaxa et al. 2013, Singh et al. 2013), which revealed that the crack bridging function of carbon nanofilaments incorporated into a cementitious matrix is significantly affected by the dispersion status, and strong surface interaction with the surrounding matrix.

Figures 6.19 (a) shows an SEM image at low magnification of specimens with 2% mass fraction of steel fibres, indicating that steel fibres were distributed homogenously in the composite. Figure6.19 (b) shows the steel fibre-matrix interface, and the micro cracks formed during the test, highlighting that although the microfibres can delay the propagation of microcracks, they do not arrest cracks with a smaller scale and stop their initiation. Due to the large difference between the diameter of the micro and nanotubes/fibres, it is not possible using SEM to show the simultaneous (synergistic) reinforcement effects of micro-scale steel fibres and nano-scale fibres.

The crack-reinforcing mechanisms of nanotubes and nanofibres in the composite can be clearly observed after the formation of the first crack. Figures 6.20 (a) and (b) respectively show the formed crack, and the carbon nanotubes along both sides of the crack. Nanotubes were ruptured and/or pulled-out of the matrix after the peak stress was reached, indicating the contribution of nanotubes in enhancing the load bearing capacity and crack-resisting characteristics. Figure 6.20 (c) shows the effect of the nanotube in reinforcing the matrix hydration products.

Similar to SEM images of the CNTs, Figure 6.21 shows the reinforcing mechanism of the carbon nanofibres. The longer nanofibres (which are around four times longer than nanotubes), act to i) provide a larger contact area with the surrounding matrix which may increase their ability to withstand pulling-out and/or rupture forces, thus higher load carrying capacity will be obtained, ii) increase the ability of nanofibres to prevent the crack propagation from nano to micron then macro scale.

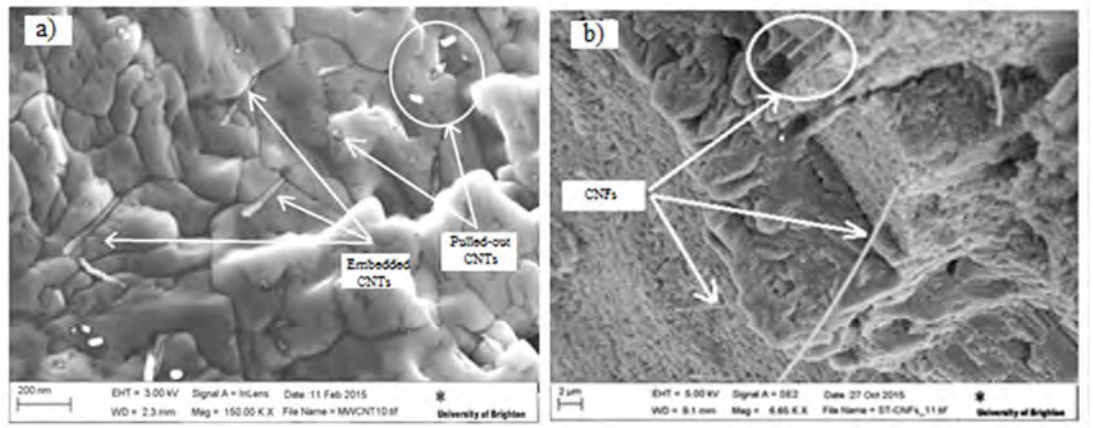

Figure 6.18 High magnification SEM images of specimens before the tensile tests containing a) carbon nanotubes and b) carbon nanofibres

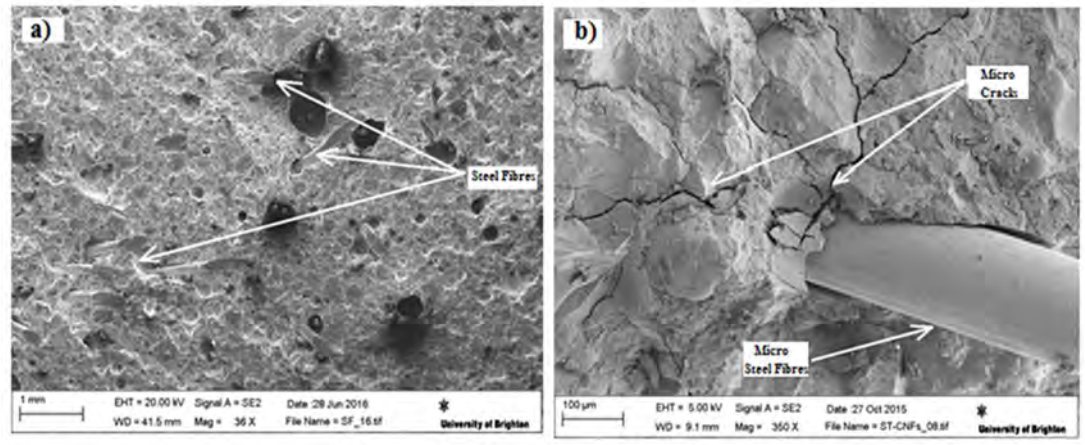

Figure 6.19 Low magnification SEM images of steel fibres images a) showing fibres dispersion, and b) microcracks propagations.

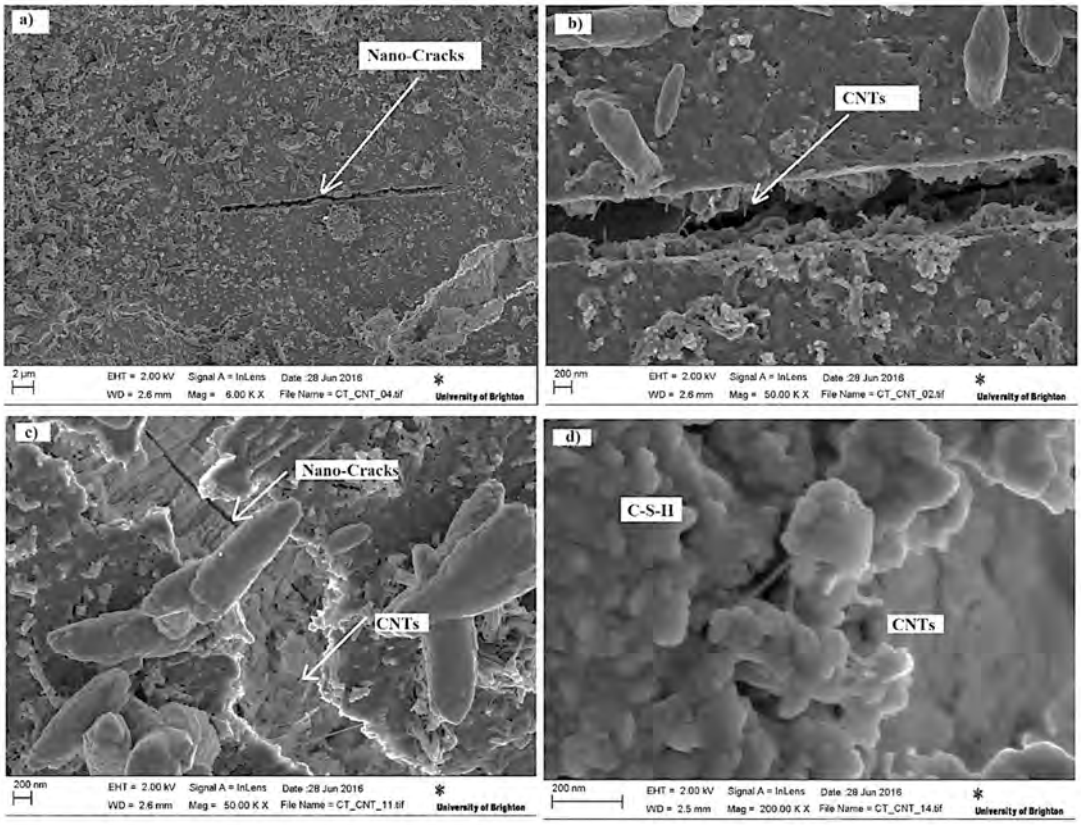

Figure 6.20 SEM images at different magnifications of cementitious composites containing CNTs; a) low-magnification image depicting the presence of a nanocrack, b) high-magnification image showing pulled-out and ruptured nanotubes along the microcrack, c) shows the multi-level scale of crack propagation, and d) shows nanotubes arresting the cement hydration products.

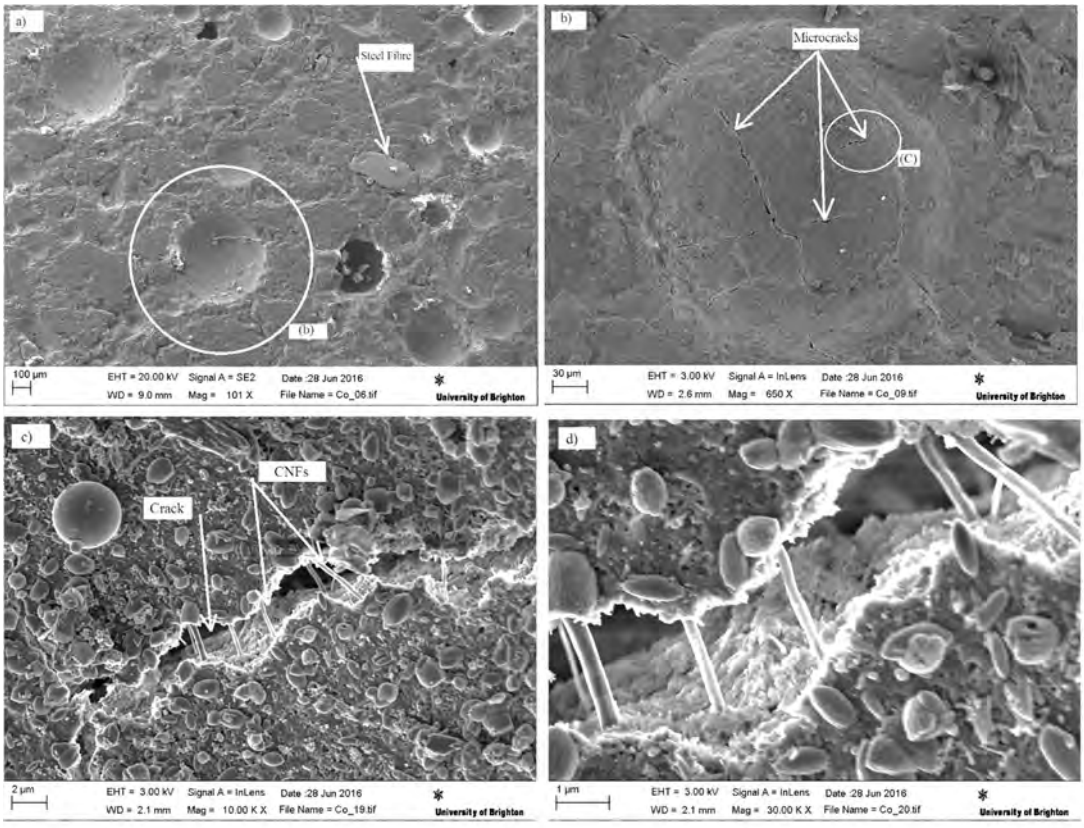

Figure 6.21 SEM images at different magnifications of cementitious composites containing CNFs; a) and b) low-magnification images depicting the presence of microcracks, c) and d) relatively high-magnification images showing nanofibres bridging across the microcracks.

Overall, the reinforcing efficiency of the CNFs in the cementitious matrix was shown to depend on their geometry and morphology, in addition to the nature of the adsorbed layer of superplasticiser (NSF). TEM images (Figure 6.22) confirm the morphology of the used nanofibres and the presence of an NSF layer on their outer surfaces. The NSF layer on the outer surface of the nanofibres acts as a linking site with the surrounding matrix which can further improve the mechanical performance (Figure 6.22a). Compared to nanotubes, the rougher surface of CNFs (consisting of conically shaped graphite planes) combined with their greater length (around four times longer than MWCNTs) acts to enhance the bond area with the matrix. Thus, a composite with a higher load transfer efficiency between the fibres and the matrix will be obtained (Figure 6.22b).

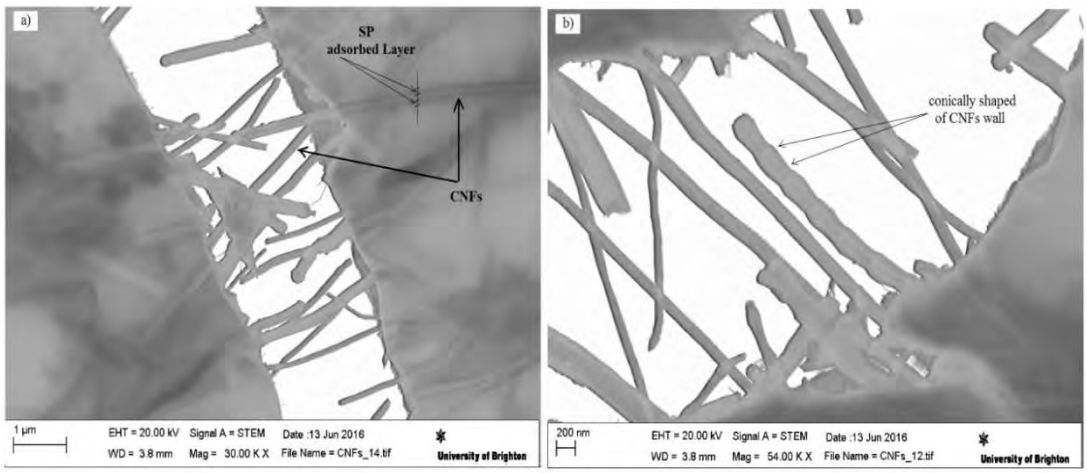

Figure 6.22 TEM images showing a) the adsorption layer of the superplasticiser on the nanofibres surface, and b) the conical Shape of CNFs

6.6 Assessment of Synergy of Nano- and Micro fibres

The use of different types and scales of fibres simultaneously for reinforcing a cementitious matrix is motivated by the concept of the multi-scale nature of the crack propagation process. The combination of nanofilaments and microfibres has been experimentally investigated with the objective to achieve effective synergy, whereby the performance of the produced composite exceeds that induced by each of the fibres alone. The synergy mechanism acts to control the cracking in the composite at different stages and begins from the nano scale. Effective synergy results in significant enhancement of the ductility, toughness, and stress-strain relationship of the composite as a result of arresting and bridging of nanocracks at early stages of loading by the effect of fibre at the nano scale, and bridging of microcracks which develop in the same time by the microfibres.

Based on the experimental results the following findings can be drawn:

- Steel fibres play a major role in delaying the development of micro-cracks, and limiting the propagation of these micro-cracks, as well as the transverse

confinement effect of the steel fibres (Amir Hossein Jodeiri* 2012, Seong-Cheol Lee 1 2015).

- Nanofilaments act as a filler and reinforcing agent resulting in a densely packed reinforced microstructure reinforced from the nanoscale, thereby enabling the applied load to be evenly transferred between the matrix and the reinforcement fibres.
- Hybridisation in this study works at nano and micro scales to delay the crack propagation, and prevent expansion cracks to the micro/macro scale by bridging the cement hydration products (leading to a higher tensile strength of the composite). At higher levels the microfibres control crack propagation. This mechanism is similar to that behind the increased strengths and energy absorption capacity, toughness, and ductility of multiscale hybrid (macro/micro) reinforced composites (Mohammadi et al. 2008, Mohammed Alias Yusof 2013).
- The significant strength gains of CNFs-composites can be attributed to i) their length which is much longer compared to nanotubes (about four times longer), and ii) their deformed geometry (conical shaped) allowing for stronger bond with the surrounding matrix, and therefore increasing the overall mechanical performance of CNFs composites (Metaxa et al. 2013).
- The strength gain with the hybrid systems can also be attributed to the effective distribution of nanotubes/fibres throughout the microstructures, which act as a nano reinforcement agent and better distribute stresses to the micro reinforcement scale.
- The effect of the nanotubes/fibres in refining the structural pores, and arresting the C-S-H hydration gel, contributes to improving the interfacial transition zone and transferring the stress over all the composite, increasing their crack resistance.
- Multiscale reinforcement is more efficient in delaying the growth and propagation of nano-micro/meso cracks before the peak load, thereby further improving the ultimate flexural tensile stress capacity.
- Bonding of nanotubes/fibres with hydration products is essential in an effective hybrid system. Use of undensified microsilica (as discussed in Chapter Four Phase-II) can enhance the dispersion of nanofilaments through the composite and at the same time prevent their re-agglomeration. The high silica content (10% replacement with the cement content), increases the pozzolanic material content

which has the capability to react with the calcium hydroxide generated from the hydration process to produce an extra gel of calcium silicate hydrate (C-S-H). This mechanism can explain the improved bond of nanotubes/fibres embedded in the C-S-H gel, as shown below. The C-S-H content has an important effect on the strength of concrete.

- $SiO_2 + Ca(OH)_2 \longrightarrow C\text{-}S\text{-}H + H_2O$

- Although there was a large difference in volume fraction/weight ratio between nanofilaments (0.175 Kg/m^3) and micro-fibres (160 kg/m^3) used in this experiment, strength gain resulted with nano and micro fibre addition separately were almost similar. The compressive strength of FRC (control mix) at all ages was almost the same (slightly low in case of CNFs composite) as the strength of nanotubes/fibres composites.

6.7 Summary

Nanofilaments (CNT, and CNF) within multiscale hybrid reinforced cementitious composites were found to contribute to multiscale reinforcement. Multiscale fibres acting to reinforce cement hydrations products in the nano scale while the longer fibres (i.e. steel fibres) arrest the microstructures and prevent the propagation of microcracks. Moreover, and for the same reason, the hybrid system was found to significantly delay the first crack formation, as the multi-scale reinforced structure increased the energy needed to initiate the cracks, and therefore contributed to obtaining a new tougher composite. Although, all of the examined nanofilenmts exhibited a positive effect in the examined composites, CNFs were found to significantly improve the mechanical performance. This can be attributed to the higher aspect ratio of CNFs compared to CNTs, which can lead to a better capability in bridging cracks and improving the load carrying capacity. SEM investigation supported the improved reinforcing efficiency of CNF over CNT, their higher aspect ratio enhancing their ability to withstand pulling-out and/or rupture forces.

The improvement resulting from the combination of nanofilaments can be attributed to i) the nanofibres' bridging mechanisms, which involve reinforcing the cement hydration products, and ii) a packing effect, with the extremely small particles acting as fillers, filling the voids (spaces) (at nano-and/or micro level) that exist within and around the ettringite products within the hydrated cement paste. Adding fibres (nano and micro to a cementitious composite can significantly increase ductile capacity and fracture toughness. Additionally, energy storing capacity is also increased, and the nanofibres can control crack width by the mechanism of fibre bridging.

Chapter Seven:

Nanocomposites as Overlay Repair/Strengthening Materials
- **Durability Performance: Shrinkage Behaviour and Sulfuric Acid Resistance**

7.1 Introduction

Construction material durability is to a large extent controlled by the resistance of the material to aggressive media, such as slightly acidic environmental waters, salt-bearing solutions etc. The ingress of gases, water or ions in aqueous solutions into materials generally takes place through connected pores and microcracks. Cracking reduces load carrying capacity of concrete structural elements, and allows the penetration of aggressive ions into the concrete element which results in corrosion of steel reinforcement, increased probability of alkali silica reaction and sulphate attack, and other durability problems(Banthia et al. 2006).

Durability degradation increases the maintenance cost and reduces the service-life of structural elements. Hence, limiting cracking is the main criterion in achieving a long-term durability and service-life. For decades, efforts have been made in concrete science and in the engineering community to develop appropriate techniques to repair or/and strengthen existing deteriorated elements to increase their service-life. To date, existing cement-based composites for such repair or strengthening applications, in principle, have been limited to cementitious composites containing randomly distributed macro/micro fibres. These fibres provide bridging forces across existing cracks, and reduce the extent of shrinkage cracking.

At present, nanofilaments (i.e. Carbon nanotubes, carbon nanofibres) are the only promising materials however that have the potential to reinforce composites from the nano scale and prevent crack initiation, therefore assisting in improving the quality and longevity of structures(Hanus and Harris 2013). Alongside the performance of nanofilaments in influencing crack behaviour, they act to fill in small composite pores and minimise connected capillary pores. Therefore, resistance to the penetration of

aggressive media, which is one of the most important parameters for the performance and long-term durability of structural materials, can also improve.

This Chapter, and Chapter Eight, addresses one the more promising applications of nanocomposites, in developing a thin-layer (35mm) repair/strengthening composite with lowered susceptibility to shrinkage and cracking. This chapter focuses on the shrinkage behaviour and ingression resistance of carbon nanotubes/fibres composites (previously optimised in Chapter Five and Chapter Six). Nanofilaments Reinforced Cementitious Composites (NRCC), and Multiscale Hybrid Reinforced Cementitious Composites (MHRCC) based on carbon nanotubes and carbon nanofibres, are investigated, using drying shrinkage, end-restrained, and base-restrained shrinkage tests. The composites' resistance to aggressive ions has also been investigated, using an accelerated test procedure to assess the behaviour of nanotubes/fibres mixtures in relation to their resistance to sulfuric acid ingress. Mechanical behaviour of the thin-layer repair/strengthening of MHRCC-CNF, and MHRCC-CNF was investigated on semi-large scale RC beams designed to simulate the performance of nanocomposites in real structural elements; the results of which are presented in Chapter Eight.

7.2 Shrinkage Performance

Several methods have been used in the past to assess shrinkage of concrete and resulting cracking (Toledo Filho et al. 2005, Oladiran 2014). In this study, free drying shrinkage and restrained shrinkage tests are the two methods that have been used to assess the shrinkage-induced cracking of cementitious composites. Other types of shrinkage such as plastic shrinkage, autogenous shrinkage, chemical shrinkage, creep relaxation, carbonation shrinkage, and shrinkage rate should be included in future work (Tada-aki Tanabe 2009). Moreover, there exist a number of dependent factors which influence the shrinkage behaviour including; raw cementitious material properties (e.g., cement, sand, and microsilica), temperature, relative humidity (RH), and volumetric size of the specimens. These parameters have been fixed during all tests to avoid their effect on the results (Noushini et al. 2014, Oladiran 2014). The

effect of variation in each of these parameters on shrinkage of composites containing nano-additives would be a useful area for future research.

Results of free and restrained shrinkage experiments on cementitious nanocomposites (NRCC-CNT, and NRCC-CNF) and multiscale hybrid reinforced cementitious composites (MHRCC-CNT, and MHRCC -CNF) are outlined and explained in details in the following subsections (summarised in the flow chart in Figure 7.1).

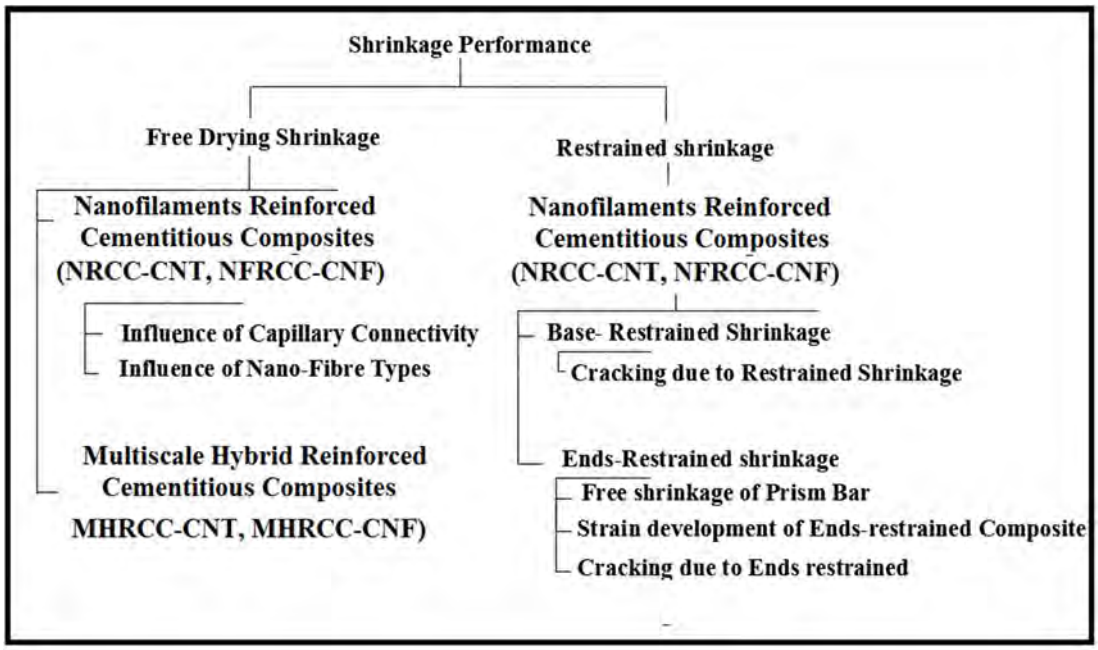

Figure 7.1 Flow chart schematically illustrating the experiments on free drying shrinkage and restrained shrinkage.

7.2.1 Free Drying Shrinkage

Drying shrinkage is defined as the time-dependent deformation of a material due to loss of water at constant temperature and relative humidity. Drying shrinkage occurs when concrete is exposed to a drying environment, and is the most widely recognized source of volume change in concrete. Generally, the structure capillary tension and the movement of interlayer water are the main shrinkage mechanisms. At present, there is no experimental or theoretical work which adequately models the behaviour of drying shrinkage in the presence of nanofilaments. In the sections below free drying shrinkage

measurements were made for all the developed composites (NRCC-CNT, NRCC-CNF; and MHRCC-CNT, MHRCC-CNF) as a function of drying time. The setup of the free drying shrinkage test is shown in Figure 7.2.

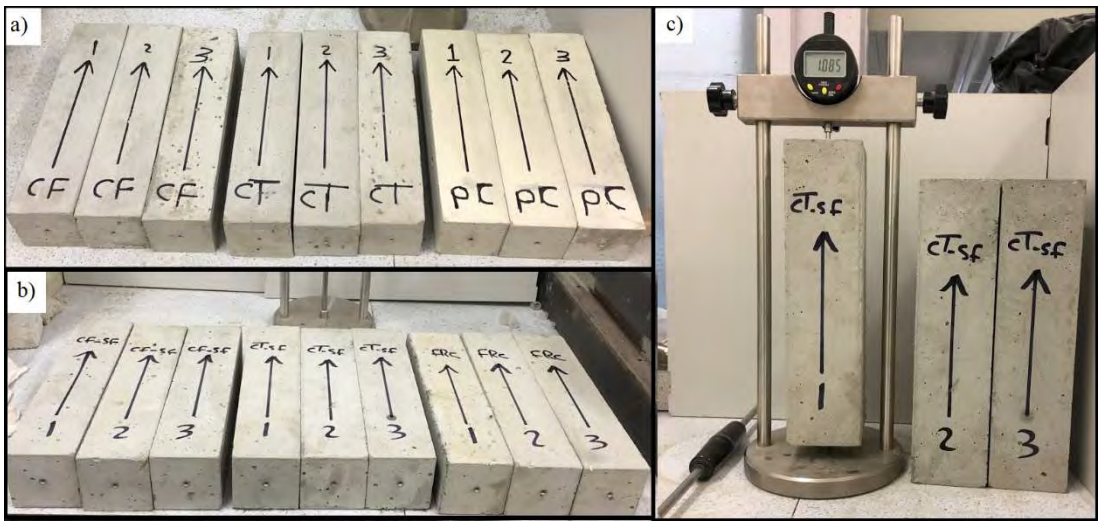

Figure 7.2 Setup of the drying shrinkage test. a) and b) show the specimens used for shrinkage tests on nanofilaments reinforced cementitious composites and multiscale reinforced cementitious composites, respectively, and c) shows shrinkage apparatus.

7.2.1.1 Shrinkage Strain of Nanofilaments Reinforced Cementitious Composites (NRCC-CNT, NRCC-CNF)

During the setting and hardening of the composite, shrinkage strain starts to develop. For normal cement mortar, an ultimate drying shrinkage strain with magnitude up to 1350 μm/m under normal lab conditions was obtained, as presented in Table 7.1. Figures 7.3(a, b, and c), and 7.4(a, b, and c) show drying shrinkage strains at early and late curing ages respectively, of (a) NRCC-CNT, (b) NRCC-CNF and (c) PC. The drying shrinkage-time relationship over 180 days shows a distinct decrease in shrinkage strain with the addition of carbon based nanofilaments (CNT, and CNF). Nanotubes and nanofibres composites showed almost the same % decrease. For these composites, the drying shrinkage under the same conditions is decreased by 85%, 71%, and 47%, at early age (from 2, 3 and 7 days respectively) compared to the shrinkage strain values of the control PC specimen. After 28 days and up to very late age (180 days) the decrease rate stabilised at about 34%.

The results indicated (Table 7.1) a greater reduction in the drying shrinkage at early age (shown in Figure 7.3). The results of PC show that the average shrinkage strain is extremely high in conventional materials. For example, at 1, 3, and 7 days, the obtained strain value of PC specimens was about 575μ, 616μ, and 725μ respectively, which represents about 43%, 47%, and 55% of the "ultimate" shrinkage respectively. In comparison, the average early shrinkage strain of CT and CF specimens was extremely low. Compared to PC, strain values were about 96μm, 160μm, 386 μm and 96μm, 161μm, 388μm, and these values represent about 7%, 12%, 30%, and 6%, 15%, 30% of the ultimate shrinkage, respectively. The greater effectiveness of the nanofilaments is consistent with their impact on the mechanical properties, and reducing the porosity.

As extensively investigated in published literature, the shrinkage of cement matrices is significantly affected by porosity, pore size, shape, and the connectivity of the capillary pores in the hydrated cement paste (see Chapter Two, Section 2.5). The addition of nano tubes and fibres decreased the matrix porosity, therefore contributing to the lower drying shrinkage. The geometry of nanofilaments and their availability as individuals rather than as agglomerates, acts to refine/fill the pores and reduce the connected capillary pores, thereby reduce the possibility of mixture bleeding and moisture losses. The connectivity of the capillary porosity in cement-based materials impacts the transport of fluids and ions to the outer surfaces. The involved drying shrinkage is a complex mechanism this is greatly influenced by the porosity. The presence of nanofilaments, to large extent, influenced the structure pore sizes, and their connectivity. These phenomena may act simultaneously and be predominant in different regions of the composite, leading to different transport mechanisms during drying.

Generally, the cementitious matrix consists of pore space and a solid phase. The pore spaces (in principle) are either connected to each other or isolated by the solid materials, and the solid phase is composed of un-hydrated cement and microsilica and hydration products (Tada-aki Tanabe 2009). The hydration process over time generally starts from individual spherical particles of cement and microsilica which gradually become interconnected to form a microstructural network. This process leads to an increase in the volume fraction of the solid phase, and decreases the

fractional connectivity of the pore phase. In cement mortar, an absence of coarse aggregate leads to increase connected capillary pores, thereby increase the evaporation percentage. The increased evaporation increases pore vapor pressure which increases drying shrinkage strain.

Table 7.1 Drying shrinkage results for PC, NRCC-CNT, and NRCC-CNF, and the decrease percentage compared to PC.

Age	PC		NRCC-CNT		NRCC-CNT		Decrease compared to PC (%)	
day	Shrinkage (μm)	SD	Shrinkage (μm)	SD	Shrinkage (μm)	SD	CT	CF
2	567.0	50.5	96.3	8.4	99.0	18.4	489	473
3	615.7	26.7	160.7	33.1	190.7	25.6	283	223
7	725.3	44.6	387.7	65.9	388.0	58.5	87	87
14	824.7	22.2	669.7	77.5	670.7	58.1	23	23
21	923.0	21.9	835.0	65.0	816.0	70.8	11	13
28	1028.4	53.9	842.0	96.3	845.0	69.3	22	22
56	1190.7	73.7	865.7	99.4	868.7	82.8	38	37
90	1298.3	60.1	950.5	90.1	970.7	97.3	37	34
120	1311.0	65.3	982.6	46.2	1033.0	51.1	33	27
180	1362.2	59.6	992.3	41.3	1040.8	59.2	37	31

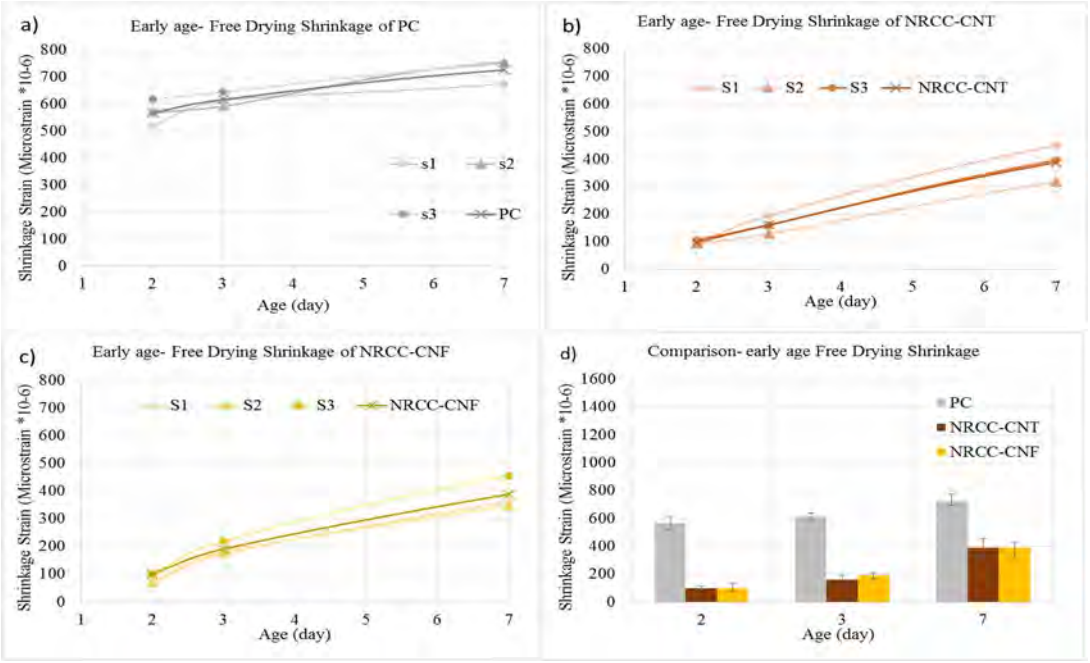

Figure 7.3 Free drying shrinkage at early age (up to 7 days) of a) cement mortar (PC), b) composite of carbon nanotubes (NRCC-CNT) and c) carbon nanofibres (NRCC-CNF). d) Shows a comparison of the early age drying shrinkage with error bars.

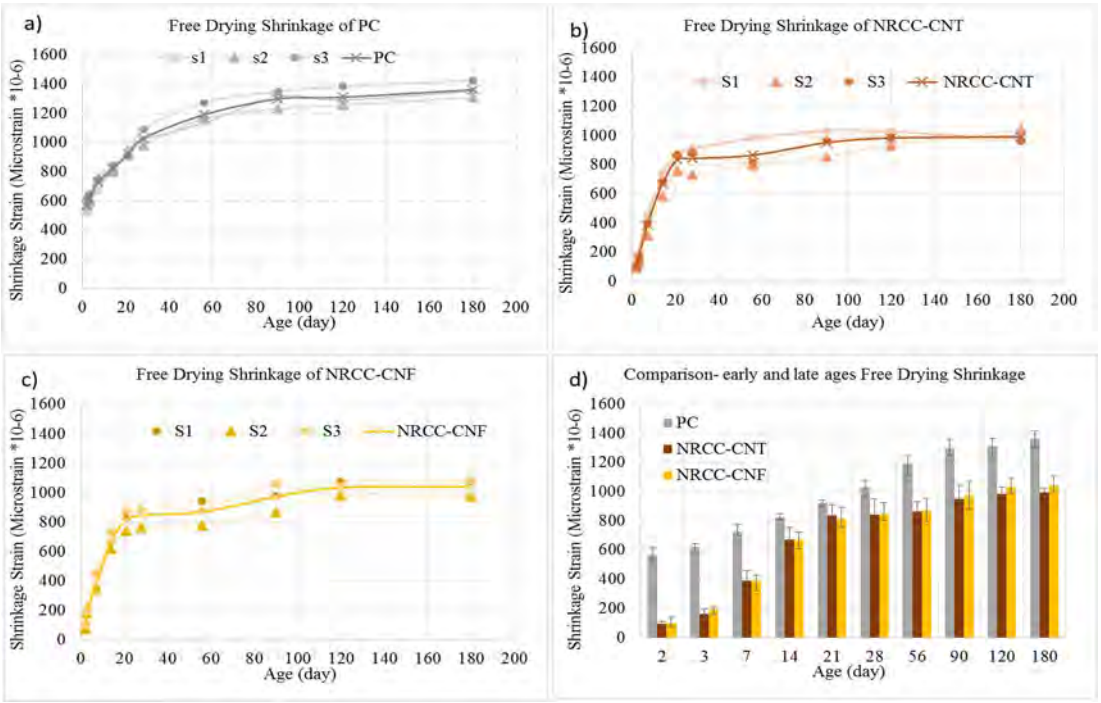

Figure 7.4 Free drying shrinkage as function of the age (up to 180 days) of a) cement mortar(PC), b) composite of carbon nanotubes (NRCC-CNT) and c) carbon nanofibres (NRCC-CNF). d) shows a comparison of the early age drying shrinkage with errors bars.

7.2.1.1.1 Influence of Capillary Connectivity on Free Drying Shrinkage.

Drying shrinkage is caused by the loss of internal water, as shown in Figure 7.5, which illustrates two cement particles at the surface of a paste subjected to drying (Radocea 1992.). When the evaporating water (W) exceeds the internal water, which moves from the inside of the concrete to the surface, stress is generated and causes the meniscus to be lowered with the increasing capillary pressure. As the diameter of the capillary pore decreases, the capillary pore pressure (and therefore the shrinkage) increases accordingly (Kejin Wang 2013).

Shrinkage of cementitious-based composites commonly occurs as a decrease in volume via four primary mechanisms: capillary tension, surface tension, disjointing pressure, and change in water within the matrix of the cement (Noushini et al. 2014). The first water to be lost from the composite due to evaporation is that held in the large capillary pores of the hardened composite, then from smaller pores, as water continues to evaporate from the capillary and gel pores, a meniscus is formed along the network of capillary pores and surface tension is created as the adsorbed water held by hydrostatic tension in the small capillaries is reduced significantly. The loss of water (free water and adsorbed water) produces tensile stress, which forces concrete to shrink. These tensile stresses are in equilibrium with compressive stresses acting in the surface layers of the concrete, and hence shrinkage of the concrete occurs ((Tada-aki Tanabe 2009).

A schematic graph was proposed by (Monteiro 2006) to represent the typical sizes of both solid and void phases of hardened cement paste, and has been modified here to include the nanofilaments used in this study (Figure 7.6). In general, capillary pores (popularly known as porosity) represent the space not filled by hydration products. Evaporation (escape) of the pore water, including the capillary water and interlayer water (in-between C-S-H gel layers) influences the drying shrinkage behaviour. Macropores and micropores refer to the capillary voids of size larger than 50nm, and smaller than 50nm, respectively. Macropores are more influential in determining the strength characteristics, whereas micropores play an important part in drying shrinkage. Capillary water within the hydrated cement paste can be separated into two categories: the water in large voids of the order of >50 nm which may be termed free

water (because its removal does not cause any volume change), and the water held by capillary tension in small capillaries (5 to 50 nm), the removal of which may cause shrinkage of the system.

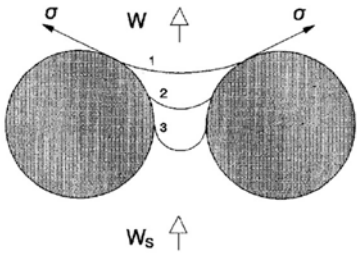

Figure 7.5 Stresses pulling the water meniscus lower between two cement particles due to moisture transfer and capillary pressure development(Radocea 1992.)

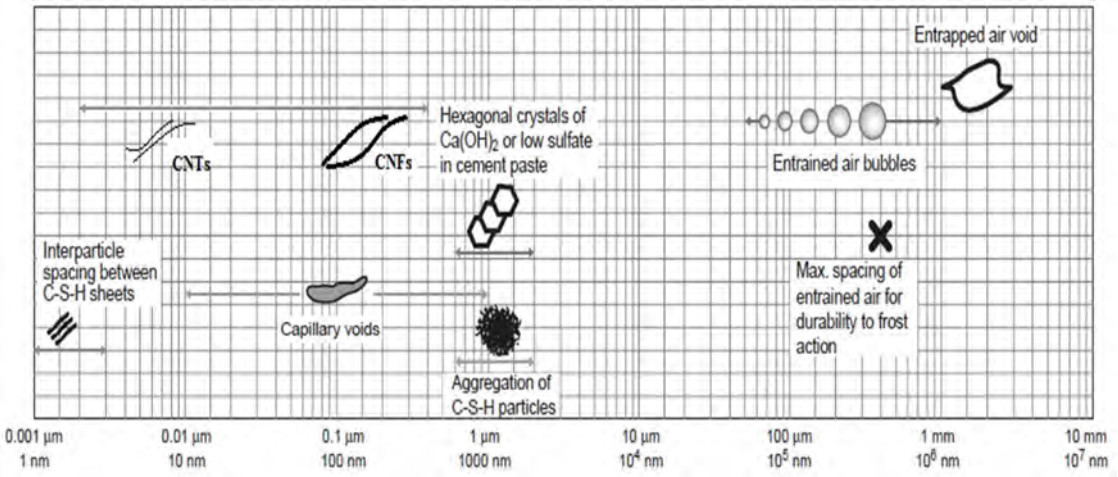

Figure 7.6 The typical size range of pores and hydration products in a hardened cement paste. CNTs, and CNFs are shown for comparison.

A typical schematic graph showing the types of water inside the composites capillary pores was proposed by (Monteiro 2006) and is shown in Figure 7.7. In this study, this graph has been modified (as shown in graph b) to represent the connected pores inside the cement mortar (in red arrows) which are the main causes of the high shrinkage of the mortar. c) shows the mechanism of nanofilaments (as green lines) in preventing the composite water escaping and evaporating. This illustrates that almost all of the free water will remain confined in the composites and contribute to the hydration

process, and thus increase the solid phase, and thereby reduce the drying shrinkage strain and cracking.

Factors reducing the drying shrinkage on one hand related to the properties of the pores such pore size distribution, pore diameter and pore connectivity, and on the other hand relate to properties of the nanofilaments themselves such as the aspect ratio, fibres spacing, fibre content, proper dispersion and distribution. Investigation of the interplay of these factors would be a profitable area of future research.

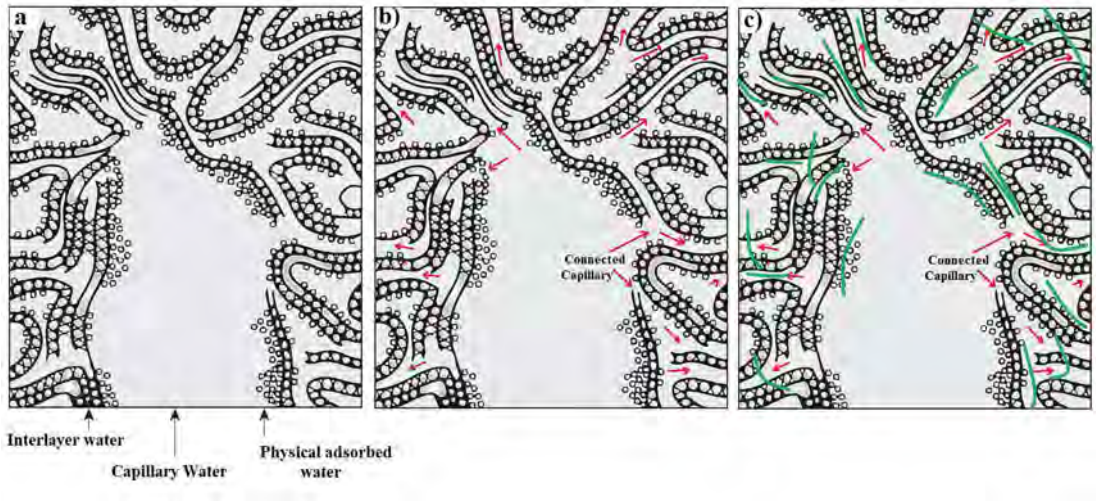

Figure 7.7 Schematic representations of different mechanisms acting on drying cement paste, a) Diagrammatic model of the types of water associated with the calcium silicate hydrate. b) Represent the connected capillary pores(red-lines), and c) represent the effect of nanotubes/fibres (in green colour) in interrupting the connected pores.

7.2.1.1.2 Influence of Nanofilament Types

Generally, mechanical strength experiments on nanofilaments reinforced cementitious composites based on carbon nanotubes and carbon nanofibres have shown considerable variation in performance and in reduction of the effect of early age cracking, (as noted in Chapter Five, and Chapter Six). These variations were mainly attributed to the higher aspect ratio of nanofibres compared to nanotubes, and the geometry of nanofibres. However, in shrinkage experiments it was observed that the free drying shrinkage strains of both types of nanofilaments composites were almost the same (Figure 7.3). Scanning Electron Microscopic (SEM) images were used to

understand the efficiency of nanofilaments in preventing evaporation and then reducing the drying shrinkage. Under (SEM) examination, pores through the composites are empty of water which is due to the sample analysis under high vacuum. Typically, the pores of cement mortar (PC) can be classified into three types; i) macropores, which are larger than 50nm and up to few microns (circled in red colour in Figure 7.8a), ii) nanopores, which are extremely fine with an average size less than 50nm (circled with yellow colours in Figure 7.8b), iii) Interlayer spaces in between C-S-H products. Together these spaces connect to form capillary voids which significantly influence the drying of the internal water.

Typical SEM images of nanotubes and nanofibres composites are shown in Figures 7.9(a-c). In these images nanotubes were found to be well-distributed and filled interlayer spaces between C-S-H gel (circulated in yellow colour in Figures 7.9(a and b). Nanofibres filled the composite micropores and macropores (Figures 7.9(c and d) circled in red colour), and were embedded through the hydration products, significantly refining the pores and decreasing the pores connectivity.

The nanofilaments significantly reduce the escape/evaporation of the water inside micro and macropores. Interrupting the connected pores allows the confined waters in the pores to be consumed by the hydration process. Hence, addition of nanofilaments changes the behaviour of the adsorbed water and interlayer water, reducing the possibility of quick evaporation and thereby reduce the drying shrinkage.

For future work it is useful to analyse the pore nature of nanofilaments reinforced cementitious composites using the MIP (Mercury Intrusion Porosimetry) technique or via image analysis.

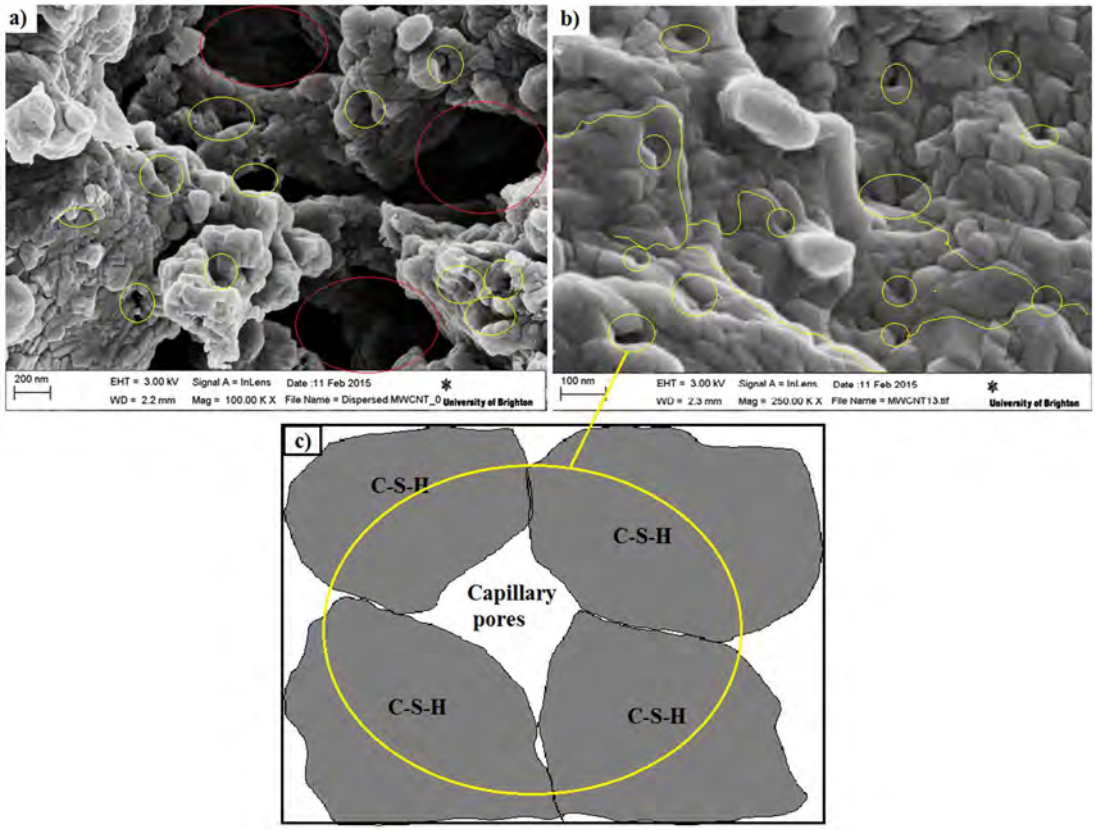

Figure 7.8 SEM images showing the structure of cement paste (PC), a) red and yellow colours represent the macropores of size greater than 50nm, and micropores of size less than 50nm, respectively, b shows the connected capillary pores, and c) is a schematic representation of the formation of capillary pores.

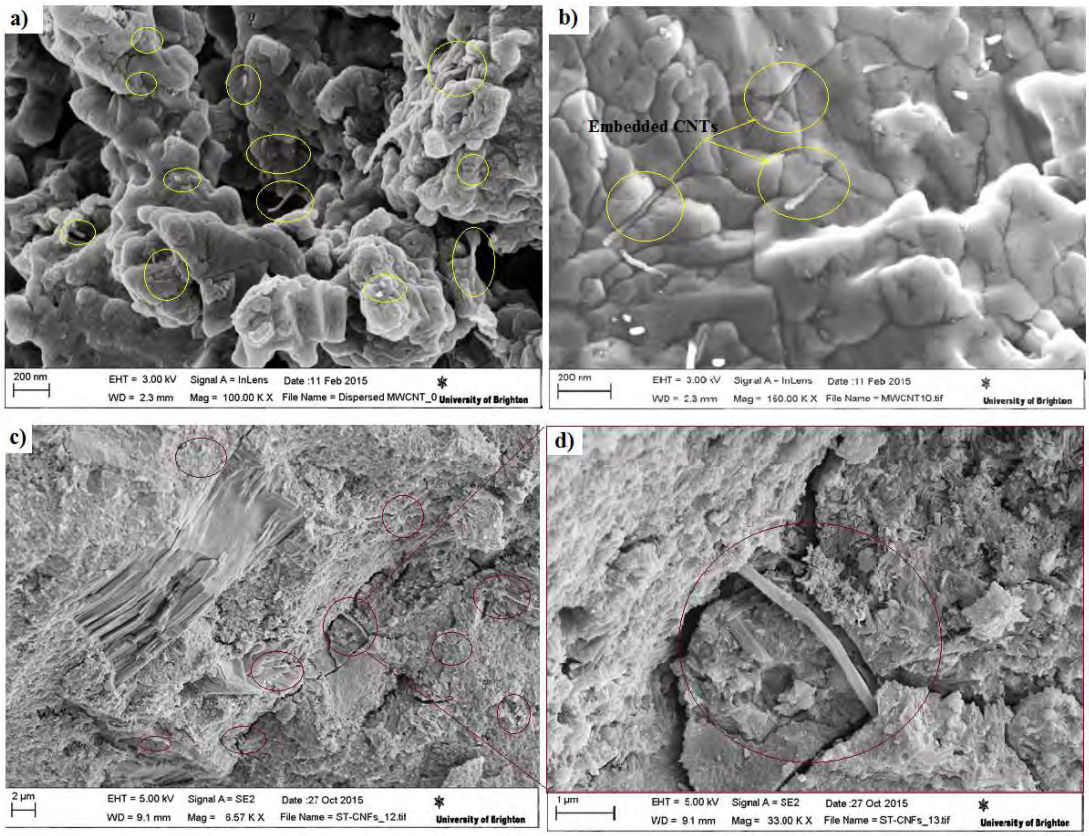

Figure 7.9 Typical SEM images of nanotubes and nanofibres composites. a) and b) show the role of carbon nanotubes in filling the extremely fine micropores and interrupting the connected capillary pores. c) and d) show the role of nanofibres in filling the micropores and macropores and interrupting the connected capillary pores.

7.2.1.2 Shrinkage Strain of Multiscale Hybrid Reinforced Cementitious Composite (MHRCC-CNT, MHRCC-CNF)

It has been a particular focus of many researchers in recent times to minimise the aforementioned shrinkage problems by inclusion of different type of micro fibres such as steel fibres in different volumetric ratios as a form of fibre reinforced composite, FRC (Carlswa 2002). In this section, free drying shrinkage of multiscale hybrid reinforced cementitious composites based on carbon nanotubes and carbon nanofibres (MHRCC-CNT, and MHRCC-CNT respectively) in addition to steel fibre reinforced composites (FRC), is analysed and discussed.

Measured free drying shrinkage strains are summarized in Table 7.2. The results of FRC, MHRCC-CNT, and MHRCC-CNF have been divided into two distinct stages: shrinkage at early age (Figure 7.10) and at late age (Figure 7.11). The early age stage is started after demoulding of the specimens and covers the first 7days of curing. Following ASTM and British Standards the drying shrinkage is measured only after drying starts. Later ages, or long term, refers (in this study) to composites at an age from 7days and beyond up to 180 days.

At early and late ages, control specimens of FRC exhibited the highest free drying shrinkage strain, whereas MHRCC-CNT, and MHRCC-CNF specimens showed lower shrinkage strain. For example, results of FRC ((Figure 7.10a) shows that the average shrinkage strain at 1, 3, and 7 days, was about 157μm, 233μm, and 361μm and this represents about 17%, 26%, and 40% of the "ultimate" shrinkage (910μm) respectively. The average early shrinkage strain of MHRCC-CNT (Figure 7.10b), and MHRCC-CNF (Figure 7.10c) specimens was about 76μm, 125μm, 184 and 82μm, 150μm, 233μm, and these values represent about 8%, 14%, 20%, and 9%, 17%, 26% of the ultimate shrinkage of FRC, respectively.

For comparison, at early age (first 7 days) and at late age (ultimate drying shrinkage) the reduction in the shrinkage as result of addition of steel fibres was about 175%, and 45% respectively, compared to shrinkage of PC. With inclusion of only nanofilaments (as discussed Section 7.2.1.1), significant reductions in the shrinkages were observed. These reductions are significantly higher compared to those of only steel fibres by about 80% at early age, with almost the same efficiency at late age. This could be attributed to the higher porosity of fibre reinforced composites (FRC), which can influence the rapid evaporation of water from the composite. Drying shrinkage of FRC has been extensively studied by a number of authors, and the drying shrinkage behaviour, in principle, is influenced by the restraint degree provided by the rigid fibres, and by the aspect ratio characteristics, volume fraction used, and the mix design of the cementitious composites.

In the hybrid system, the significant reduction observed in the drying shrinkage at early and late age was believed to be due to the effectiveness of multiscale reinforcement provided by micro steel fibre and nanofilaments, and the high aspect

ratio of both fibres, which can lead to an increase in the restrained degree of the composite. Similar to the behaviour of nanofilaments in cementitious composites (see Section 7.1.1), nanofilaments within multiscale hybrid reinforced cementitious composite can also refine/fill the composites pores and change the pore structures and capillary nature of the composite, thereby reducing the composites drying shrinkage. Steel fibres considerably decrease the drying shrinkage compared to the shrinkage of cement mortar (Figure7.12). Hardened cement mortar undergoes high drying shrinkage, whereas FRC, and nanofilaments composites have been found to a certain extent to minimise the drying shrinkage. The shrinkage behaviour of multiscale hybrid reinforced cementitious composites was found to combine the effect of each type of fibre individually.

Table 7.2 Drying shrinkage results of FRC, MHRCC-CNT, and MHRCC-CNF and the decrease percentage compared to the control mix (PC).

Age	FRC		MHRCC-CNT		MHRCC-CNF		% decrease compared to FRC	
day	Shrinkage (μm)	SD	Shrinkage (μm)	SD	Shrinkage (μm)	SD	MHRCC-CNT	MHRCC-CNF
2	157.3	13.9	76.0	13.9	81.7	7.5	107	93
3	233.0	9.8	125.3	9.8	150.3	9.3	86	55
7	361.7	8.5	184.2	8.5	233.3	11.2	96	55
14	556.7	30.4	313.3	30.4	341.0	4.4	78	63
21	713.7	9.5	381.3	9.5	400.0	13.9	87	78
28	820.7	8.5	419.3	8.5	447.0	14.2	96	84
56	872.3	27.4	455.4	27.4	549.0	20.0	92	59
90	889.7	28.7	471.3	28.7	573.5	21.1	89	55
120	906.7	19.0	486.8	19.0	581.6	15.5	86	56
180	910.3	22.7	529.1	21.2	597.8	19.5	72	52

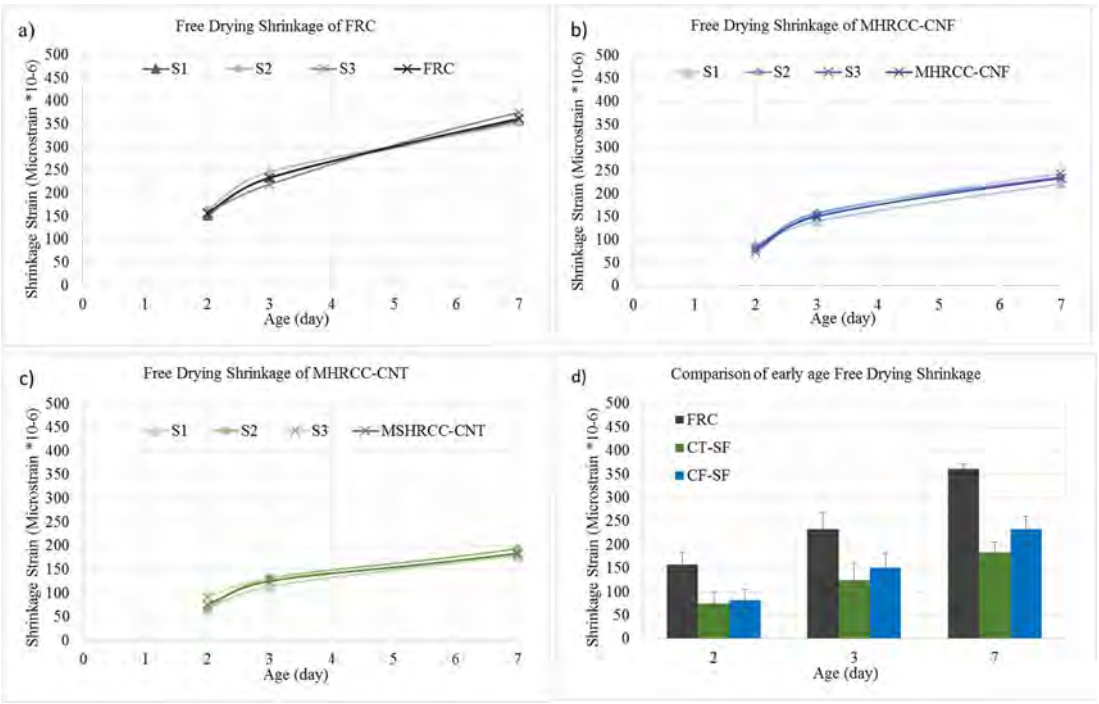

Figure 7.10 Free drying shrinkage at early age (up to 7 days) of a) FRC, b) MHRCC-CNF, and c) MHRCC-CNT. d) gives a comparison of the early age drying shrinkage with errors bars.

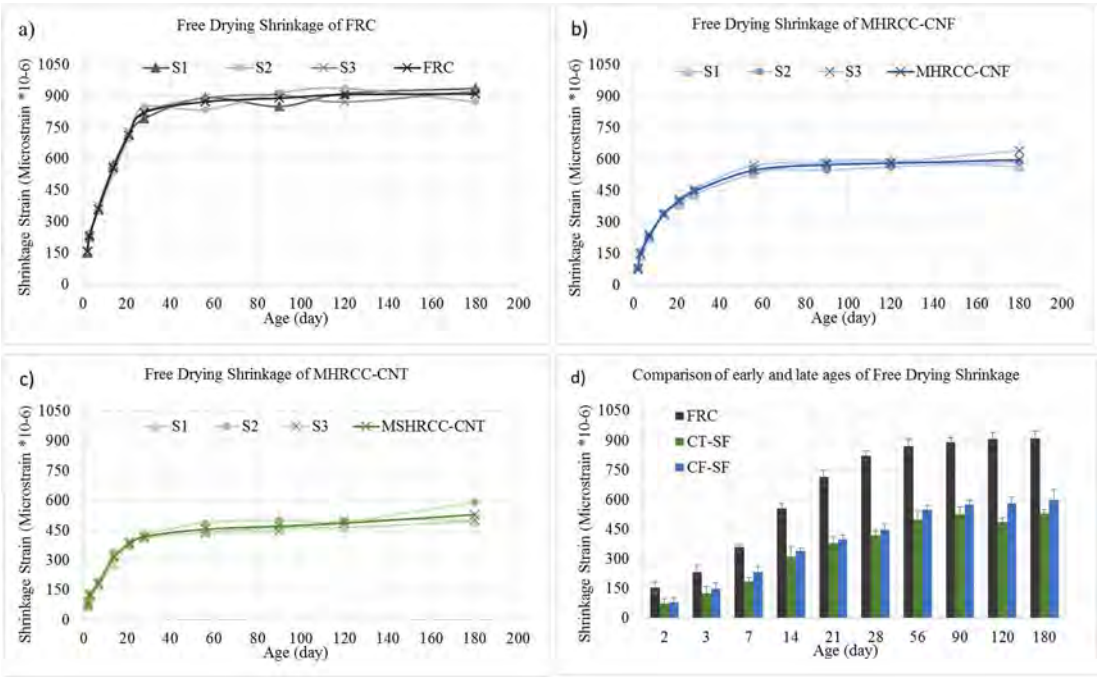

Figure 7.11 free drying shrinkage at (up to 7 days) of a) FRC, b) MHRCC-CNF, and c) MHRCC-CNT. d) represent comparison of the drying shrinkage with errors bars.

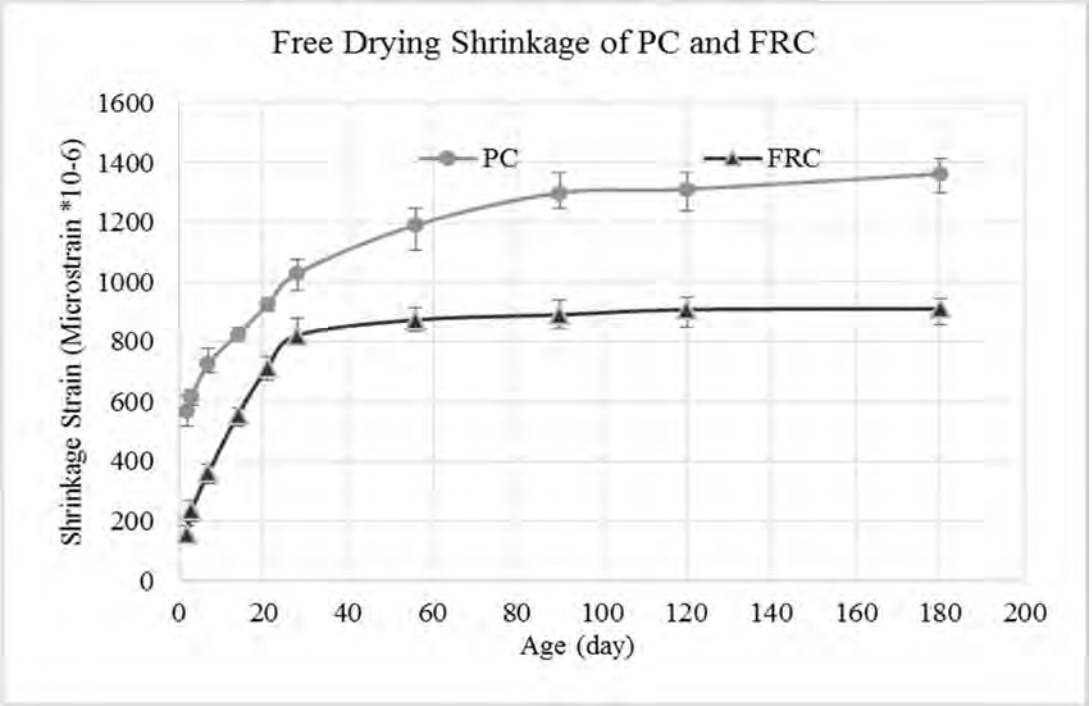

Figure 7.12 Free drying shrinkage of control mixtures of PC and FRC.

7.2.2 Restrained Shrinkage

Based on ACI 207-2R-95, cementitious based composites are restrained to some degree by volume because there is always some restraint provided either by different parts of the element itself or by the supporting elements(ACI207-2R-95 2002). The former includes the restraint provided by volume change, while the latter are always existing and can be provided by supporting elements as in real life the cement based composite is restrained to some degree. Restraining can induce tensile, compressive, or flexural stresses in the elements, depending on the type of restraint and whether the change in volume is an increase or decrease. Restraint strain that induces compressive stresses is not of concern due to the ability of composite to withstand compression, but restraint conditions which induce tensile stresses are crucial due to its effect in causing cracking at early age and under even only light service load (Zhang and Li 2001, Mindess 2007).

Many test methods have been reported in the literature to investigate the influence of microfibres on the cracking behaviour of cementitious composites exposed to shrinkage such as: End-restrained, Base restrained, and ring tests. The sections below present and discuss the restrained shrinkage over time (with specimens restrained at the base, and restrained at the ends) of cementitious nanocomposites based on carbon nanotubes and carbon nanofibres (NRCC-CNT, and NRCC-CNF) in addition to cement mortar for comparison. It is important to note that the restrained tests were performed to understand the performance of NRCC-CNT, and NRRCC-CNF through the composite and to simulate their performance in a real life application.

Several methods have been proposed in the past for the evaluation of composite restraint at the bases, and at the ends, of specimens, however to date there is no agreement on the most effective method. In this study the base restrained shrinkage behaviour and cracking potential tests were performed on thin composite overlays (35mm thick) on a concrete substrate beam, to examine the composite cracking tendency. The overlay composite is highly restrained at the base with the substrate. Shrinkage performance of a composite overlay depends significantly on the degree to which the overlay is bonded to the substrate (Carlswärd, 2006).

Experiments result from Base-Restrained Shrinkage tests are discussed first, followed by results from End Restrained Shrinkage experiments.

7.2.2.1 Base-Restrained Shrinkage

The base-restrained shrinkage test evaluates the cracking tendency of a composite overlay in addition to the restrained shrinkage behaviour. The test set up used is shown in Figure 7.13. Typically, the results of the two beams made from one batch were very similar, and average shrinkage can be used as a representative result. The restrained strain located at the top (on two lines), and side (line on each side) of the specimens were the average values of the measurements taken over two samples, and each measurement was taken over 100mm.

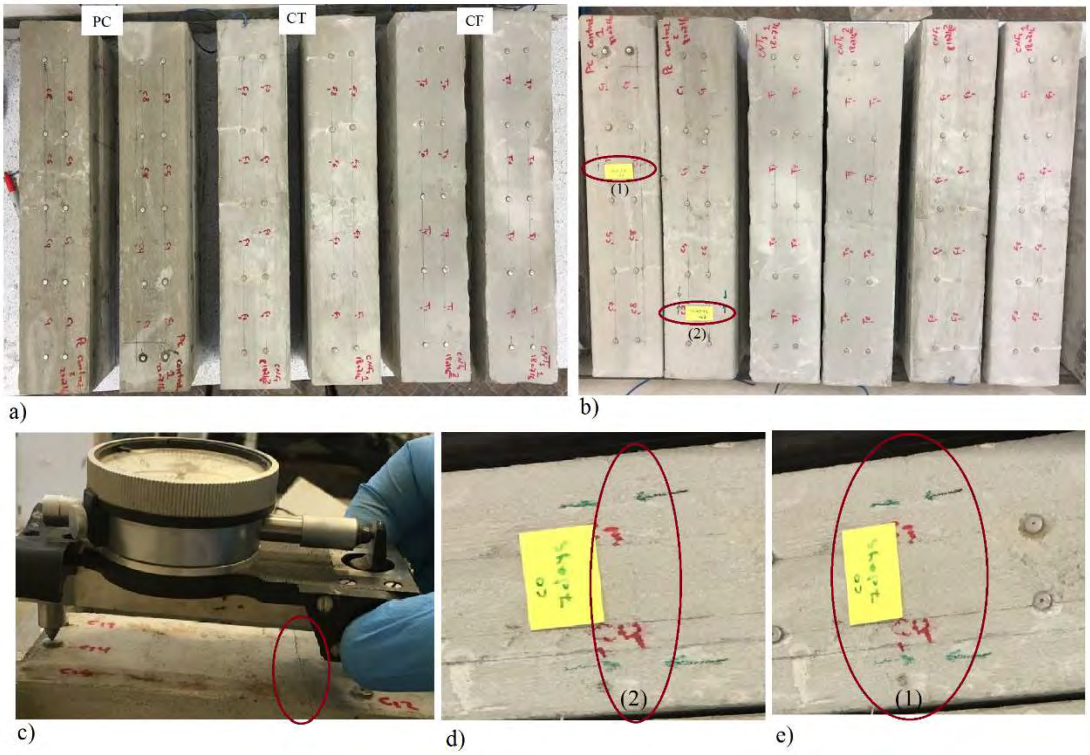

Figure 7.13 Base restrained shrinkage test set-up. a) shows the prepared beams at early age when no cracks had appeared, and b) after cracks had appeared on PC specimens (shown in c), d) and e) (zoomed images).

A summary of results from the longitudinal deformation measurements on the top and sides of the prepared beams is shown in Figures 7.14, and 7.15 for PC, NRCC-CNT, and NRCC-CNF, respectively. In the presented graphs, the maximum longitudinal strains (obtained during 150 days) have been plotted as functions of the position along the length axis. The strains were obtained simply by dividing the deformation readings by the measurement length of 100mm. In the diagrams a positive peak represents a major crack/deformation zone. However, as the gauge length was large it is likely that the positive values not only display the crack opening but also the deformation of un-cracked parts of the composite.

Figure 7.14(a1, and a2) and Figure 7.15(a1, and a2) show the average restrained shrinkages of the PC specimens at early and late age, respectively. It is evident that one-to-two dominating cracks developed in the first and third part on the top of the specimens during 7 days (segment 1 and segment 2 in Figure 7.16). Several less

extensive cracks in the micron range (which were difficult to be recognised by the naked eye) were believed to be initiated. It is furthermore clear that the width of the main cracks in both beams gradually increased after 7 days and up to 150days. The observed restrained strains on the side of the beams were lower than those observed on the top.

The results show an extremely low restrained shrinkage of nanotubes and nanofibres composites as represented in (b1, b2) and (c1, c2) in both Figure7.14, and Figure 7.15, respectively. The addition of nanotubes and nanofibres leads to almost the same reduction in shrinkage strain compared to the PC control. For instance, Figure 7.16 shows a comparison of restrained shrinkage behaviours between PC, NRCC-CNT, and NRCC-CNT (segment (1) and segment (3) were chosen for these comparisons as cracks were formed in these segments with PC samples). Incorporating nanotubes and nanofibres resulted in a reduction in shrinkage strain of about 33% and 34% in segment 1 and 42%, and 37% in segment 3 at early ages (up to 7 days) compared to those of PC. At later age the reduction in shrinkage strain of both segments was 57% and 50%, with composites of nanotubes and nanofibres, respectively. Although restrained shrinkage strain was found to increase with age, no individual and/or multiple microcracks could be observed on both nanotubes and nanofibres overlay composites. This indicates that when the overlay composite is restrained against free shrinkage (base-restrained), tensile stress develops and can cause cracks, (as observed with PC samples). Cracks logically develop from nanoscale to microscale and then to larger scale (an increase with an increase in the shrinkage stress).

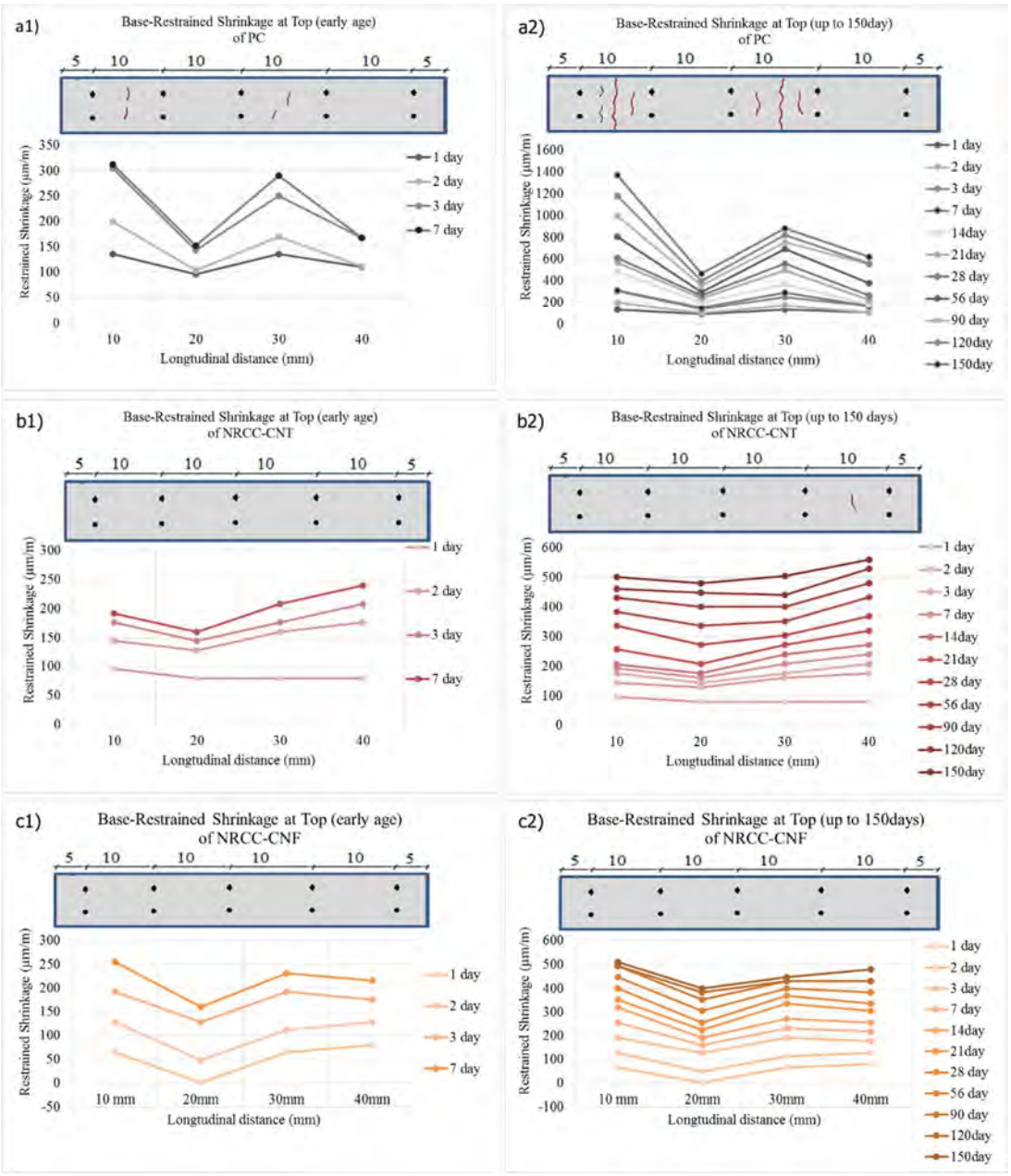

Figure 7.14 Base restrained shrinkage on top of cement mortar specimens at early and late age of (PC) a1 and a2, nanotubes composites (NRCC-CNT) b1 and b2, and nanofibres composites (NRCC-CNF) c1 and c2.

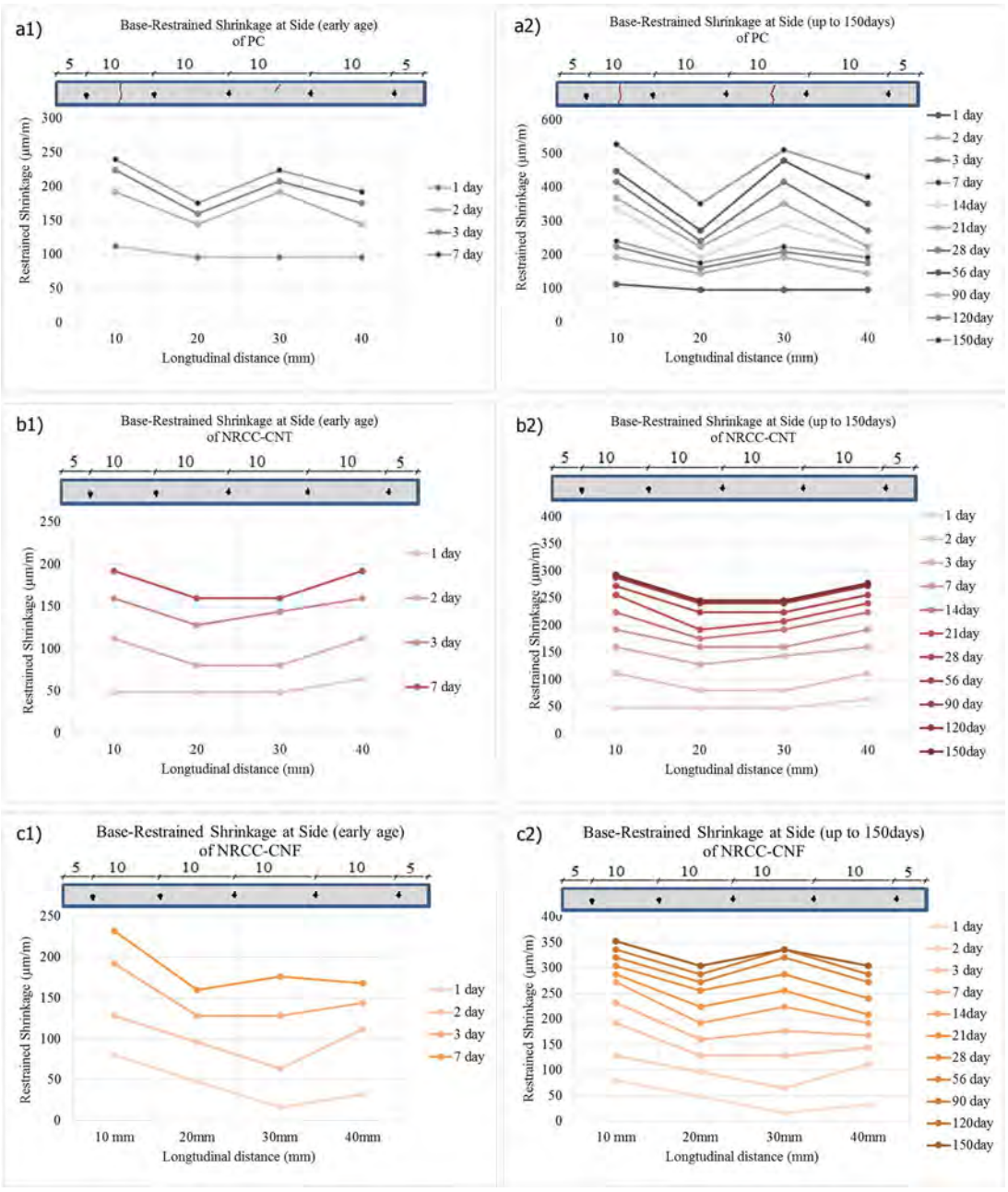

Figure 7.15 Base restrained shrinkage on side of cement mortar specimens at early and late age of (PC) a1 and a2, nanotubes composites (NRCC-CNT) b1 and b2, and nanofibres composites (NRCC-CNF) c1 and c2.

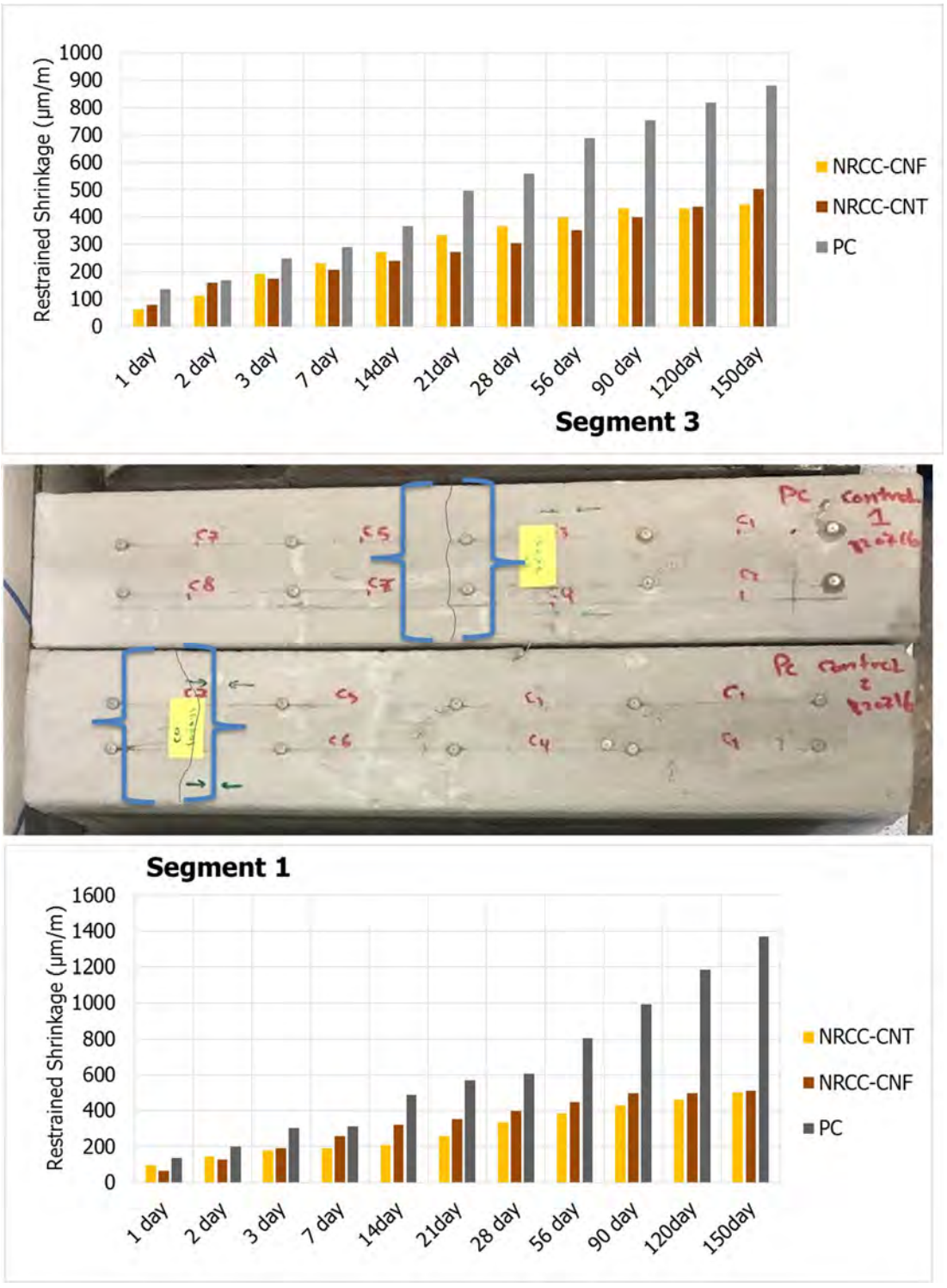

Figure 7.16 The crack development of PC specimens with age (segment (1) and segment (3). Restrained shrinkage values (top and bottom) for each segment are also shown.

7.2.2.1.1 Cracking due to Base- Restrained Shrinkage

The restrained shrinkage causes differential stresses to develop within the overlay composite. A cementitious composite develops its strength during the hydration process which occurs over a period of time, and so the strength is time-dependent. At early ages, tensile strength is limited and develops slowly and so the layer is vulnerable to cracking. Cracking occurs when the tensile stresses due to restraint exceed the tensile strength of the mortar, i.e. its resistance to cracking. With the NRCC-CNT, and NRCC-CNF overlay composites, the nanofilaments increased the composite tensile strength (investigated in Chapter Five), thus the composite strength is often much greater than the created restrain stress. Tensile relaxation and the elastic modulus of the overlay composite act to reduce the delivered restrained stress.

Figure 7.18 (a1-a2) shows the deformation and cracks that initiated in PC. Two major cracks appeared (without propagation) to a maximum width of 130µm in PC, in the region where maximum tensile stress is expected. With increasing age (around 7 day's age) the cracks began to develop (on both top and sides, about two-fold higher on top). These cracks widened to more than 30µm and up to 130µm. Figures 7.17 (b1-b2, and c1-c2) represent the deformation that was observed on the top and sides of nanotubes and nanofibres composites, respectively. From early age and up to 150 days the maximum recorded strain ranged between10-30µm (detected by using target demecs points and a mountable strain gauge), and over all the test duration no cracks were observed. Nanofilaments appear to be very effective not only in preventing crack initiation, but also in distributing the deformation strain more uniformly. Figures 7.18(b1b2-c1c2) show the shrinkage strains on the un-cracked specimens of CT, and CF overlay composites. Similar behaviour was observed on the free shrinkage specimens and this was attributed to the effectiveness of nanotubes and nanofibres in improving the overlay composite tensile strength and decreasing the porosity.

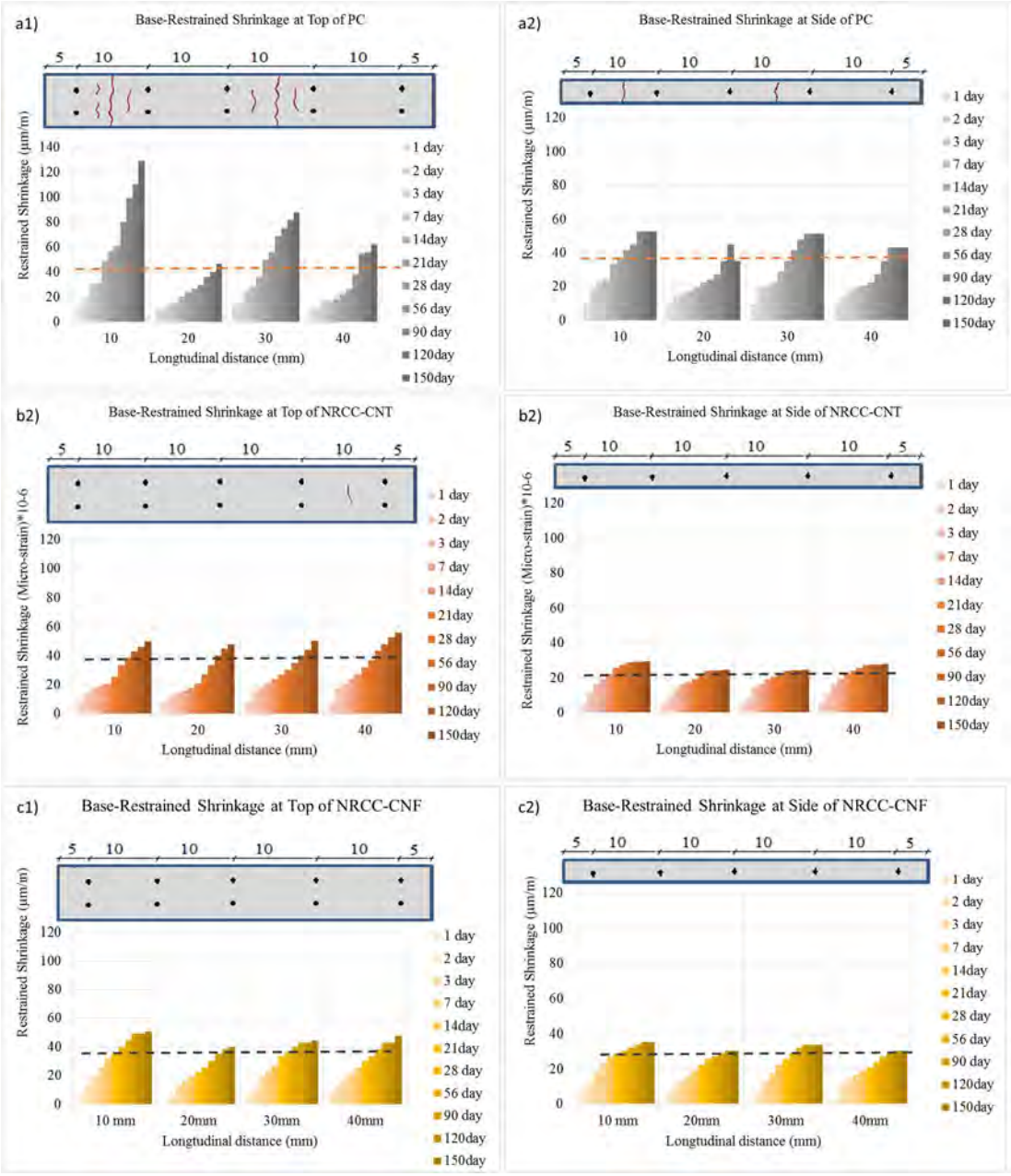

Figure 7.17 Base cracking strain and deformation of uncracked segments at early and late age of (a, and b) of PC specimens, and strain created on nano cementitious composites (d and c) of NRCC-CNT specimens, and on NRCC-CNF specimens.

Figure 7.18(a, and b) shows the overall longitudinal strains recorded on the upper and sides faces of PC and NRCC-CNT, NRCC-CNF overlays composites during 150 days. These images show that the recoded deformations, as represented by the positive line chart, are relatively stable for the NRCC-CNT, and NRCC-CNF specimens as compared to the cement mortar PC. The maximum recorded restrained strain of NRCC-CNT and NRCC-CNF (over all the specimen length) was about 38µm on top and 32µm on the sides for the NRCC-CNT and NRCC-CNF specimen as compared to 62µm and 51µm on the top and side of the PC sample, respectively. Hence, after addition of nanofilaments the crack widths were reduced by approximately 63% on the top and 59% on the sides. This occurred despite the extremely low amount of fibres used in this case, about 0.175 kg/m^3.

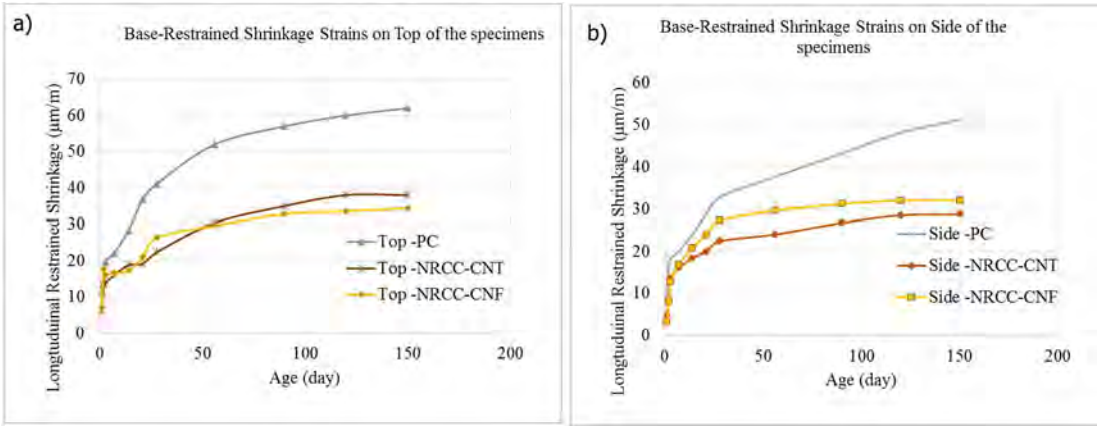

Figure 7.18 Longitudinal strains recorded on the upper faces of a PC and an NRCC-CNT, NRCC-CNF overlay respectively during 150 days.

7.2.2.2 Ends-Restrained Shrinkage (Prism Bar)

To obtain a better understanding of the shrinkage phenomena and to accurately evaluate the effect of nanotubes and nanofibres on restrain shrinkage behaviour, end restrained shrinkage tests were conducted. This type of test can produce a higher restraint strain on the composites, which increases the cracking tendency of the composite within a reasonable period. With ends restraint strain, the response of the cementitious nanocomposites exposed to imposed deformation via axial restraining at

the specimen ends is measured. Although, there is possibility of strain losses at ends of the moulds due to the ends, L-sections, was secured to the flange by means of bolts, the remaining strain comes from the curvature and contraction of the base remains high and can lead to crack initiation in the composite.

Two specimens for ends-restrained shrinkage measurement were prepared to evaluate the restrained deformation strain and crack formation. Moreover, two specimens for free shrinkage measurement were also placed in similar conditions. The rigs modified for this test were adapted from (Carlswärd 2006). Figure 7.19 shows the original end restrained shrinkage set-up.

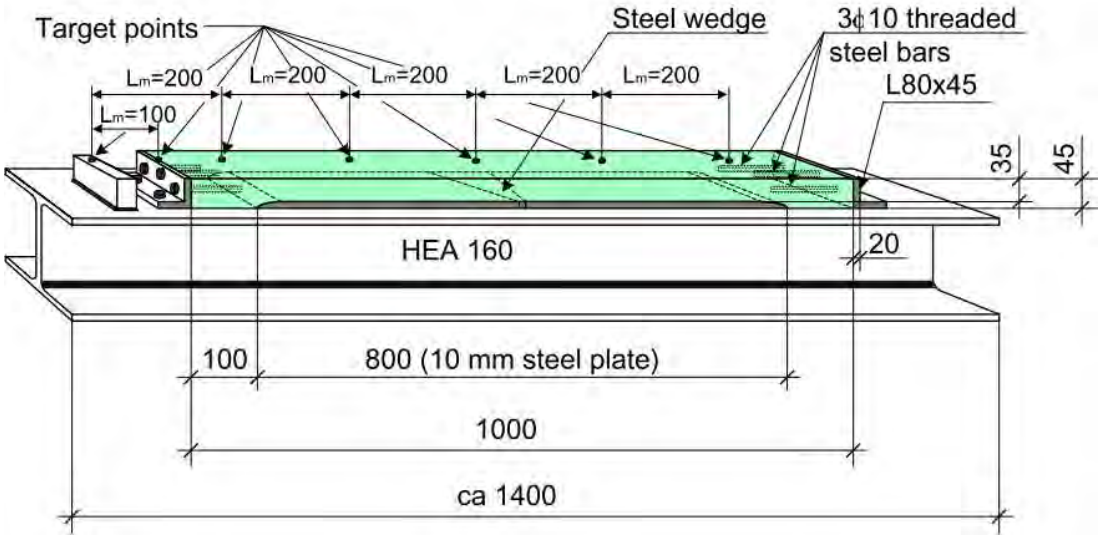

Figure 7.19 End-restrained shrinkage tests adapted from (Carlswärd 2006).

7.2.2.2.1 Free shrinkage of Prism Bar

Free drying shrinkage specimens of each mixture of PC, NRCC-CNT, and NRCC-CNF were tested over 150days (using specimens with the same geometry as end restrained specimens, Figure 7.20) to simulate an ends-restrained specimen. Figure7.21 shows that addition of nanofilaments had a positive effect on the free strains obtained at the upper face of the specimens, compared to the reference cement mortar (PC). The reduction within the studied period was about 15% and 19% at early age and 16% and 24% at late age for NRCC-CNT and NRCC-CNF, respectively. These reductions were about 15%, and 75 % less than those obtained in the standard

free drying shrinkage test (see Section 7.2.1). The reason for this most likely relates to the exposed surface area and un-stable humidity conditions. Over the duration of free shrinkage tests (standard free shrinkage tests, and prism bar tests) the humidity underwent seasonal variation, from spring to summer to winter. It was not possible to control the temperature and humidity to a fixed value for the entire test duration.

Figure 7.20 Free drying shrinkage specimens.

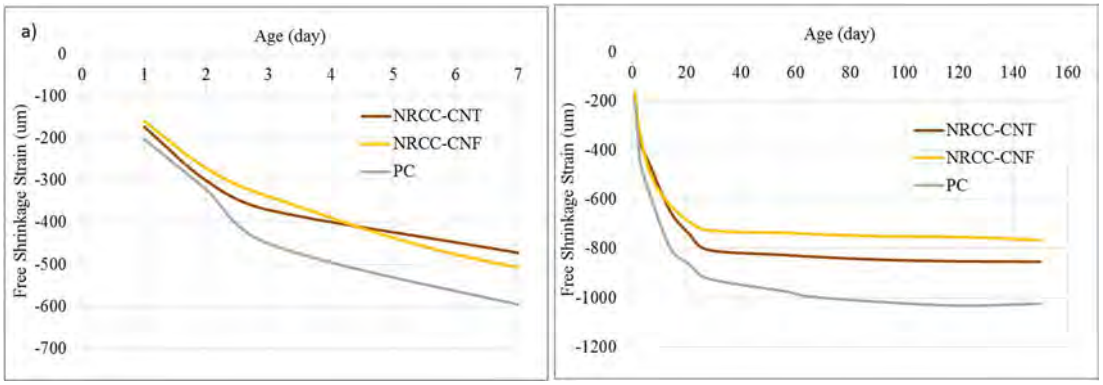

Figure 7.21 Free drying shrinkage strain of PC, NRCC-CNT, and NRCC-CNF specimens, at a) early age, b) early and late age.

7.2.2.2.2 Strain development of Ends-restrained Composite

Figure 7.22 shows the test rigs for investigating restrained shrinkage strain of cement mortar(PC) and cementitious nanocomposites based on carbon nanotubes and carbon nanofibres. Strain at the top of a specimen (at early and late age) with PC, and corresponding results for composites (NRCC-CNT), and (NRCC-CNF) are shown in Figures 7.23, 7.24, and 7.25. At early age (up to 7 days) the curve presented as the strain in un-cracked parts is the mean value of the strains measured in the areas where no cracking occurred. With increasing age, the restrained strain tended to increase and exceed the strength of the cementitious composite, and so a crack was formed after 10 days with PC specimens, and 65, and 115 days with CNTs and CNFs specimens respectively.

Crack strain is the deformation measured in the crack zone divided by the gauge length (100mm). It can be seen that cracking rapidly occurred with PC specimens due to the fact that the strain capacity of the mortar is low. Crack initiation usually occurs when the crack strain increased over the strength of the cement materials. After cracking, the strain in the un-cracked parts of the PC specimen approached the curve representing the free shrinkage. This indicates that the un-cracked segment of the specimen is totally unloaded and no stress is transferred across the crack.

The response of the specimens reinforced with nanofilaments to ends restrained shrinkage is shown in Figure 7.26 (b, and c), and was significantly different. It can be seen that the restrained strain was considerably lower than the tensile strength of the composites resulting from the addition of carbon nanofilaments. Therefore, crack initiation was considerably slower than with PC specimens. The difference in strain as compared to the free shrinkage remains even after cracking with carbon nanotubes specimens (Figure 7.26b), i.e. strain in the uncracked area was lower than the free shrinkage. This is due to nanotubes in the composites still acting to provide a degree of restraint, and their action in filling in between the pores. The response to crack initiation clearly revealed the influence of carbon nanotubes and carbon nanofibres in improving the strain capacity of the composite. This indicates that improved strain capacity is due to the ability of nanofilaments to transfer the load across the hydration

products and distribute the stress evenly over the composite. Also from Figure 7.26, a correlation between the free shrinkage and restraint shrinkage can be also made. With PC specimens, cracks were formed when the free shrinkage was about 400µm/m, whereas with NRCC-CNT and NRCC-CNF specimens, cracks were formed when the free shrinkage was about 600µm/m.

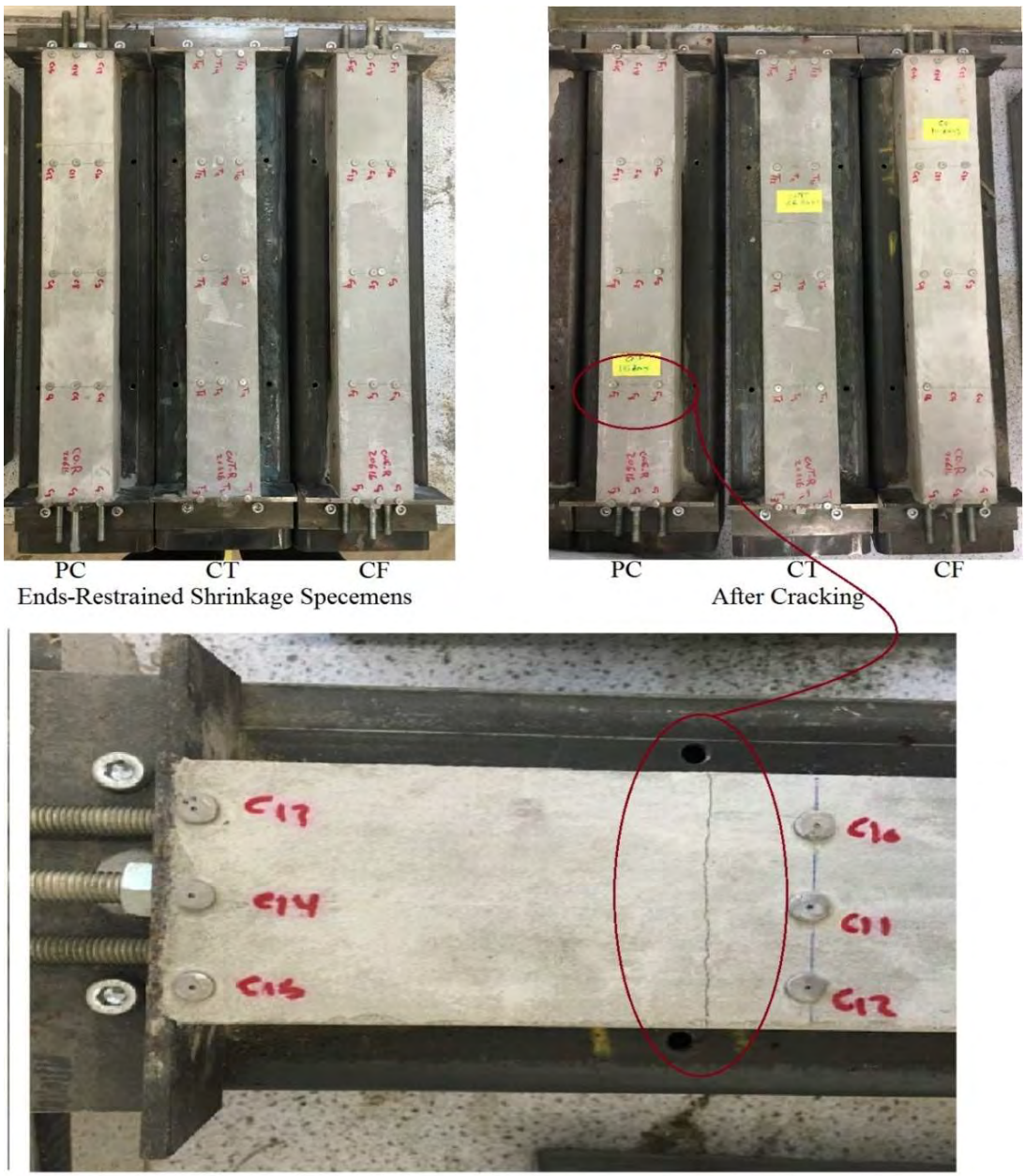

Figure 7.22 Test rigs for studying the effect of Ends-restrained shrinkage. Specimens for measuring restrained shrinkage of nano cementitious composites of NRCC-CNT, and NRCC-CNF in addition to PC.

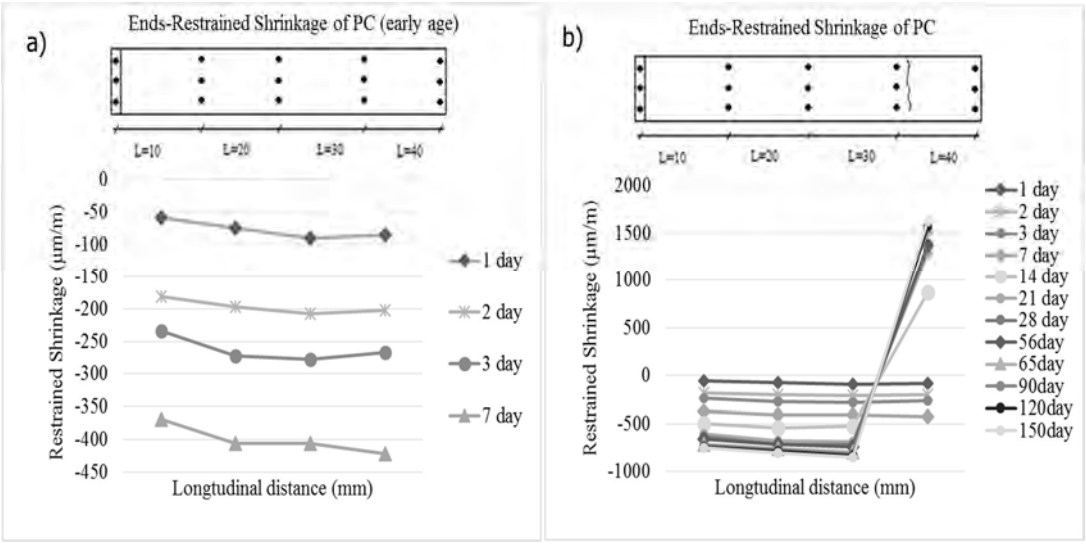

Figure 7.23 End restrained shrinkage of PC at a) early age and b) late age (up to 150 days).

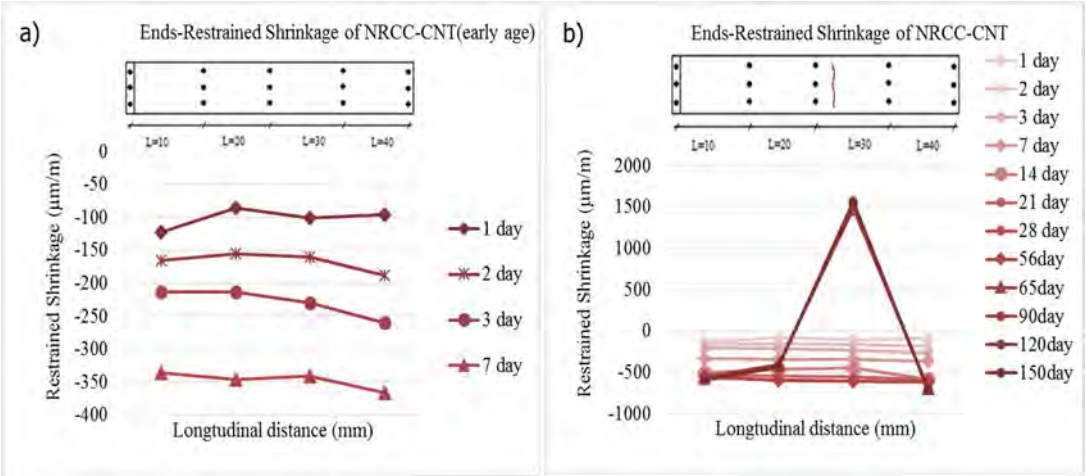

Figure 7.24 End restrained shrinkage of NRCC-CNT at a) early age and b) late age (up to 150 day).

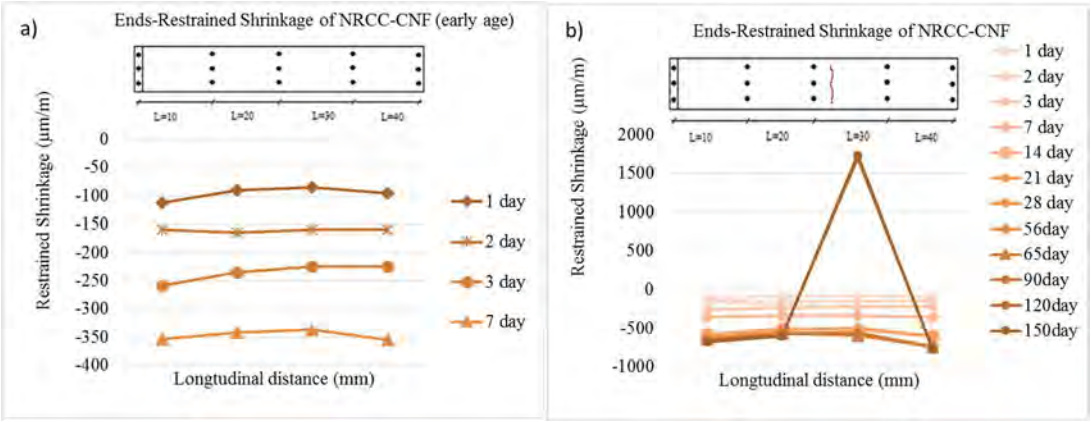

Figure 7.25 End restrained shrinkage of NRCC-CNF at a) early age and b) late age (up to 150 day).

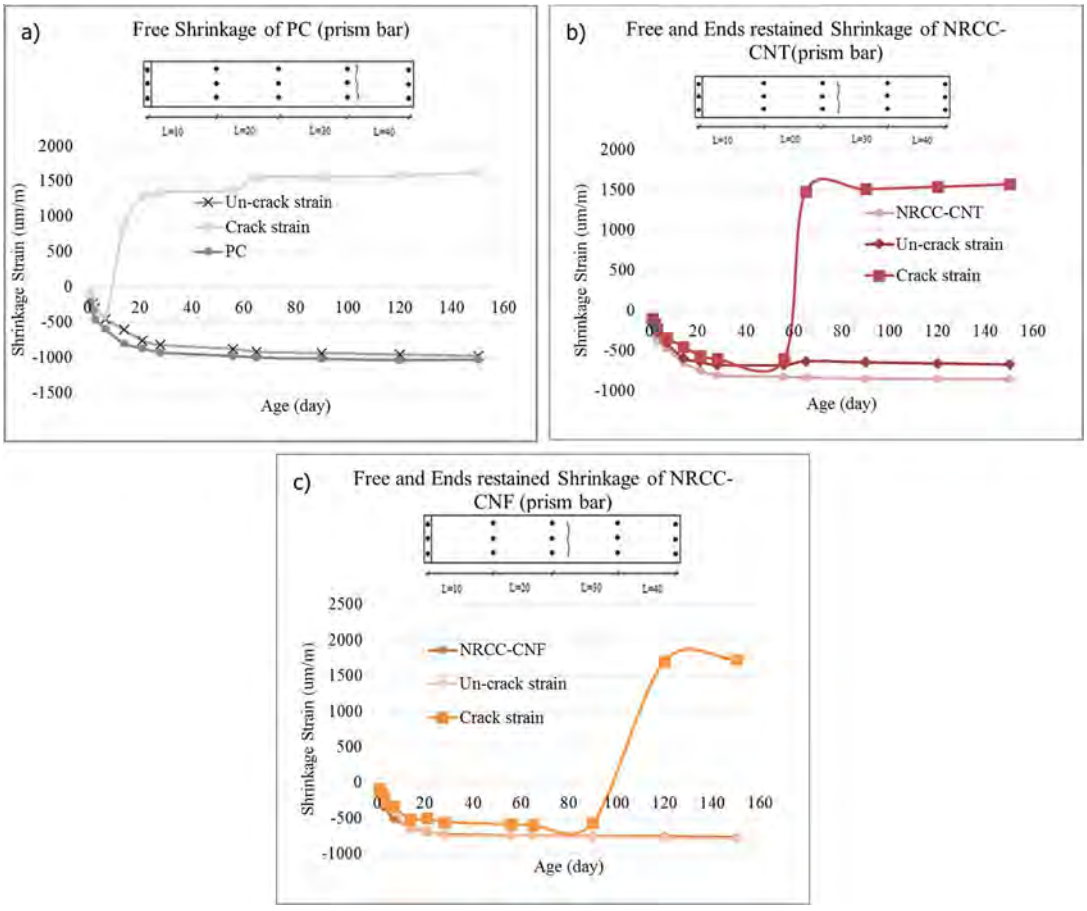

Figure 7.26 Measured strain development at the exposed upper face of a restrained specimen as well as the corresponding measured free shrinkage (prism specimen) at the top. a) PC (b) NRCC-CNT, and c) NRCC-CNF. Un-cracked refers to the strain value of un-cracked parts of the specimen.

7.2.2.2.3 Cracking due to Ends Restrained Shrinkage

Figure 7.27 shows a summary of the obtained results, showing time to cracking, and crack width at the top at the examined specimens. It was noticed that multiple cracking did not occur in any case, and the crack width (directly calculated from the strain measurements following the procedure illustrated in Figure 7.27a) became stable after formation in the range of (12-20) um as shown in Figure 7.27b. The term un cracked is the mean value of the measured strains in un-cracked parts of the specimen, i.e. obtained over the three measuring lengths where no crack was detected. L_m is the measuring distance of 100 mm and L_{m1} is the distance after cracking.

From the results, it can be concluded that while the addition of nanofilaments significantly prolonged the time until crack initiation, they did not affect the crack propagation. Inclusion of nanofilaments delayed the cracking until after 65 to 115 days at a corresponding free shrinkage strain of about 600µm/m. A rather unusual trend was also noticed, in that a crack in PC specimens developed near to the ends, whereas with NRCC-CNT and NRCC-CNF specimens cracks develop in the middle of the specimens. This may be related to cracks forming in the weakest sections, which may depend on small deviations in geometry or material irregularities.

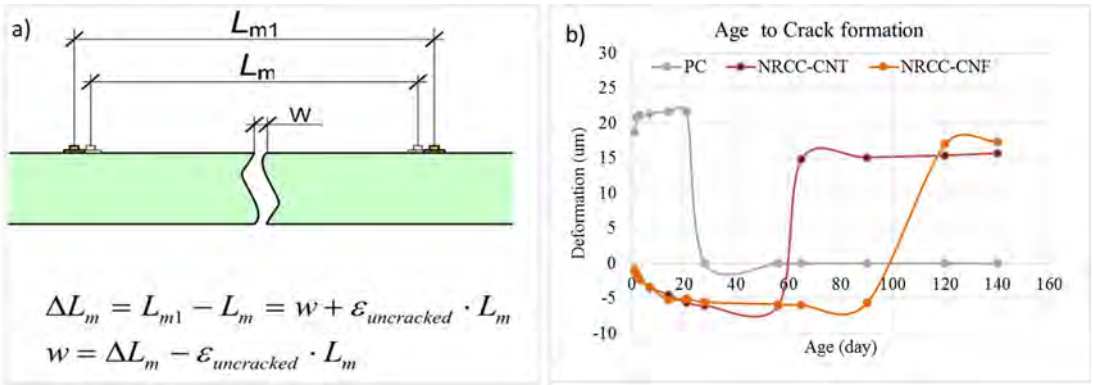

Figure 7.27 a) Principles for calculation of crack widths. Lm is the measuring length, Lm1 is the distance after cracking and un-cracked is the strain in un-cracked parts(Carlswärd 2006). b) time to crack formation.

7.3 Resistance of CNTs/Fs Cementitious Composites against ingress of aggressive media, such as Sulfuric Acid Attack

7.3.1 Overview

Acid resistance is one of the most important parameters to extend the service life of structural elements. Sulfuric acid attack and degradation processes are highly complex, but in principle, when the microstructure of the composite is porous and connected capillary pores relatively common, the diffusion rate of acid ions through the composite will accelerate the chemical reactions with the cement hydration products. These reactions result in the conversion of calcium hydroxide to calcium sulfate (gypsum) which, in turn, may be converted to calcium sulfoaluminate (ettringite). Theses produces are responsible for a large volume expansion which leads to an increase in internal pressure and deterioration of the matrix(Chang et al. 2005, Bassuoni and Nehdi 2007, Girardi et al. 2010).

An improvement in accelerated testing as a way of predicting durability was proposed in these experiments. The behaviour of nanofilaments reinforced cementitious composites of NRCC-CNT, and NRCC-CNF, and multiscale hybrid reinforced cementitious of MHRCC-CNT, and MHRCC-CNF were examined in relation to long-term exposure to sulfuric acid solutions. Change in crushing load, mass loss, and microstructures (through SEM images) were used for assessing the composites' durability performance under acid attack.

7.3.2 Measured Crushing Load

The results of the crushing load and standard compressive strength at 28 days for each composite in addition to control mixes are presented in Table 7.3, and Table 7.4. The results are represented in term of crushing load rather than compressive strength, as the specimen's surface area became irregular after the immersion in acid solution for 90 days which could affect the compressive strength calculation.

The standard 28-day crushing load of each composite was used for comparison after immersion in the acid solution. Figure 7.28 shows the relative change of crushing load against the immersion time up to 90 days for all composites. The relative change of crushing load of a composite relative to control specimens at 28 days was the

percentage loss in the crushing load, and loss in mass. After immersion, all of the cubic specimens of each composite showed a decrease in the crushing load but at very different rates. Greater decreases were noticed with control cubes (cement mortar (PC) and steel fibre composite (FRC)). Incorporation of nanofilaments gave a higher ability to resist acid attack. The residual crushing load ratio (which is defined as the ratio of crushing load after immersion in the acid (H_2SO_4) solution to the crushing load before immersion) was highest for NRCC-CNF, and MHRCC-CNF samples, followed by the NRCC-CNT, and MHRCC-CNT (as shown in Figure7.28). Compared to PC and FRC, residual crushing load ratio of NRCC-CNT, and NRCC-CNF, and MHRCC-CNT, and MHRCC -CNF was about 35%, 73%, and 19%, 22% respectively.

In the literature, it has been reported that hydration products are vulnerable to acid attack, (Kumar Mehta 2006). Following addition of nanofilaments to the mixture, the hydration products (mainly C-S-H gel) were found to be less vulnerable to acid environments, since nanofilaments in such acidic environment act to restrict access of acid ions to the composite body, and act to decrease the pore volume and the matrix became denser. As discussed in section, nanofilaments act to reduce the porosity by refining/filling the structural pores, act as reinforcing elements across hydration products, and prevent crack initiation, thereby leading to a well compacted composite. The high variation between the effect of nanofilaments types (carbon nanotubes and carbon nanofibres) on acid attack are mainly attributed to the geometry of nanofibres, and their higher aspect ratio.

Ion migration from the acid solution into the composite depends on the sulphate concentration of the solution, and the composite pore structure. The reaction between the acid ions and cement hydration product takes place when sulphate ions diffuse into the matrix. Higher degradation occurs when the exposed composite shows physical signs of degradation such as expansion, notable cracking, surface erosion or softening of the cement paste matrix.

The effect of sulfuric acid in corrosion of the composite) can generally be characterized by the following reactions (Bassuoni and Nehdi 2007).

$$Ca(OH)_2 + H_2SO_4 \rightarrow CaSO_4.2H_2O$$

$$CaSiO_2.2H_2O + H_2SO_4 \rightarrow CaSO_4 + Si(OH)_4 + H_2O$$

$3CaO.Al_2O_3.12H_2O + 3(CaSO_4.2H_2O) + 14H_2O \rightarrow 3CaO.Al_2O_3.3CaSO_4.32H_2O.$

Products that appeared on the outer surface of the specimens (after removal from the solution) are mainly gypsum, which is associated with volume expansion (by a factor of 2.2 compared to the volume of reactants).These expanded mineral products induce significant tensile stresses, resulting in cracking and spalling (Liu et al. 2012). Further reaction of gypsum with calcium aluminate phases in the cementitious matrix can form ettringite, which gives more volume increase (up to a factor of 7) than that of gypsum, thus leading to more micro- and macro-cracking. In addition, sulfuric acid decomposes the cementitious matrix by decalcifying calcium silicate hydrate (C–S–H), thus contributing to strength loss.

Table 7.3 Standard crushing load after 28 day and 90 day immersions in sulfuric acid of NRCC-CNT and NRCC-CNF in addition to cement mortar (PC).

Nanofilaments Reinforced Cementitious Composite								
Mix	Standard Crushing Load (kN)			Crushing Load After 90 days Acid Immersion			Load change (%)	Mass Loss (%)
	Crushing load (kN)	Average Crushing load (kN)	Standard Deviation (SD)	Crushing load (kN)	Average Crushing load (kN)	Standard Deviation (SD)		
PC	135.6	128.3	8.7	95.2	101.9	5.1	-25.8	19.4
	116.0			102.9				
	133.2			107.7				
NRCC-CNT	183.2	164.4	13.3	132.6	137.9	6.9	-19.2	11.6
	154.4			147.6				
	155.6			133.4				
NRCC-CNF	172.0	170.3	4.6	181.9	176.3	6.0	3.4	9.8
	175.0			178.9				
	164.0			168				

Table 7.4 Standard crushing load after 28 day and 90-day immersion in sulfuric acid of MHRCC-CNT and MHRCC -CNF in addition to cement mortar (PC).

Multiscale hybrid reinforced cementitious composites								
Mix	Standard Crushing Load (kN)			Crushing Load After 90 days Acid Immersion			load change (%)	Mass Lose (%)
	load (kN)	Average (kN)	SD	load (kN)	Average (kN)	SD		
FRC	176.0	176.7	1.5	145.2	150.3	5.2	-17.6	9.1
	178.8			148.1				
	175.3			157.4				
MHRCC -CNT	185.3	186.5	1.1	180.8	178.1	2.2	-4.7	4.9
	188.0			178.1				
	186.3			175.5				
MHRCC -CNF	194.3	185.5	7.1	188.2	189.5	6.6	2.1	4.2
	176.8			182.2				
	185.5			198.1				

7.3.3 Measured Weight Loss

After 90 days of exposure, acid-attacked surfaces of the specimens were cleaned with distilled water. Chemical resistance was then evaluated by determining the weight loss (WL) of the specimens using (Eq.7.1).

$$WL\ (\%) = \frac{W1 - W2}{W1} \times 100 \qquad \text{(Eq.7.1)}$$

Where:

W2 =weight (g) at time 90day

W1= Initial weight (g) before exposure to sulfuric acid.

The weight loss results are shown in Figure 7.28 (a-b). Specimens of PC and FRC (Controls) show the highest weight loss after immersion in the acid solution.

In general, and as indicated by previous studies, weight loss in control specimens occurred due to their porous microstructures which allow ingress of sulfuric acid during immersion in acid. Reaction of acid ions involves an increase in volume of the reacting solids (Rizkalla 1989). The formation of these products leads to excessive expansion and cracking which gradually causes the surface layer of cement mortar to fail, generating a significant weight reduction in the specimens. Inclusion of nanofilaments had a pronounced effect on reducing the weight loss results, for example, carbon nanotubes reduced the mass loss by about 40% and 46% in NRCC-CNT, and MHRCC-CNT, respectively, whereas carbon nanofibres reduced the weight loss by about 50%, and 54% in NRCC-CNF, and MHRCC-CNF, respectively. The positive effect of nanofilaments in reducing the weight loss could be attributed to reduced diffusion of acid ions which reduces the harmful reactions, and reduces the leaching of calcium salts from the impermeable surface thereby increasing the acid resistance. Continuous cement hydration process could also act to reduce the weight loss due to formation of hydration products leading to weight gain.

In Figure 7.28b a relatively small gain in the weight of NRCC-CNF was observed, which is probably due to the hydration process and formation of C-S-H gels.

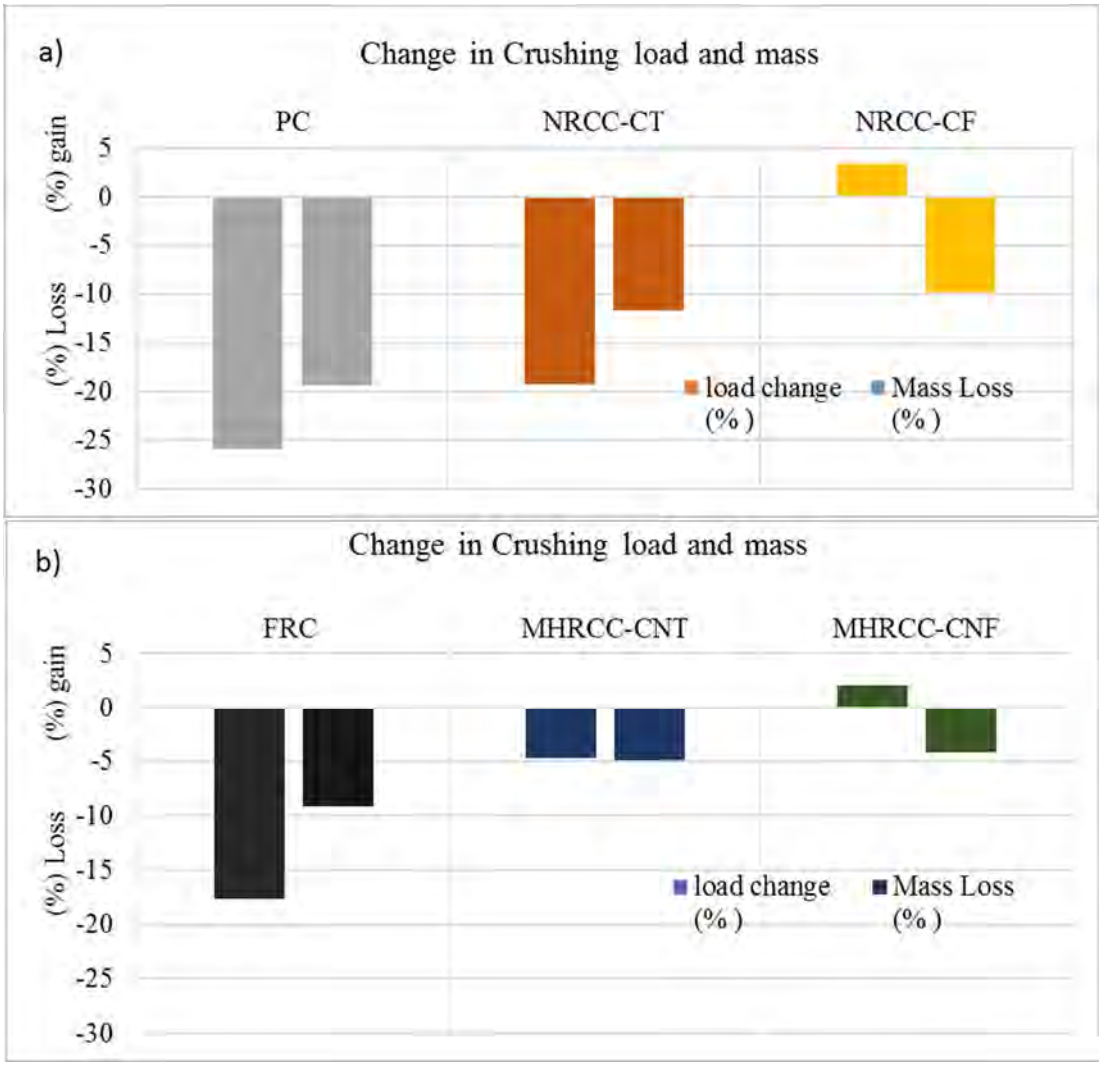

Figure 7.28 Rate of crushing load change and weight loss for a) PC and nano cementitious composites, and b) FRC and multiscale hybrid reinforced cementitious composites after immersion in sulfuric acid.

7.3.3 Visual Inspection

Typical surface appearances of the cubic specimens of eighteen cementitious mortar/composites after 90 days' immersion in 5% sulphuric acid are shown in Figure7.29, and Figure7.30.

Visual inspection indicated that all specimen surfaces became significantly rougher after immersion in acid, which appeared to indicate that the outer surface layers of Portland cement composite were vulnerable to acid attack. The weakened structure of

PC and FRC after immersion in acid meant that these specimens significantly deteriorated on applying crushing load. This could be attributed to their pore structures causing massive reactions between calcium hydroxide and the acid which makes the deterioration proceed from the exterior to the interior faster. The nanotubes and nanofibres specimens were relatively unaffected by the sulfuric acid attack.

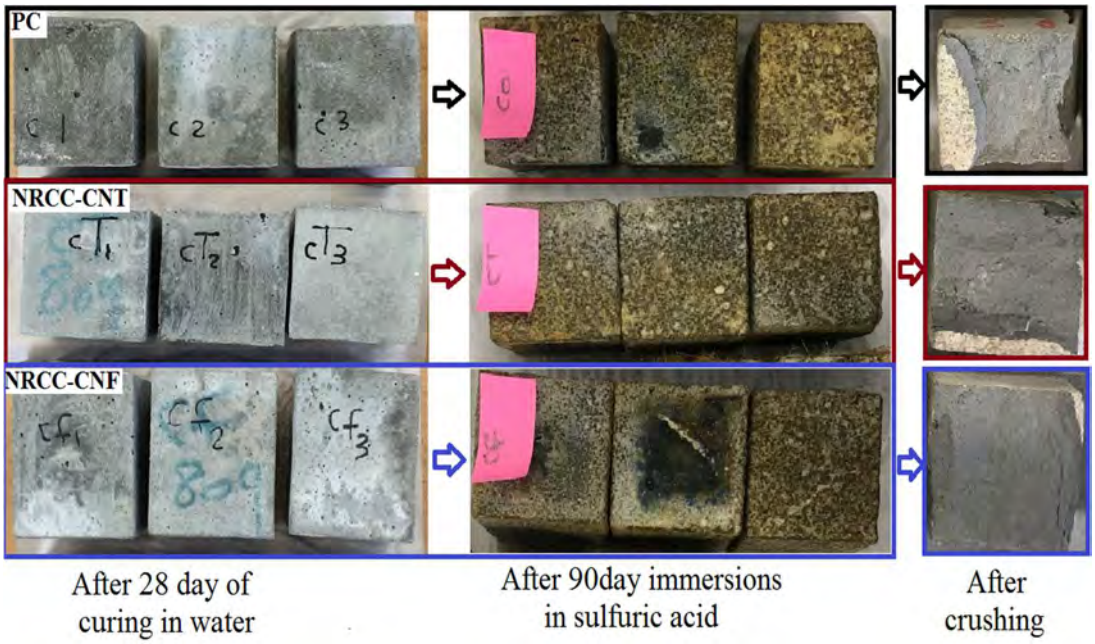

Figure 7.29 Cement mortar (PC) and cementitious nanocomposites specimens (NRCC-CNT, and NRCC-CNF) after: curing for 28day in water, immersion in sulfuric acid, and after crushing.

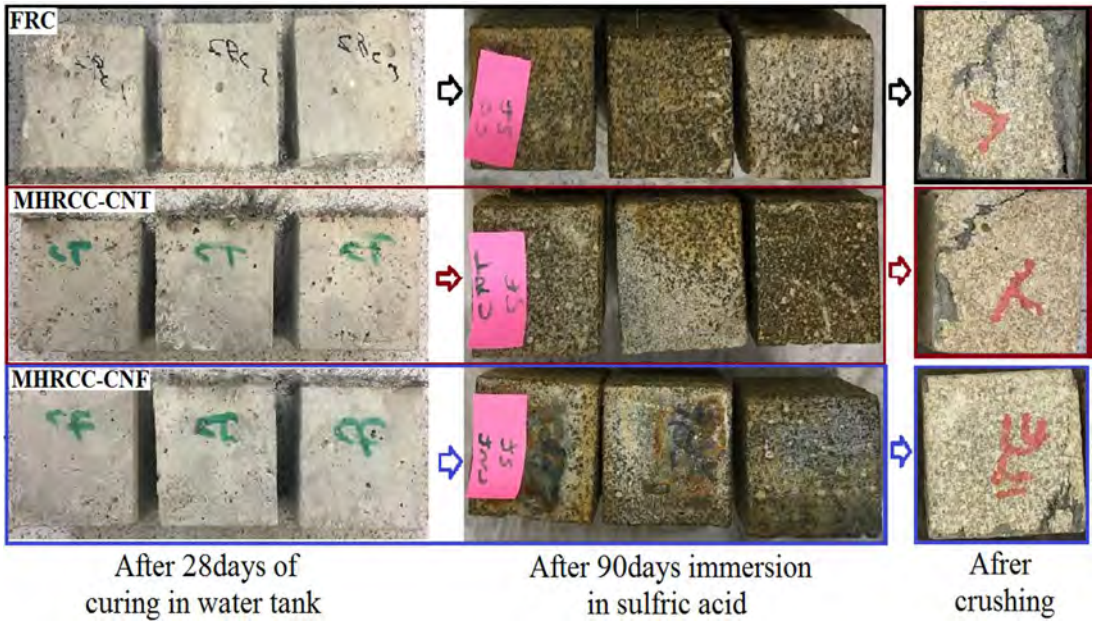

Figure 7.30 Fibre reinforced composite (FRC) and nano multiscale hybrid composites specimens (MHRCC-CNT, and MHRCC-CNF) after: curing for 28day, immersion in sulfuric acid, and after crushing.

7.3.4 Microstructural Analysis

For further examine the effect of incorporated of carbon nanofilaments in composites exposed to an acid environment, sampled were imaged under scanning electronic microscopy (SEM). Typical samples of approximately 5mm thickness x10mm x10mm length and width were taken from broken cubes of PC, CNTs, and CNFs after immersion in sulfuric acid for 90 days. Two samples for each mixture were examined, one from the surface of the specimens and the second sample from the middle of the specimens.

Figures 7.31 shows typical images of PC samples (outer and middle regions) after immersion in acid solution. There were clear microcracks and increased porosity in the imaged areas. Hydration products of calcium silicate hydroxide, ettringite and calcium carbonate crystals can be observed, but calcium hydroxide crystals were not found, as these may have been consumed in reactions with the acid. Images of the

outer and middle regions of PC samples show that the structure in each is almost identical which could be a sign that the acid attacked through all the sample.

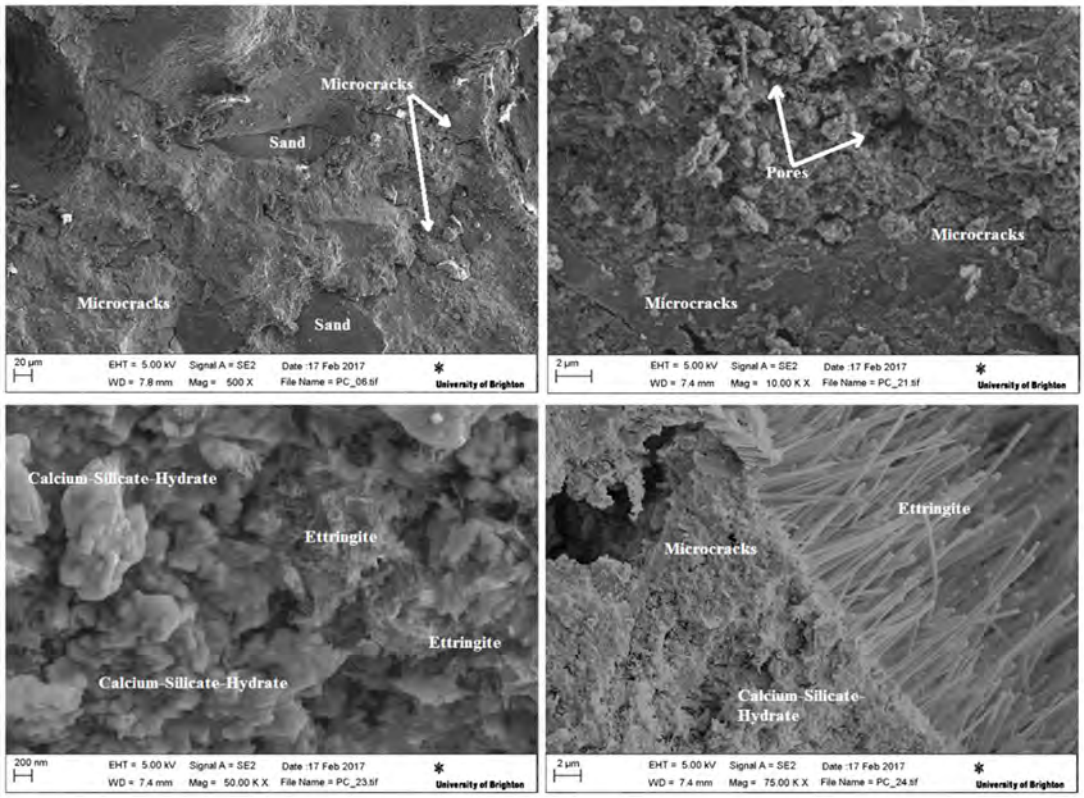

Figure 7.31 SEM images of PC samples after immersion in acid for 90 days showing microcracks and numerous ettringite patches.

Figure 7.32, and Figure 7.33 show typical images of samples containing carbon nanotubes and carbon nanofibres respectively, (a, b) show low and high magnification images of the region near the acid-exposed surface, and (c, d) show low and high magnification images of the middle region of the cube samples. In the middle regions, no cracks were observed in the interfacial zone and around the fine aggregate (sand).This result supports previous studies and clearly indicates that the acid attack is a surface phenomenon in these samples: the deterioration starts at the surface of the composite and progresses inwards. These micrographs show that the deterioration is smaller in the middle regions of NRCC-CNT and NRCC-CNF specimen than in the region near the acid exposed surface which supports the data showing improvement in the crushing load and less mass loss.

The images of PC show needle-like structures that are visible in several locations. These are gypsum and ettringite. These products were rarely visible on images of carbon nanotubes and carbon nanofibres composites (NRCC-CNT and NRCC-CNF).

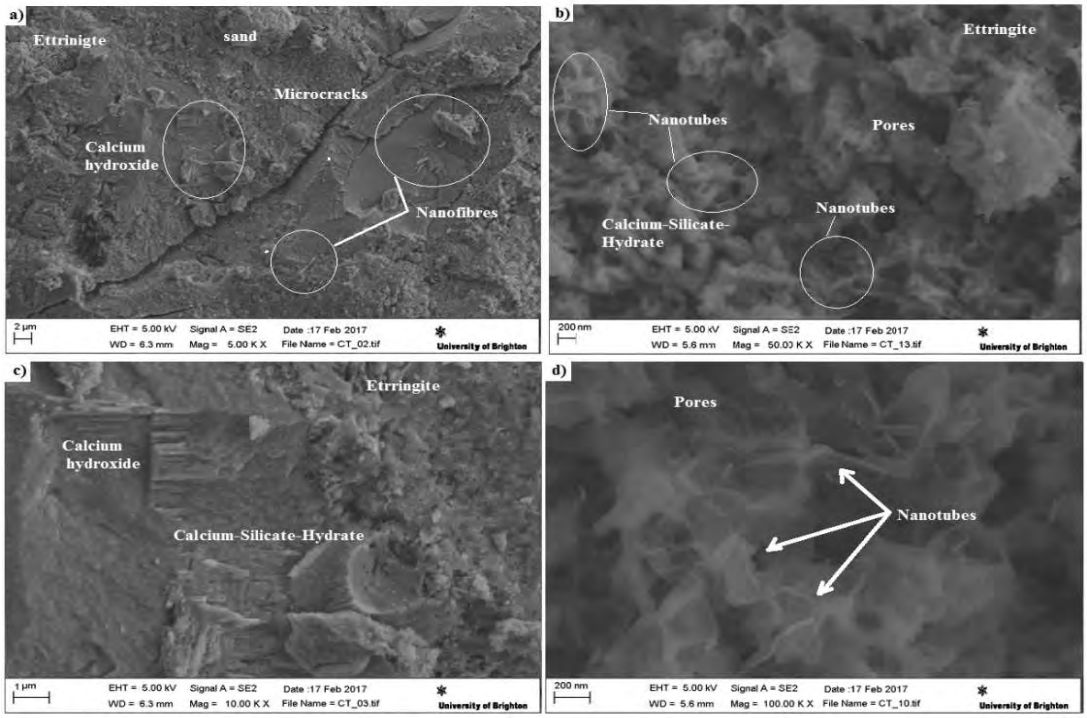

Figure 7.32 SEM images of NRCC-CNT samples after immersion in acid for 90 days (a, b) from sample near to exposed surface, and c, d) images taken at the middle of samples.

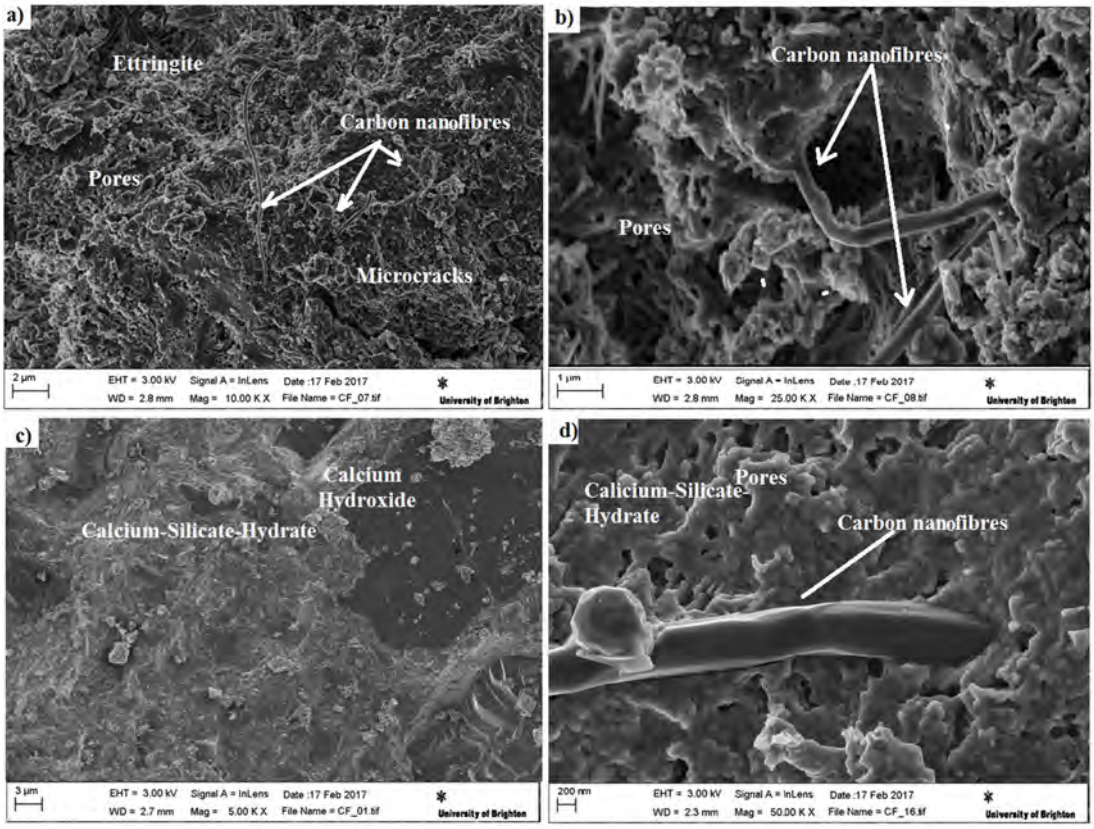

Figure 7.33 SEM images of NRCC-CNF samples after immersion in acid for 90 days (a, b) from sample near to exposed surface, and c, d) images taken at the middle of samples.

7.4 Summary

-Shrinkage Experiments

In this chapter, an experimental study on shrinkage (free drying shrinkage and restrained shrinkage) of nanofilaments reinforced cementitious composites (NRCC-CNT, and NRCC-CNF) and multiscale hybrid reinforced cementitious composites (MHRCC-CNT, and MHRCC-CNF) was performed to evaluate their long-term performance. Base restrained shrinkage, and ends restrained shrinkages were adopted for assessing cracking potential in these materials when used as overlay composites (i.e. repair materials). Based on results analysed, the following conclusions were drawn:

- Free drying shrinkage results for carbon nanotubes and carbon nanofibres composites at early and late age (up to 180days) indicated that all nanomaterials mixes exhibited lower drying shrinkage than the control. The geometry of nanofilaments, and the higher degree of fibre dispersion can refine the pores, and interrupt the paths of the continuous capillary pores, and thus reduce the possibility of mixture bleeding/evaporation.
- In base restrained shrinkage tests, cementitious nanocomposites (as thin overlay composites) exhibited a superior resistance to crack initiation. Visible cracks were observed in control samples within the first ten days, as the restraint conditions resulting from the bond with the substrate induced tensile stresses which are higher that the tensile strength of the overlay, and can lead to cracking. No cracks were observed with nanofilaments composites over all testing durations due to the improved tensile strength of the composites and reinforcement at the nano scale.
- In ends restrained shrinkage, the high strain formed through the samples gives a clear indication of the difference between nanotubes and nanofibres composites. The higher aspect ratio and deformed outer surface of carbon nanofibres (compared to nanotubes) contributes to enhancing the performance of nanofibres composites, as these factors enhance the composite's resistance to facture/and pulling out under restraint conditions.
- Due to the superior performance of nanofilaments in reinforcing the cement structure at the nanoscale, the risk of cracking in hybrid composite overlays is reduced and their durability service is enhanced (further investigated in chapter Eight).
- Although the reinforcing of micro cracks controls crack propagation, microfibres do not contribute to preventing crack initiation at the nanoscale, whereas nanofibres can. Hence, the use of fibres in the nano scale is the only agent that can reinforce the cementitious composite at the nano scale and prevent crack initiation.

-Sulfuric Acid Resistance

As examined with crushing load, mass loss and SEM images, exposure to sulfuric attack is an effective indicator to evaluate the durability performance of cementitious nanocomposites and multiscale hybrid reinforced cementitious composites. The load crushing results shows the effect of nanofilaments in improving the resistance of the nanofilaments composites to sulfuric acid attack. Nanofilaments reinforce across the composite hydration products, prevent crack initiation, reduce the composite porosity, improve the bulk density, and thereby restrict ion diffusion into the composite body. SEM examinations showed that while cracking of the cement mortar samples (PC) was found, the nanofilaments interfacial zone in the NRCC-CNT, and NRCC-CNF specimens remained continuous without cracking under acid attack. The better condition of interfacial zones in the nano cementitious composite could be an important factor in its better performance under sulphuric acid attack.

Chapter Eight:

Nanocomposites for structural Repair/ Strengthening:

- **Multiscale Hybrid nanocomposites in Repairing/ Strengthening RC Concrete**

8.1 Introduction

Concrete is the most widely used construction material for civil infrastructure all over the world. However, concrete structures suffer from a lack of durability associated with cracking, which is one of the most serious issues facing reinforced concrete infrastructures worldwide. The concept of repair and strengthening of reinforced concrete (RC) members in existing structures has gathered significant interest in the last few years, as this is a more economic and sustainable solution to increase the flexural strength, increase the stiffness, reduce the deflections under service load, and increase durability against environmental effect etc., Therefore, this concept reduces the cost associated with periodic maintenance and extend service life, compared to demolition and reconstruction (Iqbal et al. 2016).

In recent years, for such repair and strengthening application, high-performance fibre-reinforced composites exhibiting outstanding strength and ductility and strain-hardening behaviour have been developed. These properties can be achieved by designing a mixture based on a low water-to-binder (water/cementitious) ratio, high amount of admixtures and pozzolanic cementitious materials, and by adding a high volume of micro fibres. Despite their beneficial properties however, the application of fibre-reinforced composites (for example high strength steel fibre composites) in real structures has been limited due to their high cost, heavy density, lack of design and analysis techniques, and their high potential of early-age shrinkage cracking(Yoo et al. 2013, Yoo et al. 2014, Shi et al. 2015). The early age cracks could be increased under tensile stress, allowing penetration of chloride, moisture, and oxygen to the substrate, leading to deterioration of the repaired element.

Deterioration usually begins through concrete cover (cracks, spalling, delamination, etc), thickness of cover in most structures between 20mm-40mm. Concrete cover

deterioration can permanently increase stresses in the remaining original concrete and reduce the yielding strength of reinforcement bars, and deteriorate the bond at the steel-concrete interface. These effects can significantly reduce the service life of the structure and even change the failure mode of the structure from ductile to brittle(Schmidt et al. 2012, Bastos et al. 2016).

In this chapter, the potential application of the developed composites (MHRCC-CNT, and MHRCC-CNT, as a layer repair/strengthening material were examined. Due to the improved mechanical and durability performance (investigated in Chapter Six and Chapter Seven), the composites applied to reconstruct and strengthen degraded RC beams, improve the beams mechanical and durability properties, and extend their service life. RC beams have been repaired/strengthened (in thin scale 35mm) using the developed composites. The investigation includes determining the flexural strength capacity of the repaired/strengthening RC beams in comparison to conventional repair/strengthening material such FRC.

8.2 Test Program:

8.2.1 RC Beams Details and Preparation:

Multiscale hybrid reinforced cementitious composites based on carbon nanotubes (MHRCC-CNT) and based on carbon nanofibres (MHRCC-CNF), described in Chapter Six, were applied as thin layer to rehabilitate beams subjected to flexural loads. Eight reinforced concrete beams (half-scale) were prepared for this objective; two reference beams of normal concrete with dimensions of 100mm×200mm×1400mm which labelled as RC1, and RC2, and six beams of 100mm×165mm×1400mm for repair and strengthening. Beams were labelled as FRC1, FRC2, for those repaired/strengthened with conventional materials (FRC), and CNTRC1, CNTRC2 and CNFRC1, CNFRC2 for those beams repaired/strengthened with a layer of MHYCN-CNT, and MHYCN-CNF composites, respectively
The beams were reinforced with 2Φ10mm steel bars in tension and compression and stirrups of Φ8mm at 100mm c/c were placed, beam design of both control and pre-

damage beams are shown in Figure 8.1, and Figure 8.2, respectively.

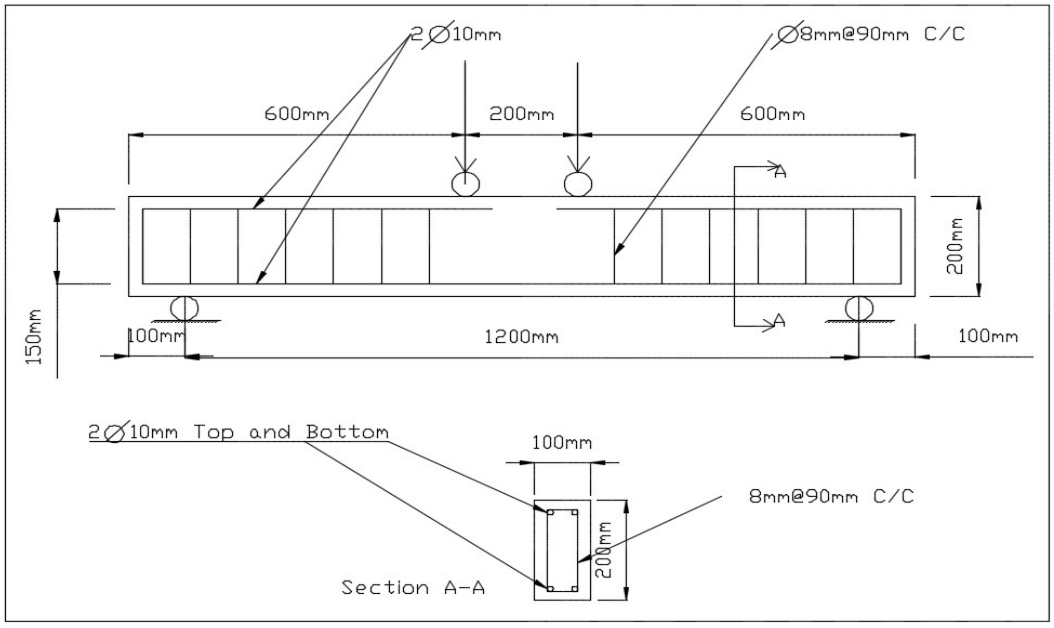

Figure 8.1 Schematic of four-point bending specimen configuration of control beams.

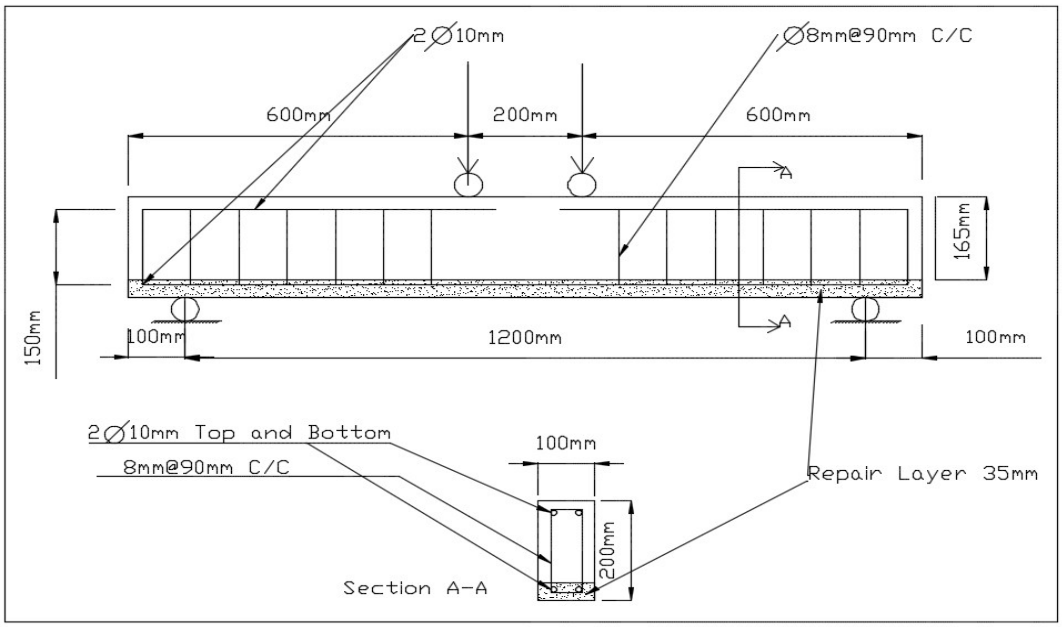

Figure 8.2 Schematic of Four-point bending specimen configuration of repaired/strengthen beams.

8.2.2 RC Beams, Control and Substrate, Casting and Curing Procedure:

Two RC beams as controls, and six RC beams as substrate (35mm cut-depth) were prepared as follows:

Normal concrete mixture was designed of Portland cement Type I, coarse aggregate maximum size of 20mm, fine silica sand, and w/c ratio of 0.45. The mixture was cast in the beam moulds in two layers, and each layer was compacted using an air needle concrete vibrator for about 5 second for each insertion. The upper surface of the concrete reference beams was smoothly finished after casting was completed using a hand trowel. Substrate concrete beams were cast to a depth of 165mm, the remaining depth of 35mm on the tensile zone will be repaired with the proposed composites. After 48 hours, beams were removed from their moulds and then thick tissues were placed over the beams and wetted down (and kept wet over the curing time), then a plastic sheet was placed over the beams. Figure 8.3(a-c) shows the reinforcement and mould preparation, casting steps, and demoulding of RC beams. Cubes of 100mm x100mm x 100mm and cylindrical specimens of 100mm in diameter and 200mm in height were tested in order to obtain the compressive strength and splitting tensile strength of both concrete substrate and the composites.

Figure 8.3 Preparations and casting steps of RC controls and substrates beams.

8.2.3 Preparing the Substrate and Applying the Nanocomposite layer:

In this study, MHRCC-CNT, MHRCC-CNF composites have been used (i.e. layer of 35mm applied) in repair/strengthening of six beams (pre-damaged). These composites have been chosen due to their significant improved mechanical and durability properties which have been previously investigated in Chapter Six and Chapter Seven, respectively. The cut-depth of concrete substrate beams were substituted with layers of FRC, MHRCC-CNT, and MHRCC -CNF composites, respectively (two beams for each composite). The procedure of prepare the substrate surfaces before applying the layer as follows:

- After 3 months of curing, surface of the substrate (in the tensile zoon) was levelled using an air needle gun (an effective tool to remove several millimetres from the concrete surface). At the same time, needle gun application was performed to roughen the surface.
- After surface preparation and cleaning, the tensile zone of the beam was positioned upward and wooden mould plates were re-positioned on the beam substrate. The tensile zone of the beam was positioned upwards due to it is not possible to apply the layer in the normal position (the tensile zone positioned in the downward position).
- The concrete internal surface was kept wet, i.e., in the saturated condition. This action was adopted in order to avoid excessive absorption of water by the surface to be repaired. The formation of a film of water on the surface of the beam was also eliminated to avoid any problems regarding the anchorage of the cementitious composite.
- The prepared repair/strengthening composite mixture (method explained in Chapter Three) was manually placed into the moulds in one layer and compacted using a concrete vibrator on the outside surface of the moulds.
- Figure 8.4 shows the procedure of preparing the substrate surface, and cleaning the longitudinal and transversal bars of rust and of dust (using water jetting). The repair/strengthening layer was then applied.
- After three months of repairing date (applying the layer), these beams were tested under flexural test.

Figure 8.4 Preparation the surface of RC concrete substrate and casting the repair/strengthening layer.

8.3 Materials Mechanical Properties

Mean compressive strength values were obtained from the average of three 100mm cubes tested in conjunction with test beams. Compressive strength was tested using a crusher machine in accordance with ASTM C39/C39M-05(2005). Three cylinders were also prepared and tested for splitting tensile strength which is a measure of the

tensile strength is of concrete (ASTM C496/C496M-04). Analysis of the bond strength between the repair composite and the concrete substrate is suggested to be addressed in future work, as this is crucial in preventing delamination and spalling of concrete. The nominal yield strength of the steel reinforcement was 415MPa.

8.4 Test Setup and Instrumentation

All specimens were tested under a four-point bending test by using monotonic loading up to failure. The span of the beams was 1200mm and the distance between the load points was 200mm, and shear span for both sides was 500mm (as shown above in Figure 8.5).

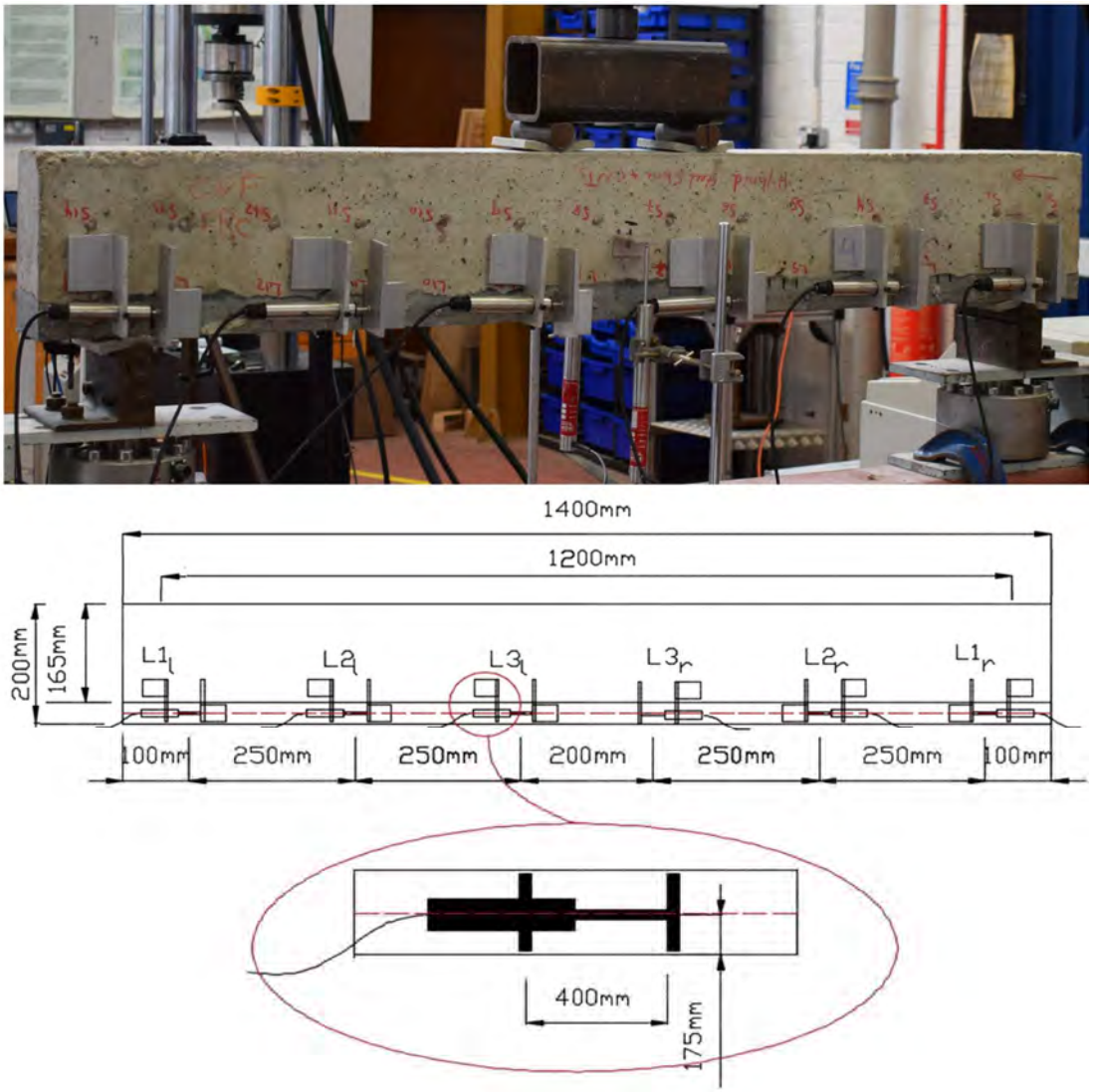

Figure 8.5 Flexural test and LVDTs set-up.

Two LVDTs (connected to the testing machine) were used on both sides to measure the deflection at mid-span. Deflection values obtained from the two mid-span LVDTs were averaged for each record. As slippage between the substrate and repair/strengthening composite layer could occur, for the repaired beams six LVDTs were laterally placed on one side of the beam to monitor sliding. The LVDTs' output data were recorded every 6 seconds using a data logger.

Structural behaviour of beams was observed and monitored throughout the tests, by recording the loads, and the corresponding vertical displacements. After testing, a comparison of the behaviour of control beams (RC1, RC2), and repaired/strengthened beams (FRC1, FRC2, CNTRC1, CNTRC2, and CNFRC1, CNFRC2) was then conducted. Tests were performed in the Laboratory of Structures in the School of Environment and Technology, University of Brighton. Testing was performed using a Zwick/Roell servo hydraulic closed-loop test machine with a load cell capacity of 200kN controlled at a displacement rate of 0.36 mm/min.

8.5 Analysis of Test Results and Discussion

8.5.1 Overview

To assess the validity of using thin layers of MHRCC-CNT, and MHRCC-CNF as repair and strengthening systems, test results were analysed and compared to results of normal strength concrete RC beams and beams repaired using conventional materials (i.e. steel fibre reinforced concrete FRC).

Test results were analysed based on cracking behaviour, strain distribution across the depth of the repair/strengthening composite, vertical mid span deflection, ductility, and ultimate flexural load and failure mode.

8.5.2 Mechanical Properties and Shrinkage Behaviour

Mechanical properties of the concrete substrate and the repair/strengthening materials in term of compressive strength and splitting tensile strength, and free drying shrinkage of both repair composite (Chapter Seven) and substrate concrete (normal concrete (NC)) are summarised in Table8.1. Figure 8.6 shows the drying shrinkage strains of NC, MHRCC-CNT, and MHRCC-CNF composites at early and late ages. The observed findings can be summarised as follows.

- The shrinkage behaviour of NC, and MHRCC-CNT, and MHRCC-CNF was almost the same, whereas a significant difference in the shrinkage between RC and FRC was observed: shrinkage strain of FRC at 28 days was found to be higher by about 43%. Although, the composite can resist crack formation at early ages and against the effect of restrained shrinkage, stresses due to differential shrinkage between the concrete substrate and the FRC layer could immediately cause cracking, and these stresses limit the capacity of the composite and influence its service life. It has been previously noted that the combined effect of restrained shrinkage, drying shrinkage and differential shrinkage between the concrete substrate and the composite is the most significant factor affecting long-term service life of the conventional repair techniques. (Jafarifar 2012).
- The low shrinkage strains observed with composites of MHRCC-CNT (420 microstrain), MHRCC-CNF (447 microstrain) reduce the possibility of cracks initiation as a result of volumetric changes.
- The bond strength between the concrete substrate and repair/strengthening composites is significantly influenced by the substrate surface preparation and the mechanical strength of the added layer. The higher the mechanical strength and the rougher the surface, the higher the bond strength, and accordingly there is less possibility of delamination or de-bonding, and high restrain strain could occur(Ombres 2011, Ladani et al. 2015). The induced restraint stress increases with an increase in the bond strength that results from applying the composite layer on rough surfaces (due to frictional resistance imposed by the rough surfaces of the concrete substrate). These stresses could cause tensile stresses to build up at locations of restraint. Tensile stresses cause cracks when these are higher than the

tensile strength of the composite, and in the absence of reinforcement agents at the nano scale (such with FRC composite), cracks start at the nano scale and propagate towards the top face.

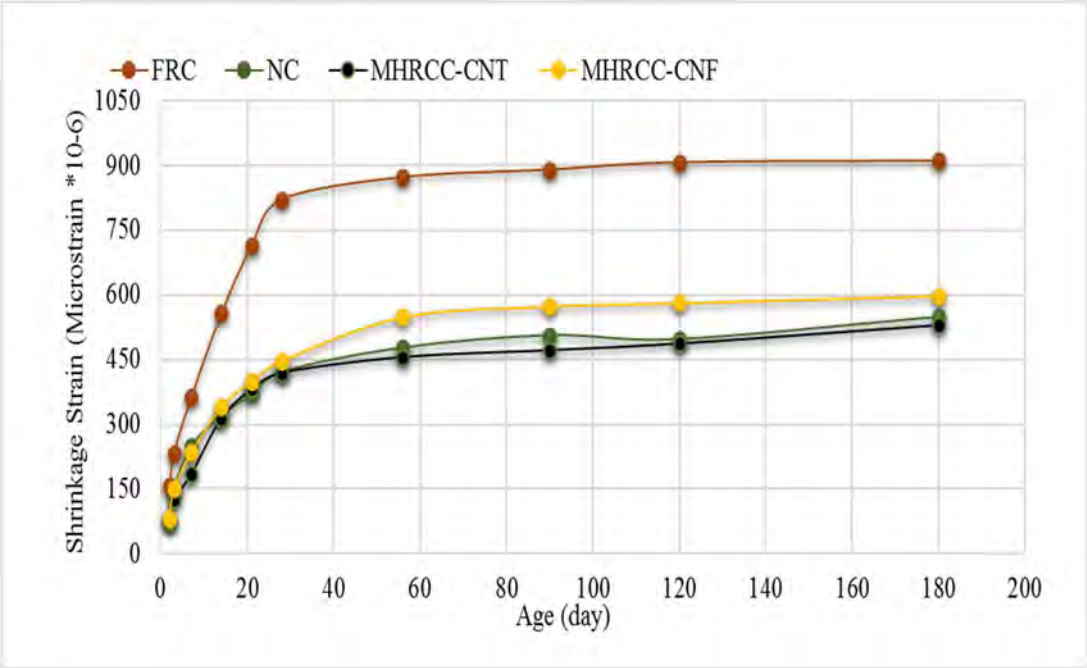

Figure 8.6 Comparison between the drying shrinkage behaviour of normal concrete (NC), and Fibre reinforced composite (FRC), and Multiscale hybrid reinforced cementitious composites based on carbon nanotubes (MHRCC-CNT) and carbon nanofibres (MHRCC-CNF) (Chapter Seven).

Table 8.1 Mechanical properties of substrate concrete and the Repair/Strengthening Composite.

Beam ID		Substrate Concrete			Repair/Strengthening Composite		
		Compressive Strength (MPa)	Tensile Strength (MPa)	Free shrinkage (micro strain)	Compressive Strength (MPa)	Splitting Tensile trength (MPa)	Free shrinkage (micro strain)
I	RC1	32.50	3.03	421.6			
	RC2	29.33	2.68				
II	FRC1	NA	NA	NA	65.17	7.74	820.7
	FRC2	NA	NA	NA		8.47	
III	NTRC1	NA	NA	NA	74.6	11.5	420
	NTRC2	NA	NA	NA		11.90	
IV	NFRC1	NA	NA	NA	74.2	12.82	447
	NFRC2	NA	NA	NA		12.45	

8.5.3 Flexural Behaviour of RC Beams

Flexural strength, crack pattern, crack formation, and failure mode were monitored throughout testing to assess the performance of the added layers compared to the reference beams. The results were discussed as follows.

8.5.4 Cracking Behaviour: Under Monotonic Flexural Loading

8.5.4.1 Control Beams

The control beams of RC1, and RC2 were tested, as a reference for the repaired beams, under four-point loading after 3 months of curing. Figure 8.7 shows the failure mode of the specimens (flexural failure).

Figure 8.7 Crack pattern of control beam specimens RC1, a) during the first crack formation, b) before reaching the ultimate load and c) after failure.

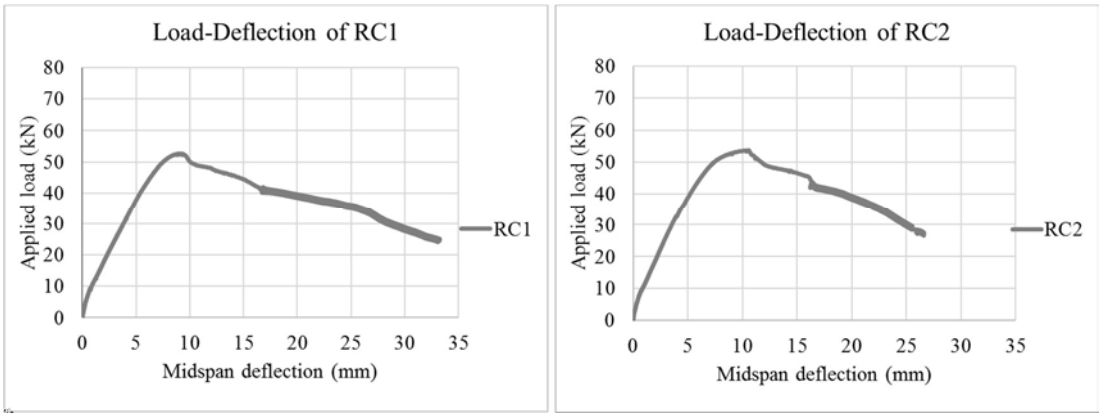

Figure 8.8 Load deflection curves of RC1, and RC2 control beams

The identical beams RC1 and RC2 behaved in the expected manner under flexural loading, load deflection cures are shown in Figure 8.8. The appearance of flexural first cracks, at the bottom of the beam, occurred at a load of 8kN and at an imposed displacement of about 0.95mm. These cracks were widened and distributed as loading proceeded along the 60mm middle span of the specimen. This occurred because this was the length along which the maximum bending moment was applied. With continuous loading and up to and the ultimate flexural load of 53.2kN (and corresponding maximum displacement of 9.5mm), many new flexural cracks formed and widely speared in the tension zoon (underneath the loading points), flexure-shear cracks did not appear. During post-cracking and with the load decreasing, minor flexure-shear cracks gradually began to appear (hairline shear) near to the supports area. At the end of the beam test, all inelastic deformation was concentrated in the critical crack region, while only hairline shear deformations were detected.

8.5.4.2 RC Beams Repaired Using FRC Layer

Conventional cementitious materials (i.e. FRC composite) were used for repair/strengthening in specimens FRC1 and FRC2(explained in Table 8.1). The results of these beams were useful for comparison with the behaviour of those beams repaired with the nanotubes/fibres composites (MHRCC-CNT, and MHRCC-CNF). Figure 8.9 shows photographs of the cracking pattern under flexural loading until failure.

Figure 8.9 Crack pattern of beams repaired using FRC composites a) during first crack formation, b) before reaching the ultimate load and c) after failure.

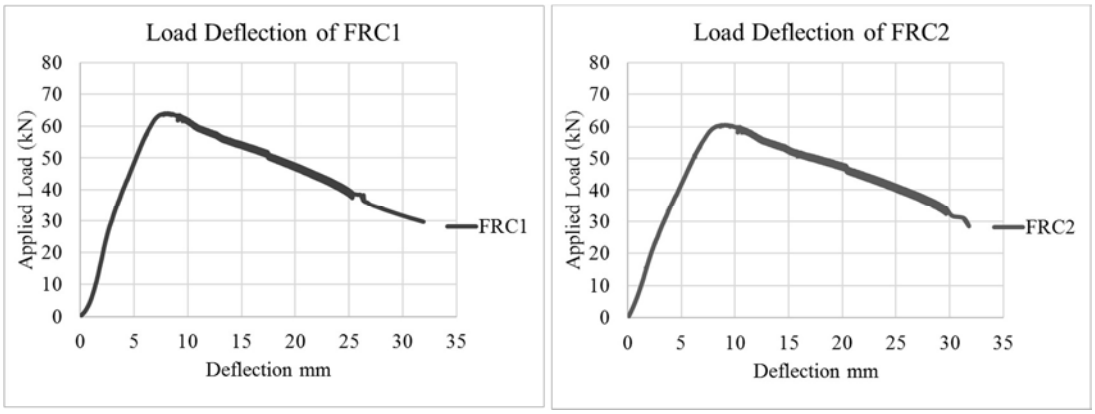

Figure 8.10 Load deflection curves of FRC1, and FRC2 control beams.

In both beams, the first flexural crack was observed at an average load and displacement of 18kN, and 2mm respectively. The maximum displacement was observed when the applied flexural load reached its ultimate value of 62.2kN, and 9.25mm. As the applied displacement and load increased, the propagation of the localised flexural crack (that led to the flexural failure) continued and exceeded the FRC layer, up to the ultimate loading when the maximum width recorded on the bottom of the layer was about 8mm. Cracks did not open widely during the post-cracking behaviour of the beam, since the presence of the steel fibre delays crack initiation and arrests their propagation, and no flexure-shear cracks formed. Load-deflection curves of FRC1, and FRC2 are shown in Figure 8.10.

8.5.4.3 RC Beams Repaired Using MHRCC-CNT Layer

Identical beams of NTRC1, and NTRC2 were repaired/strengthened using a layer of the composite prepared based on carbon nanotubes (MHRCC-CNT). The pattern of cracking and crack propagation during flexural testing and up to failure are shown in Figure 8.11

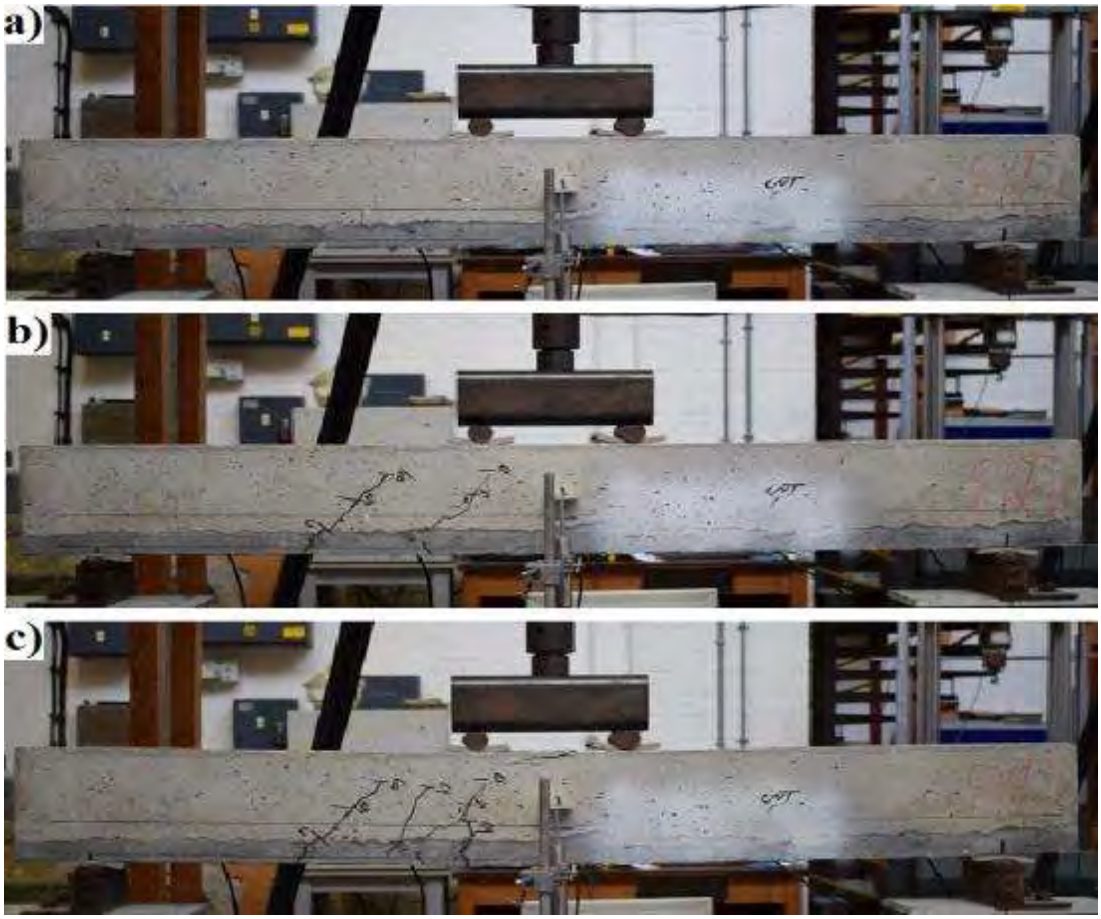

Figure 8.11 Crack pattern of beams repaired using CNTs-Hybrid fibre composites a) during first crack formation, b) before reaching the ultimate load and c) after failure.

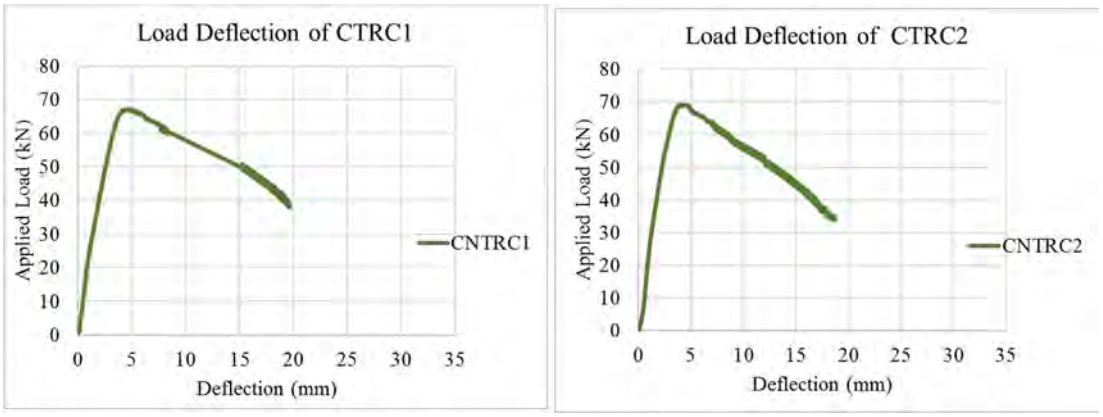

Figure 8.12 Load deflection curves of CNTRC1, and CNTRC2 beams.

During the test process, the first flexural crack was observed at a load and displacement of 24.5kN, and 1.04mm, and the deflection corresponding to peak load (4.7mm) was observed at an ultimate load of 68.3kN. Without changing the quantity of longitudinal steel or the cross section of the beams, the stiffness of the beams was significantly improved with the use of MHRCC-CNT in a thin layer in the tension zone, giving rise to a steeper load-deflection curve. In addition, a thin layer (35mm) of hybrid nanotubes and steel fibres composites was found to cause a distinct reduction in the number of the cracks initiated during loading. Moreover, the synergistic effect of the composite also delayed and reduced the formation and width of the localised cracks. At ultimate flexural strength, the maximum crack width was about 4mm (Figure 8.10C). The load deflection curves for NTRC1, and NTRC2 are presented in Figure 8.12.

8.5.4.4 RC Beams Repaired Using MHRCC-CNF Layer

Beams of NFRC1, and NFRC2 were repaired/strengthened using a layer of composite prepared using carbon nanofibres. Crack patterns until failure are shown in Figure 8.13

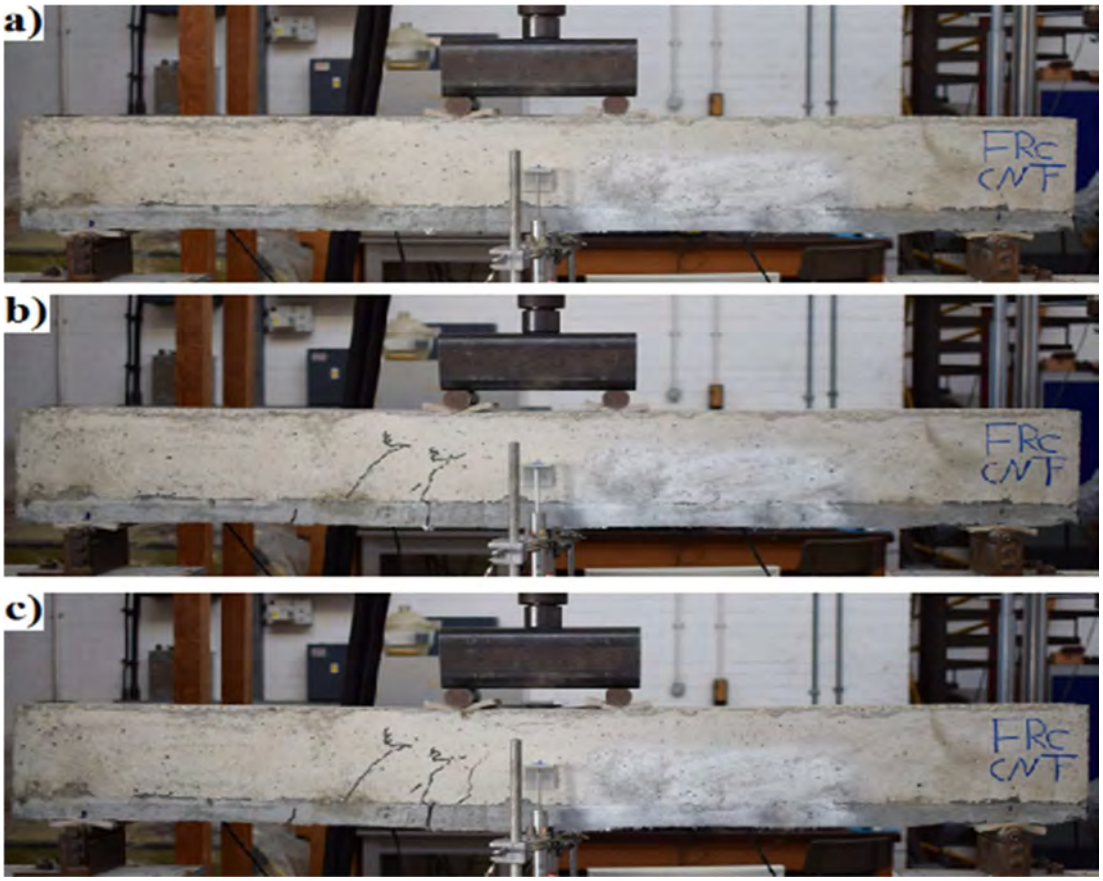

Figure 8.13 Crack pattern of beams repaired using CNFs-Hybrid fibre composites a) during first crack formation, b) before reaching the ultimate load and c) after failure.

Similar to CNTRC1, and CNTRC2, up to the point at which the ultimate flexural load was reached a distinct reduction in the number of created cracks was observed. In both beams, the first flexural crack was observed at a load and displacement of 23 kN, 1.0mm, respectively, whereas at ultimate flexural load (i.e.70.8kN) the maximum deflection was about 5.7mm. Moreover, the stiffness was also improved, showing the same trend as that observed in CNTRC1, and CNTRC2. Cracks did not open widely during the post-cracking behaviour of the beam, as the synergistic effect of the steel fibre and nanofibres delayed crack initiation and widening (i.e. arrested crack propagation), and no flexure-shear cracks formed. Up to ultimate loading the flexural main crack in the repair/strengthening layer had grown to about 4mm and had propagated upward to the substrate concrete, as shown in Figure 8.13C.

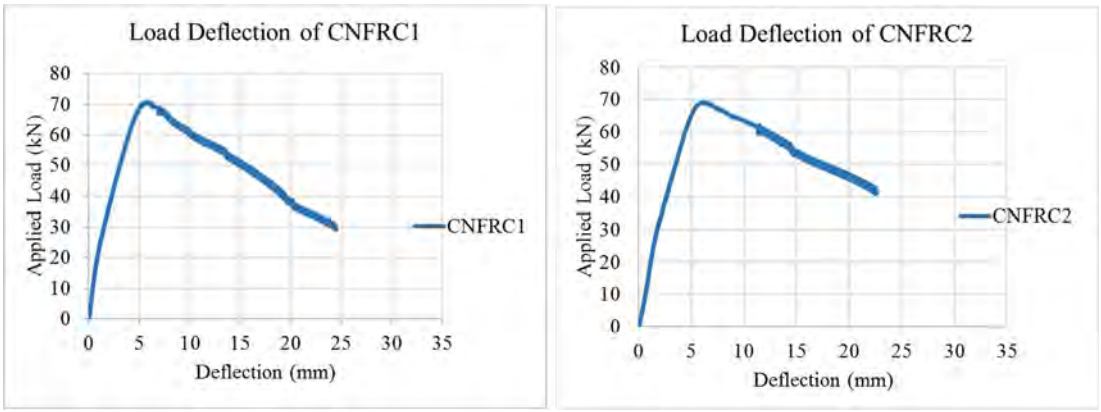

Figure 8.14 Load deflection curves of CNFRC1, and CNFRC2 beams.

The load deflection curves for CNFRC1, and CNFRC2 are presented in Figure 8.14 Composites based on carbon nanofibres were found to further increase in load carrying capacities of the beams compared to the beams repaired/strengthened using composites based on carbon nanotubes. However, the major improvements are observed in the stiffness of the beams.

The formation of cracks that occurred as a result of the yielding of embedded steel reinforcement in all repaired beams generated high stresses in the layer across the cracks. In general, however, it was found that use of a thin layer of multiscale hybrid reinforced cementitious composite based on carbon nanotubes (MHRCC-CNT) and based on carbon nanofibres (MHRCC-CNF) gave a remarkable improvement in the mechanical properties compared to a strengthening layer of FRC composite.

8.5.5 Load-Deflection Curves

The control beams failed, as expected, under flexure with extensive yielding of the longitudinal tension reinforcement, followed by crushing of the concrete in the compression zone. The failure of all the repair/strengthened beams was a flexural failure, as shown in (Figure 8.7C, Figure 8.9C, Figure 8.11C, and Figure 8.13C). No signals of deterioration, before failure, could be seen at the bottom side of the repair/strengthening layer. In addition, no evidence of de-bonding between the composite layer and the concrete substrate was observed even after yielding of the

reinforcement and formation of numbers of cracks adjacent to the existing main flexural crack. The control beam specimens were used as a baseline to compare the remaining strengthening beam specimens.

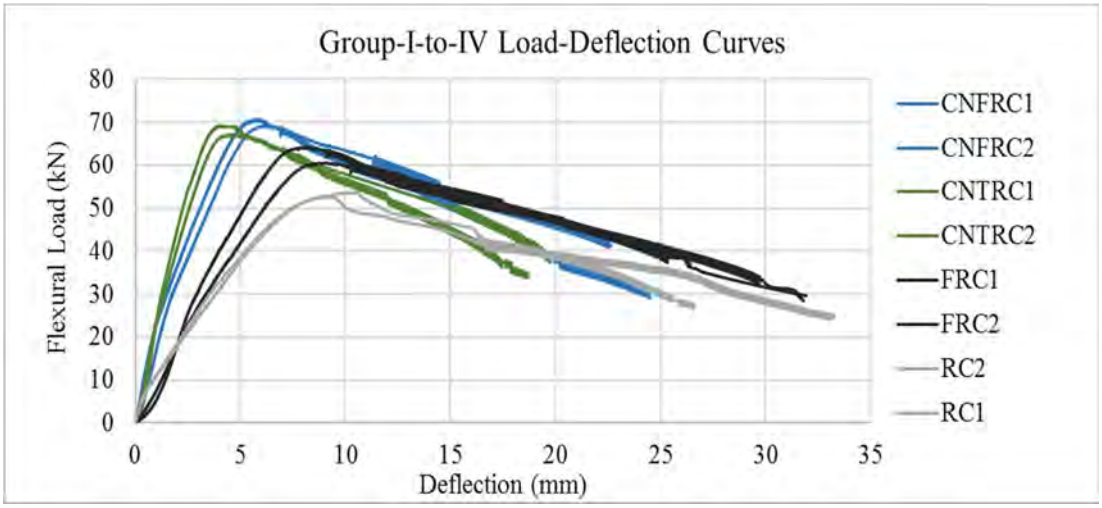

Figure 8.15 Load vs.deflection curves for beams of (RC1, and RC2), (FRC1, and FRC2), (CNTRC1, and CNTRC2), and (CNFRC1, and CNFRC2).

Figure 8.15 shows a comparison of Load versus mid span deflection response of each group. The general response can be divided into three stages of behaviour:
The first stage was characterized by an approximately linear relationship between the load and the mid-span deflection. During this stage of behaviour, the section was uncracked and both the reference and repaired beams behave essentially elastically. The second stage represents the behaviour beyond the initiation of first cracks until the yield point in the longitudinal tension reinforcements was reached. This is shown by an increased slope of the load versus mid-span deflection curve. The stiffness of the beams repaired with a thin layer of carbon nanotubes and nanofibres hybrid fibre composite was improved significantly (slightly greater with composites of CNF) compared to normal concrete beams and beams repaired with a layer of FRC. The end of this stage occurs when the main steel reinforcement starts to exhibit inelastic behaviour. The third stage was characterized by a decreasing slope of the load versus mid-span deflection curve, where the tension steel reinforcement reaches the strain hardening stage. In this stage, all curves decreased with load in a similar manner. The

bonding between the old concrete surface and the repair/strengthening layer was sufficient, as no horizontal cracks were noted in any place along the interface in any of the repaired beams.

For more understanding the comparison between the tested RC beams, the deflection behaviour between the controls and repaired/strengthened beams at distance of "L/480 (2.5mm)", "L/240 (5mm)", and at the peak were obtained (where L: is the free span between supports which is about 1200mm in the tested beams). The results obtained are summarized in Table 8.2 and from the results the following comparison can be drawn. Compared to the normal control beams (RC):

- The FRC layer increased the flexural load at deflection of 5mm and the deflection at peak by 24%, and 22% respectively, whereas, at deflection of 2.5mm the enhancement was marginal (4%).
- With both composites (MHRCC-CNT, and MHRCC-CNF), there are significant improvements in peak loads (compared to FRC beams), however, the major improvements are noticed in the stiffness of the beams. The layer of composites MSHRCC-CNT, and MSHRCC-CNF were found to significantly improve the load at deflection of 2.5mm, i.e. increases of 144%, and 93% were obtained.
- An increase in load capacity of the beam by about twofold at early loading and by about one-third at peak loading is observed without changing the quantity of longitudinal steel or the cross section of the beam. The greatest increase in ultimate load was about 22%, 30%, and 34% in beams repaired/strengthened using FRC layers, composites based on carbon nanotubes MSHRCC-CNT, and composites based on carbon nanofibres MSHRCC-CNF, respectively.
- Compared to MHRCC-CNT, the composites of MHRCC-CNF increased the stuffiness by about 35%, while the ultimate flexural load was decreased by 11%.

Table 8.2 Ultimate load capacity, and percentage increases observed with different strengthening / repair layers compared with control specimens.

Beam ID	At 2.5 mm (l/480) deflection			At 5mm (l/240) deflection			At peak deflection		
	Load (kN)	Average Load (kN)	% Inc. w.r.t. Ref. beam	Load (kN)	Average Load (kN)	% Inc. w.r.t. Ref. beam	Load (kN)	Av. Load (kN)	% Inc-reas
RC1	21.5	21.5		38	38.0		52.7	52.7	
RC2	20.4			39.2			53.6		
FRC1	25.3	22.4	4	47.3	47.3	24	64.2	64.2	22
FRC2	23.5			42.2			60.6		
CNTRC1	49.7	52.5	144	67.1	66.8	76	67.2	68.3	30
CNTRC2	55.2			66.5			69.3		
CNFRC1	43.83	41.5	93	67.9	66.5	75	70.8	70.0	33
CNFRC2	39.1			65.1			69.2		

8.5.6 Ductility Ratios

The ductility of a beam can be defined as its ability to sustain inelastic deformation without loss in its load carrying capacity prior to failure. Following this definition, ductility can be expressed in terms of deformation and can be calculated as the ratio of ultimate deformation to deformation at yield.

In the present work, ductility indices are expressed as the ratio between the deflection (δu), at an ultimate condition, and the deflection (δy), at the yield (Eq.8.1), as shown in Figure 8.16.

$$\mu_{\Delta} = \delta u / \delta y \qquad \text{(Eq.8.1)}$$

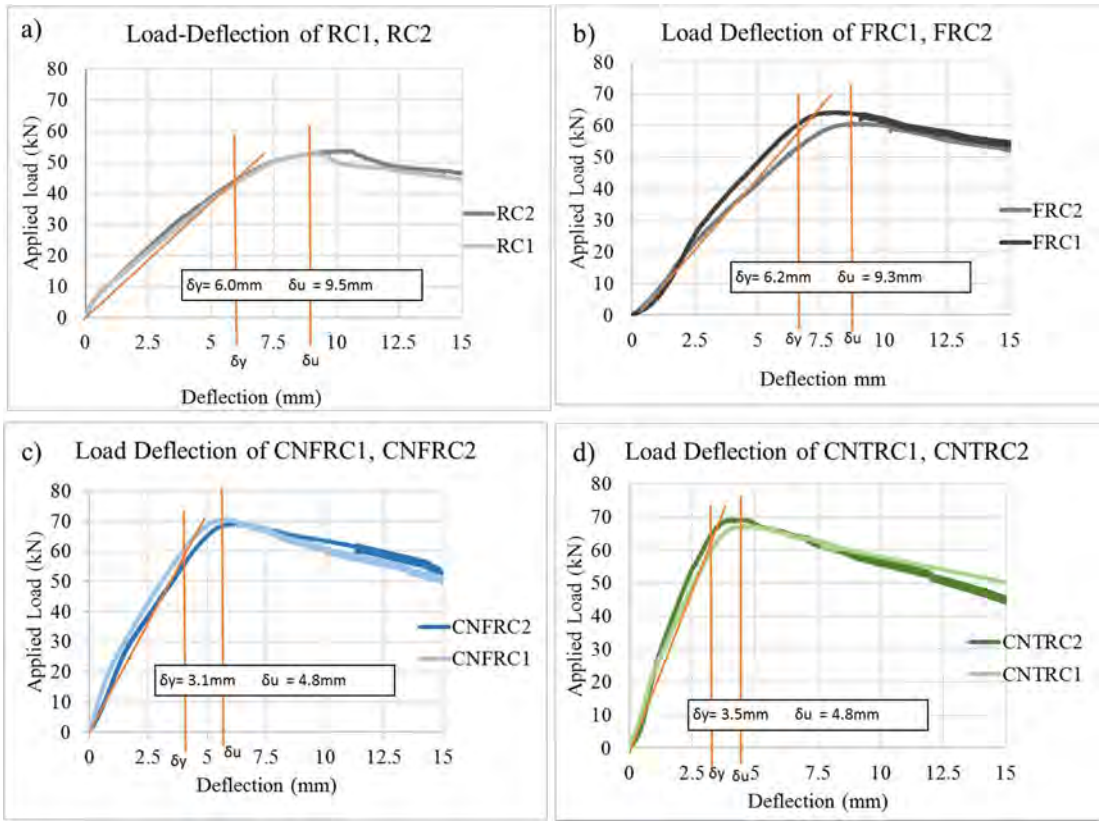

Figure 8.16 Load vs. deflection curves for beams of (RC1, and RC2), (FRC1, and FRC2), (CNTRC1, and CNTRC2), and (CNFRC1, and CNFRC2) explaining the method followed to determine the deflection(δu) at an ultimate condition, and the deflection(δy), at the yield.

Table 8.3 Ductility ratio for the tested beams.

Beam ID	Yield Load (kN)	Ultimate Load (kN)	δy (mm)	δu (mm)	Ductility ratio δy/δu	Average ductility (%)	Reduction in ductility (%)
RC1	44.5	52.9	6.0	9.0	1.5	1.58	0
RC2	44.8	53.5	6.0	10.0	1.7		
FRC1	55.6	63.9	6.0	9.0	1.5	1.50	-5
FRC2	53.2	60.5	6.3	9.5	1.5		
CNTRC1	62.3	67.2	3.1	4.8	1.5	1.52	-4
CNTRC2	65.5	69.2	3.2	4.8	1.4		
NFRC1	65.3	70.5	3	4.8	1.5	1.51	-4
NFRC2	65.1	69.1	3.5	5	1.3		

Table8.3 summarises the ductility indices for all tested beams. In accordance with the recommendations of the FIB (1990), the ductility index should exceed this minimum recommended value to prevent the occurrence of sudden failure. The minimum allowable ductility index of concrete types C35/45 or lower should be approximately 1.7, and 2.6 for concrete types of grade higher than C35/45. The acceptable ductility index ensures that the internal reinforcement experiences plastic deformation in order to provide the desired warning prior to failure of the member. Although the repair/strengthening layers of both composites significantly enhanced the stiffness, and showed good improvement in the ultimate load, these composites did not produce ductile behaviour, as evidenced by the percentages in Table 8.3. In a reinforced beam (such as the reference beam), failure is initiated by yielding of the steel reinforcement, followed, after considerable deformation at no substantial loss of load carrying capacity, by concrete crushing and ultimate failure. In contrast, in the stiffer repaired beam, the tension zone is reinforced internally with longitudinal steel bars and externally with the repair/strengthening layer, therefore there is usually a substantial reserve capacity of steel yielding. Prior to the steel reinforcement yielding, the beam can still carry increasing loads until flexural cracks occur in the repair/strengthening composite.

8.5.7 Slippage Between the Concrete Substrate and the Repair Layer

The distribution of repair/strengthening composite strains at the mid span of the repaired beam specimens was measured using six lateral LVDTs glued on mid-width of the repair layer.

LVDT data were recorded during testing, and collected from the datalogger after completion of the test. Next a synchronized between datalogger data and the loads data from the actuator (Zuick matchine). The load-lateral displacement curve represents the slippage between the substrate and the repair layer. The recoded lateral displacement from the LVDTs as a function of flexural load was approximately constant, and no significance could be obtained. This could be attributed to the high bond between the layer and the composite, and that no slippage occurred during the test.

8.6 Summary

A detailed experimental program was carried out to test the effectiveness of the multiscale hybrid reinforced cementitious composites based on carbon nanotubes (MHRCC-CNT) and carbon nanofibres (MHRCC-CNF) developed in Chapters Six, in terms of their utilization for repairing/strengthening of flexural RC beams. The repaired/strengthening layers have been applied to the beams to reconstruct a cut-depth of 35mm in the tension zone. The layer capacities have been compared to reference beams (i.e. normal concrete beams, and beams reconstructed (repairing/strengthening) by applying a layer of the conventional composites of FRC). From the obtained results, there is a remarkable improvement in the stiffness and bending strength of beams tested after repair/strengthening with thin layers of MHRCC-CNT and MHRCC-CNF. They exhibited significant stiffness over FRC (conventional repair/strengthening materials). Stiffness of MHRCC-CNT, and MHRCC-CNF beams were significantly increased at mid-span deflection of 2.5mm, with the average of around 94, and 144%, respectively.

It may be concluded that addition of a thin layer of strain hardening material, such as the MHRCC developed and tested here, is an effective technique in improving the stiffness and bending behaviour of flexural members, in addition to increasing their ultimate flexural load.

Chapter Nine:
Conclusions and Further Work

9.1 Overview

This thesis has examined the feasibility of using carbon-based nano-additives (carbon nanotubes, carbon nanofibres, and graphene oxide) in producing cementitious composites with improved mechanical and durability performance. Objectives toward achieving this goal are summarised in four points and discussed over five results chapters. The objectives include:1) investigate facile technique to overcome the main relevant challenges (i.e. dispersion) with the use of nano-additives with cementitious materials, 2) produce nano-additives reinforced cementitious composite, and multiscale hybrid reinforced cementitious composite, containing various type of nano-additives dispersed following the dispersion technique, 3) examine the shrinkage behaviour (through the tests of free drying shrinkages, and base-restrained shrinkages and end-restrained shrinkages), and durability properties in term of their resistance to sulfuric acid resistance, 4) examine the potential application of the proposed composites as thin layer (35mm) repair and strengthening to reconstruct degraded concrete element (RC beams). A summary of the main conclusions drawn from the experimental work presented in this thesis is given below:

9.2 Facile Dispersion Technique (Chapter Four)

Through this chapter (over three Phases), a facile method for dispersion of carbon nanotubes in different concentrations has been optimised. The influence of ultrasonication, surfactant, and use of mineral admixtures has been investigated.

In Phase I the effects of three different sonication intensities and various treatment times on dispersion of nanotubes in water and their impact on the properties of cementitious composites (compressive and tensile strength) were assessed. The results indicated that high sonication intensity (i.e. 100% amplitude) applied over a short treatment duration (up to 5 min) using 0.025% of MWCNTs gave a high concentration of well dispersed nanotubes in water, which subsequently significantly improved the mechanical strengths of cement composites. In Phase II, it was found that surfactants

such as PCE, NSF, MC are effective dispersants for nanotubes in aqueous solution, and that reasonable surfactant content can improve stability of the dispersed nanotubes. Mechanical strength results highlighted that use of surfactant based superplasticisers (either PCE, or NSF) in a ratio of 1:10 (MWCNTs-to surfactant) led to a distinct improvement in composite strength. In phase III, the work on novel dispersion techniques was extended to include use of undensified microsilica (USF) to improve and prevent the re-agglomeration of nanotubes through the composite. It was found that USF particles fill in pores and voids in between the nanotubes, which densifies and reinforces the hydrating gel structure. In addition, pozzolanic reactions occur between the silica-rich USF particles and cement hydration products leading to formation of additional Calcium Silicate Hydrate (C-S-H) which acts to improve the bond between the nanotubes and surrounding matrix.

9.3 Development of Nano-Additives Cementitious Composites (Chapter Five)

In this chapter, the development of nano-additives cementitious composites based on low added amounts (0.025 wt.% cement) of functionalised carbon nanotubes, carbon nanofibres, and graphene oxide was investigated. The nano suspensions were prepared following the dispersion technique developed in Chapter Four. Mechanical strengths were generally enhanced with all the used nano-additives. The origin of the ability of these materials to increase the strength gain can be attributed to:

- The sufficient dispersion of the nano reinforcing agents used acting to reinforce the cement hydration products (such as calcium silicate hydrates and ettringite). Thus, the crack arresting ability of nanotubes/fibres is likely to increase tensile resistance when the composite begins cracking, i.e. the fibres in the nanoscale increase crack arresting ability and delay nano cracks to microcracks' propagation, and then cracking at the macroscopic level. The used dispersion techniques contribute in increasing the coverage density of surfactant molecules on the surfaces of nanotubes/fibres, which may act as a cross-linker between the cement matrix and the nano-additives. The presence of nanotubes/fibres/graphene sheets may also inhibit the growth or propagation of internal cracks and help to transfer load. The distribution of nano-additives throughout the microstructure densifies

the material and reinforces the hydration products, and acts as a nano strengthening agent, better distributing stresses at the micro scale.

- The availability of surfactant molecules (through non-covalent) and -COOH groups (through covalent bond) on functionalised nanotubes walls, and graphene oxide sheets are likely to be effective cross-linking agents. These agents bridge between the tubes/sheets and surrounding matrix and thereby play a positive role in enhancing the load transfer between them and the matrix, as it tends to enhance the mechanical interlocking coupled with chemical cross-linking type bonding.
- The geometry of CNFs compared to MWCNTs (i.e. their outer surfaces are conically shaped and angled with respect to the longitudinal fibre axis) can lead to improve bonding with the surrounding matrix, bridging of cracks and improving the load carrying capacity. In addition, their longer fibre length (around four times longer compared to MWCNTs) can lead to better capability in bridging cracks and thus improving the load carrying capacity.
- The possibility of nanotubes /fibres, or graphene sheets to form a homogenous inter-connecting entangled network of nanotubes in the matrix with some overlapping each other, the matrix is therefore restrained from failure until a fail in the bond or pullout/fracture in the tube/fibre/sheets occurs.

From the above experimental results (Sections 9.2, 9.3) it can be concluded that the suggested dispersion technical processing route (to disperse at 0.025% MWCNTs, F-MWCT, CNFs, and FLGO) represents a considerable advancement over previous methods. The technique of high-intensity sonication over short time intervals is an effective (and scalable) dispersion method, which can generate desired dispersion levels and be used to reproducibly manufacture structurally-enhanced cementitious composite materials.

9.4 Development of Multiscale Hybrid Reinforced Cementitious Composites (Chapter Six)

In this chapter, the development of new types of hybrid composites, termed multiscale hybrid reinforced cementitious composites based on nanofilaments, i.e. carbon nanotubes (MHRCC-CNT, and carbon nanofibres MHRCC-CNF, were investigated. The mechanism of the multiscale system is that the shorter fibres (nanofilaments) act to reinforce the cement hydration products at the nano scale, while the longer fibres (i.e. steel fibres) arrest the microstructures and prevent the propagation of microcracks. This synergistic effect significantly delays the first crack formation. Moreover, the hybrid system increases the composite packing effect, as nanofilaments also act as fillers, filling the voids (spaces) (at nano-and/or micro level) that exist within and around the ettringite products within the hydrated cement paste. Although both carbon nanotubes and carbon nanofibres exhibited a distinct effect, the performance of the latter was higher, and led to the greatest improvement in the composite mechanical performance. This can be attributed to the higher aspect ratio of CNFs compared to CNTs, which can lead to a better capability in bridging cracks and improving the load carrying capacity. SEM investigation supported the improved reinforcing efficiency of CNFs over CNTs, their higher aspect ratio is enhancing their ability to withstand pulling-out and/or rupture forces.

Based on the mechanical properties obtained, application of multi scale hybrid reinforcement in cementitious composites increased significantly the energy needed to initiate cracks. Hence these materials can provide new, tougher, crack-free composites, with improved fracture toughness, and energy storing capacity.

9.5 Shrinkage Behaviour and Sulfuric Acid Resistance (Chapter Seven)

9.5.1 Shrinkage Behaviour

The cracking tendency (through base-restrained shrinkage and end-restrained shrinkage) and free drying shrinkage tests of the developed composites were investigated in Chapter Seven. Base restrained shrinkage and ends restrained

shrinkages were adopted for assessing cracking potential in these composites under restraint conditions, such as when using them as overlay composites (i.e. repair materials).

Carbon nanotubes and carbon nanofibres in both composites exhibited a significant reduction in the free drying shrinkage strain compared to cement mortar. The geometry and high aspect ratio, and higher dispersion degree, of the nanofilaments through the composite can significantly refine the nano/micro pores, and interrupt the paths of continuous capillary pores, and thus reduce the possibility of mixture bleeding/evaporation. Moreover, base restrained shrinkage tests, and ends restrained shrinkage, revealed that nanofilament cementitious composites exhibited a superior resistance to crack initiation. Visible cracks were observed in control samples within the first ten days, whereas no cracks were observed with nanofilament composites over all testing durations, which were attributed to the improved tensile strength of the composites and the presence of reinforcement agents at the nano scale. The higher aspect ratio and deformed outer surface of carbon nanofibres (compared to nanotubes) contribute to enhancing the performance of nanofibres composites, as these factors enhance the composite's resistance to facture/and pulling out under restraint conditions.

9.5.2 Sulfuric Acid Resistance

Sulfuric acid attack tests were carried out to give an indication of the effect of nanofilaments (nanotubes, and nanofibres) on the resistance of these composites to sulfuric acid attack. The nanofilaments were found to increase the composite resistance to aggressive ions, and act to reinforce across the composite hydration products, prevent crack initiation, reduce the composite porosity, improve the bulk density, and thereby restrict ion diffusion into the composite body. SEM examination showed that while cracking of the control cement mortar samples (PC) was found, the nanofilament interfacial zone in both composites specimens remained continuous without cracking under acid attack. The improved interfacial zones in the nano cementitious composites could be an important factor in their better durability performance under sulphuric acid attack.

Hence, the shrinkage, cracking tendency, and durability tests on nanofilament cementitious composites give an indication of superior performance of nanofilaments in reinforcing the cement structure at the nanoscale, reducing the risk of material deterioration, as crack formation from the nano scale is limited.

9.6 Thin Layer Repair and Strengthening Composites-Potential Application (Chapter Eight)

The potential use of the developed crack-free composites, i.e. multiscale hybrid reinforced cementitious composites based on carbon nanotubes (MHRCC-CNT) and based on carbon nanofibres (MHRCC-CNF), in repairing/strengthening applications was investigated in Chapter Eight. Thin layers (35mm) of these composites were applied to reconstruct RC large scale beams in the tension zone. The strengthening capacities of the nano- and hybrid- composite layers have been compared to reference beams (i.e. normal concrete beams, and beams reconstructed (repaired/strengthened) by applying a layer of conventional FRC composites). From the obtained results, there is a remarkable improvement in the stiffness and bending strength when applying the nano and hybrid materials. They exhibited significant stiffness improvement, about twofold over FRC (i.e. conventional repair/strengthening materials).

It may be concluded that the flexural members repaired/strengthened with a thin layer of crack-free composite such as MHRCC is an effective technique in improving the stiffness and bending behaviour of flexural members in addition to their ultimate flexural load.

9.7 Limitations of the Current Research

Despite the extensive experimental work undertaken during this thesis, time, resource and practical limitations mean that some aspects of the work require extension and further validation, as follows:

The experiments to optimise the dispersion technique were limited to use of one type (i.e. length and diameter/width) of nanotubes, nanofibres, and graphene sheets. The detailed effect of ultrasonication parameters such the temperature delivered during

sonication and the effect of probe diameters on dispersion were not covered. Analytically, to date, quantitative techniques to evaluate the dispersion of CNTs/CNFs within the aqueous solution are not available, and the available methods, such as tests through absorbance (Uv-vis absorbance spectrometry) values and TEM images, are semi-qualitative. The evaluation of dispersion level though the cement composite, through SEM images, may not be a completely representative method since it only covered a limited area on the top surface of the investigated sample. In addition, the post-treatment length of nanotubes and nanofibres, and dimensions of graphene sheets, was not measured to verify the breakage/defects due to the ultrasonication process.

9.8 Suggestions for Future Work

Based on the results presented here, the following aspects might usefully be considered for future work:

1- The effect of high intensity sonication over various durations on the integrity/structure of nanotubes/Fibres/ graphene sheets.
2- The effect of rising suspension temperature as a result of high sonication intensity on the performance of nanotubes through the cementitious composites.
3- The chemical adsorption mechanism, effect of different molecular weights of PCE, NFS, and MC on dispersion, and absorption on the nanotubes outer walls, of surfactant agents on nanotubes following high ultrasonication intensity.
4- Improvement of the bond strength between nano-additives and the surrounding cementitious matrix by using various ultrafine supplementary pozzolanic materials, at different addition percentages.
5- Use of ultrasonication techniques to refine undensified microsilica and generate silica particles in the same size scale as nano- additives, which could be a useful technique to improve the bond between nano-additives and the surrounding cementitious materials, and prevent their re-agglomeration through the matrix.
6- The performance of multi scale fibres (nanotubes/fibres, and steel fibres) could be influenced by many factors, including: casting and placement technique, specimen

size, and geometry and fibres content. Varying these parameters could be a useful area for optimising effective multiscale hybrid composites.

7- The durability performance of multi scale hybrid reinforced cementitious composites, such as resistance to corrosion, chloride pentation, carbonation, freeze- thaw, sulfate resistance, etc.

8- Use of modern strain gauges to accurately determine the deformation/cracks tendency of nano cementitious composites, including use of ring tests (as a standard test) to evaluate the restrained shrinkage, and large rigs to evaluate the end-restrained shrinkage.

9- Investigate the effect of plastic shrinkage, autogenous shrinkage, chemical shrinkage, creep relaxation, carbonation shrinkage, and shrinkage rate, nano-additives reinforced cementitious composites.

10- Investigate the effect of variation in environment temperature, relative humidity (RH), and volumetric size of the specimens on shrinkage behaviour of nano-additives reinforced cementitious composites.

11- Methods of improving the dispersion of nano-additives for cementitious application on large scale should be investigated, since it is encouraging to use nano composite for large structural application.

At present, certain technical aspects partly explain the limited use of nano-additive containing composites in construction applications, not least the relatively high price of the nano material, and the production scale of nanomaterials (production is typically relatively small-scale). The effective portion of nanomaterials that could be added, the dispersion technique, the sensitivity of the material to mixing procedures and mix proportions, and the variability of mechanical properties as a function of casting conditions, are all areas that require confirmation or standardisation, and could form useful directions for further research.

References .

AASHTOT132 (2000). "Standard Method of Test for Tensile Strength of Hydraulic Cement Mortars," In American Association of State Highway and Transportation Officials, Standard Specifications for Transportation Materials and Methods of Sampling and Testing, Washington, DC, ."

Abu Al-Rub, R. K., Ashour, A. I. and Tyson, B. M. (2012). "On the aspect ratio effect of multi-walled carbon nanotube reinforcements on the mechanical properties of cementitious nanocomposites." Construction and Building Materials 35(0): 647-655.

Abu Al-Rub RK, T. B., Yazdanbakhsh A, Grasley Z. (2012). "Mechanical properties of nanocomposite cement incorporating surface-treated and untreated carbon nanotubes and carbon nanofibers." ASCE J Nanomech Micromech 2(1):1–6.

ACI207-2R-95 (2002). Effect of Restraint, Volume Change, and Reinforcement on Cracking of Mass Concrete. ACI 207.2R-95.

ACI544.1R-96 (2002). State-of-the-Art Report on Fiber Reinforced Concrete Reported by ACI Committee 544.

Adam J., B., Claire E., L. and Jamie S., Q. (2011). "Parametric analysis of sonication and centrifugation variables for dispersion of single walled carbon nanotubes in aqueous solutions of sodium dodecylbenzene sulfonate." Carbon 49(15): 5213-5228.

Adresi, M., Hassani, A., Javadian, S. and Tulliani, J.-M. (2016). "Determining the Surfactant Consistent with Concrete in order to Achieve the Maximum Possible Dispersion of Multiwalled Carbon Nanotubes in Keeping the Plain Concrete Properties." Journal of Nanotechnology 2016: 1-9.

Agboola, A. E., Pike, R. W., Hertwig, T. A. and Lou, H. H. (2007). "Conceptual design of carbon nanotube processes." Clean Technologies and Environmental Policy 9(4): 289-311.

Ahmed Ibrahim, A. (2011). Aspect Ratio Effect of Functionalized/Non-Functionalized Multiwalled Carbon Nanotubes on the Mechanical Properties of Cementitious Materials. Master's thesis, Texas A&M University. Available electronically from http : / /hdl .handle .net /1969 .1 /ETD -TAMU -2011 -08 -10197.

Ahmed Sbia, L., Peyvandi, A., Soroushian, P., Lu, J. and Balachandra, A. M. (2014). "Enhancement of Ultrahigh Performance Concrete Material Properties with Carbon Nanofiber." Advances in Civil Engineering 2014: 1-10.

Alhelfi, A. and Sundén, B. (2016). "Predictions of Temperature and Pressure Fields Due to Collapse of a Bubble in Sulfuric Acid Solution Under Ultrasound." Journal of Thermal Science and Engineering Applications 8(4): 041010-041010-041016.

Amir Hossein Jodeiri*, R. J. Q. (2012). "Effect of Wirand FS7-II Steel Wire Fibre on Flexural Capacity of Reinforced Concrete Beam." Journal of Civil Engineering Research 6: 100-107.

Anette, J. (2011). Effects of Steel Fibres on Cracking in Reinforced Concrete, Chalmers university of technolog

Antoine, E. N. (2003). "Engineered Steel Fibers with Optimal Properties for Reinforcement of Cement Composites." Journal of Advanced Concrete Technology Vol. 1, No. 3, 241-252, November 2003 / Copyright © 2003 Japan Concrete Institute.

Antonello Di, C., Valeria, E. and Antonella, F. (2014). "Non-covalent and reversible functionalization of carbon nanotubes." Beilstein J Nanotechnol 5: 1675-1690.

Anurag, S. (2014). Processing, characterization and sliding wear behavior of functionalized carbon nanotube reinforced epoxy matrix composite Master of Technology.

Arteaga-Arcos, J. C., Chimal-Valencia, O. A., Yee-Madeira, H. T. and Díaz de la Torre, S. (2013). "The usage of ultra-fine cement as an admixture to increase the compressive strength of Portland cement mortars." Construction and Building Materials 42(0): 152-160.

Ashour, A. I. (2011). Aspect Ratio Effect of Functionalized/Non-Functionalized Multiwalled Carbon Nanotubes on the Mechanical Properties of Cementitious Materials. Master's thesis, Texas A&M University. Available electronically from http : / /hdl .handle .net /1969 .1 /ETD -TAMU -2011 -08 -10197.

ASTMC39/C39M-17 ASTMC39/C39M-17, Standard Test Method for Compressive Strength of Cylindrical Concrete Specimens, ASTM International, West Conshohocken, PA, 2017, www.astm.org.

ASTMC157 (2014). ASTM C157 / C157M-08(2014)e1, Standard Test Method for Length Change of Hardened Hydraulic-Cement Mortar and Concrete, ASTM International, West Conshohocken, PA, 2014, www.astm.org.

ASTMC230/C230M-14 Standard Specification for Flow Table for Use in Tests of Hydraulic Cement, ASTM International, West Conshohocken, PA, 2014, www.astm.org.

Babak, F., Abolfazl, H., Alimorad, R. and Parviz, G. (2013). "Predicting the impact of multiwalled carbon nanotubes on the cement hydration products and durability of cementitious matrix using artificial neural network modeling technique." ScientificWorldJournal 2013: 103713.

Balaguru, S. (1992). " Fiber-Reinforced Cement Composites, McGraw-Hill Inc., New York, ."

Banthia, N., Gupta, R. and Mindess, S. (2006). "Development of fiber reinforced concrete repair materials." Canadian Journal of Civil Engineering 33(2): 126-133.

Banthia, N. and Sappakittipakorn, M. (2007). "Toughness enhancement in steel fiber reinforced concrete through fiber hybridization." Cement and Concrete Research 37(9): 1366-1372.

Barick, A. K. and Tripathy, D. K. (2011). "Preparation, characterization and properties of acid functionalized multi-walled carbon nanotube reinforced thermoplastic polyurethane nanocomposites." Materials Science and Engineering: B 176(18): 1435-1447.

Bassuoni, M. T. and Nehdi, M. L. (2007). "Resistance of self-consolidating concrete to sulfuric acid attack with consecutive pH reduction." Cement and Concrete Research 37(7): 1070-1084.

Bastos, G., Patiño-Barbeito, F., Patiño-Cambeiro, F. and Armesto, J. (2016). "Nano-Inclusions Applied in Cement-Matrix Composites: A Review." Materials 9(12): 1015.

Baughman RH, Z. and AA, d., Heer (2002). "Carbon nanotubesthe route toward applications. Science 2002;." 297((5582):): 787–792.

Bhushan, B. (2010). Carbon nanofibers. In: Springer handbook of nanotechnology, Springer Science & Business Media.

Bin Donga, Y. S., Yonghui, L., Jie, Y., Jingkun, X. and Liqiang, Z. (2011). "Dispersion of carbon nanotubes by carbazole-tailed amphiphilic imidazolium ionic liquids in aqueous solutions." J Colloid Interface Sci 356(1): 190-195.

Bo, Z., Shu Jian, C., Asghar H., K., Frank, C., C.M, W. and Wen Hui, D. (2015). "Effect of ultrasonication energy on engineering properties of carbon nanotube reinforced cement pastes." Carbon 85: 212-220.

Brandt, A. M. (2008). "Fibre reinforced cement-based (FRC) composites after over 40 years of development in building and civil engineering." Composite Structures 86(1-3): 3-9.

BS-EN12390-3 (2009). Testing hardened concrete. Compressive strength of test specimens.

BSEN197-1:2000 Cement. Composition, specifications and conformity criteria for common cements

C109M-16a, A. C. Standard Test Method for Compressive Strength of Hydraulic Cement Mortars (Using 2-in. or [50-mm] Cube Specimens), , ASTM International, West Conshohocken, PA, 2016, www.astm.org.

C192M-13a, A. C. Standard Practice for Making and Curing Concrete Test Specimens in the Laboratory, ASTM International, West Conshohocken, PA, 2013, www.astm.org.

C496M-11, A. C. Standard Test Method for Splitting Tensile Strength of Cylindrical Concrete Specimens, ASTM International, West Conshohocken, PA, 2004, www.astm.org.

C1609M-12, A. C. Standard Test Method for Flexural Performance of Fiber-Reinforced Concrete (Using Beam With Third-Point Loading), ASTM International, West Conshohocken, PA, 2012, www.astm.org.

Carlswa, J. (2002). Steel fibre reinforced concrete toppings exposed to shrinkage and temperature deformations PhD.

Carlswärd, J. (2006). Shrinkage cracking of steel fibre reinforced self compacting concrete overlays Test methods and theoretical modelling.

Carsten, V. (2010). Ultrafine particles in concrete: Influence of ultrafine particles on concrete properties and application to concrete mix design.

Centonze, G., Leone, M. and Aiello, M. A. (2012). "Steel fibers from waste tires as reinforcement in concrete: A mechanical characterization." Construction and Building Materials 36(0): 46-57.

Chadwick, R. (2008). Polymer Functionalization Strategies for the Suspension of Carbon Nanotubes in Bulk Polymers, McMaster University.

Chaipanich, A., Nochaiya, T., Wongkeo, W. and Torkittikul, P. (2010). "Compressive strength and microstructure of carbon nanotubes–fly ash cement composites." Materials Science and Engineering: A 527(4–5): 1063-1067.

Chang, Z.-T., Song, X.-J., Munn, R. and Marosszeky, M. (2005). "Using limestone aggregates and different cements for enhancing resistance of concrete to sulphuric acid attack." Cement and Concrete Research 35(8): 1486-1494.

CheapTubes (2017). Cheap Tubes Inc https://www.cheaptubes.com/product/multi-walled-carbon-nanotubes-8-15nm/.

Chen, Collins, Macleod, Pan, Duan and Wang (2011). "Carbon nanotube–cement composites: A retrospect." The IES Journal Part A: Civil & Structural Engineering 4(4): 254-265.

Chen, S. J., Zou, B., Collins, F., Zhao, X. L., Majumber, M. and Duan, W. H. (2014). "Predicting the influence of ultrasonication energy on the reinforcing efficiency of carbon nanotubes." Carbon 77: 1-10.

Chen, S. J. W., Wei Sagoe-Crentsil, Kwesi Collins, Frank Zhao, Xiao Ling Majumder, Mainak Duan, Wen Hui (2016). "Distribution of carbon nanotubes in fresh ordinary Portland cement pastes: understanding from a two-phase perspective." RSC Adv. 6(7): 5745-5753.

Chunyu Li, T.-W. C. (2003). "Elastic moduli of multi-walled carbon nanotubes and the effect of van der Waals forces." Composites Science and Technology 63(11): 1517-1524.

Clésia C., N., Mauro, K., Clarivaldo S., S. and Marco A. Z., A. (2001). "Use of Ultrasonic Baths for Analytical Applications: A New Approach for Optimisation Conditions."

Coleman, J. N., Khan, U., Blau, W. J. and Gun'ko, Y. K. (2006). "Small but strong: A review of the mechanical properties of carbon nanotube–polymer composites." Carbon 44(9): 1624-1652.

Cwirzen, A., Habermehl-Cwirzen, K., Nasibulin, A. G., Kaupinen, E. I., Mudimela, P. R. and Penttala, V. (2009). "SEM/AFM studies of cementitious binder modified by MWCNT and nano-sized Fe needles." Materials Characterization 60(7): 735-740.

Cwirzen, A., Habermehl-Cwirzen, K. and Penttala, V. (2008). "Surface decoration of carbon nanotubes and mechanical properties of cement/carbon nanotube composites." Advances in Cement Research 20(2): 65-73.

Danoglidis, P. A., Konsta-Gdoutos, M. S., Gdoutos, E. E. and Shah, S. P. (2016). "Strength, energy absorption capability and self-sensing properties of multifunctional carbon nanotube reinforced mortars." Construction and Building Materials 120: 265-274.

Datsyuk, V., Landois, P., Fitremann, J., Peigney, A., Galibert, A. M., Soula, B. and Flahaut, E. (2009). "Double-walled carbon nanotube dispersion via surfactant substitution." Journal of Materials Chemistry 19(18): 2729.

Díez-Pascual, A. M., Gómez-Fatou, M. A., Ania, F. and Flores, A. (2015). "Nanoindentation in polymer nanocomposites." Progress in Materials Science 67: 1-94.

El-Sayed, N., Latipa, K., Jamal, K., Lyazzat, B. and Craig, W. (2014). "Effects of Surfactants on the Properties of Mortar Containing Styrene/Methacrylate Superplasticizer." The Scientific World Journal 2014: 10.

Eric W., W., Paul E., S. and Charles M., L. (1997). "Nanobeam Mechanics: Elasticity, Strength, and Toughness of Nanorods and Nanotubes." Science 277(5334): 1971-1975.

Ezeokonkwo, J. C. a. N., C. U (2011). "Uniaxial Compressive Strength of Polypropylene Fibre Reinforced Sandcrete Cubes." Scholarlink Research Institute Journals, University of Nigeria, Nsukka, Enugu State, Nigeria.

Fakharifar, M., Dalvand, A., Arezoumandi, M., Sharbatdar, M. K., Chen, G. and Kheyroddin, A. (2014). "Mechanical properties of high performance fiber reinforced cementitious composites." Construction and Building Materials 71: 510-520.

Fakhim, B., Hassani, A., Rashidi, A. and andGhodousi, P. (2014). "Preparation and mechanical properties of graphene oxide: cement nanocomposites." ScientificWorldJournal 2014: 276323.

Fan, W., Stoffelbach, F., Rieger, J., Regnaud, L., Vichot, A., Bresson, B. and Lequeux, N. (2012). "A new class of organosilane-modified polycarboxylate superplasticizers with low sulfate sensitivity." Cement and Concrete Research 42(1): 166-172.

Farman, A., Laurence, R., Jean-Marc, L. e. e., Laurent, D. and Fabrice, M. (2014). "Efect of sonication conditions: solvent, time, temperature and reactor type on the preparation of micron sized vermiculite particles. Ultrasonics " 21 Sonochemistry, Elsevier,: pp.1002-1009.

Ferrari, L., Bernard, L., Deschner, F., Kaufmann, J., Winnefeld, F., Plank, J. and Jennings, H. (2012). "Characterization of Polycarboxylate-Ether Based Superplasticizer on Cement Clinker Surfaces." Journal of the American Ceramic Society 95(7): 2189-2195.

Frank, C., John, L. and Wen Hui, D. (2012). "The influences of admixtures on the dispersion, workability, and strength of carbon nanotube–OPC paste mixtures." Cement and Concrete Composites 34(2): 201-207.

Fusion, H. (2017). "http://www.sonicator.com/."

Gdoutos, E. E., Konsta-Gdoutos, M. S. and Danoglidis, P. A. (2016). "Portland cement mortar nanocomposites at low carbon nanotube and carbon nanofiber content: A fracture mechanics experimental study." Cement and Concrete Composites 70: 110-118.

Geng Ying, L., Pei Ming, W. and Xiaohua, Z. (2005). "Mechanical behavior and microstructure of cement composites incorporating surface-treated multi-walled carbon nanotubes." Carbon 43(6): 1239-1245.

George Turner, R. H., Tapsell Gerald (2014). "Concrete and Carbon Nanofibers." Proc. of the Intl. Conf. on Advances In Engineering And Technology - ICAET-2014(978-1-63248-028-6 doi: 10.15224/ 978-1-63248-028-6-03-94).

Ghorabi, S. R., Laleh Madaeni, Sayed Siavash Zinadini, Sirus Derakhshan, Ali Ashraf (2012). "Effects of three surfactant types of anionic, cationic and non-ionic on tensile properties and fracture surface morphology of epoxy/MWCNT nanocomposites." Iranian Polymer Journal 21(2): 121-130.

Girardi, F., Vaona, W. and Di Maggio, R. (2010). "Resistance of different types of concretes to cyclic sulfuric acid and sodium sulfate attack." Cement and Concrete Composites 32(8): 595-602.

Gojny, F. H., Nastalczyk, J., Roslaniec, Z. and Schulte, K. (2003). "Surface modified multi-walled carbon nanotubes in CNT/epoxy-composites." Chemical Physics Letters 370(5-6): 820-824.

Graphenea. (2010). "Available at http://www.graphenea.com/." Graphenea Inc. Cambridge Coworking Center 1 Broadway Cambridge, MA 02142 United States Retrieved March, 2015.

Grünewald, S. (2004). Performance-Based Design of Self-Compacting Fibre Reinforced Concrete, Department of Structural and Building Engineering, Delft University of Technology, Delft, .

Haghi and Sabu, T. (2015). Carbon nanotubes: Theoretical Concepts and Research Strategies for Engineers. Apple Academic Press, Inc. 3333 Mistwell Crescent, Oakville, ON L6L 0A2 Canada.

Hamzaoui, R., Bennabi, A., Guessasma, S., Khelifa, R. and Leklou, N. (2012). "Optimal Carbon Nanotubes Concentration Incorporated in Mortar and Concrete." Advanced Materials Research 587: 107-110.

Han, B., Yu, X. and Ou, J. (2011). Multifunctional and Smart Carbon Nanotube Reinforced Cement-Based Materials. Nanotechnology in Civil Infrastructure. K. Gopalakrishnan, B. Birgisson, P. Taylor and N. Attoh-Okine, Springer Berlin Heidelberg: 1-47.

Hantel, M. M. (2013). Graphite Oxide and Graphene Oxide Based Electrode Materials for Electrochemical Double Layer Capacitors. PhD Phd Thesis.

Hanus, M. J. and Harris, A. T. (2013). "Nanotechnology innovations for the construction industry." Progress in Materials Science 58(7): 1056-1102.

Hoheneder, J. (2012). "Smart Carbon Nanotube/fiber and Pva Fiber- Reinforced Composites for Stress Sensing and Chloride Ion Detection." Thesis and Desertations Paper 32.

Hou, D., Lu, Z., Li, X., Ma, H. and Li, Z. (2017). "Reactive molecular dynamics and experimental study of graphene-cement composites: Structure, dynamics and reinforcement mechanisms." Carbon 115: 188-208.

Hui, Z., Zhong, Z. and Claudia, B. (2004). "Comparison of short carbon fibre surface treatments on epoxy composites: I. Enhancement of the mechanical properties." Composites Science and Technology 64(13–14): 2021-2029.

Iijima, S. (2002). "Carbon nanotubes: past, present, and future." Physica B: Condensed Matter 323(1-4): 1-5.

In-Yup Jeon1, D. W. C., Nanjundan Ashok Kumar1 and Jong-Beom Baek1 (2011). Functionalization of Carbon Nanotubes Carbon Nanotubes - Polymer Nanocomposites. S. Yellampalli, World's largest Science, Technology & Medicine Open Access book publishe.

Inna, S. J. G. A. J. (2013). "Effect of Pozzolanic Additives on Structure and Chemical Durability of Concrete." Procedia Engineering 57: 1005-1012.

Iqbal, S., Ali, A., Holschemacher, K., Bier, T. A. and Shah, A. A. (2016). "Strengthening of RC beams using steel fiber reinforced high strength lightweight self-compacting concrete (SHLSCC) and their strength predictions." Materials & Design 100: 37-46.

Iravani, S. (1996). "Mechanical properties of high-performance concrete." ACI Materials Journal, 93(5), 416-426.".

Irshidat, M. R., Al-Saleh, M. H. and Al-Shoubaki, M. (2015). "Using carbon nanotubes to improve strengthening efficiency of carbon fiber/epoxy composites confined RC columns." Composite Structures 134: 523-532.

Islam, R., Bergey, Johnson,Yodh (2003). "High weight fraction surfactant solubilization of singlewall carbon nanotubes in water." ano Letters,vol.3,no. 2, pp. 269–273, 2003.

Ivan, M. (2006). "High-performance Hybrid-fibre Concrete: Development and Utilisation." Universiteit van Belgrado, Servië.

Jafarifar, N. (2012). Shrinkage behaviour of steel-fibre-reinforced-concrete pavements.

Jonas, C. (2006). Shrinkage cracking of steel fibre reinforced self compacting concrete overlays: Test methods and theoretical modelling.

Jorge, F. d., AssedNaked, H. and Laia, H. (2013). "Analysis of the Behavior of Carbon Nanotubes on Cementitious Composites." ISRN Nanomaterials 2013: 1-17.

Jose , L. F. J. M. d. C., and Juan Ángel García (2014). "Carbon Nanotube-Cement Composites in the Construction Industry: 1952-2014. A State of the Art Review." 2nd International Conference on Emerging Trends in Engineering and Technology (ICETET'2014).

Junrong, Y., Nadia, G., Cor E., K. and Joachim, L. (2007). "Controlling the dispersion of multi-wall carbon nanotubes in aqueous surfactant solution." Carbon 45(3): 618-623.

Karabanova, L. V., Whitby, R. L. D., Bershtein, V. A., Korobeinyk, A. V., Yakushev, P. N., Bondaruk, O. M., Lloyd, A. W. and Mikhalovsky, S. V. (2013). "The role of interfacial chemistry and interactions in the dynamics of thermosetting polyurethane–multiwalled carbon nanotube composites at low filler contents." Colloid and Polymer Science 291(3): 573-583.

Kawashima, S., Hou, P., Corr, D. J. and Shah, S. P. (2013). "Modification of cement-based materials with nanoparticles." Cement and Concrete Composites 36: 8-15.

Keitetsu, R., Tetsushi, K. and Kajima, T. (2013). Strain Hardening Cement Composites: Structural Design and Performance: State-of-the-Art Report of the RILEM Technical Committee 208-HFC, SC3.

Kejin Wang, S. M. S., Sri Sritharan, Hasitha Seneviratne, Xin Wang, Qizhe Hou (2013). Investigation into Shrinkage of High-Performance Concrete Used for Iowa Bridge Decks and Overlays, Institute for Transportation Iowa State University 2711 South Loop Drive, Suite 4700 Ames, IA 50010-8664.

Kerdnawee, K., Termvidchakorn, C., Yaisanga, P., Pakchamsai, J., Chookiat, C., Eiad-ua, A., Wongwiriyapan, W., Chaiwat, W., Ratchahat, S., Faungnawakij, K., Suttiponparnit, K. and Charinpanitkul, T. (2017). "Present Advancement in Production of Carbon Nanotubes and Their Derivatives from Industrial Waste with Promising Applications." KONA Powder and Particle Journal 34(0): 24-43.

Kerienė, J., Kligys, M., Laukaitis, A., Yakovlev, G., Špokauskas, A. and Aleknevičius, M. (2013). "The influence of multi-walled carbon nanotubes additive on properties of non-autoclaved and autoclaved aerated concretes." Construction and Building Materials 49(0): 527-535.

Khalaj, G. and Nazari, A. (2012). "Modeling split tensile strength of high strength self compacting concrete incorporating randomly oriented steel fibers and SiO2 nanoparticles." Composites Part B: Engineering 43(4): 1887-1892.

Khalifa, A. (2015). Processing and Characterisation of Cementitious Materials Reinforced with Fibres, The University of Warwick.

Khanna, V., Bakshi, B. R. L. and L., J. (2008). "Carbon Nanofiber Production, Life Cycle Energy Consumption and Environmental Impact." Energy Consumption and Environmental Impact From Carbon Nanofiber 12(3): 394-410.

Kim, H. K., Nam, I. W. and Lee, H. K. (2014). "Enhanced effect of carbon nanotube on mechanical and electrical properties of cement composites by incorporation of silica fume." Composite Structures 107: 60-69.

Kim, J. J. and Reda Taha, M. (2014). "Experimental and Numerical Evaluation of Direct Tension Test for Cylindrical Concrete Specimens." Advances in Civil Engineering 2014: 1-8.

Kim, S. W., Kim, T., Kim, Y. S., Choi, H. S., Lim, H. J., Yang, S. J. and Park, C. R. (2012). "Surface modifications for the effective dispersion of carbon nanotubes in solvents and polymers." Carbon 50(1): 3-33.

Kong, F.-r. P., Li-sha Wang, Chen-man Zhang, De-la Xu, Nai (2016). "Effects of polycarboxylate superplasticizers with different molecular structure on the hydration behavior of cement paste." Construction and Building Materials 105: 545-553.

Krister, H., Bo, J., Bengt, K. and Bjorn, L. (2003). Surfactants and Polymers in Aqueous Solution. Krister Holmberg, Bo Jonsson, Bengt Kronberg and Bjorn Lindman.

Kumar Mehta, P. J. M. M. (2006). Concrete Microstructure, Properties, and Materials.pdf, New York Chicago San Francisco Lisbon London Madrid, Mexico City Milan New Delhi San Juan Seoul, Singapore Sydney Toronto.

Ladani, R. B., Wu, S., Kinloch, A. J., Ghorbani, K., Zhang, J., Mouritz, A. P. and Wang, C. H. (2015). "Improving the toughness and electrical conductivity of epoxy nanocomposites by using aligned carbon nanofibres." Composites Science and Technology 117: 146-158.

Lee, S.-C., Oh, J.-H. and Cho, J.-Y. (2015). "Compressive Behavior of Fiber-Reinforced Concrete with End-Hooked Steel Fibers." Materials 8(4): 1442-1458.

Li, G. Y., Wang, P. M. and Zhao, X. (2005). "Mechanical behavior and microstructure of cement composites incorporating surface-treated multi-walled carbon nanotubes." Carbon 43(6): 1239-1245.

Li, G. Y., Wang, P. M. and Zhao, X. (2007). "Pressure-sensitive properties and microstructure of carbon nanotube reinforced cement composites." Cement and Concrete Composites 29(5): 377-382.

Li, H., Xiao, H.-g. and Ou, J.-p. (2004). "A study on mechanical and pressure-sensitive properties of cement mortar with nanophase materials." Cement and Concrete Research 34(3): 435-438.

Li, V. C. W., Hwai-Chung (1992). "Conditions for Pseudo Strain-Hardening in Fiber Reinforced Brittle Matrix Composites." Applied Mechanics Reviews 45(8): 390-398.

Li, X., Korayem, A. H., Li, C., Liu, Y., He, H., Sanjayan, J. G. and Duan, W. H. (2016). "Incorporation of graphene oxide and silica fume into cement paste: A study of dispersion and compressive strength." Construction and Building Materials 123: 327-335.

Liew, K. M., Kai, M. F. and Zhang, L. W. (2016). "Carbon nanotube reinforced cementitious composites: An overview." Composites Part A: Applied Science and Manufacturing 91: 301-323.

Liliana Olenic, S. P., Valer Almasan and Alexandru R. Biris, Ed. (2010). Electrochemical and Adsorption Properties of Catalytically Formed Carbon Nanofibers. National Institute for Research and Development of Isotopic and Molecular Technologies Romania. INTECH, Croatia, SCIYO.COM.

Liu, C.-X. C., Jin-Woo (2012). "Improved Dispersion of Carbon Nanotubes in Polymers at High Concentrations." Nanomaterials 2(4): 329-347.

Liu, Q., Xu, Q., Yu, Q., Gao, R. and Tong, T. (2016). "Experimental investigation on mechanical and piezoresistive properties of cementitious materials containing graphene and graphene oxide nanoplatelets." Construction and Building Materials 127: 565-576.

Liu, S., Li, L., Wang, Z., Wang, J. and Rao, M. (2012). "Study on Strength and Microstructure of Cement Pastes Containing Limestone Powder under Flowing Acid Solution Condition." ISRN Ceramics 2012: 1-6.

Liu, W.-W., Chai, S.-P., Mohamed, A. R. and Hashim, U. (2013). "Synthesis and characterization of graphene and carbon nanotubes: A review on the past and recent developments." Journal of Industrial and Engineering Chemistry(0).

Lu, L., Ouyang, D. and Xu, W. (2016). "Mechanical Properties and Durability of Ultra High Strength Concrete Incorporating Multi-Walled Carbon Nanotubes." Materials 9(6): 419.

Lu, Z., Hou, D., Ma, H., Fan, T. and Li, Z. (2016). "Effects of graphene oxide on the properties and microstructures of the magnesium potassium phosphate cement paste." Construction and Building Materials 119: 107-112.

Luo, J., Hou, D., Li, Q., Wu, C. and Zhang, C. (2017). "Comprehensive performances of carbon nanotube reinforced foam concrete with tetraethyl orthosilicate impregnation." Construction and Building Materials 131: 512-516.

Lv, S., Ma, Y., Qiu, C., Sun, T., Liu, J. and Zhou, Q. (2013). "Effect of graphene oxide nanosheets of microstructure and mechanical properties of cement composites." Construction and Building Materials 49(0): 121-127.

Madhavi, Pavithra, Singh, S. B., Raj, S. B. V. and Paul, S. (2013). " Effect of Multiwalled Carbon Nanotubes On Mechanical Properties of Concrete ". chennai city, India : international journal of scientific research, . ." 2: 2277 - 8179.

Makar, M. (2005). Carbon nanotube/cement composites-early results and potential applications, Proceedings of the 3rd International Conference on Construction Materials: Performance,. Innovations and Structural Implications. Vancouver, B.C., Canada,: pp.1-10.

Mann, S. (2006). "Nanotechnology and Construction <Nanotech and Construction Nanoforum report_259_9089.pdf>."

Maria, K.-G., Zoi S, S. and Shah, S. P. (2010). "Multi-scale mechanical and fracture characteristics and early-age strain capacity of high performance carbon nanotube/cement nanocomposites." Cement and Concrete Composites 32(2): 110-115.

Maria, K.-G., Zoi S, S. and Surendra, P. S. (2010). "Highly dispersed carbon nanotube reinforced cement based materials." Cement and Concrete Research 40(7): 1052-1059.

Marks, J. (2013). "Engineered cementitious composites: applications and impact of high tensile, self-healing concrete." University of Pittsburgh Swanson School of Engineering.

Marsh, D. H. R., G. A. Zaka, M. H. Whitby, R. J. Khlobystov, A. N. (2007). "Comparison of the stability of multiwalled carbon nanotube dispersions in water." Phys Chem Chem Phys 9(40): 5490-5496.

Martin-Gullon, I., Vera, J., Conesa, J. A., González, J. L. and Merino, C. (2006). "Differences between carbon nanofibers produced using Fe and Ni catalysts in a floating catalyst reactor." Carbon 44(8): 1572-1580.

Martin Tr¨ubertini, F. (2011). Numerical Modeling of High Performance Fiber Reinforced Cementitious Composites.

MC, C.-F. (1993). " Comité euro-international du béton: Ceb-fip model code 1990, bulletin d'information, no. 213/214. Lausanne: Thomas telford services ltd."

Mechtcherine, V. (2013). "Novel cement-based composites for the strengthening and repair of concrete structures." Construction and Building Materials 41: 365-373.

Mendoza, O., Sierra, G. and Tobón, J. I. (2014). "Effect of the reagglomeration process of multi-walled carbon nanotubes dispersions on the early activity of nanosilica in cement composites." Construction and Building Materials 54(0): 550-557.

Metaxa, Z., Konsta-Gdoutos, M. and Shah, S. (2010). "Carbon Nanofiber-Reinforced Cement-Based Materials." Transportation Research Record: Journal of the Transportation Research Board 2142: 114-118.

Metaxa, Z. S., Konsta-Gdoutos, M. S. and Shah, S. P. (2013). "Carbon nanofiber cementitious composites: Effect of debulking procedure on dispersion and reinforcing efficiency." Cement and Concrete Composites 36(0): 25-32.

Metaxa, Z. S., Seo, J.-W. T., Konsta-Gdoutos, M. S., Hersam, M. C. and Shah, S. P. (2012). "Highly concentrated carbon nanotube admixture for nano-fiber reinforced cementitious materials." Cement and Concrete Composites 34(5): 612-617.

Mindess, A. B. a. S. (2007). Fibre Reinforced Cementitious Composites, byTaylor & Francis 2 Park Square, Milton Park,Abingdon,Oxon OX14 4RN

Mittal, G., Dhand, V., Rhee, K. Y., Park, S.-J. and Lee, W. R. (2015). "A review on carbon nanotubes and graphene as fillers in reinforced polymer nanocomposites." Journal of Industrial and Engineering Chemistry 21: 11-25.

Mohammad Iqbal, K. (2007). A novel method for measuring porosity of high strength concrete. 7th Saudi Engineering Conference (SEC7), Department of Civil Engineering, College of Engineering King Saud University, Kingdom of Saudi Arabia.

Mohammadi, Y., Singh, S. P. and Kaushik, S. K. (2008). "Properties of steel fibrous concrete containing mixed fibres in fresh and hardened state." Construction and Building Materials 22(5): 956-965.

Mohammed Alias, Y., Norazman Mohamad, N., Ariffin, I., Ng Choy, P., RisbyMohd, S. and andMuhammad Azani, Y. (2013). "Performance of Hybrid Steel Fibers Reinforced Concrete Subjected to Air Blast Loading " Advances in Materials Science and Engineering.

Mohammed Alias Yusof, N. N., 1 Ariffin Ismail,2 Ng Choy Peng,1 RisbyMohd Sohaimi,1 andMuhammad Azani Yahya1 (2013). "Performance of Hybrid Steel Fibers Reinforced Concrete Subjected to Air Blast Loading." Advances in Materials Science and Engineering.

Mokhtar, M. M., Abo-El-Enein, S. A., Hassaan, M. Y., Morsy, M. S. and Khalil, M. H. (2017). "Mechanical performance, pore structure and micro-structural characteristics of graphene oxide nano platelets reinforced cement." Construction and Building Materials 138: 333-339.

Monteiro, P. K. M. P. J. M. (2006). <Concrete Microstructure, Properties, and Materials.pdf>, McGraw-Hill New York Chicago San Francisco Lisbon London, Madrid Mexico City Milan New Delhi San Juan Seoul,Singapore Sydney Toronto.

Morsy, M. S., Alsayed, S. H. and Aqel, M. (2011). "Hybrid effect of carbon nanotube and nano-clay on physico-mechanical properties of cement mortar." Construction and Building Materials 25(1): 145-149.

Mudimela, P. R., Nasibulina, L. I., Nasibulin, A. G., Cwirzen, A., Valkeapää, M., Habermehl-Cwirzen, K., Malm, J. E. M., Karppinen, M. J., Penttala, V., Koltsova, T. S., Tolochko, O. V. and Kauppinen, E. I. (2009). "Synthesis of Carbon Nanotubes and Nanofibers on Silica and Cement Matrix Materials." Journal of Nanomaterials 2009: 1-4.

Musmar, M. (2013). "Tensile strength of steel fiber reinforced concrete." Contemporary Engineering Sciences 6: 225-237.

Musso, S., Tulliani, J.-M., Ferro, G. and Tagliaferro, A. (2009). "Influence of carbon nanotubes structure on the mechanical behavior of cement composites." Composites Science and Technology 69(11-12): 1985-1990.

Nadiv, R., Shtein, M., Refaeli, M., Peled, A. and Regev, O. (2016). "The critical role of nanotube shape in cement composites." Cement and Concrete Composites 71: 166-174.

Nanoshel. (2014). "Smart nano-materials in construction Industry ", from https://www.nanoshel.com/product/smart-nano-materials-construction-industry/.

Nanowerk, S. (2011). "Global carbon nanotubes market - industry beckons." from http://www.nanowerk.com/spotlight/spotid=23118.php.

Nataraja, M., Dhang, N. and Gupta, A. (1999). " Stress-strain curves for steel-fiber reinforced concrete under compression. Cement Concr. Compos. 1999, 21, 383–390.".

Nemkumar, B. and Jean-François, T. (1995). "Test Methods for Flexural Toughness Characterization of Fiber Reinforced Concrete:." ACI Materials Journal, 1(92): pp. 48–57.

Nemkumar, B. and Vivek, B. (2013). "Performance Synergy in Hybrid Fiber Reinforced Concrete Under Impact." Journal of Frontiers in Construction Engineering 2: PP. 75-82.

Nemkumar Banthia*1, V. B. (2013). "Performance Synergy in Hybrid Fiber Reinforced Concrete Under Impact." Journal of Frontiers in Construction Engineering 2: PP. 75-82.

Noushini, A., Vessalas, K., Arabian, G. and Samali, B. (2014). "Drying Shrinkage Behaviour of Fibre Reinforced Concrete Incorporating Polyvinyl Alcohol Fibres and Fly Ash." Advances in Civil Engineering 2014: 1-10.

Novoselov, K. S. G., A. K. Morozov, S. V. Jiang, D. Zhang, Y. Dubonos, S. V. Grigorieva, I. V. Firsov, A. A. (2004). "Electric Field Effect in Atomically Thin Carbon Films." Science 306(5696): 666-669.

Oladiran, O. G. (2014). ASSESSMENT OF RESTRAINED SHRINKAGE CRACKING OF CONCRETE THROUGH ELLIPTICAL RINGS. PhD, Brunel University.

Ombres, L. (2011). "Flexural analysis of reinforced concrete beams strengthened with a cement based high strength composite material." Composite Structures 94(1): 143-155.

Oxana V., K., Boris I., K. and Edgar Gerardo de Casas, O. (2013). "Dispersion of carbon nanotubes in water and non-aqueous solvents." RSC Advances 3(47): 24812.

Pacheco-Torgal, F. and Jalali, S. (2011). "Nanotechnology: Advantages and drawbacks in the field of construction and building materials." Construction and Building Materials 25(2): 582-590.

Pakravan, H. R., Latifi, M. and Jamshidi, M. (2017). "Hybrid short fiber reinforcement system in concrete: A review." Construction and Building Materials 142: 280-294.

Pan, Z., Wu, C., Liu, J., Wang, W. and Liu, J. (2015). "Study on mechanical properties of cost-effective polyvinyl alcohol engineered cementitious composites (PVA-ECC)." Construction and Building Materials 78: 397-404.

Parveen, S., Rana, S. and Fangueiro, R. (2013). "A Review on Nanomaterial Dispersion, Microstructure, and Mechanical Properties of Carbon Nanotube and Nanofiber Reinforced Cementitious Composites." Journal of Nanomaterials 2013: 1-19.

Parveen, S., Rana, S., Fangueiro, R. and Paiva, M. C. (2015). "Microstructure and mechanical properties of carbon nanotube reinforced cementitious composites developed using a novel dispersion technique." Cement and Concrete Research 73: 215-227.

Passant, Y. (2015). Novel dispersion technique of carbon nanotube in combination with nano silica in cement composites to enhance its mechanical properties. Master of science. Cairo, Egypt; 28–30.

Peng-Cheng, M., Siddiqui, N. A., Marom, G. and Kim, J.-K. (2010). "Dispersion and functionalization of carbon nanotubes for polymer-based nanocomposites: A review." Composites Part A: Applied Science and Manufacturing 41(10): 1345-1367.

Peyvandi, A., Sbia Libya, A., Soroushian, P. and Sobolev, K. (2013). "Effect of the cementitious paste density on the performance efficiency of carbon nanofiber in concrete nanocomposite." Construction and Building Materials 48(0): 265-269.

Peyvandi, A., Soroushian, P., Abdol, N. and Balachandra, A. M. (2013). "Surface-modified graphite nanomaterials for improved reinforcement efficiency in cementitious paste." Carbon 63: 175-186.

Pouria, P., Michelle R., N., Dorina, B. and Dorel, F. (2011). "Effect of surface treatment on the post-peak residual strength and toughness of polypropylene/polyethylene-blended fiber-reinforced concrete." Journal of Composite Materials 45(20): 2047-2054.

Radocea, A. (1992.). " A Study on the Mechanism of Plastic Shrinkage of Cement-Based Materials. PhD thesis. Göteborg: Chalmers University of Technology Göteborg.".

Rance, G. A., Marsh, D. H., Nicholas, R. J. and Khlobystov, A. N. (2010). "UV–vis absorption spectroscopy of carbon nanotubes: Relationship between the π-electron plasmon and nanotube diameter." Chemical Physics Letters 493(1-3): 19-23.

Rashid, A. A.-R., Ahmad I., A. and Bryan M., T. (2012). "On the aspect ratio effect of multi-walled carbon nanotube reinforcements on the mechanical properties of cementitious nanocomposites." Construction and Building Materials 35(0): 647-655.

Rastogi, R. K., Rahul Tripathi, S. K. Sharma, Amit L. Kaur, Inderpreet Bharadwaj, Lalit M. (2008). "Comparative study of carbon nanotube dispersion using surfactants." Journal of Colloid and Interface Science 328(2): 421-428.

Rhee, I., Kim, Y. A., Shin, G.-O., Kim, J. H. and Muramatsu, H. (2015). "Compressive strength sensitivity of cement mortar using rice husk-derived graphene with a high specific surface area." Construction and Building Materials 96: 189-197.

Richardson, A. and Heather, M. (2013). "Improving the Performance of Concrete using 3D Fibres." Procedia Engineering 51(0): 101-109.

RILEM (2006). RILEM TC HRC : RILEM Proceedings PRO 49: International RILEM Workshop on High Performance Fiber Reinforced Cementitious Composites (HPFRCC) in Structural Applications.

Rizkalla, E. K. A. a. S. H. (1989). "Response of Concrete to Sulfuric Acid Attack." ACI MATERIALS JOURNAL.

Rossi, A. P., Mallier Y. (1987). "Effect of steel fibres at two stages: the material and the structure. ." Mater Struct ;20:436–9.

Rovnaník, P., Šimonová, H., Topolář, L., Bayer, P., Schmid, P. and Keršner, Z. (2016). "Carbon nanotube reinforced alkali-activated slag mortars." Construction and Building Materials 119: 223-229.

Ruoff, R. S., Qian, D. and Liu, W. K. (2003). "Mechanical properties of carbon nanotubes: theoretical predictions and experimental measurements." Comptes Rendus Physique 4(9): 993-1008.

Şahin, Y. and Köksal, F. (2011). "The influences of matrix and steel fibre tensile strengths on the fracture energy of high-strength concrete." Construction and Building Materials 25(4): 1801-1806.

Şahmaran, M., Lachemi, M., Hossain, K. M. A. and Li, V. C. (2009). "Internal curing of engineered cementitious composites for prevention of early age autogenous shrinkage cracking." Cement and Concrete Research 39(10): 893-901.

Şahmaran, M. and Li, V. (2010). "Engineered Cementitious Composites." Transportation Research Record: Journal of the Transportation Research Board 2164: 1-8.

Said, S. H. and Razak, H. A. (2015). "The effect of synthetic polyethylene fiber on the strain hardening behavior of engineered cementitious composite (ECC)." Materials & Design 86: 447-457.

Samuel, C., Zhu, P., Jay G., S., Chien Ming, W. and Wen Hui, D. (2014). "Nano reinforced cement and concrete composites and new perspective from graphene oxide." Construction and Building Materials 73: 113-124.

Sanchez, F. and Ince, C. (2009). "Microstructure and macroscopic properties of hybrid carbon nanofiber/silica fume cement composites." Composites Science and Technology 69(7–8): 1310-1318.

Sanchez, F. and Sobolev, K. (2010). "Nanotechnology in concrete – A review." Construction and Building Materials 24(11): 2060-2071.

Santillan-Jimenez, E., Perdu, M., Pace, R., Morgan, T. and Crocker, M. (2015). "Activated Carbon, Carbon Nanofiber and Carbon Nanotube Supported Molybdenum Carbide Catalysts for the Hydrodeoxygenation of Guaiacol." Catalysts 5(1): 424-441.

Santos, H. M., Lodeiro, C. and Capelo-Martínez, J.-L. (2008). " The Power of Ultrasound, in Ultrasound in Chemistry: Analytical Applications (ed J.-L. Capelo-Martínez), Wiley-VCH Verlag GmbH & Co. KGaA, Weinheim, Germany. doi: 10.1002/9783527623501.ch1."

Saptarshi, S., B., B. and Nagesh R., I. (2013). "Can Carbon Nanotubes Make Wonders in Civil/Structural Engineering?" Progress in Nanotechnology and Nanomaterials Vol. 2(Iss. 4): PP. 117-129.

Sarfarazi, V., Ghazvinian, A., Schubert, W., Nejati, H. R. and Hadei, R. (2016). "A New Approach for Measurement of Tensile Strength of Concrete." Periodica Polytechnica Civil Engineering 60(2): 199-203.

Schmidt, M., Fehling, E., Glotzbach, C., Fröhlich, S. and Piotrowski, S. (2012). Ultra-High Performance Concrete and Nanotechnology in Construction, Kassel.

Seong-Cheol Lee 1, J.-H. O. a. J.-Y. C., * (2015). "Compressive Behavior of Fiber-Reinforced Concrete with End-Hooked Steel Fibers " materials 8: 1442-1458.

Sham, M.-L. and Kim, J.-K. (2006). "Surface functionalities of multi-wall carbon nanotubes after UV/Ozone and TETA treatments." Carbon 44(4): 768-777.

Shang, Y., Zhang, D., Yang, C., Liu, Y. and Liu, Y. (2015). "Effect of graphene oxide on the rheological properties of cement pastes." Construction and Building Materials 96: 20-28.

Shao, H., Chen, B., Li, B., Tang, S. and Li, Z. (2017). "Influence of dispersants on the properties of CNTs reinforced cement-based materials." Construction and Building Materials 131: 186-194.

Sharma, S. and Kothiyal, N. C. (2016). "Comparative effects of pristine and ball-milled graphene oxide on physico-chemical characteristics of cement mortar nanocomposites." Construction and Building Materials 115: 256-268.

Sharma, S. and Kothiyal, N. C. (2016). "Facile growth of carbon nanotubes coated with carbon nanoparticles: A potential low-cost hybrid nanoadditive for improved mechanical, electrical, microstructural and crystalline properties of cement mortar matrix." Construction and Building Materials 123: 829-846.

Shi, C., Wu, Z., Xiao, J., Wang, D., Huang, Z. and Fang, Z. (2015). "A review on ultra high performance concrete: Part I. Raw materials and mixture design." Construction and Building Materials 101, Part 1: 741-751.

Shu, X. R., Qianping Liu, Jiaping Zhao, Hongxia Zhang, Qian Wang, Xiumei Yang, Yong Liu, Jinzhi (2016). "Tailoring the solution conformation of polycarboxylate superplasticizer toward the improvement of dispersing performance in cement paste." Construction and Building Materials 116: 289-298.

Siddique, R. and Mehta, A. (2014). "Effect of carbon nanotubes on properties of cement mortars." Construction and Building Materials 50(0): 116-129.

Singh, A. P., Gupta, B. K., Mishra, M., Govind, Chandra, A., Mathur, R. B. and Dhawan, S. K. (2013). "Multiwalled carbon nanotube/cement composites with exceptional electromagnetic interference shielding properties." Carbon 56(0): 86-96.

Sobolkina, A., Mechtcherine, V., Khavrus, V., Maier, D., Mende, M., Ritschel, M. and Leonhardt, A. (2012). "Dispersion of carbon nanotubes and its influence on the mechanical properties of the cement matrix." Cement and Concrete Composites 34(10): 1104-1113.

Song, K., Zhang, Y., Meng, J., Green, E., Tajaddod, N., Li, H. and Minus, M. (2013). "Structural Polymer-Based Carbon Nanotube Composite Fibers: Understanding the Processing–Structure–Performance Relationship." Materials 6(6): 2543-2577.

Sorelli, L., Constantinides, G., Ulm, F.-J. and Toutlemonde, F. (2008). "The nano-mechanical signature of Ultra High Performance Concrete by statistical nanoindentation techniques." Cement and Concrete Research 38(12): 1447-1456.

SpaSojević, A. (2008). Structural implications of ultra-high performance fibre-reinforced concrete in bridge design.

Stähli, P. and van Mier, J. G. M. (2007). "Manufacturing, fibre anisotropy and fracture of hybrid fibre concrete." Engineering Fracture Mechanics 74(1-2): 223-242.

Stark, J. (2011). "Recent advances in the field of cement hydration and microstructure analysis." Cement and Concrete Research 41(7): 666-678.

Stynoski, P., Mondal, P. and Marsh, C. (2015). "Effects of silica additives on fracture properties of carbon nanotube and carbon fiber reinforced Portland cement mortar." Cement and Concrete Composites 55(0): 232-240.

Sun, L. D. a. J. (2016). Mechanical Properties of Carbon Nanotubes-Polymer Composites. Carbon Nanotubes - Current Progress of their Polymer Composites.

Syed Mazharul, I., Raja Rizwan, H. and Md. Abu Zakir, M. (2012). "Fiber-reinforced concrete incorporating locally available natural fibers in normal- and high-strength concrete and a performance analysis with steel fiber-reinforced composite concrete." Journal of Composite Materials 46(1): 111-122.

Tada-aki Tanabe, K. S., Okayama University, Hirozo Mihashi, Ryoichi Sato, Koichi Maekawa, Hikaru Nakamura (2009). Creep, Shrinkage and Durability Mechanics of Concrete and Concrete Structures. 009 Taylor & Francis Group, London,.

Tamimi, A., Hassan, N. M., Fattah, K. and Talachi, A. (2016). "Performance of cementitious materials produced by incorporating surface treated multiwall carbon nanotubes and silica fume." Construction and Building Materials 114: 934-945.

Tian, H., Zhang, Y. X., Ye, L. and Yang, C. (2015). "Mechanical behaviours of green hybrid fibre-reinforced cementitious composites." Construction and Building Materials 95: 152-163.

Tobias, H. (2015). Investigation of a Novel Self-Healing Cementitious Composite Material System, Cardiff University.

Toledo Filho, R. D., Ghavami, K., Sanjuán, M. A. and England, G. L. (2005). "Free, restrained and drying shrinkage of cement mortar composites reinforced with vegetable fibres." Cement and Concrete Composites 27(5): 537-546.

Tong, T., Fan, Z., Liu, Q., Wang, S., Tan, S. and Yu, Q. (2016). "Investigation of the effects of graphene and graphene oxide nanoplatelets on the micro- and macro-properties of cementitious materials." Construction and Building Materials 106: 102-114.

Tong, Y., Zhao, S., Ma, J., Wang, L., Zhang, Y., Gao, Y. and Xie, Y. M. (2014). "Improving cracking and drying shrinkage properties of cement mortar by adding chemically treated luffa fibres." Construction and Building Materials 71: 327-333.

Torabian Isfahani, F., Li, W. and Redaelli, E. (2016). "Dispersion of multi-walled carbon nanotubes and its effects on the properties of cement composites." Cement and Concrete Composites 74: 154-163.

Tragazikis, I. K., Dassios, K. G., Exarchos, D. A., Dalla, P. T. and Matikas, T. E. (2016). "Acoustic emission investigation of the mechanical performance of carbon nanotube-modified cement-based mortars." Construction and Building Materials 122: 518-524.

Trettin, K. T. (2005). "Nanotubes fur hochleistungsbetone (nanotubes for highperformance concretes)." Betonwerk und Fertigteil-Technik/Concr Precast Plant Technol 71(2): 20–21.

Tyson, B. M., Abu Al-Rub, R. K., Yazdanbakhsh, A. and Grasley, Z. (2011). "Carbon Nanotubes and Carbon Nanofibers for Enhancing the Mechanical Properties of Nanocomposite Cementitious Materials." Journal of Materials in Civil Engineering 23(7): 1028-1035.

Tyson, B. M., Abu Al-Rub, R. K., Yazdanbakhsh, A. and Grasley, Z. (2011). "A quantitative method for analyzing the dispersion and agglomeration of nano-particles in composite materials." Composites Part B: Engineering 42(6): 1395-1403.

Vaisman, L., Wagner, H. D. and Marom, G. (2006). "The role of surfactants in dispersion of carbon nanotubes." Advances in Colloid and Interface Science 128–130(0): 37-46.

Victor Chabot, B. K., 1 Brent Sloper,1 Costas Tzoganakis,1 and Aiping Yua, (2013). " high yield production and purification of few layer graphene by Gum Arabic assisted physical sonication."

Wang, B., Guo, Z., Han, Y. and Zhang, T. (2013). "Electromagnetic wave absorbing properties of multi-walled carbon nanotube/cement composites." Construction and Building Materials 46(0): 98-103.

Wang, H., Gao, X. and Wang, R. (2017). "The influence of rheological parameters of cement paste on the dispersion of carbon nanofibers and self-sensing performance." Construction and Building Materials 134: 673-683.

Wang, Q., Wang, J., Lv, C.-x., Cui, X.-y., Li, S.-y. and Wang, X. (2017). "[New Carbon Materials 2016, 31(6): 574–584]. Rheological behavior of fresh cement pastes with a graphene oxide additive." Carbon 114: 755.

Wang, W., Ruiz, I., Guo, S., Favors, Z., Bay, H. H., Ozkan, M. and Ozkan, C. S. (2014). "Hybrid carbon nanotube and graphene nanostructures for lithium ion battery anodes." Nano Energy 3(0): 113-118.

Wille, K. and Loh, K. (2010). "Nanoengineering Ultra-High-Performance Concrete with Multiwalled Carbon Nanotubes." Transportation Research Record: Journal of the Transportation Research Board 2142: 119-126.

Wilson, M. A., Carter, M. A. and Hoff, W. D. (1999). "British Standard and RILEM water absorption tests: A critical evaluation." Materials and Structures/Mat6riaux et Constructions 32: 571o578

Xiao-Lin, X., Yiu-Wing, M. and Xing-Ping, Z. (2005). "Dispersion and alignment of carbon nanotubes in polymer matrix: A review." Materials Science and Engineering: R: Reports 49(4): 89-112.

Xu, S., Jintao, L. and Qinghua, L. (2015). "Mechanical properties and microstructure of multi-walled carbon nanotube-reinforced cement paste." Construction and Building Materials 76: 16-23.

Yan Yan, H. and Eugene M., T. (2012). "Dispersion of Carbon Nanotubes: Mixing, Sonication, Stabilization, and Composite Properties." Polymers 4(4): 275-295.

Yan, Y. H. and Eugene, M. T. (2012). "Dispersion of Carbon Nanotubes: Mixing, Sonication, Stabilization, and Composite Properties." Polymers 4(4): 275-295.

Yazdanbakhsh, A., Grasley, Z., Tyson, B. and Abu Al-Rub, R. (2012). "Challenges and Benefits of Utilizing Carbon Nanofilaments in Cementitious Materials." Journal of Nanomaterials 2012: 1-8.

Yazdanbakhsh, A., Grasley, Z., Tyson, B. and Abu Al-Rub, R. K. (2011). "Dispersion quantification of inclusions in composites." Composites Part A: Applied Science and Manufacturing 42(1): 75-83.

Yit Thai, O., Abdul Latif, A., Sharif Hussein Sharif, Z. and Soon Huat, T. (2010). "A review on carbon nanotubes in an environmental protection and green engineering perspective." Brazilian Journal of Chemical Engineering Fracture Mechanics.

Yonghui Liu, L. Y., Shaohua Zhang, Jie Yuan, Lijuan Shi, Liqiang Zheng (2010). "Dispersion of multiwalled carbon nanotubes by ionic liquid-type Gemini imidazolium surfactants in aqueous solution." Colloids and Surfaces A: Physicochem. Eng. Aspects: 359 (2010) 2066–2070.

Yoo, D.-Y., Min, K.-H., Lee, J.-H. and Yoon, Y.-S. (2014). "Shrinkage and cracking of restrained ultra-high-performance fiber-reinforced concrete slabs at early age." Construction and Building Materials 73: 357-365.

Yoo, D.-Y., Park, J.-J., Kim, S.-W. and Yoon, Y.-S. (2013). "Early age setting, shrinkage and tensile characteristics of ultra high performance fiber reinforced concrete." Construction and Building Materials 41: 427-438.

Yu, H., Danni, L., Penghui, L., Qingbin, L. and Guoqiang, S. (2014). "Fracture toughness enhancement of cement paste with multi-walled carbon nanotubes." Construction and Building Materials 70 (2014) 332–338.

Yu M, L. O., Dyer MJ, Kelly TF, Ruoff RS. (2000). "Strength and breaking mechanism of multiwalled carbon anotubes under tensile load. Science 2000;287:637–40.".

Yurtseven, A. E. (2004). Determination of mechanical properties of hybrid fiber reinforced concrete, Middle east technical university.

Zdenek, B., Peter J.M., B., Vít, Š. and Jan, Z. (2009). Nanotechnology in Construction 3: Proceedings of the NICOM3. Springer-Verlag Berlin Heidelberg.

Zhang, H., Zhang, Z. and Breidt, C. (2004). "Comparison of short carbon fibre surface treatments on epoxy composites: I. Enhancement of the mechanical properties." Composites Science and Technology 64(13–14): 2021-2029.

Zhang, J. and Li, V. C. (2001). "Influences of Fibers on Drying Shrinkage of Fiber-Reinforced Cementitious Composite." Journal of Engineering Mechanics 127(1): 37-44.

Zhou, C., Li, F., Hu, J., Ren, M., Wei, J. and Yu, Q. (2017). "Enhanced mechanical properties of cement paste by hybrid graphene oxide/carbon nanotubes." Construction and Building Materials 134: 336-345.

Zhu, P. J. M. B. a. A. P. (2004). "Application of nanotechnology in construction Summary of a state-of-the-art report." RILEM TC 197-NCM: 'Nanotechnology in construction materials' Materials and Structures / Matériaux et Constructions 37: pp 649-658.

Zhu, X. H., Kang, X. J., Yang, K. and Yang, C. H. (2017). "Effect of graphene oxide on the mechanical properties and the formation of layered double hydroxides (LDHs) in alkali-activated slag cement." Construction and Building Materials 132: 290-295.

Zoi, M., Maria, K.-G. and Surendra, S. (2010). "Carbon Nanofiber-Reinforced Cement-Based Materials." Transportation Research Record: Journal of the Transportation Research Board 2142: 114-118.

Appendix

Conferences and Publications

- Alrekabi, S., Cundy, A., Lampropoulos A., and Savina, I.N. (2016), Experimental Investigation on the Effect of Ultrasonication on Dispersion and Mechanical Performance of Multi-Wall Carbon Nanotube-Cement Mortar Composites. International Journal of Civil, Environmental, Structural, Construction and Architectural Engineering, 111 (3). pp. 268-274.

- Alrekabi, S., Cundy, A., Lampropoulos A., and Savina, I.N. (2016), Experimental investigation of the effect of superplasticizer/surfactant aided aqueous dispersion of multi-walled Carbon nanotubes on workability and mechanical properties of cementitious composites. Proceedings of the 25th Workshop and Colloquium, OTH Regensburg, (East BavarianUniversity of Technology), Regensburg, Germany, 2-3 March, 2016.

- Alrekabi, S., Cundy, A., Lampropoulos A., and Savina, I.N. (2016). Effect of Microsilica on the Dispersion of Carbon Nanotubes within a Cementitious Composite. Young Researchers' Forum III Innovation in Construction Materials 12 April 2016.

- Alrekabi, S., Cundy, A., Whitby R.L.D., Lampropoulos A., and Savina, I.N. (2017). Effect of Undensified Silica Fume on the Dispersion of Carbon Nanotubes within a Cementitious Composite. Applied Nanotechnology and Nanoscience International Conference 2016. IOP Conf. Series: Journal of Physics: Conf. Series 829 (2017) 012011.

Journal:

- Alrekabi, S., Cundy, A., Lampropoulos A., Whitby R.L.D., and Savina, I.N. (2016). Mechanical performance of novel cement-based composites prepared with nano-fibres, and hybrid nano- and micro-fibres. Composite Structures Journal. (Under review).

- Alrekabi, S., Cundy, A., Lampropoulos A., Whitby R.L.D., and Savina, I.N. (2017). The Effect of High Intensity Sonication on the Dispersion of Carbon-Based Nanofilaments in Cementitious Composites, and its Impact on Mechanical Performance. Materials and Design (Under review)**.**